TUM School of Life Sciences

Lipocalin 13 in Systemic Energy Homeostasis

Lea Katharina Bühler

Vollständiger Abdruck der von der TUM School of Life Sciences der Technischen Universität München zur Erlangung des akademischen Grades eines Doktors der Naturwissenschaften genehmigten Dissertation.

Vorsitzender:		Prof. Dr. Dirk Haller
Prüfende/-r der Dissertation:	1.	Prof. Dr. Ilona Grunwald Kadow
	2.	Prof. Dr. Stephan Herzig

Die Dissertation wurde am 22.10.2020 bei der Technischen Universität München eingereicht und durch die TUM School of Life Sciences am 16.02.2021 angenommen.

Abstract

As the prevalence of diabetes has reached epidemic proportions, finding an effective and safe anti-diabetic drug has become a major focus of medical research. Exploiting endogenous circulating factors, which play crucial roles in energy homeostasis, has become a promising avenue. In this context, the hepatokine lipocalin 13 (LCN13) has emerged as potential insulin sensitizer and biomarker for type 2 diabetes (T2D).

In this study, we investigated the role of LCN13 in systemic metabolic control and inter-organ communication. Suppressing hepatic LCN13 production in healthy wild type mice by liponanoparticle (LNP)-mediated small interfering RNA (siRNA) transfer had no effects on glucose clearance, insulin sensitivity or lipid metabolism. In line with this, increasing LCN13 availability in healthy wild type mice by either adeno-associated virus (AAV)-mediated hepatic overexpression or by administration of recombinant mammalian LCN13 protein did not influence glucose homeostasis. Also, in the context of genetically or diet-induced diabetes, LCN13 treatment did not reveal any beneficial impact on glucose or lipid metabolism. Furthermore, manipulation of LCN13 expression did not affect mRNA levels of other lipocalin family members. In contrast to our *in vivo* studies, LCN13 consistently enhanced glucose-stimulated insulin secretion (GSIS) by both primary islets and the β-cell line MIN6 in an isolated *in vitro* system.

In summary, albeit promoting insulin secretion *in vitro*, LCN13 did not affect the metabolic phenotype of healthy or diabetic mice *in vivo*. In light of publications assessing other lipocalin family members, we conclude that the role of LCN13 in energy metabolism seems to be more delicate and complex than previously thought. We discuss possible confounding factors that could underlie the discrepancies between these and previously published results and how to unravel the yet unknown components affecting the actions of LCN13.

Zusammenfassung

Die Prävalenz von Diabetes steigt weltweit und hat mittlerweile ein epidemisches Ausmaß erreicht. Dies verdeutlicht die Dringlichkeit der Herstellung von neuen, effektiveren Antidiabetika. Im Blut zirkulierende Faktoren spielen eine wichtige Rolle im menschlichen Stoffwechsel und stellen in diesem Zusammenhang ein vielversprechendes therapeutisches Ziel dar. Ein Kandidat ist hierbei das Hepatokin Lipokalin 13 (LCN13), dem in der Literatur eine Insulin-sensitivierende Wirkung und eine Rolle als Biomarker für Typ 2 Diabetes (T2D) zugeschrieben wurde.

Diese Studie hatte das Ziel, die Rolle von LCN13 im Metabolismus und in der Organ-Kommunikation näher zu charakterisieren. Die Inhibition der LCN13-Produktion in der Leber von gesunden Wildtyp-Mäusen mittels Liponanopartikel (LNP) vermitteltem small interfering RNA (siRNA) Transfer hatte keine negativen Auswirkungen auf die Insulinsensitivität, den Glukose- oder Lipidstoffwechsel. Auch die leberspezifische Überexpression von LCN13 mithilfe von Adeno-assoziierten Viren (AAV) oder die Gabe von rekombinantem LCN13-Protein, das in Säugetierzellen hergestellt wurde, hatte keinen Einfluss auf die Glukosehomöostase in gesunden Wildtyp-Mäusen. In Übereinstimmung mit unseren Ergebnissen in gesunden Tieren zeigte die leberspezifische Überexpression von LCN13 in Mäusen mit Stoffwechselstörungen keinen positiven Einfluss auf den Glukose- oder Fettstoffwechsel. Dies umfasste sowohl adipöse Mäuse, die mit einer fettreichen Diät gefüttert wurden, als auch db/db-Mäuse, ein genetisches Mausmodell für vererbte Fettleibigkeit und Diabetes. Wir konnten zudem zeigen, dass die Veränderung der LCN13-Expression keinen Einfluss auf die mRNA-Level anderer Mitglieder der Lipokalin Proteinfamilie hat. Im Gegensatz zu diesen *in vivo*-Ergebnissen erhöhte LCN13 die Glukose-stimulierte Insulinsekretion (GSIS) von primären Langerhans-Inseln und der Betazelllinie MIN6 *in vitro*.

Zusammenfassend kann gesagt werden, dass LCN13 keinen Einfluss auf den metabolischen Phänotyp von gesunden oder adipösen und diabetischen Mäusen hatte, obwohl es die Insulinsekretion von Betazellen *in vitro* förderte. Vor dem Hintergrund bereits veröffentlichter Daten anderer Lipokaline schließen wir, dass die Rolle von LCN13 im Stoffwechsel störungsanfälliger und komplexer ist als bisher angenommen. Wir diskutieren mögliche Störfaktoren, die die Diskrepanzen zwischen dieser und bereits veröffentlichter Studien erklären könnten, und Möglichkeiten zu deren Identifikation.

Acknowledgements

In the first place, I would like to thank Stephan Herzig. Thank you for giving me the opportunity to be a part of your great research group and institute. I am especially grateful for our inspiring scientific discussions, your constant support, motivating nature and optimistic way of thinking, which taught me how to deal with setbacks during my PhD project.
I am also very grateful to Ilona Grunwald Kadow and Mauricio Berriel Diaz for the scientific exchange and your great ideas during the thesis advisory committee meetings, which helped to move this project forward.

Thanks to all IDC members, the atmosphere at the institute was very motivating and enriching. I did not only have great co-workers but also found true friends.
Special thanks go to Adriano Maida. You were a fantastic supervisor. I admire your scientific knowledge, your ability to troubleshoot and your encouraging nature. Besides being an outstanding scientist you are also one of the most warm-hearted and empathetic persons I have ever met. Thank you for everything.
Many thanks also to Anastasia Georgiadi. Your passion for science is contagious. Thank you for sharing your broad scientific knowledge and for supporting me far beyond protein production.
Special thanks also go to Elena. You were an amazing support, especially during my maternity leave. Thanks for always being there for me – not only in the lab, but also as a friend.
Moreover, I am ever so grateful to Andrea. Thanks for all the hours we spent in the DMF together and for the hugs when I needed them the most.
Thanks also to Ana, Asrar, Eveline, Götz, Katarina, Nina, Phivos and Susi for the scientific exchange and for always standing by my side. You made my time at the IDC so much more enjoyable and I cannot thank you enough for that.
I would also like to express my thanks to Miri, the fairy godmother of the institute. You helped me to find my way through the bureaucracy jungle and shared one or the other late-night pizza with me. Thanks for becoming such a wonderful friend.

I am especially thankful to my family, Basirou and Naomi. You helped me to keep my sanity in stressful times. You are the most important people in my life.
I love you.

Table of Contents

1. Introduction

1.1 Physiological Blood Glucose Homeostasis

1.1.1 Multi-Hormonal Model of Glucose Regulation

Maintaining blood glucose levels within a narrow range was classically attributed to a bi-hormonal model. This encompasses the key anabolic hormone insulin, which is responsible for glucose lowering after the ingestion of a meal, and the antagonistic catabolic hormone glucagon, which induces endogenous glucose production upon fasting (Aronoff et al., 2004). After meal ingestion, increased circulating glucose levels are sensed by pancreatic β-cells which respond by secreting insulin in a pulsatile manner (Weigle, 1987). Insulin in turn ensures blood glucose disposal by various mechanisms (Figure 1a; reviewed in Aronoff et al., 2004; Haeusler et al., 2018). Key features are the induction of glucose uptake by primarily muscle but also adipocytes as well as the inhibition of hepatic glucose output. The latter is achieved, on one hand, by promoting glycogen synthesis. On the other hand, insulin can inhibit hepatic gluconeogenesis in both direct and indirect manner (Hatting et al., 2018). Indirect suppression of gluconeogenesis as well as glycogenolysis is for example achieved by insulin's inhibiting effect on glucagon secretion by pancreatic α-cells. Of note, insulin also promotes lipogenesis while inhibiting lipolysis. This leads to a decline in circulating free fatty acids (FFA)/non-esterified fatty acids (NEFA) known to support hepatic gluconeogenesis as well as to negatively influence insulin sensitivity in liver and muscle (discussed below). In the fasted state, glucagon secretion increases due to diminished insulin inhibition. Glucagon ensures sufficient blood glucose levels by enhancing endogenous glucose production via the induction of both glycogen breakdown and gluconeogenesis.

It however became clear that gut-derived factors also play a pivotal role in glycemic control, as glucose taken up orally resulted in a stronger insulin response than glucose infused intravenously (Elrick et al., 1964). This amplification in insulin secretion called the 'incretin effect' could mainly be attributed to glucagon-like peptide-1 (GLP-1) and glucose-dependent insulinotropic peptide (GIP; Drucker, 2006). GLP-1 further reinforces the action of insulin by inhibiting glucagon secretion, slowing down gastric emptying and promoting satiety (Edholm et al., 2010; Nauck et al., 2002; Ramracheya et al., 2018). These effects can also be exerted by islet amyloid polypeptide (IAPP), or amylin, which is yet another component of the multi-hormonal model governing glucose homeostasis (Gedulin et al., 1997; Morley and Flood, 1991; Young et al., 1996). IAPP is secreted alongside with insulin as it co-localizes with insulin in the secretory granules of β-cells (Kahn et al., 1990; Lukinius et al., 1989).

Besides the aforementioned GIP and GLP-1 there are several other gut-derived hormones which regulate systemic metabolism. In the following some of them will be highlighted (reviewed in Sun et al., 2019). Oxyntomodulin (OXM) is secreted alongside with GLP-1. Besides enhancing insulin secretion in a glucose-dependent manner, it promotes satiety and energy expenditure. Peptide YY (PYY) is another gut-derived hormone which is co-secreted with GLP-1. Like GLP-1, it slows down gastric emptying and reduces food intake. Ghrelin, a counter-regulatory hormone which is released under fasting conditions, acts, amongst others, as appetite stimulant, promotes lipogenesis and increases glucagon secretion, while inhibiting insulin release.

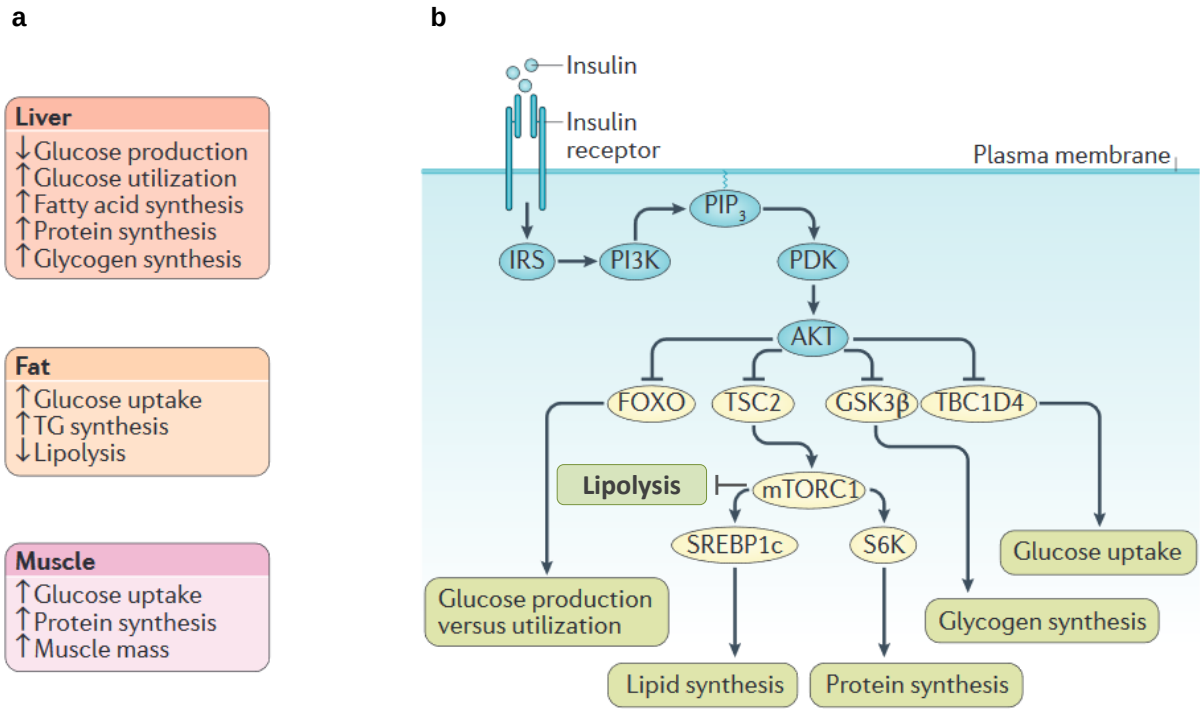

Figure 1 | Insulin Signalling Cascade and Downstream Metabolic Effects

(**a**) Key effects of insulin on liver and peripheral organs. (**b**) Insulin signalling cascade: an overview of crucial factors translating the insulin signal into metabolic changes. See text for details. FOXO, forkhead box O transcription factor; GSK3β, glycogen synthase kinase 3 beta; IRS, insulin receptor substrate; mTORC1, mammalian target of rapamycin complex 1; PDK, 3-phosphoinositide-dependent protein kinase-1; PI3K, phosphatidylinositol 3-kinase; PIP_3, phosphatidylinositol (3,4,5)-trisphosphate; S6K, ribosomal protein S6 kinase beta-1; SREBP1, sterol regulatory element-binding protein-1; TBC1D4, TBC1 domain family member 4; TSC2, tuberous sclerosis complex 2. Figure was adapted and modified from (Haeusler et al., 2018)

1.1.2 Insulin Signalling Cascade

After binding to the insulin receptor (IR), which is located at the plasma membrane of basically all cells, insulin can activate various signalling pathways and cellular responses (Figure 1b; reviewed in Haeusler et al., 2018):

The principle mechanism of IR signal transduction is based on tyrosine phosphorylation. Insulin binding elicits receptor dimerization and subsequent cross-phosphorylation of the IR. This autophosphorylation by the receptor tyrosine kinase of the IR generates docking sites for insulin receptor substrates (IRS) which are phosphorylated by the IR kinase upon binding. Consequently, IRS recruit and activate the catalytic subunit of phosphoinositide 3-kinase (PI3K) which in turn converts phosphatidylinositol 4,5-bisphosphate (PIP_2) at the plasma membrane into phosphatidylinositol 3,4,5-trisphosphate (PIP_3). PIP_3 recruits 3-phosphoinositide-dependent protein kinase-1 (PDK) which directly phosphorylates the serine/threonine kinase AKT/protein kinase B (PKB) at the threonine residue 308 (Thr308). AKT gets fully activated by a second phosphorylation at the serine residue 473 (Ser473) by the mechanistic target of rapamycin complex 2 (mTORC2). Once activated, AKT phosphorylates multiple substrates at serine/threonine residues, thereby facilitating many of the known insulin downstream effects.

For instance, AKT-mediated phosphorylation of TBC1 domain family member 4 (TBC1D4), a RAB GTPase-activating protein, leads to its inactivation. This allows activated RAB proteins to promote glucose transporter type 4 (GLUT4) translocation to the plasma membrane where it allows insulin-induced glucose uptake in muscle and adipocytes (Ishikura et al., 2007; Leto and Saltiel, 2012; Sano et al., 2007).

Another major effect of insulin-induced AKT activation is the inhibition of glycogen synthase kinase 3 beta (GSK3β) which permits glycogen synthase activity and thereby glucose storage in the form of glycogen (Cross et al., 1995).

Forkhead family box O (FOXO) transcription factors are AKT targets which exert insulin-induced effects at the transcriptional level. AKT-dependent nuclear exclusion and inactivation of FOXO promotes glucokinase expression while inhibiting glucose-6-phophatase expression. By that, glucose utilisation is favoured over hepatic glucose output (Haeusler et al., 2014). Furthermore, AKT activates the transcription factor sterol regulatory element-binding protein-1 (SREBP1c) which promotes lipid synthesis by inducing, for example, acetyl-CoA carboxylase (ACC) and fatty acid synthase (FAS). The underlying signal cascade involves AKT-dependent inhibition of protein tuberous sclerosis 2 (TSC2), which allows for the activation of mTORC1. mTORC1 subsequently phosphorylates and inhibits lipin1 and CREB regulated transcription coactivator 2 (CRTC2) which normally prevent SREBP1c transcriptional activity and nuclear translocation, respectively (Haeusler et al., 2018).

Besides fostering lipogenesis, insulin inhibits lipolysis via mTORC1-mediated activation of early growth response protein 1 (EGR1) which is a transcriptional repressor of adipose triglyceride lipase (ATGL) (Chakrabarti et al., 2013).

Insulin-dependent activation of mTORC1 furthermore induces protein synthesis via its downstream target ribosomal protein S6 kinase (S6K; Ruvinsky and Meyuhas, 2006).

Insulin signalling is tightly regulated. In healthy individuals, this is achieved by multiple negative feedback loops. Insulin-induced receptor internalization followed by lysosomal degradation, lipid and protein phosphatases as well as pseudosubstrates of the IR kinase are means to attenuate insulin signalling (Haeusler et al., 2018). Another crucial component of insulin-induced negative feedback loops is inhibitory phosphorylation. While tyrosine phosphorylation activates both IR and IRS, serine/threonine phosphorylation, including S6K/mTORC1-facilitated IRS serine phosphorylation, leads to signal attenuation (Copps and White, 2012). Aberrant lipid-induced IR/IRS serine phosphorylation constitutes one basis for obesity-related insulin resistance (discussed below).

1.1.3 Molecular Drivers of Insulin Secretion

Not only insulin signalling, but also insulin secretion is governed by a complex regulatory network. How metabolic components can induce and amplify insulin secretion of pancreatic β-cells is still an area of intensive research. In this section key aspects of 'fuel-induced insulin secretion' will be highlighted (reviewed by Prentki et al., 2013).

Glucose is the primary stimulus for the induction of insulin secretion. Especially, the expression of glucokinase (GK) allows β-cells to act as glucose sensors. This hexokinase isoenzyme is characterized by its low glucose affinity, sigmoidal glucose dependency and, importantly, by the lack of any negative feedback control (Prentki et al., 2013). Besides glucose, also other nutrients such as amino acids, FFA and hormones like GLP-1 can enhance insulin secretion; however, exclusively in a glucose-dependent manner (see Figure 2). The central trigger of insulin exocytosis is an increase in cytoplasmic Ca^{2+} concentration. In short, glucose oxidation by both glycolysis and the Krebs cycle leads to the generation of reduced nicotinamide adenine dinucleotide (NADH) and flavin adenine dinulceotide ($FADH_2$) molecules. Electrons deriving from both NADH and $FADH_2$ fuel the mitochondrial respiratory chain leading to the reduction of oxygen to water. Simultaneously, protons are pumped across the inner mitochondrial membrane generating a proton-motive force fueling ATP-synthase-dependent adenosine triphosphate (ATP) production (oxidative phosphorylation/OXPHOS). An increased $\frac{\mathrm{ATP}}{\mathrm{ADP}}$ ratio leads to the closure of the nucleotide-sensitive K_{ATP}/SUR1 channel complex and subsequently to plasma membrane depolarisation and opening of voltage-sensitive L-type Ca^{2+} channels. The resulting Ca^{2+} influx promotes exocytosis of insulin granules by a complex interplay

between Ca^{2+} binding proteins, such as the calcium sensor synaptogamin, and calcium-activated protein kinases (Barclay et al., 2005; Brose et al., 1992; Gustavsson et al., 2012; Tang et al., 2006). Besides glucose, also activated FFA (FA-CoA) and the amino acid glutamine can enter the Krebs cycle to fuel OXPHOS. The latter is hydrolyzed to glutamate and further converted to α-ketoglutarate by glutamate dehydrogenase (GDH). This anaplerotic reaction is potentiated by leucine which is an allosteric activator of GDH. Another anaplerotic reaction providing intermediates for the Krebs cycle is the carboxylation of pyruvate to oxalacetate by pyruvate carboxylase (PC). Anaplerotic reactions allow for intermediates to exit the Kebs cycle (cataplerosis) and to act as metabolic coupling factors (MCF) in order to amplify insulin secretion. The generation of these MCF and mechanisms of how they translate metabolic cues into insulin secretion are summarized in the following (see also Figure 2).

Citrate, isocitrate and malate deriving from the Krebs cycle can enter pyruvate cycles which results in the generation of NAD^+, ensuring glycolytic flux, as well as reduced nicotinamide adenine dinucleotide phosphate (NADPH), malonyl-CoA and acyl-CoA. NADPH was suggested to promote redox-regulated posttranslational modification of exocytosis proteins via glutaredoxin and to act on voltage-dependent K^+ (Kv) channels (Ivarsson et al., 2005; MacDonald et al., 2003; Reinbothe et al., 2009). NADPH-driven Kv closure prevents membrane repolarisation and thereby augments insulin secretion. Malonyl-CoA allosterically inhibits carnitinepalmitoyltransferase I (CPT-I) which is accompanied by suppressed mitochondrial β-oxidation and a higher flux of FFA through the glycerolipid/FFA (GL/FFA) cycle. This results in an increased accumulation of lipid signalling molecules which subsequently enhance glucose-stimulated insulin secretion (GSIS; Chen et al., 1994b). It was speculated that acyl-CoA molecules deriving from pyruvate and GL/FFA cycles could play essential roles in acylation-based regulation of proteins involved in exocytosis (Prentki et al., 2013). Supporting this idea, protein acetylation was demonstrated to be important in the regulation of both glucose and fatty acid metabolism in β-cells (Zhang et al., 2019).

Besides the described pyruvate cycles, the reduction of the glycolysis intermediate dihydroxyacetone phosphate (DHAP) to glycerol-3-phosphate (Gro3P) also generates NAD^+ molecules. Gro3P and FFA-CoA enter the GL/FFA cycle which generates lipid signalling molecules such as monoacylglycerols (MAG) by sequential lipogenic and lipolytic reactions. MAG were shown to bind and activate mammalian homologue of UNC-13-1 (Munc13-1) which is involved in vesicle priming and required for sustained insulin release (Kang et al., 2006; Zhao et al., 2014).

Another mechanism which augments cytoplasmic Ca^{2+} levels relies on receptors located at the plasma membrane. In this context, FFA can bind to their plasma membrane receptor FFAR1/GPR40 which is highly expressed on β-cells. GPR40 activation results in phospholipase C (PLC)-mediated generation of diacylglycerol (DAG) and inositol 1,4,5-

triphosphate (IP_3). IP_3 opens Ca^{2+} channels at the endoplasmic reticulum and thereby amplifies intracellular Ca^{2+} levels which, however, seems to play only a minor role in the amplification of insulin secretion (Mancini and Poitout, 2013). DAG on the other hand can activate protein kinase C and D1 (PKC and PKD1) which have been implicated in post-translational modification of exocytosis proteins and actin remodelling (Ferdaoussi et al., 2012; Trexler and Taraska, 2017).

Besides nutrients, also hormones, such as incretins and leptin, are regulators of insulin secretion (Fu et al., 2013). The underlying mechanism of GLP-1-induced insulin secretion comprises activation of adenylate cyclase, subsequent cyclic adenosine monophosphate (cAMP) production and cAMP-mediated activation of protein kinase A (PKA) as well as exchange protein directly activated by cAMP 2/cAMP-regulated guanine nucleotide exchange factor II (Epac 2/cAMP-GEFII). PKA-derived phosphorylation was shown to potentiate K_{ATP}/SUR1 channel complex closure, while opening voltage-dependent calcium channels (VDCC; Kanno et al., 1998; Light et al., 2002). Epac2 was reported to support exocytosis via calcium-dependent binding of RIM2, Picollo and RAB3 (Ozaki et al., 2000; Shibasaki et al., 2004). The counter-regulatory hormone leptin was shown to inhibit pancreatic insulin secretion by PI3K-mediated activation of phosphodiesterase 3B (PDE3B) which in turn hydrolysis cAMP (Marroquí et al., 2012; Zhao et al., 1998).

Another class of MCF was sugested to be represented by reactive oxygen species (ROS) which are generated by the mitochondrial respiratory chain as well as by the NADPH oxidase (Pi et al., 2007; Prentki et al., 2013). This is however a matter of debate (Deglasse et al., 2019).

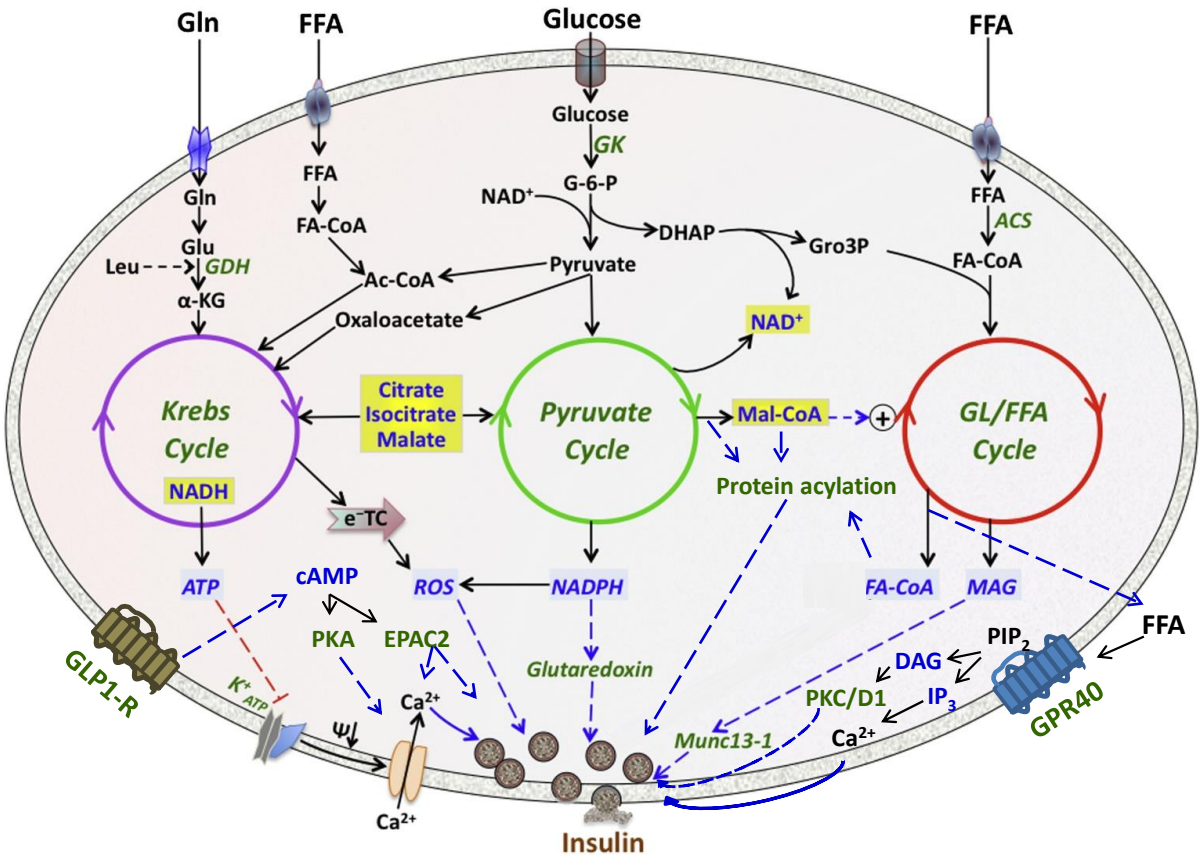

Figure 2 | Triggering and Amplifying Pathways of Insulin Secretion

Insulin secretion is triggered by a rise of cytoplasmic Ca^{2+} levels. During glycolysis glucose is metabolized to pyruvate which fuels the Krebs cycle. In the latter reduced nicotinamide adenine dinucleotide (NADH) and flavin adenine dinucleotide ($FADH_2$) are produced which subsequently pass electrons through the mitochondrial respiratory chain at the inner mitochondrial plasma membrane to generate adenosine triphosphate (ATP). ATP in turn facilitates the closure of ATP-sensitive potassium channels (K^+_{ATP}) located at the plasma membrane leading to membrane depolarisation and opening of voltage-sensitive L-type calcium channels. Besides glucose, also free fatty acids (FFA) and amino acids like glutamine (Gln) can fuel ATP production. Via entering pyuvate cylces and the glycerolipid/FFA (GL/FFA) cycle, these three different nutrient classes generate a diverse set of additional metabolic coupling factors which amplify glucose-stimulated insulin secretion (GSIS). FFA as well as glucagon-like peptide-1 (GLP-1) can further potentiate insulin secretion via receptor mediated signalling. Ac-CoA, acetyl-coenzyme A; ACS, acetyl-CoA synthetase; α-KG, alpha-ketoglutarate; cAMP, cyclic adenosine monophosphate; EPAC2, exchange protein directly activated by cAMP 2; DAG, diacylglycerol; DHAP, dihydroxyacetone phosphate; e^-TC, electron transport chain; FA-CoA, acyl-coenzyme A; GDH, glutamate dehydrogenase; GK, glucokinase; G-6-P, glucose-6-phosphate; Gln, glutamine; Glu, glutamate; GPR40, G-protein-coupled receptor 40; Gro3P, glycerol 3-phosphate; IP_3, inositol 1,4,5-trisphosphate; Leu, leucine; MAG, monoacylglycerol; Mal-CoA, malonyl-coenzyme A; Munc13-1, mammalian homologue of UNC-13-1; PIP_2, phosphatidylinositol 4,5-bisphosphate; NAD^+, oxidized nicotinamide adenine dinucleotide; NADPH, reduced nicotinamide adenine dinucleotide phosphate; PKA, protein kinase A; PKC, protein kinase C; PKD1, protein kinase D 1; ROS, reactive oxygen species. Solid arrows show direct and/or established interactions. Dashed arrows symbolize indirect or not fully established actions. Figure was adapted and modified from (Prentki et al., 2013).

1.2 Type 2 Diabetes Mellitus

With reaching epidemic proportions, diabetes has become a global health burden and its rate of incidence is still rapidly rising. While in 1980 4.7% (108 million adults) of the world's population was estimated to have diabetes, in 2019 9.3% (463 million adults) lived with diabetes (International Diabetes Federation, 2019). If this trend continues, 700 million adults (global prevalence of 10.9%) are predicted to have diabetes in 2049. Diabetes is a metabolic disease characterized by hyperglycemia due to absolute or relative insulin deficiency. Uncontrolled diabetes can lead to various long-term complications including cardiovascular disease (CVD), neuropathy, nephropathy and retinopathy which were estimated to be responsible for 11.3% of global deaths in 2019 (Forbes and Cooper, 2013; International Diabetes Federation, 2019). This underscores the urgency of finding more effective anti-diabetic drugs than those currently available.

Diabetes is classically divided into Type 1 and Type 2 Diabetes (T1D, T2D) which differ in the underlying cause of insulin insufficiency. While T1D manifests due to autoimmune destruction of the insulin-producing β-cells (absolute insulin deficiency), T2D is characterized by insulin resistance of peripheral organs (relative insulin deficiency). The conventional classification in T1D and T2D has however been refined by the identification of five distinct T2D subgroups which differ in disease progression and risk for diabetic complications (Ahlqvist et al., 2018; Zaharia et al., 2019). Therefore, diabetes should be regarded as a heterogeneous disease highlighting the need for personalized treatment strategies. Here, we focus on T2D, discussing risk factors, its pathogenesis and current therapeutic strategies.

1.2.1 The Link between Obesity and Insulin Resistance

Even though T2D is associated with various genetic predispositions (Ali, 2013), the modern lifestyle characterized by overnutrition and a lack of exercise together cause obesity, and are key drivers of the observed epidemic rise in T2D (Bluher, 2019; Colberg et al., 2010; Kahn et al., 2006b). Both factors, namely genetic predisposition and obesity act in concert to provoke systemic insulin resistance in muscle, liver, adipose tissue, kidney, gastrointestinal tract, vasculature, brain as well as pancreatic α- and β-cells (DeFronzo et al., 2015). Obesity, in particular the abdominal/visceral fat mass strongly correlates with insulin resistance (Carey et al., 1996). Comparing insulin responsiveness of visceral and peripheral fat, Zierath *et al.* observed a selective decreased antilipolytic effect in visceral fat (Zierath et al., 1998). This was explained by lower IRS-1 expression as well as reduced tyrosine phosphorylation of IR and IRS-1 and resulting diminished PI3K activity. Importantly, in contrast to peripheral adipocytes, visceral ones secrete FFA directly in the portal circulation which may explain their detrimental effect on liver metabolism. Ectopic lipid accumulation in peripheral organs such as liver and

muscle is linked to insulin resistance (Lara-Castro and Garvey, 2008). Increased fat depots contribute to the establishment of reduced insulin sensitivity via multiple mechanisms outlined in the following.

Lipotoxicity. When the storage capacity of adipose tissue is exceeded, harmful lipid species accumulate in non-adipose tissues. A rise in plasma FFA levels, for instance, results in an increase of intracellular DAG concentrations in liver and muscle (Erion and Shulman, 2010). In muscle, this glyceride in turn activates PKC-θ leading to enhanced phosphorylation of IRS-1 serine residues, an effect associated with reduced tyrosine phosphorylation and curtailed PI3K activity (Griffin et al., 1999; Yu et al., 2002). Likewise, DAG-mediated PKC-ε activation in liver interferes with IRS-2 tyrosine phosphorylation (Samuel et al., 2004; Samuel et al., 2007). Thereby, insulin receptor signalling is inhibited in these key insulin-responsive organs. Besides PKC and DAG, there are other key mediators of lipid-induced insulin resistance. For example, obesity and lipid infusion in mice, were shown to increase the activity of the double-stranded RNA-dependent protein kinase (PKR; Nakamura et al., 2010). The authors report PKR-mediated regulation of IRS-1 serine phosphorylation in a JUN N-terminal kinase (JNK)-dependent and -independent manner. This in turn promoted insulin resistance in primary mouse embryonic fibroblast (MEF) cells. In line with this, PKR knockout mice exhibited increased insulin signalling in liver and adipose tissue, however not in skeletal muscle (Nakamura et al., 2010). Moreover, saturated fatty acids were shown to alter the membrane distribution of the proto-oncogene tyrosine-protein kinase c-Src which leads to its activation and the induction of insulin resistance in mouse adipose tissue in a JNK-dependent manner (Holzer et al., 2011). Furthermore, increased exposure to long-chain saturated fatty acids, such as palmitate, is associated with insulin resistance in humans and was shown to not only promote DAG accumulation but also ceramide production in C2C12 myotubes (Chavez and Summers, 2003; Riccardi et al., 2004). In line with this, ceramide synthase enzyme 6 (CERS6) expression is upregulated in adipose tissue of obese humans, while CerS6-deficient mice are characterized by reduced C16:0 ceramides and are protected from high fat diet (HFD)-induced obesity and glucose intolerance (Turpin et al., 2014). Ceramide promotes insulin resistance by inhibiting AKT via two distinct mechanisms. First, ceramide blocks AKT translocation to the plasma membrane and promotes its dephosphorylation by induction of protein phosphatase 2A in 3T3-L1 adipocytes (Stratford et al., 2004). Furthermore, ceramide was shown to induce suppressor of cytokine signalling (*Socs)-3* mRNA expression in adipocytes both *in vitro* and *in vivo* (Yang et al., 2009). SOCS-3 is thought to promote insulin resistance by competing with IRS-1 for binding to Tyr960 moieties of the IR. Thereby, IRS-1 phosphorylation and its subsequent association with p85, the regulatory subunit of PI3K, is inhibited (Emanuelli et al., 2001).

Chronic Inflammation. Obesity is accompanied by an increase in infiltrating macrophages in adipose tissue (Weisberg et al., 2003). Myeloid cells, in turn, have been shown to play a pivotal role in inducing systemic insulin resistance via nuclear factor kappa-B (NF-κB)-mediated inflammatory pathways (Arkan et al., 2005). In line with this, fatty acids were shown to induce Toll-like receptor 4 (TLR4) signalling in adipocytes and macrophages leading to the induction of proinflammatory signalling pathways, such as NF-κB-driven production of tumor necrosis factor alpha (TNF-α) and interleukin 6 (IL-6) *in vitro* and *in vivo* (Shi et al., 2006). TLR4 deficient female mice, showed increased systemic insulin sensitivity accompanied by reduced activation of inflammatory gene expression in adipose and liver tissue (Shi et al., 2006). Other studies highlighted the pivotal role of JNK in fatty acid-induced insulin resistance. Saturated fatty acids were, for example, shown to activate JNK by signalling through TLR2 and TLR4 (Huang et al., 2012). JNK, in turn, was required for proinflammatory macrophage polarization and obesity-induced insulin resistance in mice (Han et al., 2013). Thus, fatty-acid induced insulin resistance is highly interconnected with innate immunity and inflammation. The macrophage-derived proinflammatory cytokines TNF-α and IL-6 orchestrate insulin resistance by promoting lipolysis as well as inhibiting downstream signalling of the IR (Nonogaki et al., 1995; Zhang et al., 2002). The latter was shown to be mediated by P38 mitogen-activated protein kinases (MAPK) and inhibitor of nuclear factor kappa-B kinase (IKK) driven inhibitory serine phosphorylation of both IR and IRS-1 (de Alvaro et al., 2004). TNF-α was shown to induce SOCS-3 mainly in white adipose tissue (WAT) of mice (Emanuelli et al., 2001). Similarly, another study suggested a paracrine effect of IL-6 on SOCS-3 expression in WAT of obese individuals (Rieusset et al., 2004).

Altered Adipocyte Secretome. While the secretion of insulin resistance-promoting adipokines is enhanced, insulin sensitizing ones are less expressed in obese patients (Arita et al., 1999; Yang et al., 2005). Adipose-derived retinol-binding protein 4 (RBP4) was, for example, shown to induce insulin resistance in muscle by impairing insulin receptor signalling and to promote hepatic gluconeogenesis by inducing phosphoenolpyruvate carboxykinase (PEPCK; Yang et al., 2005). Likewise, resistin (resistance to insulin) was identified as an adipokine upregulated in mouse models of diet- and genetically induced obesity and diabetes where it was shown to contribute to impaired glucose tolerance and insulin resistance (Steppan et al., 2001). Mechanistically, resistin was reported to reduce 5' adenosine monophosphate-activated protein kinase (AMPK) activation in skeletal muscle, adipose tissue and liver in rats, while inducing SOCS-3 in adipose tissue of mice (Satoh et al., 2004; Steppan et al., 2005). In humans, resistin expression is responsive to inflammatory stimuli and is detected in mononuclear cells rather than in adipocytes (Fain et al., 2003; Kunnari et al., 2009). Increased levels seem to be linked to obesity, while its role in insulin resistance and diabetes in humans is still a matter of debate (Lazar, 2007; Schwartz and Lazar, 2011). The adipokine leptin acts

as an adipostat as it is released in direct proportion to the size of the adipose tissue depot in mice and humans (Considine et al., 1996; Zhang et al., 1994). It increases energy expenditure and promotes satiety in mice (Campfield et al., 1995; Halaas et al., 1995; Pelleymounter et al., 1995). Genetic loss of leptin in humans leads to hyperphagia and severe obesity which was improved by the administration of recombinant leptin and its suppressive action on energy intake (Farooqi et al., 1999). Obese humans, however, display increased leptin levels and leptin resistance leading to disrupted leptin signalling in the central nervous system and to an intake of excess calories (Considine et al., 1996; Woods et al., 2000). In contrast, circulating adiponectin levels are reduced in obese mice and humans, where it negatively correlates with insulin resistance and is a predictive marker for T2D and decreased insulin sensitivity (Arita et al., 1999; Daimon et al., 2003; Hu et al., 1996; Lindsay et al., 2002; Yamamoto et al., 2004). Mitochondrial dysfunction in adipose tissue, a common feature of T2D, was suggested to be the cause of reduced adiponectin secretion (Wang et al., 2013). Adiponectin improves insulin sensitivity by signalling through AMPK, peroxisome proliferator-activated receptor alpha (PPAR-α) and p38 MAPK (Yamauchi et al., 2003; Yamauchi et al., 2001). Thereby, it enhances β-oxidation in liver and muscle, increases glucose uptake in muscle and decreases hepatic gluconeogenesis (Berg et al., 2001; Combs et al., 2001; Combs et al., 2004; Yamauchi et al., 2003; Yamauchi et al., 2002; Yamauchi et al., 2001).

Mitochondrial Dysfunction. The aforementioned mitochondrial dysfunction arises from oxidative stress-induced enhancement of uncoupling protein-2 (UCP-2) activity and increased levels of ROS (Rains and Jain, 2011). Both FFA and glucose are key drivers of the increased oxidative stress observed in diabetic patients. Defective mitochondria show an impaired fatty acid oxidation leading to an accumulation of DAG and, via the above mentioned pathway, to insulin resistance (Rains and Jain, 2011).

Endoplasmic Reticulum Stress. Obesity is also linked to insulin resistance by endoplasmic reticulum (ER) stress and the unfolded protein response (UPR). Obesity-related ER stress was shown to lead to defective insulin signalling by inositol-requiring enzyme 1 alpha (IRE-1α)–dependent activation of JNK and subsequent serine phosphorylation of IRS-1 (Boden et al., 2008; Ozcan et al., 2004).

1.2.2 Pancreatic β-Cell Failure: the Key Element in T2D Development

Most obese, insulin-resistant individuals do not develop hyperglycemia, as pancreatic β-cells hold an extensive capacity to compensate for the lack of insulin responsiveness by extending both β-cell mass and function (Butler et al., 2003; Chen et al., 2017a; Kahn et al., 1993; Polonsky et al., 1988).

Mezza *et al.* reported that chronic insulin resistance under euglycemia in humans was associated with an increase in β-cell mass by 50% due to transdifferentiation of both ductual cells and α-cells into β-cells (Mezza et al., 2014). Another study also reported insulin-glucagon double-positive cells in patients with impaired glucose tolerance (IGT) and newly diagnosed diabetes. However, their data suggested neogenesis of β-cells from pancreatic endocrine precursor cells as driving force behind the increased β-cell mass (Yoneda et al., 2013). Another link between α-cells and β-cell compensation is the induction of intra-islet GLP-1 production which was reported in insulin resistant states such as obesity and T2D. Intra-islet-derived GLP-1 was shown to play an important role in β-cell compensation by promoting β-cell survival, expansion as well as insulin expression and secretion (Kilimnik et al., 2010; Li et al., 2005; Linnemann et al., 2015). Mechanistically, GLP-1 transactivation of epidermal growth factor receptor (EGFR) followed by the PI3K-AKT-FOXO1 signalling cascade promotes β-cell proliferation and survival via pancreatic and duodenal homeobox 1 (PDX1; Buteau et al., 2003; Buteau et al., 2006). Interestingly, IL-6 was identified as inducer of GLP-1 expression by intestinal L and pancreatic α-cells in mice, linking chronic inflammation in diabetes to β-cell compensation (Ellingsgaard et al., 2011). A further potential mechanism behind the increasing β-cell mass observed in hyperinsulinemic, insulin-resistant patients includes insulin-driven inhibition of FOXO1 (Kitamura et al., 2002; Okamoto et al., 2006). Also, glucose has been implicated as positive regulator of β-cell mass. GK and IRS-2 were shown to be critical for β-cell hyperplasia in response to HFD-induced insulin resistance in mice (Terauchi et al., 2007). It was suggested that glucose oxidation leads to Ca^{2+}-dependent activation of cAMP response element-binding protein (CREB), which in turn induces the expression of IRS-2 and in the following β cell replication via FOXO1 nuclear exclusion (Terauchi et al., 2007; Weir and Bonner-Weir, 2007). The contribution of transdifferentiation, neogenesis and replication to the development of new β-cells warrants further investigation.

The reported increase in β-cell mass can however not explain the extent of hyperinsulinemia observed in obese nondiabetic patients (Kahn et al., 1993; Polonsky et al., 1988). This is rather relying on adapted β-cell function (Chen et al., 2017a). Compensatory hyperinsulinemia is mediated, amongst others, by enhanced glucose and lipid metabolism in β-cells. Islets of different rat models characterized by hyperinsulinemia revealed enhanced catalytic activity of GK and increased flux through PC and the malate-pyruvate and citrate-pyruvate shuttles (Chen et al., 1994a; Liu et al., 2002). The thereby accelerated glucose oxidation and

anaplerosis contribute to enhanced insulin secretion by the elevated production of MCF such as ATP and NADPH (Prentki et al., 2013). Furthermore, investigating insulin secretion and fatty acid metabolism in islets derived from insulin-resistant Zucker fatty fa/fa (ZF) rats, led to the conclusion that insulin resistance promotes lipolysis as well as increased flux through the GL/FFA cycle in β-cells (Nolan et al., 2006). This, in turn, leads to the accumulation of further lipid-based MCF which augment GSIS (Nolan et al., 2006; Prentki et al., 2013).

Hyperglycemia and T2D will only emerge if β-cells fail to meet the increased insulin demand (Kahn, 2001). At the time of T2D diagnoses, β-cell mass is already decreased by 50 to 80% (Chen et al., 2017a). This reduction is attributed to increased apoptosis rather than impaired proliferation (Butler et al., 2003). Furthermore, islets from T2D patients were reported to have an increased proportion of glucagon producing α-cells, to be smaller in size and to exhibit compromised GSIS (Deng et al., 2004). Overall, β-cell failure is driven by multiple components:

Age. β-cell function is reported to negatively correlate with aging in humans (Chang and Halter, 2003).

Genetic Susceptibility. Genetic predispositions can render β-cells susceptible to dysfunction. This includes for example single nucleotide polymorphisms (SNPs) in the transcription factor 7-like 2 (TCF7L2) gene which is associated with defects in both insulin secretion and the incretin effect (Grant et al., 2006; Lyssenko et al., 2007).

Glucolipotoxicity. Elevated glucose levels together with saturated FFA were shown to synergistically induce β-cell death both in the rat INS 832/13 cell line as well as in isolated primary human islets (El-Assaad et al., 2003). Mechanistically, glucolipotoxicity alters lipid partitioning (promotion of fatty acid esterification with a concomitant reduction of lipid oxidation/detoxification) and causes mitochondrial dysfunction, cholesterol and ceramide deposition as well as ROS production which all seem to be involved in the observed β-cell death (El-Assaad et al., 2010). Oxidative stress, for instance, enhances UCP-2 activity and by that diminishes ATP levels and GSIS (Lowell and Shulman, 2005). Glucolipotoxicity also induces ER stress-promoted β-cell cell death (Back and Kaufman, 2012).

Amyloid Deposits. IAPP deposits are commonly found in islets of T2D patients (Cooper et al., 1987). These deposits are associated with ER stress-mediated apoptosis and with β-cell dysfunction, caused by disrupting cell-to-cell contacts and, thereby, insulin secretion (Guardado-Mendoza et al., 2009; Huang et al., 2007; Ritzel et al., 2007).

Reduced Incretin Effect. In T2D, β-cells are hyposensitive to GLP-1 and GIP (Nauck et al., 2004; Vilsboll et al., 2002). Importantly, pharmacological levels of GLP-1, but not GIP, are still able to elicit insulinotropic effects (Nauck et al., 1993).

Functional Exhaustion. Persistent insulin resistance is thought to impose a high secretion burden on β-cells which leads to their functional exhaustion, dedifferentiation, and in the long run to apoptosis (Chen et al., 2017a).

1.2.3 The Establishment of Hyperglycemia and Dyslipidemia in T2D

The impact of both insulin resistance and insulin deficiency on peripheral organs leads to a rise in blood glucose and FFA levels. How different organs contribute to this phenomenon is summarized in the next section (see also Figure 3).

Muscle. In the muscle, insulin resistance leads to a reduction in glucose uptake and glycogen synthesis which decreases glucose clearance from the blood (Kelley et al., 1996; Shulman et al., 1990).

Adipose Tissue. Adipocytes which are resistant to the antilipolytic effect of insulin permanently secrete FFA (Fraze et al., 1985). The elevated exposure of the liver to FFA subsequently results in an increased hepatic triglyceride synthesis and very-low-density lipoprotein (VLDL) output by an insulin-independent, substrate push mechanism (Samuel and Shulman, 2016; Vatner et al., 2015).

Liver. The liver further increases blood glucose levels by an aberrant hepatic glucose output. Gluconeogenesis, not glycogenolysis, seems to be the driving force behind the elevated glucose production (Consoli et al., 1989; Magnusson et al., 1992; Wajngot et al., 2001). Besides insulin resistance and insulin deficiency, increased hepatic glucose secretion is mainly driven by hyperglucagonemia (Baron et al., 1987), although increased glucagon sensitivity and increased substrate delivery also play an important role (DeFronzo et al., 2015). The latter involves the delivery of glucose and glycerol due to muscle and adipocyte insulin resistance, respectively (Samuel and Shulman, 2016). Furthermore, increased FFA release from adipocytes promotes gluconeogenesis by the acetyl-CoA-mediated activation of PC (Adina-Zada et al., 2012).

α-cells. As insulin is vital for the regulation of glucagon secretion, insulin resistance at the level of α-cells was reported to be a possible explanation for the observed hyperglucagonemia in T2D patients (Ferrannini et al., 2007; Kawamori et al., 2009). An additional underlying mechanism could be hyperglycemia-induced β- to α-cell transdifferentiation (Brereton et al., 2014; Talchai et al., 2012).

Gastrointestinal tissue. GIP exerts glucagonotropic effects, while GLP-1 inhibits glucagon secretion (Chia et al., 2009; Meier et al., 2003; Nauck et al., 2002; Ramracheya et al., 2018).

Of relevance, the lack of GLP-1-mediated inhibition on glucagon secretion seems to contribute to hyperglucagonemia in T2D (Defronzo, 2009). Besides the liver, also the intestine is a gluconeogenic organ. In rats, intestinal gluconeogenesis (IGNG) was shown to mainly rely on glutamine as glucose precursor and to be insulin-sensitive (Croset et al., 2001). IGNG was shown to be an important contributor to endogenous glucose production (EGP) after prolonged fasting and in streptozotocin-diabetic states in rats (Mithieux et al., 2004).

Kidney. In healthy individuals the kidney contributes to glucose homeostasis by reabsorbing more than 99% of the renal glomeruli-filtered glucose. This was shown to be mediated by the sodium-glucose cotransporters SGLT1 and SGLT2 on the apical side of the early and late proximal tubule, respectively (Vallon et al., 2011). In mice and patients with T2D, SGLT2 expression is upregulated which increases renal glucose reabsorption and thereby the threshold of glucose excretion which sustains hyperglycemia (Umino et al., 2018; Wilding, 2014). Besides its role in glucose reabsorption, the kidney is known for its gluconeogenic capacity. In humans after an overnight fast, the kidney accounts for 20-25% of EGP, while the liver is responsible for 75-80% (Gerich, 2010). Similar to the liver, kidney gluconeogenesis is insulin-responsive and increased in the post-absorptive state in T2D patients compared to healthy individuals (Meyer et al., 1998).

In summary, insulin resistance and progressive β-cell failure are the core defects which eventually lead to uncontrolled hyperglycemia and frank diabetes. Hyperglycemia was shown to be strongly associated with microvascular and macrovascular complications of T2D, with the latter being the most common cause of diabetes-associated deaths (Stratton et al., 2000). Therefore, the main goal of anti-diabetic drugs is to reach glycemic control.

1.2.4 Therapies to Combat T2D

The above summarized key events of diabetes etiopathology offer a broad number of targets which could be exploited as therapy options. Their overall aim is to control glycemia, as improved glycemic control in newly diagnosed T2D patients significantly reduces the risk of at least microvascular complications (UK Prospective Diabetes Study (UKPDS) Group, 1998). A ten year post-interventional follow-up of the same patients showed that the risk reduction for diabetic complications persisted (Holman et al., 2008). Of note, other studies have ascribed no or solely a moderate benefit of glycemic control to the reduction of diabetic complications (Action to Control Cardiovascular Risk in Diabetes Study Group, 2008; ADVANCE Collaborative Group, 2008; Duckworth et al., 2009; NICE-SUGAR Study Investigators, 2009; Reaven et al., 2019; Rodríguez-Gutiérrez and Montori, 2016; Turnbull et al., 2009). While reducing blood glucose levels, it is of uttermost importance to avoid harmful hypoglycaemia

which is associated with an increased mortality risk (Gerstein et al., 2008). Independently of glycemic control, anti-diabetic drugs should also have anti-hyperlipidemic as well as anti-hypertensive properties. Main classes of anti-diabetic drugs and guidelines for the management of T2D-associated hyperglycemia are listed hereinafter (see also Figure 3).

Healthy Lifestyle. Combined dietary intervention and physical exercise with demonstrated blood glucose lowering effects are core elements of the therapeutic strategy for overweight and obese T2D patients (Davies et al., 2018). The positive impact of physical exercise on glucose disposal stems from insulin-independent GLUT-4 induction and translocation as well as improved mitochondrial function (Stanford and Goodyear, 2014). Besides the implementation of a healthy lifestyle, there are several oral and injectable glucose-lowering medication options for T2D patients.

Metformin. Because of the proven efficacy, safety, tolerability and low cost, metformin is the recommended first-line T2D drug (Davies et al., 2018). Its major effect is the suppression of hepatic glucose production which results in lower fasting plasma glucose and glycated hemoglobin (HbA1c) levels (Cusi et al., 1996). One possible mechanism of action was reported to be the inhibition of the mitochondrial glycerophosphate dehydrogenase in liver (Madiraju et al., 2014). Of note, metformin also decreases plasma VLDL triglyceride levels which was suggested to be driven by glucose uptake and metabolism in brown adipose tissue (Geerling et al., 2014). Metformin, which is orally taken, is associated with gastrointestinal side effects while it does not promote weight gain or hypoglycaemic events, a common side effect of other anti-diabetic drugs (Kahn et al., 2006a; U.K. Prospective Diabetes Study Group, 1995). As metformin does not prevent β-cell failure, hyperglycemia progressively re-emerges which makes the intake of additional medications necessary (Kahn et al., 2006a; Turner et al., 1999; U.K. Prospective Diabetes Study Group, 1995).

SGLT2 Inhibitors. Decreasing the higher renal reabsorption of glucose observed in T2D is the rationale behind using of SGLT2 inhibitors (SGLT2i). These oral medications reduce the maximum renal glucose reabsorptive capacity and lower the threshold at which glucose is excreted in the urine (DeFronzo et al., 2013). Even though, SGLT2i paradoxically induce EGP, the increased glucosuria lowers plasma glucose levels. The associated decrease in glucotoxicity was reported to exert beneficial effects on insulin sensitivity and β-cell function (Ferrannini et al., 2014; Merovci et al., 2014). Clinical trials revealed lower HbA1c levels, reduced blood pressure, weight loss as well as less cardiovascular and renal complications upon SGLT2i inhibitor treatment. However, adverse effects include genitourinary tract infections, diabetic ketoacidosis and bone fractures (Adeghate et al., 2019).

Dipeptidyl Peptidase 4 Inhibitors and GLP-1 Receptor Agonists. Another strategy to improve glycemic control in T2D patients is to exploit the beneficial effects of GLP-1, namely the increase of insulin secretion with a concomitant reduction of postprandial glucagon release, the reduction of gastric emptying and the suppression of appetite (Stonehouse et al., 2008). There are two drug classes which promote GLP-1 signalling via different mechanism, firstly dipeptidyl peptidase 4 inhibitors (DPP4i) which increase the stability of endogenous GLP-1 and secondly GLP-1 receptor agonists (GLP-1RA). GLP-1 exhibits a low half-life due to rapid degradation initialized by DPP4 (Deacon et al., 1995; Mentlein et al., 1993). Therefore orally given, competitive DPP4i extend the availability of endogenous GLP-1. The main consequence of DPP4i treatment is the reduction of gluconeogenesis. This is driven by increased insulin and concomitantly reduced glucagon secretion (Balas et al., 2007). GLP-1RA, which are administered via subcutaneous injection, suppress gluconeogenesis and slow down gastric emptying (Cervera et al., 2008). Comparing DPP4i and GLP-1RA, the latter is superior in promoting glycemic control and weight loss (Aroda et al., 2012; DeFronzo et al., 2008). This greater efficacy could be explained by a higher pharmacological plasma concentration of GLP-1 compared to the endogenously stabilised postprandial GLP-1 availability (DeFronzo et al., 2008). In contrast to other diabetic drugs, DPP4i and GLP-1RA exhibit fewer side effects, with mild to moderate gastrointestinal events being the most common (DeFronzo et al., 2008). Additionally, GLP-1RA administration revealed beneficial effects on cardiovascular outcomes (Marso et al., 2016a; Marso et al., 2016b).

Thiazolidinediones. Thiazolidinediones (TZD) are oral medications which improve insulin sensitivity by acting as peroxisome proliferator-activated receptor gamma (PPAR-γ) agonists (Ibrahimi et al., 1994). In adipocytes, they inhibit lipolysis resulting in decreased plasma FFA levels (Mayerson et al., 2002; Miyazaki et al., 2001). Thereby, they reduce the lipotoxic stress on peripheral organs which improves both insulin sensitivity and β-cell function. Furthermore, they reduce proinflammatory cytokine secretion such as TNF-α, while adiponectin output is increased (Hofmann et al., 1994; Maeda et al., 2001). Besides the relieving effect on plasma FFA levels and beneficial secretome changes, TZD induce lipogenic genes such as fatty acid synthase and acetyl-CoA carboxylase which explains the weight gain observed in TZD-treated patients (Kahn et al., 2006a; Way et al., 2001). However, this weight gain is associated with a favourable fat redistribution from abdominal to subcutaneous fat depots (Carey et al., 2002; Mayerson et al., 2002). Apart from indirect effects due to altered adipocyte metabolism, TZD also directly inhibit gluconeogenesis in liver of obese Zucker Diabetic Fatty (ZDF) rats by repressing gluconeogenic genes such as PEPCK and by promoting glucose metabolism via the induction of GK (Way et al., 2001). The same study showed that in muscle, TZD favour glucose utilization by pyruvate dehydrogenase kinase 4 (PDK4) downregulation further promoting glucose uptake (Way et al., 2001). The key success of TZD lies in the improvement

and preservation of β-cell function (Miyazaki et al., 2002). This together with improved insulin sensitivity explains why TZD show a prolonged glycemic control superior to the duration managed by other anti-diabetic drugs such as metformin or sulonylureas monotherapies when given as initial treatment to patients with recently diagnosed T2D (Kahn et al., 2006a). Besides weight gain, edema, congestive heart failure and bone fractures are safety concerns arising from TZD treatment (Davies et al., 2018; Kahn et al., 2006a).

Sulfonylureas. Sulfonylureas (SU) are orally taken insulin secretagogues which promote hyperinsulinaemia to overcome insulin resistance. Mechanistically, they bind to the sulfonylurea receptor 1 (SUR1) subunit of the K_{ATP}/SUR1 channel complex promoting its closure, membrane depolarisation and thereby insulin secretion (Inagaki et al., 1995). Lowering HbA1c levels come at the expense of weight gain, increased hypoglycaemic events and maybe even induction of β-cell apoptosis (Maedler et al., 2005; UKPDS U.K. Prospective Diabetes Study Group, 1995). Furthermore, treatment with SU is associated with an increase in cardiovascular events and death (Roumie et al., 2012; Simpson et al., 2006). Due to the listed side effects, SU are mostly recommended if other combinatorial treatment regimes have failed or if costs are a major issue (Davies et al., 2018). Proceeding β-cell dysfunction diminishes the initial benefits of SU on plasma glucose levels (UKPDS Kahn et al., 2006a; Turner et al., 1999; U.K. Prospective Diabetes Study Group, 1995).

Insulin. Insulin injection is recommended for patients with severe hyperglycemia, usually after other combinatorial treatment regimes have failed (Davies et al., 2018). Insulin in combination with metformin, SGLT2i, GLP-1RA, TZD and SU has been shown to improve glycemic control (Gough et al., 2014; Holman et al., 2007; Rosenstock et al., 2002; Wilding et al., 2012). Observed adverse side effects include weight gain and the risk of hypoglycaemia.

Regarding the sequence of anti-diabetic medication, following recommendations are given by the American Diabetes Association (ADA) and the European Association for the Study of Diabetes (EASD; Davies et al., 2018):
The first-line treatment of T2D is comprised of metformin and the initiation of a healthy lifestyle. If the clinical target is not met, the stepwise addition of other anti-diabetic drugs is preferred over an initial combination therapy. The choice of which glucose-lowering drug should be added is based on the patient characteristics and preference (patient-centered approach). Established comorbidities such as atherosclerotic CVD, heart failure or chronic kidney disease are indicators for SGLT2i and GLP-1RA which showed beneficial effects on cardiovascular outcomes (Adeghate et al., 2019; Marso et al., 2016a; Marso et al., 2016b). Apart from those comorbidities, the favoured medication depends on the parameter of major concern including hyperglycemia (DPP4i, GLP-1RA, SGLT2i, TZD), weight gain (GLP-1RA, SGLT2i) or costs (SU, TZD). Patients with severe hyperglycemia are advised to use insulin. In summary,

although many treatment options for T2D exist, the inability to maintain glycaemic control, due to progressive β-cell loss, and side effects such as hypoglycaemia and weight gain emphasize the need for new anti-diabetic drugs.

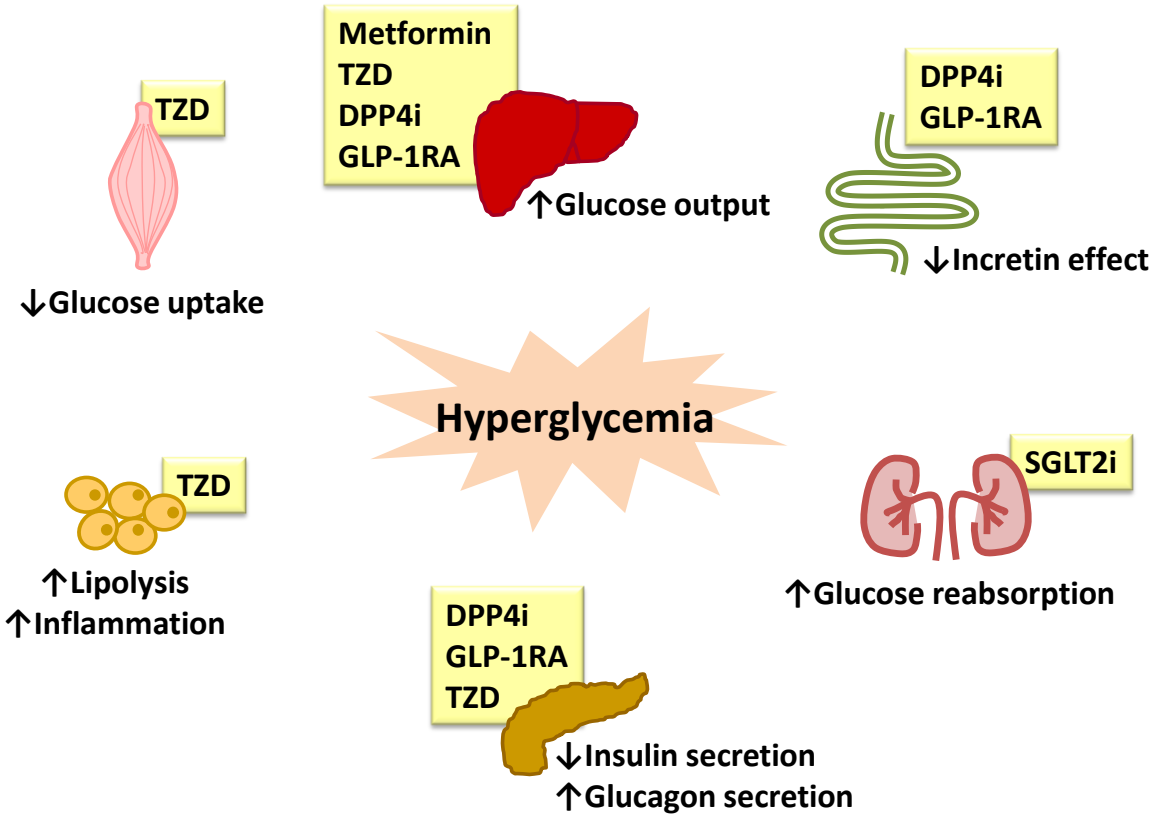

Figure 3 | Metabolic Dysfunctions Contributing to Hyperglycemia and T2D as well as Current Treatment Options

Hyperglycemia establishes due to various organ dysfunctions. Anti-diabetic drugs, which are depicted in yellow boxes, target different aspects of these aberrant processes. See text for details. DPP4i, dipeptidyl peptidase 4 inhibitors; GLP-1RA, glucagon-like peptide 1 receptor agonists; SGLT2i, sodium dependent glucose co-transporter inhibitors; TZD, thiazolidinediones. Figure is based on (DeFronzo et al., 2015).

A new concept for the treatment of T2D is the development of single-molecule peptides combining beneficial properties of different metabolically relevant hormones such as glucagon GLP-1 and GIP (Brandt et al., 2018). Glucagon and GLP-1 receptor co-agonists were, for example, shown to improve glucose tolerance and obesity as well as to restore leptin responsiveness in different mouse models of obesity (Clemmensen et al., 2014; Day et al., 2009; Pocai et al., 2009). Likewise, GIP and GLP-1 co-agonists were shown to improve hyperglycemia, induce weight loss and have insulinotropic effects in rodents, monkeys and humans (Finan et al., 2013). Moreover, a GLP-1-gastrin dual agonist (ZP3022) improved glycaemic control and increased β-cell mass in db/db mice (Fosgerau et al., 2013). By designing a triagonist for glucagon, GLP-1 and GIP receptors, obesity, hyperglycemia and hepatic steatosis was improved in various mouse models of obesity and diabetes to an extent superior to dual co-agonists and monoagonists (Finan et al., 2015).

Besides the described peptide multiagonists, peptide/nuclear hormone combinations are another promising treatment strategy for T2D (Brandt et al., 2018). In this setting, the uptake of nuclear receptor ligands, such as estrogen, dexamethasone and the thyroid hormone T3 is restricted to target cells expressing the receptor of the conjugated peptide hormone (Brandt et al., 2018). A (GLP-1)-estrogen conjugate as well as a glucagon-T3 conjugate were shown to improve obesity, dyslipidemia and hyperglycemia in DIO (diet-induced obese) mice (Finan et al., 2016; Finan et al., 2012). Intriguingly, a GLP-1/dexamethasone conjugate was shown to not only improve obesity and hyperglycemia but also to counteract hypothalamic and systemic inflammation in obese mice (Quarta et al., 2017). As various multiagonists have already entered clinical trials, there might be soon new pharmacological options for T2D patients available, which are not only effective in lowering hyperglycemia but also in reducing weight, while exhibiting a convincing safety profile (Brandt et al., 2018).

1.3 Hepatokines: Emerging Key Players in Metabolic Control

As exemplified in the previous section, harnessing hormonal circuits between metabolic tissues is a promising avenue for novel T2D treatments. It is becoming increasingly clear that also tissues other than the specialized endocrine organs regulate energy metabolism by the secretion of organokines which can act in auto-, para- as well as endocrine manner (Castillo-Armengol et al., 2019; Chung and Choi, 2020). The hepatocyte secretome, for example, was shown to consist of 538 proteins, so called hepatokines, of which 168 were classically secreted via an N-terminal signal peptide (Meex et al., 2015). Steatotic hepatocytes revealed that 19% of the hepatic secretome was influenced by HFD. The authors reported that the altered secretome induced insulin resistance in skeletal muscle and proinflammatory responses in macrophages. This together with an increasing body of evidence suggests that liver-derived

proteins do not only regulate peripheral metabolism in health, but can also actively contribute to metabolic dysfunction (Meex and Watt, 2017). In the following, two major hepatokines with opposing effects will be exemplified: fetuin-A which causes insulin resistance and fibroblast growth factor 21 (FGF21) which, in contrast, acts as insulin sensitizer.

The first hepatokine to be described fetuin-A is mainly expressed by the liver and is a natural inhibitor of the IR tyrosine kinase (Mathews et al., 2000; Srinivas et al., 1993). Fetuin-A knockout (KO) mice show improved glucose tolerance, increased insulin sensitivity and are resistant to HFD-induced weight gain (Mathews et al., 2002). Increased fetuin-A levels are linked to non-alcoholic fatty liver disease (NAFLD) and the metabolic syndrome (Haukeland et al., 2012; Ix et al., 2006; Stefan et al., 2006). Furthermore, high circulating fetuin-A levels are associated with insulin resistance and are a predictive marker for T2D (Ix et al., 2008; Mori et al., 2006; Stefan et al., 2008; Stefan and Haring, 2013; Stefan et al., 2006). Mechanistically, fetuin-A promotes lipid-induced insulin resistance by forming a ternary complex with FFA and TLR4 which in turn induces proinflammatory cytokine release by macrophages and adipocytes (Mukhopadhyay and Bhattacharya, 2016; Pal et al., 2012). In light of these results, fetuin-A was postulated to be `the missing link in lipid-induced inflammation´ (Heinrichsdorff and Olefsky, 2012). In humans, circulating FFA together with fetuin A act in concert to predict insulin resistance (Stefan and Haring, 2013), which makes the fetuin A-TLR4 interaction a promising target for new anti-diabetic therapy.

With its multiple positive metabolic actions, FGF21 is another potential anti-diabetic drug candidate. Administration of FGF21 to *ob/ob* and *db/db* resulted in reduced systemic glucose and triglyceride levels and FGF21-transgenic mice were shown to be resistant to HFD-induced weight gain due to increased energy expenditure (Kharitonenkov et al., 2005; Xu et al., 2009). Furthermore, FGF21 ameliorates hepatic steatosis and insulin sensitivity, induces browning in white adipose tissue and enhances β-cell function and survival (Fisher et al., 2012; Wente et al., 2006; Xu et al., 2009). Paradoxically, FGF21 levels are increased in patients with obesity, NAFLD, T2D and are a predictive marker for insulin resistance, hepatic steatosis and the metabolic syndrome (Chavez et al., 2009; Dushay et al., 2010; Mraz et al., 2009; Mutanen et al., 2014; Zhang et al., 2008b). This contradiction could be explained by a compensatory upregulation of FGF21 due to metabolic stress or by the presence of a FGF21 resistant state (Meex and Watt, 2017). In the first clinical proof of concept, a biopharmaceutically optimized FGF21 analogue called LY2405319 was able to improve dyslipidemia, however not fasting glucose levels, in patients with obesity and T2D (Gaich et al., 2013). Recently, the PEGylated FGF21 analogue Pegbelfermin (BMS-986036) was reported by a phase 2a study to significantly lower hepatic lipid content in patients with non-alcoholic steatohepatitis (NASH; Charles et al., 2019). These data show that FGF21 indeed holds great potential as a diabetes,

obesity and NASH drug. Moreover, it is currently investigated further by ongoing clinical trials (https://clinicaltrials.gov/).

Hepatokines are not only promising therapeutics but also promising biomarker candidates. As exemplified above, individual hepatokines correlate with specific metabolic dysfunctions such as insulin resistance, T2D and NASH. Generating a profile of favourable and pathological hepatokines could help to detect metabolic diseases, stage their progression and allow for personalized medicine (Figure 4; Iroz et al., 2015).

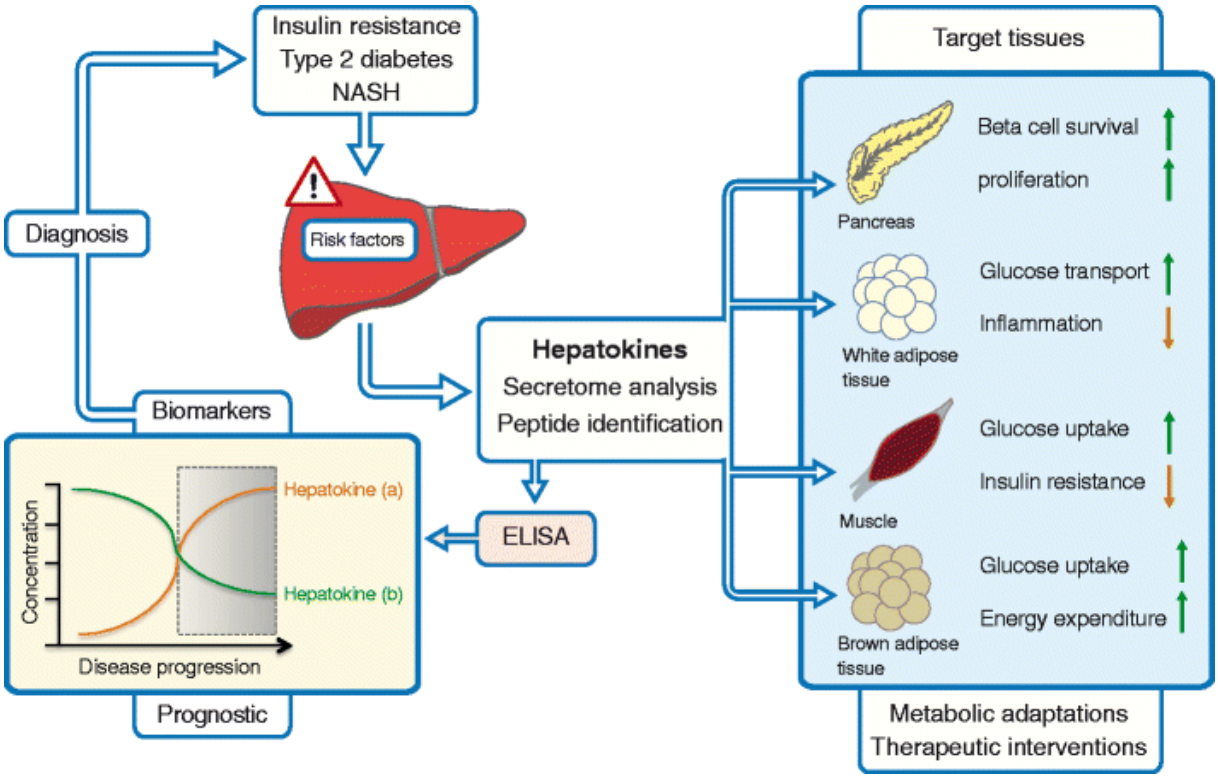

Figure 4 | Utilizing Hepatokines in Diagnosis and Therapy

The liver is participating in systemic metabolism by releasing hepatokines. This secretion pattern is altered by pathological changes including insulin resistance, T2D and NASH. The identification of beneficial and detrimental hepatokines could establish a personalized profile of secreted hepatokines enabling disease diagnosis and judgment of progression. At the same time this hepatokine profile could indicate the appropriate therapeutic approach to improve the disease phenotype. Figure was adapted from (Iroz et al., 2015).

1.4 The Lipocalin Protein Family

Lipocalins, which are small secreted proteins, hold great potential to function as biomarkers for various diseases including inflammatory diseases, cancer and importantly also for diabetes (Abella et al., 2015; Charkoftaki et al., 2019; Xu and Venge, 2000). Lipocalin family members share a highly conserved tertiary structure, despite low sequence similarities (Flower, 1996; Schiefner and Skerra, 2015). The core of this common folding motif is comprised of a β-barrel with a hydrophobic pocket acting as an internal ligand binding site. The β-barrel consists of eight antiparallel β-strands which are connected via seven loops. While the N-terminus closes one side of the barrel, the other site is in an open conformation, flanked by four of these loops which are highly variable in amino acid sequence, length and conformation (Schiefner and Skerra, 2015; Schlehuber and Skerra, 2005). The amino acid composition and the overall structure of both the β-barrel cavity and the loops at the cavity entrance determine ligand specificity. Ligands encompass chemically sensitive and poorly soluble odorants (e.g. pheromones), retinoids, steroids and lipids (Flower, 1996; Schlehuber and Skerra, 2005). Lipocalins were classically ranked among transport proteins. One of the best characterized lipocalin, RBP4, for example, stabilizes and transports the oxidation-prone retinol from liver to peripheral tissues (Flower, 1996). While retinol binding by RBP4 is highly specific, other lipocalins show a rather promiscuous ligand-binding capacity (Redl, 2000). Lipocalins are thought to elicit their physiological function by binding to plasma membrane receptors on target cells (Flower, 2000). Binding of RBP to the cell surface receptor stimulated by retinoic acid 6 (STRA6), for example, facilitates retinol uptake by its direct diffusion into the cell membrane (Chen et al., 2016). Another characteristic of lipocalins is their ability to form non-covalent or covalent complexes with macromolecules. For instance, most of plasma RBP4 is non-covalently associated with transthyretin. This extends its half-life by preventing its kidney-mediated filtration (Flower, 1996).

1.4.1 Lipocalin 13

Besides being transport proteins, several lipocalin family members have been reported to play an active role in energy metabolism (Table 1). One of these is lipocalin 13 (LCN13), also known as odorant-binding protein 2a (OBP2A). In humans, it was detected in the mucus covering the olfactory cleft where it is believed to contribute to odour detection by transporting specific odorants (Briand et al., 2002). Furthermore, LCN13 was suggested to play a role in male fertility as it is part of an epididymal lipocalin gene cluster in mice (Suzuki et al., 2004). LCN13 seems to be also expressed in liver, muscle and pancreas from where it is secreted into the blood stream of mice (Cho et al., 2011). The first connection to energy metabolism was drawn by Rui *et al.* who noted reduced LCN13 expression in mice upon fasting as well as

in mice with either genetic (db/db) or HFD-induced diabetes (Cho et al., 2011). In agreement, our group found decreased hepatic *Lcn13* mRNA levels in patients with T2D where it negatively correlated with fasting glucose levels (Ekim Ustunel et al., 2016). Transgenic overexpression of LCN13 in wild type mice was shown to protect against diet-induced hyperglycemia, glucose intolerance and insulin resistance (Cho et al., 2011). In line with this, αLCN13 administration worsened glucose tolerance in wild type mice (Sheng et al., 2011). Restoring LCN13 levels in db/db, ob/ob and HFD mice, which exhibit reduced LCN13 levels, by adenovirus-mediated overexpression or administration of exogenous recombinant LCN13 improved glucose clearance and insulin sensitivity (Cho et al., 2011; Sheng et al., 2011). Mechanistically, the authors demonstrated that LCN13 increased insulin signalling, glucose uptake and suppressed hepatic glucose production (Cho et al., 2011). Besides glucose handling, LCN13 also affected lipid metabolism by inhibiting lipogenic genes, while inducing β-oxidation (Sheng et al., 2011). In agreement, LCN13 transgenic mice were protected against HFD-induced liver steatosis and adenoviral-mediated LCN13 overexpression in ob/ob mice resulted in an improved liver phenotype (Sheng et al., 2011). We could show that transforming growth factor beta-like stimulated clone (TSC) 22 D4, which positively correlated with tumour-induced body wasting and which reduced lipogenesis and hepatic VLDL output, is a direct transcriptional repressor of the *Lcn13* gene (Ekim Ustunel et al., 2016; Jones et al., 2013). Beneficial effects of TSC22D4 knockdown in db/db mice on glucose tolerance were partly mediated by LCN13, as double knockdown of TSC22D4 and LCN13 could reverse the favourable phenotype elicited by knocking down solely TSC22D4.

Table 1 | Summary of Lipocalin Family Members with Reported Functions in Metabolic Control

Lipocalin	Metabolic Function	Tissue/Serum Level	References
LCN2	• Insulin sensitivity ↑/↓/↔ • Insulin secretion ↑/↓ • Glucose tolerance ↑/↓/↔ • Glucose uptake ↓ • Liver steatosis ↓ • Dyslipidemia ↓ • β-oxidation ↑ • BW/fat mass ↑/↓/↔ • Energy expenditure (NW)↑/(OB)↔ • Food intake ↑/↓ • Thermogenesis ↑/↓ • Mitochondrial function ↑ • Autophagy ↓ • Inflammation ↑/↓/↔	• Obesity ↑/↔ • T2D ↑/↓ • Fasting ↑ • Glucose/lipid ingestion ↑	• (Akelma et al., 2012) • (Capulli et al., 2018) • (Chan et al., 2016) • (De la Chesnaye et al., 2015) • (Guo et al., 2010) • (Ishii et al., 2017) • (Jun et al., 2011) • (Law et al., 2010) • (Lim et al., 2015) • (Mosialou et al., 2017) • (Paton et al., 2013) • (Schmid et al., 2016) • (Yan et al., 2007) • (Wang et al., 2007) • (Zhang et al., 2008a) • (Zhang et al., 2014)
LCN5	• Insulin sensitivity ↑ • Glucose tolerance ↑ • Mitochondrial biogenesis and function ↑	• Negatively correlated with BW and fat mass	• (Seldin et al., 2018)
LCN13/ OBP2A	• Insulin sensitivity ↑ • Glucose tolerance ↑ • Glucose uptake ↑ • Gluconeogenesis ↓ • Hepatic steatosis ↓ • Lipogenesis ↓ • β-oxidation ↑	• Obesity ↓/↔ • T2D ↓ • Fasting ↓	• (Cho et al., 2011) • (Ekim Ustunel et al., 2016) • (Sheng et al., 2011)
LCN14/ OBP2B	• Insulin sensitivity ↑ • Glucose tolerance ↑ • Gluconeogenesis ↓ • Hepatic steatosis ↔ • Adipose glycerol efflux ↓ • Locomotor activity ↑	• Obesity ↓ • T2D ↓ • Fasting ↓ • Refeeding ↑	• (Lee et al., 2016)

Lipocalin	Metabolic Function	Tissue/Serum Level	References
APOD	• Insulin sensitivity ↓ • Glucose tolerance ↓ • Hepatic steatosis↑/↔ • Dyslipidemia↓ • Cross-talk with Ob-Rb • Polymorphism associated with changed serum lipid parameters, T2D, obesity and hyperinsulinemia	• Obesity ↑ • T2D ↑/↓ • Atherosclerosis ↑	• (Baker et al., 1994) • (Brahimaj et al., 2017) • (Desai et al., 2002) • (Do Carmo et al., 2009) • (Liu et al., 2001) • (Perdomo and Henry Dong, 2009) • (Perdomo et al., 2010) • (Sreekumar et al., 2002) • (Vijayaraghavan et al., 1994)
APOM	• Insulin sensitivity ↑/↔ • Insulin secretion via bound S1P ↑ • β-cell survival via S1P analogue FTY720 ↑ • Glucose tolerance ↑/↓ • Triglyceride clearance ↓ • Fat mass ↑ • BAT activity ↓ • Mitochondrial function ↑ • Protects against atherosclerosis • SNP associated with metabolic traits of T2D	• Obesity ↑/↓ • T2D ↓ • Metabolic syndrome ↓ • Caloric restriction ↑	• (Christoffersen et al., 2011) • (Christoffersen et al., 2018) • (Dullaart et al., 2009) • (Kurano et al., 2014) • (Kurano et al., 2020) • (Moon et al., 2013) • (Sramkova et al., 2019) • (Wolfrum et al., 2005) • (Zhou et al., 2011)
MUP1	• Insulin sensitivity (liver)↔ • Insulin sensitivity (muscle) ↑ • Glucose tolerance ↑ • Gluconeogenesis ↓ • Lipogenesis ↓ • Mitochondrial biogenesis and function ↑ • Energy expenditure ↑ • Locomotor activity ↑	• Obesity ↓ • T2D ↓ • Caloric restriction ↓ • Fasting ↓ • Refeeding ↑ • Exercise↑	• (De Giorgio et al., 2009) • (Hui et al., 2009) • (Kleinert et al., 2018) • (van Schothorst et al., 2006) • (Zhou et al., 2009)

Lipocalin	Metabolic Function	Tissue/Serum Level	References
PTGDS	• Insulin sensitivity ↑/↔ • Glucose tolerance ↑/↓/↔ • Liver steatosis ↓ • Adipogenesis ↑ • Protects against obesity • Protects against atherosclerosis • Mediates positive VSG effects • SNP associated with atherosclerosis	• Obesity ↑ • T2D ↔ • Metabolic Syndrome ↓ • RYGB ↑	• (Cheung et al., 2013) • (Cipollone et al., 2004) • (Fujimori et al., 2007) • (Hamano et al., 2002) • (Kumar et al., 2015) • (Kumar et al., 2016) • (Kumar et al., 2018) • (Kumar et al., 2020) • (Miwa et al., 2004) • (Ragolia et al., 2005) • (Ragolia et al., 2008) • (Tanaka et al., 2009) • (Urbanet et al., 2015) • (Virtue et al., 2012)
RBP4	• Insulin sensitivity ↓ • Glucose tolerance ↓ • Gluconeogenesis ↑ • SNPs associated with metabolic complications	• Obesity ↑ • T2D ↑ • NAFLD ↑/↔ • Exercise ↓	• (Alkhouri et al., 2009) • (Cengiz et al., 2010) • (Chen et al., 2017b) • (Codoner-Franch et al., 2016) • (Graham et al., 2006) • (Milner et al., 2009) • (Terra et al., 2013) • (Wu et al., 2008) • (Yang et al., 2005)

APOD, apolipoprotein D; APOM, apolipoprotein M; BW, body weigth; LCN2, lipocalin 2; LCN5, lipocalin 5; LCN13/OBP2A, lipocalin 13/odorant binding protein 2a; LCN14/Obp2b, lipocalin 14/odorant binding protein 2b; MUP1, major urinary protein 1; NAFLD, non alcoholic fatty liver disease; NW, normal weight; OB, obese; Ob-Rb, long form of the leptin receptor; PTGDS, prostaglandin D2 synthase; RBP4, retinol-binding protein 4; RYGB, Roux-en-Y gastric bypass; S1P, sphingosine 1-phosphate; VSG, vertical sleeve gastrectomy; ↑, upregulated; ↓, downregulated; ↔, unchanged.

1.5 Aim of this Study

Over the past decades, T2D has become a major global socioeconomic burden. Current treatment regimes are often unable to maintain glycemic control and come at the expense of unwanted, sometimes severe side effects. It is becoming increasingly clear that metabolic health is sustained by extensive inter-tissue communication via circulating organokines. In this regard, we have previously shown that the hepatokine LCN13/OBP2A plays a crucial role in glycemic control and that its hepatic mRNA levels negatively correlate with T2D in humans (Ekim Ustunel et al., 2016). Understanding the precise role of LCN13 in the pathophysiology of diabetes could therefore help to develop new diagnostic and pharmacological solutions for T2D patients.

Here, we aimed to further address the importance of LCN13 in health and disease. For this purpose, we performed LNP-mediated, liver-specific knockdown of LCN13 and raised endogenous LCN13 levels by either AAV-mediated hepatic LCN13 overexpression or by administration of recombinant mammalian LCN13 protein in mice. To decipher its role in metabolic dysfunction, we tested the curative and preventive potential of LCN13 in HFD-fed and db/db mice. We furthermore studied the impact of altered LCN13 levels on the expression of other lipocalin family members. Interestingly, a potential receptor for odorant-binding proteins (OBP) and/or their cargo was found to be expressed by the β-cell line MIN6 (Blache et al., 1998). Moreover, other lipocalin family members, such as APOM, were shown to promote both insulin secretion and β-cell survival (Kurano et al., 2014; Moon et al., 2013). This together with the fact that β-cell failure is the key driver in the establishment of hyperglycemia and diabetes prompted us to also study the effects of LCN13 on β-cell function.

2. Materials and Methods

2.1 Materials

2.1.1 Devices

Table 2 | Devices

Device	Name	Company
-20° freezer	Mediline Lgex 3410	Liebherr
-86°C freezer	HFU400TV	Thermo Fisher Scientific
Bacterial shaking incubator	IS1	Axon
Benchtop centrifuge	AllegraX-15R	Beckman Coulter
Benchtop centrifuge	Microfuge 20	Beckman Coulter
Benchtop centrifuge	Centrifuges 5427R	Eppendorf
Cell counter	Countess II Automated Cell Counter	Thermo Fisher Scientific
Cell culture hood	HeraSafe KS	Thermo Fisher Scientific
Cell culture incubator	Heracell™ 240i CO_2 Incubator	Thermo Fisher Scientific
Column chromatography system	ÄKTA pure 25	GE Healthcare
Dissecting microscope	SMZ745 / SMZ745T	Nikon
Electrophoresis chambers	Mini-Gel-Tank	Invitrogen
Electrophoresis chambers	Agarose gel tanks	EMBL (Heidelberg)
Fridge	Mediline LKUv 1610	Liebherr
Fume hood	Scala 1500	Waldner
Gel imaging system	ChemiDoc XR+	Bio-Rad
Glucometer	Accu-Chek Performa Glucometer	Roche
Glucometer	StatStrip Xpress Glucose Meter	Nova Biomedical
Heater and magnetic stirrer	RSM-10HS	PHOENIX Instrument
Heating block	ThermoMixer® C	Eppendorf
Ice machine	AC	Scotsman
Incubator shaker	New Brunswick™ S41i CO2	Eppendorf
Inverted microscope	ECLIPSE Ts2	Nikon
Microbiological incubator	Heratherm™ Compact	Thermo Fisher Scientific
Microplate reader	Varioskan Lux	Thermo Fisher Scientific
Microwave	R-93ST-A	Sharp
Multichannel pipette	Eppendorf Research® plus	Eppendorf
Multichannel pipette with adjustable tip spacing	8 Channel VOYAGER, 12.5 µL	Integra

Multipipette	Multipette® E3/E3x	Eppendorf
PCR machine	Mastercycler® Nexus Thermal Cyclers	Eppendorf
pH meter	pH 3210	WTW
Pipette Boy	Eppendorf® Easypet® 3 electronic pipettor	Eppendorf
Pipettes	Eppendorf Research® plus	Eppendorf
Power supply	PowerPac™ HC Power Supply	Bio-Rad
Real-Time PCR System	QuantStudio 6	Thermo Fisher Scientific
Scale	AX124M	Ohaus
Scale	AX5202M	Ohaus
Serum analyzer	AU480 Chemistry Analyzer	Beckman Coulter
Shaker	Tilt Shaker WS 10	Edmund Bühler
Shaker	Universal Shaker SM 30 A	Edmund Bühler
Shaker for ELISA plates	Microplate Shaker	VWR international
Shaker for incubator	Orbi-Shaker™ CO2	Benchmark Scientific
Sonicator	SONOPULS HD 2070.2	BANDELIN electronic
Spectrophotometer	NanoDrop2000c	Thermo Fisher Scientific
Superspeed centrifuge	Sorvall LYNX 6000	Thermo Fisher Scientific
Tissue homogeniser	Mixer Mill MM 400	Retsch
Tube roller	RS-TR 5/10	PHOENIX Instrument
Vacuum concentrator	Concentrator plus	Eppendorf
Vortexer	Vortex7-2020	Neolab
Water purification system	Advantage A10	Milli-Q
Waterbath	Aqualine AL 12	LAUDA
Western blot imaging system	ChemiDoc MP	Bio-Rad
Western blot transfer system	Trans-Blot® Turbo™ Transfer System	Bio-Rad

2.1.2 Consumables

Table 3 | Consumables

Name	Company
1.1ml Z-Gel	SARSTEDT
25/75/150cm^2 flasks	Cellstar
500 µm cell strainer	PluriSelect
Corning® 500 mL Bottle Top Vacuum Filter, 0.45 µm Pore	Sigma-Aldrich
Corning® Costar® Ultra-Low Attachment 6 Well Plates	Sigma-Aldrich
Micro tube	
Falcon tubes (15ml, 50ml)	SARSTEDT
Gel loading pipette tips	Alpha Laboratories
Glassware	Schott
HisTrap™ HP 5ml chromatography columns	GE Healthcare
Microvetten CB 300 µL K2 EDTA	SARSTEDT
Minisart® Syringe Filter, PES, 0.22 µm	SARTORIUS
Nitrile gloves	Kimtech
Nitrocellulose membrane (0.2 µm)	Bio-Rad
NORM-JECT® Syringes	Henke Sass Wolf
Novex Tris-Glycine Mini Gels	Invitrogen
PCR tubes	SARSTEDT
Petri dishes	Falcon
Pipette filter tips	STARLAB
qPCR plates (384 wells)	Life Technologies
Scalpels	Lance Paragon Ltd
Spectra/por 1 Dialysis Membranes, MWCO 6000 to 8000	Spectrum Laboratories
Sterile Pasteur pipettes	VWR international
U100 insulin syringes	BD Micro-fine+
Wypall®X60 Wischtücher	VWR international

2.1.3 Chemicals and Reagents

Table 4 | Chemicals and Reagents

Name	Company
Agarose	Bio-Rad
Alanyl-glutamin	Sigma-Aldrich
Albumin Bovine Fraction V, Protease-Free	Serva
Ampicillin	Sigma-Aldrich
Bovine Serum Albumin, heat shock fraction, suitable for RIA, pH 5.2, ≥96%	Sigma-Aldrich
BrdU (5-Bromo-2′-deoxyuridine)	Sigma-Aldrich
Bromophenol blue	Sigma-Aldrich
Calcium chloride ($CaCl_2$)	Carl Roth
Chloroform	Carl Roth
Coomassie brilliant blue R 250	Sigma-Aldrich
D-(+)-Glucose solution (100 g/L)	Sigma-Aldrich
D-Glucose	AppliChem
Dithiothreitol (DTT)	Sigma Aldrich
DNA Gel Loading Dye (6x)	Thermo Fisher Scientific
Ethanol (EtOH)	Carl Roth
Exendin-4 (Ex-4)	Sigma Aldrich
Glycerol	Sigma Aldrich
Glycine	Sigma-Aldrich
Halt Protease and Phosphatase Inhibitor Cocktail, EDTA-free (100X)	Thermo Fisher Scientific
Halt™ Protease Phosphatase Inhibitor-Cocktail	Thermo Fisher Scientific
HEPES	Sigma-Aldrich
Histopaque®-1077 sterile-filtered, density: 1.077 g/mL	Sigma-Aldrich
Histopaque®-1119 sterile-filtered, density: 1.119 g/mL	Sigma-Aldrich
Huminsulin® Normal (100 IE/mL)	Lilly
Hydrochloric acid (HCl)	Sigma-Aldrich
Imidazole	AppliChem
Isopropanol	Sigma-Aldrich
Kanamycin	AppliChem
LB Agar (Luria/Miller)	Carl Roth
LB broth	Sigma-Aldrich
Lipofectamine 3000 Reagent	Thermo Fisher Scientific
Lipofectamine™ 3000 Transfection Reagent	Thermo Fisher Scientific
Magnesium sulphate ($MgSO_4$)	Sigma-Aldrich
Methanol (MeOH)	Honeywell Riedel-de Haën

Monopotassium chloride (KH_2PO_4)	Carl Roth
Oligonucleotides	Sigma-Aldrich
Ponceau S solution	Sigma-Aldrich
Potassium chloride (KCl)	Sigma-Aldrich
Puromycin dihydrochloride from Streptomyces alboniger	Sigma-Aldrich
Recombinant Mouse Lipocalin-13 Protein	R&D Systems
S.O.C. Medium	Invitrogen
SDS	Carl Roth
Skim milk powder	Sigma-Aldrich
Sodium bicarbonate ($NaHCO_3$)	Carl Roth
Sodium chloride (NaCl)	Carl Roth
Sodium phosphate ($NaHPO_4$)	Carl Roth
SuperSignal™ West Femto Substrate	Thermo Fisher Scientific
SYBR™ Safe™ DNA gel stain	Invitrogen
Taqman gene expression master mix	Applied Biosystems
Tris	Carl Roth
Triton-X	Carl Roth
TRIzol™ Reagenz	Invitrogen
Trypan Blue solution	Sigma-Aldrich
Trypsin-EDTA (0.05%), phenol red	Thermo Fisher Scientific
TurboTransfer Buffer	Bio-Rad
Tween 20	Sigma-Aldrich

2.1.4 Solutions and Buffers

Table 5 | Solutions and Buffers

Name	Company
Acidic ethanol	70% (v:v) EtOH, 0.18 M HCl
Blocking buffer	1x TBS-T with 5% (w/v) skim milk
Collagenase solution (per mouse)	6 mg collagenase P in 6 mL HBSS medium, 1% (w:v) BSA
Coomassi destaining solution	50% (v:v) H_2O, 40% (v:v) EtOH, 10% (v:v) acetic acid
Coomassi staining solution	0.25% (w:v) Coomassie Blue R-250
Elution Buffer	0.2 M NaCl, 0.02 M $NaHPO_4$, 400 mM imidazole, pH 7.2
Histopaque-1100	45.5% (v:v) Histopaque-1077 and 54.5% (v:v) Histopaque-1119
Krebs-Ringer buffer	2.54 mM $CaCl_2$, 10 mM HEPES, 4.74 mM KCl, 1.19 mM KH_2PO_4, 118.5 mM NaCl, , 25 mM $NaHCO_3$, 1.19 mM $MgSO_4$

LB Agar	40 g LB Agar (Luria/Miller) in 1 L distilled water
LB Medium	20 g LB broth in 1 L distilled water
SDS loading buffer (5x)	250 mM Tris/HCl (pH 6.8), 0.5 M DTT, 10% (w/v) SDS, 50% (v:v) glycerol, 0.01% (w/v) bromophenol blue
SDS running buffer (10x)	0.25 M Tris, 1.92 M Glycine, 1% (w/v) SDS
TAE (10x)	0.4 M Tris/HCl (pH 7.7), 10 mM EDTA, 0.2 M acetic acid
TBS (10x)	0.2 M Tris, 1.5 M NaCl (pH 7.8)
TBS-T (1x)	1x TBS with 0.1% (v:v) Tween 20
WB1	0.2 M NaCl, 0.02 M $NaHPO_4$, 5 mM imidazole (pH 7.2)
WB2	0.2 M NaCl, 0.02 M $NaHPO_4$, 20 mM imidazole (pH 7.2)

2.1.5 Commercial Kits

Table 6 | Commercial Kits

Kit	Company
Insulin ELISA	ALPCO
LabAssay™ Phospholipid	WAKO Chemicals GmbH
MinElute PCR Purification Kit	QIAGEN
NEFA-HR(2) assay kit	WAKO Chemicals GmbH
Pierce™ BCA™ Protein-Assay	Thermo Fisher Scientific
QIAGEN Plasmid Mega Kit	QIAGEN
QIAprep Spin Miniprep Kit	QIAGEN
QIAquick Gel Extraction Kit	QIAGEN
Quantitect Reverse Transcription Kit	Qiagen
Serum Analyzer kits	Beckman Coulter
Serum Triglyceride Determination Kit	Sigma-Aldrich
Total cholesterol assay kit	Randox Laboratories

2.1.6 Antibodies

Table 7 | Antibodies

Antibody	Host Species	Dilution	Company/Catalog No.
LCN13	Sheep	1:400	R&D Systems/AF7974
anti-human IgG H&L	Rabbit	1:1000	Abcam/ab6759
anti-sheep IgG-HRP	Rabbit	1:1000	Santa Cruz Biotechnology/ sc-2924

2.1.7 Enzymes and Corresponding Buffers

Table 8 | Enzymes and Corresponding Buffers

Enzyme/Buffer	Company
Collagenase P	Roche
Phusion High-Fidelity DNA Polymerase	Thermo Fisher Scientific
Phusion HF Buffer (5x)	Thermo Fisher Scientific
Restriction Enzymes	New England BioLabs (NEB)
CutSmart® Buffer (10x)	NEB
T4 DNA Ligase	NEB
T4 DNA Ligase Reaction Buffer (10x)	NEB

2.1.8 Molecular Weight Markers

Table 9 | Molecular Weight Markers

Marker	Company
GeneRuler 1 kb DNA Ladder	Thermo Fisher Scientific
GeneRuler 100 bp DNA Ladder	Thermo Fisher Scientific
Precision Plus Protein™ Kaleidoscope™ Prestained Protein Standards	Bio-Rad

2.1.9 Oligonucleotides

2.1.9.1 Primers for Sequencing

Table 10 | Primers for Sequencing

Name	Sequence (5'→ 3')
SP-6xHis-Fc-LCN13-pEFIRES-PURO_Fwd1	GTCTTACTGACATCCACTT
SP-6xHis-Fc-LCN13-pEFIRES-PURO_Fwd2	GCTGAATGGCAAGGAGTA
SP-6xHis-Fc-LCN13-pEFIRES-PURO_Fwd3	CGGTGTGCGTTTGTCTATAT
SP-6xHis-Fc-LCN13-pEFIRES-PURO_Rev1	TGTATCTTATACACGTGGCT
SP-6xHis-Fc-LCN13-pEFIRES-PURO_Rev2	ATGATCCTCTAGCTAGAGTCG
pdsAAV2-LP1-LCN13_Fwd1	GCTTAAATACGGACGAGGACAG
pdsAAV2-LP1-LCN13_Rev1	CTATAGTGAGTCGTATTAAGTACTCT
pdsAAV2-LP1-LCN13_Rev2	AACCACAACTAGAATGCAGTGA

2.1.9.2 Primers for Cloning Construct SP-6xHis-Fc-LCN13-pEFIRES-PURO

Table 11 | Primers for Cloning Construct SP-6xHis-Fc-LCN13-pEFIRES-PURO

Name	Sequence (5'→ 3')
NotI-Lcn13_Fwd	GGCCGCACAGGAAGCCCCGCCAGAT
LCN13-TGA-XbaI_Rev	GTGAATTCTAGATCAGTCACTTTCAACACATTTATCTCCGAT

2.1.9.3 Primers for Cloning Construct pdsAAV2-LP1-LCN13

Table 12 | Primers for Cloning Construct pdsAAV2-LP1-LCN13

Name	Sequence (5'→ 3')
NheI-SacI-Kozak-LCN13 _Fwd	ATCAATGCTAGCGAGCTCGCCACCAtgAAGAGCCTGCTCCTC
LCN13-TAG-SacI-NotI_Rev	GTGAATGCGGCCGCCTAGCTATCTAGAGCTCCTAGTCACTTTCAACAC ATTTATC

2.1.10 Plasmids

Table 13 | Plasmids

Name	Source
pDGΔVP	(Grimm et al., 1998)
p5E18-VD2/8	(Gao et al., 2002)
pAdDest-LCN13-FLAG	kind gift of Dr. Bilgen Üstünel
pdsAAV2-LP1-GFPmut-miNC	(Rose et al., 2011)
SP-6xHis-Fc-pEFIRES-PURO	kind gift of Dr. Anastasia Georgiadi
pdsAAV2-LP1-GFPmut	Personally contributed
pdsAAV2-LP1-LCN13	Personally contributed
SP-6xHis-Fc-LCN13-pEFIRES-PURO	Personally contributed

2.1.11 Taqman Probes

Table 14 | Taqman Probes

Target	Probe ID	Company
Apod	Mm01342307_m1	Life Technologies
Apom	Mm00444525_m1	Life Technologies
Lcn2	Mm01324470_m1	Life Technologies
Lcn3	Mm00440138_m1	Life Technologies
Lcn4	Mm03048210_m1	Life Technologies
Lcn5	Mm00468329_m1	Life Technologies
Lcn13	Mm00463685_m1	Life Technologies
Lcn14	Mm01328294_g1	Life Technologies
Mup1	Mm03647538_g1	Life Technologies
Pparg	Mm00440940_m1	Life Technologies
Ptgds	Mm01330613_m1	Life Technologies
Rbp4	Mm00803264_g1	Life Technologies
Scd1	Mm00772290_m1	Life Technologies
Tbp	Mm01277042_m1	Life Technologies

2.1.12 Cell Lines

Table 15 | Eukaryotic Cell Lines

Cell line	Source
CHO-S	kindly provided by Dr. Anastasia Georgiadi
MIN6	kindly provided by Dr. Susumu Seino of Kobe University (Minami et al., 2000)

Table 16 | Bacterial Strains

Name	Company
One Shot™ TOP10 Chemically Competent E. coli	Invitrogen
SURE 2 Supercompetent Cells	Agilent

2.1.13 Media and Supplements

Table 17 | Media and Supplements

Name	Company
Alanyl-glutamin	Sigma-Aldrich
CD OptiCHO™ Medium	Life Technologies
DMEM	Gibco
DMEM/F-12	Gibco
DPBS	Life Technologies
Fetal bovine serum (FBS)	Thermo Fisher Scientific
Hank's Balanced Salt Solution	Sigma-Aldrich
L-Glutamine	Thermo Fisher Scientific
Opti-MEM Reduced Serum Media	Thermo Fisher Scientific
Penicillin/Streptavidin (P/S)	Thermo Fisher Scientific
RPMI 1640	Gibco
β-mercaptoethanol	Sigma-Aldrich

2.1.14 Rodent Diets

Table 18 | Rodent Diets

Diet	Company/Reference Number
10% low fat diet	Research Diets/D12492i
60% high fat diet	Research Diets/D12450Ji
Regular rodent chow diet	Altromin Spezialfutter GmbH & Co. KG/1314

2.1.15 Software

Table 19 | Software

Software	Company
ApE – a plasmid editor	Freeware
EndNote	Clarivate Analytics
Graphpad Prism 8	GraphPad Software Inc.
Image Lab	BioRad
Inkscape	Freeware
Microsoft Office	Microsoft Cooperation

2.2 Methods

2.2.1 Animal Studies

All animal studies were performed in accordance with the national animal welfare legislation and were approved by the state ethics committee and the government of Upper Bavaria. Performed experiments were covered by the licenses 55.2-1-54-2532-164-2015 and 55.2-1-55-2532-49-2017.

2.2.1.1 Husbandry and General Study Outlines

Mice were housed under specific pathogen-free conditions with a 12:12 h light-dark cycle and free access to water and food. Exclusively male mice were used for all studies. An overview of used mouse strains, vendors and the corresponding experiments are listed in Table 20.

Table 20 | Mouse Strains and Corresponding Experiments

Mouse Strain	Vendor	Study
C57Bl6/N	Charles River	LCN13 tissue expression screen – Figure 5 Wild type mice injected with recombinant Fc-LCN13 – Figure 8 HFD study to test therapeutic potential of LCN13 – Figure 10/11 Islet isolation – Figure 18
C57Bl6/N	Janvier	LCN13 knockdown study – Figure 6/7/16 HFD study to test preventive potential of LCN13 – Figure 9/12
B6.BKS(D)-Leprdb/J (000697)	Jackson	db/db mice study to test therapeutic potential of LCN13 – Figure 13/14/17 AAV titration study – Figure 15
C57BL/6J (000664)	Jackson	Wild type controls for the db/db background: db/db mice study to test therapeutic potential of LCN13 – Figure 13/14/17 AAV titration study – Figure 15

For islet isolation, 8 to 12-week-old mice were used. To test the therapeutic potential of LCN13, 5-week-old mice were fed a HFD for 14 weeks, before AAVs were injected. To test LCN13's potential to prevent metabolic dysfunctions evoked by HFD, mice were injected with AAVs at the age of 7 weeks and HFD feeding was initiated 5 weeks later. In all db/db studies, mice received AAVs at the age of 7 weeks. In the LCN13 knockdown study, LNPs were administered to 8-week-old mice. Studies were terminated by sacrificing mice ad libitum by cervical dislocation between 9 a.m. and 1 p.m. Blood was retrieved by decapitation. Serum was

acquired by spinning down whole blood in 1.1ml Z-Gel tubes (SARSTEDT) at 10 000 g and RT for 10 min, after which the serum above the gel was pipette into new tubes. Harvested organs were weighed and together with the serum snap frozen in liquid nitrogen. Murine samples were stored at -80°C.

2.2.1.2 Assessment of Glucose and Insulin Tolerance

Before metabolic phenotyping, mice were fasted for 5 or 16 h (8 a.m. to 1 p.m. and 6 p.m. to 10 a.m., respectively). Experiment-specific fasting times as well as injected glucose and insulin doses are summarized in Table 21.

Table 21 | Experimental Details of Metabolic Phenotyping

Study	Metabolic Test	Fasting (h)	Dose
LCN13 knockdown study – Figure 6	GTT	5	2 g/kg D-glucose
	ITT	5	1 U/kg insulin
Wild type mice injected with recombinant Fc-LCN13 – Figure 8	GTT	5	2 g/kg D-glucose
HFD study to test preventive potential of LCN13 – Figure 9/12	GTT	5	2 g/kg D-glucose
	ITT	5	0.75, 1.2 and 1.5 U/kg insulin
HFD study to test therapeutic potential of LCN13 – Figure 10	GTT	16	1 g/kg D-glucose
	ITT	5	1 and 1.5 U/kg insulin
db/db mice study to test therapeutic potential of LCN13 – Figure 13	GTT	16	1 g/kg D-glucose
	ITT	5	2 U/kg insulin
AAV titration study – Figure 15	GTT	5	1 g/kg D-glucose
	ITT	5	3 U/kg insulin

Blood glucose levels were measured at the tail vein using a glucometer at 0, 15, 30, 60 and 120 min or at 0, 20, 40, 60 and 90 min after i.p. glucose and insulin injection, respectively. To determine plasma insulin levels, blood samples were taken up into EDTA-coated capillary tubes from the tail vein, before injections were performed. After spinning down at 2000 g and RT for 5 min, plasma was transferred to new tubes. Plasma insulin levels were measured with a mouse insulin enzyme-linked immunosorbent assay (ELISA) kit from ALPCO according to the manufacturer's instructions. To assess insulin resistance, the homeostasis model

assessment (HOMA) index was calculated [fasting blood glucose (mmol/l) x fasting plasma insulin (µIU/mL) / 22.5].

2.2.1.3 Assessment of Lipid Parameters in Serum and Liver

Lipid parameters in blood, such as cholesterol, high density lipoprotein (HDL), low density lipoprotein (LDL), alanine transaminase (ALT) and aspartate aminotransferase (AST) were measured using designated kits and the AU480 chemistry analyzer from Beckman Coulter.

For hepatic lipid levels, frozen liver tissue was weighed, before 1.5 mL chloroform: methanol (2:1) was added. After tissue lysis using the tissue homogeniser Mixer Mill MM 400 from Retsch (two rounds of 30 Hz for 30 s each), samples were spun down briefly and mixed on a thermomixer at 1400 rpm and room temperature (RT) for 20 min. Subsequently, samples were spun down at 13000 rpm and 20°C for 30 min and 1 mL of supernatant was transferred to a new tube. After adding 200 µL of 150 mM NaCl, samples were shaken vigorously and spun down at 2000 rpm and 20°C for 5 min. 200 µL of the lower organic phase was transferred into new tubes containing 40 µL of chloroform:Triton-X (1:1) solution. Samples were dried overnight using a vacuum concentrator (at 30°C with brakes off) 200 µL dH_2O was added to the remaining solution and, after mixing well, samples were placed on a rotating wheel at RT for 1 h. Samples were stored at -80°C and were vortexed, before lipid assays were performed. Cholesterol and NEFA levels were measured using 10 µL of extract while for triglycerides 8 µL and for phospholipids 2 µL were used. Hepatic lipid levels were measured using commercially available kits (Table 6) according to the manufacturer's instructions.

2.2.1.4 Isolation of Primary Islets of Langerhans

After cervical dislocation and opening of the abdominal cavity, the hepato-pancreatic duct was clamped under a dissecting microscope at the ampulla where it meets the intestine. 3 mL collagenase solution were slowly injected at the bifurcation where the cystic and the hepatic ducts meet. After dissection, the inflated pancreas was incubated in 3 mL collagenase in a 50 mL falcon tube in a 37 °C warm waterbath for 15 min. The tube was gently shaken after 7.5 min and vigorously after 15 min. To stop collagenase action, 20 mL ice-cold HBSS medium supplemented with 1% BSA was added and all following steps were conducted on ice. After centrifugation (290 g at 4°C for 2 min), the supernatant was discarded and the pellet was resuspended in 15 mL HBSS medium supplemented with 1% BSA. The suspension was transferred through a 500 µm cell strainer into a new 50 mL falcon tube. After spinning down (290 g at 4°C for 2 min), the supernatant was discarded and the cell pellet was resuspended

by gently vortexing in histopaque 1100. The resulting cell suspension was slowly overlaid with 5 mL HBSS supplemented with 1% BSA. After centrifugation (900 g in a swinging-bucket rotor at 4°C for 15 min with medium acceleration and no brake), islets were transferred from the interface between histopaque and medium into a new 50 mL Falcon tube using a sterile pasteur pipette. Islets were washed twice with 25 mL HBSS medium supplemented with 1% BSA and were subsequently transferred in 10 mL islet culturing media (RPMI supplemented with 10% FBS, 1% penicillin-streptomycin) into a 10 cm Petri dish. Using a 200 µL pipette, islets were handpicked in 6 cm dishes containing 4 mL islet culturing medium (100 islets per dish). The next day, islets were used for glucose-induced insulin secretion assays.

2.2.2 Cloning and Microbiology Techniques

2.2.2.1 Cloning of the Construct pdsAAV2-LP1-LCN13

The full length mouse LCN13 coding sequencing (NCBI Reference Sequence: NM_153558.1; 176 amino acids) with the stop codon replaced by a Flag tag sequence (DYKDDDDK) had been cloned into the pAd/BLOCK-iT™-DEST expression vector (Thermo Fisher Scientific) and was received as kind gift from Dr. Bilgen Üstünel. From this vector (pAdDest-LCN13-FLAG), the full length mouse LC13 coding sequence without the Flag tag was cloned into pdsAAV2-LP1-GFPmut-miNC, replacing the mutated GFP and miNC cassettes of the latter. In short, full-length LC13 coding sequence was amplified from the pAdDest-LCN13-FLAG vector by polymerase chain reaction with 5'NheI and 3'NotI overhangs (PCR; for used primers see Table 12). The PCR product and the pdsAAV2-LP1-GFPmut-miNC were digested using the restriction enzymes NheI/NotI, removing the GFPmut-miNC sequence from the latter, before they were ligated. To generate a control vector harbouring the mutated GFP sequence without the miNC cassette, the pdsAAV2-LP1-GFPmut-miN vector was digested with NotI only.

2.2.2.2 Cloning of the Construct SP-6xHis-Fc-LCN13-pEFIRES-PURO

The coding sequence of LCN13 without the sequence of the signal peptide (encoding for the first 18 amino acids) was amplified from the pAdDest-LCN13-FLAG vector by PCR (for used primers see Table 11). Both the resulting PCR product and the mammalian expression vector SP-6xHis-Fc-pEFIRES-PURO were NotI/XbaI digested and subsequently ligated.

2.2.2.3 PCR

PCR was used to isolate the LCN13 coding sequence from the pAdDest-LCN13-FLAG vector in order to subsequently clone it into diverse vectors (see above). The formula of the PCR reaction mixes and the PCR amplification parameters are shown in Table 22 and 23. Annealing temperatures were calculated using the NEB Tm online calculator tool. 25 cycles of amplification were used.

Table 22 | PCR Reaction Mix

Component	Volume (µL)
Phusion HF Buffer (5x)	10
dNTP mix (10 mM)	1
Fwd and Rev primers (10 µM)	5
Template DNA (10 ng)	2
Phusion Polymerase	0.5
Nuclease-free water	31.5

Table 23 | PCR Settings

Step	Temperature (°C)	Time
Initial Denaturation	95	30 sec
Denaturation	95	10 sec
Annealing	primer-specific	20 sec
Extension	72	1 min/kb of DNA to be amplified
Refrigeration	4	on hold

2.2.2.4 Restriction Digest

For restriction digestion of vectors and PCR-amplified inserts, following protocol was used:

Table 24 | Restriction Digestion

Component	Amount
Vector/insert	3 µg/1 µg
Enzyme(s)	1 µL
Fast Digest Buffer (10x)	5 µL
Nuclease-free water	Up to 50 µL

Digests were incubated in a static incubator at 37°C overnight. Uncut vectors and single-digested vectors were included as controls.

2.2.2.5 Agarose Gels for Analysis of Digested DNA Fragments

In order to analyze restriction digests, 0.8 – 2% agarose gels (m/v) were prepared depending on the DNA fragment size by dissolving agarose in 1x TAE buffer by microwaving. After cooling down, 1x SYBR Safe DNA gel stain was added and the agarose solution was poured in designated chambers. DNA samples to be analyzed were mixed with 1x loading dye, before they were loaded onto the solidified gel. DNA bands were visualized using a ChemiDoc XR+ gel imaging system from Bio-Rad and, if applicable, cut out from the gel and transferred to a 2 mL Eppendorf tube for purification. Small amounts of amplified, double-digested inserts were run on an agarose gel to ensure their intactness. The rest of the inserts were subsequently purified using the MinElute PCR Purification Kit (QIAGEN) according to the manufacturer's protocol. Double-digested vectors were loaded completely on the agarose gel, followed by purification using the QIAquick Gel Extraction Kit (QIAGEN) as recommended by the manufacturer.

2.2.2.6 Ligation and Bacterial Transformation

Ligation reactions were set up in a 3:1 (insert:vector) ratio (Table 25).

Table 25 | Ligation Reaction

Component	Amount
Insert	60 fmol
Vector	20 fmol
Ligase	1 µL
Buffer (5x)	4 µL
Nuclease-free water	Up to 20 µL

Ligation reactions were incubated at RT for 1 h, before bacteria were transformed. To determine the percentage of self-ligation, a vector-only control was included. For mammalian LCN13 expression vectors, One Shot TOP10 Chemically Competent E. coli (Invitrogen) were used, for AAV vectors recombinase-deficient Sure 2 Supercompetent Cells (Agilent) were transformed. In short, bacteria were thawed on ice and incubated for another 30 min on ice after adding 2 µL of the ligation mix. Then, bacteria were heat shocked for 30 s at 42°C on a thermoblock and immediately placed on ice for 1 min. 250 µL of S.O.C. media was added and tubes were incubated horizontally in a shaking incubator at 225 rpm and 37°C for 1 h. 80 µL of the transformed bacteria was plated on appropriate antibiotic selection plates which were inverted and incubated overnight at 37°C. One plate without bacteria and one plate with

untransformed bacteria served as control for contamination and functional antibiotics, respectively.

2.2.2.7 Plasmid DNA Isolation and Clone Validation

Single colonies were picked into 2.5 mL LB medium containing the appropriate antibiotic and allowed to grow at 37°C overnight. One tube containing LB medium and antibiotic without bacteria served as control for bacterial contamination. Plasmid DNA was isolated from 2 mL of each culture tube using the QIAprep Spin Miniprep Kit (QIAGEN) according to the manufacturer's protocol. The remaining 0.5 mL was stored at 4°C and used for the preparation of glycerol stocks (300 µL bacterial culture + 300 µL 50% glycerol solution), after the positive clones had been identified. For clone validation, restriction digests and agarose-based analysis of inserts was conducted as described above. Positive clones were sent to Eurofins Genomics for sequencing (for primers see Table 10).

2.2.2.8 AAV Production

AAVs were generated by Vigene Biosciences [Rockville (Maryland), USA]. Besides the AAV cis plasmids pdsAAV2-LP1-LCN13 and pdsAAV2-LP1-GFPmut, the adenoviral helper plasmid pDGΔVP (Grimm et al., 1998) and the mutated p5E18-VD2/8 expression vector (Gao et al., 2002) were amplified from their corresponding glycerol stocks. In short, an inoculation loop was used to transfer a small amount of each frozen glycerol stock into 2 mL LB medium containing 50 µg/mL ampicillin in the morning. In the evening the bacterial culture was added to 400 mL ampicillin-containing LB medium in a 1 L Erlenmeyer-flask. In order to obtain the needed amount of plasmids required to be sent to Vigene (Table 26), 4 bacterial culture flasks were set up for the helper plasmid pDGΔVP, 2 flasks for the mutated p5E18-VD2/8 expression vector and 1 flask for each of the AAV cis plasmids. The next day, plasmids were purified using the QIAGEN Plasmid Mega Kit according to the manufacturer's instructions. DNA was dissolved in 900 µL Tris-EDTA (TE) buffer at 4°C overnight.
Unless indicated otherwise, each mouse was injected with $5x10^{11}$ AAVs (in 100 µL PBS) via the tail vein.

Table 26 | Identity and Amount of Plasmids Sent to Vigene

Plasmid	Amount required (mg)	Amount sent (mg)
pdsAAV2-LP1-LCN13	0.5-1	0.67
pdsAAV2-LP1-GFPmut	0.5-1	0.66
pDGΔVP	1-2	1.17
p5E18-VD2/8	1-2	1.33

2.2.2.9 Liponanoparticle Production

To knockdown LCN13 specifically in hepatocytes, we exploited liponanoparticles (LNP) carrying a LCN13-targeted siRNA or a luciferase-targeted control siRNA. Both siRNA design, synthesis, lead identification by a dual luciferase-reporter gene assay as well as packaging into LNPs was performed by Axolabs GmbH (Kulmbach, Germany). The LNP formulation was based on Axolabs' proprietary lipid XL-10. These LNPs deliver the majority of siRNA to hepatocytes, when administered via the tail vein. The selected, most potent siRNA sequence is shown in Table 27.

Unless indicated otherwise, mice received LNPs at a dose of 0.5 mg/kg (in 200 µL PBS) via the tail vein.

Table 27 | LCN13-targeted siRNA packaged in LNPs

Strand	Sequence (5'→ 3')
Sense strand	cuGuGAGAAuAAuaGcucAdTsdT
Antisense strand	UGAGCuAUuAUUCUcAcAGdTsdT

A, C, G, U = RNA nucleotides; dT = DNA nucleotide; a, c, u = 2′-O-methylated nucleotides; s = phosphorothioate linkages.

2.2.3 RNA and Protein Detection

2.2.3.1 RNA Isolation and qPCR

Total RNA was extracted from homogenized mouse tissues using TRIzol Reagent (Thermo Fisher Scientific) according to the manufacturer's instructions. cDNA was prepared using the Quantitect Reverse Transcription Kit (QIAGEN). In short, total RNA was diluted to 65 ng/µL. Genomic DNA was eliminated by incubating 9 µL of total RNA (585 ng) with 1x gDNA Wipeout Buffer at 42°C for 2 min. Afterwards, 4.5 µL of the reverse-transcription reaction master mix (Table 28) was added to the samples.

Table 28 | Reverse-Transcription Reaction Master Mix

Component	Volume (µL/sample)
Reverse transcriptase	0.75
RT buffer (5x)	3
RT primer mix	0.75

Samples without reverse transcriptase were always included as negative controls. Reverse transcription was performed at 42°C for 30 min, after which the enzyme was inactivated by incubation at 95°C for 3 min. For downstream qPCR analysis, cDNA samples were diluted 1:6 by adding 75 µL H_2O to each sample (final DNA concentration: 6.5 ng/µL).

For qPCR, the TaqMan probe-based qPCR was used which was run on the Quantstudio 6 quantitative PCR machine (Life Technologies). In detail, 2.5 µL of the pre-diluted cDNA (16.25 ng) and 5.5 µL of the qPCR master mix (Table 29) was pipetted into each well of a 384 qPCR plate at least in duplicates. Each run was conducted with 50°C for 2 min and 95°C for 10 min (hold stage) and 40 cycles of 95°C for 15 s and 60°C for 1 min (PCR stage). Data was analyzed by the ΔΔCt method. The TATA-box binding protein (TBP) mRNA levels were used for normalization.

Table 29 | qPCR Master Mix

Component	Volume (µL/sample)
TaqMan Master Mix	4
Primer-probe	0.2
Nuclease-free water	1.3

2.2.3.2 Western Blot

Western blotting was conducted to estimate the purity and to validate the identity of the in-house produced mammalian recombinant Fc-LCN13 protein. Furthermore, hepatic LCN13 overexpression and subsequent secretion into the blood circulation was validated by western blot. Ready-to-use Novex tris-glycine mini gels (Invitrogen) were used for all western blots. Loaded protein amounts as well as the percentage of gels are summarized in Table 30. Proteins were separated by SDS-PAGE in 1x SDS-running buffer at 80 V for initial 30 min and afterwards at 120 V until the loading dye reached the end of the gel. To assess the purity of the produced mammalian recombinant proteins, gels were stained with coomassie brilliant blue R250. For antibody-based detection of LCN13, nitrocellulose membranes and transfer stacks (6 layer of Wypall®X60) with the size of the gels were soaked in 1x Turbo-Transfer Buffer for 3 min. Protein transfer onto nitrocellulose membranes was conducted using the Trans-Blot®

Turbo™ Transfer System from Bio-Rad with following assembly:
Anode (+)-6x transfer stacks-nitrocellulose membrane-SDS gel-6x transfer stacks-(-).
Membranes were blocked using 5% (w/v) skimmed milk in 1x TBS-T at RT for 1 h. After 3 sequential washing steps in TBS-T for 5 min each, membranes were immunoblotted with the primary antibody at 4°C overnight. The next day, membranes were washed as described above and incubated, if applicable, with the corresponding secondary antibody at RT for 1 h. After washing, proteins were detected using the SuperSignal West Substrate from Thermo Fisher Scientific, as well as the ChemiDoc XRS+ imaging system and the program Image Lab from Bio-Rad.

Table 30 | Percentage of Protein Gels and Loaded Protein Amounts

Protein	Application	Amount (µg)	Gel (%)
Recombinant Fc and Fc-LCN13	Coomassi	5	2-24
	αLCN13/αhuman IgG	2.6	10
Circulating LCN13	αLCN13	~24 (1:20 dilution)	12

2.2.4 Cell Culture

Unless indicated otherwise, primary cells and cell lines were incubated at 37°C in a humidified incubator containing 5% CO_2 and 21% O_2.

2.2.4.1 Generation of MIN6 Pseudo-Islets

MIN6-m9 cells were cultured in DMEM supplemented with 20% FBS, 1% penicillin-streptomycin, 0.01% β-mercaptoethanol and 2 mM glutamine. For pseudo-islet formation, $2x10^5$ MIN6-m9 cells were seeded in 2 mL culture medium per well of an ultra-low attachment 6 well plate. After three days of shaking at 70 rpm and 37°C, pseudo-islets reached sizes comparable to primary mouse islets and were used for glucose-stimulated insulin secretion assay.

2.2.4.2 GSIS

MIN6 pseudo-islets or primary islets were washed in Krebs-Ringer buffer (KRB) supplemented with low glucose (2.8 mM). 10 intact islets spanning various sizes (e.g. 4 small, 4 medium, 2 big islets) were transferred into 300 µL KRB buffer with low glucose per well of ultra-low attachment 6 well plates for 1 h at 37°C. Caution was taken in order to have similar sized islets across the different wells. Plates were kept in an angled position throughout the experiment. Afterwards, islets were transferred in 300 µL KRB buffer with low (2.8 mM) or high (16.7 mM) glucose and different treatments. PBS and Exendin-4 (Ex-4; 10 nM) were used as negative and positive controls, respectively. Recombinant bacterial LCN13 was used at a concentration of 10 nM. Pseudo-islets and primary islets were exposed to the different treatments for 2 and 1 h, respectively. Islets were subsequently transferred into 1.5 ml Eppendorf tubes containing 150 µL acidic ethanol. After centrifugation (1000 rpm at 4°C for 1 min), 150 µL of the secretion media was transferred into 1.5 ml Eppendorf tubes. Collected islets and secretion media were stored at -20°C until further analysis.

Insulin content and secretion was measured using the mouse insulin ELISA kit from ALPCO according to the manufacturer's instructions. For islet insulin content, islets were sonicated in acidic ethanol (3 pulses of 30 Hz for 1 second) and diluted 1:1530. Collected supernatants were either analyzed undiluted (2.8 mM glucose samples), in a dilution of 1:15 (16.7 mM glucose samples) or in a dilution of 1:40 (16.7 mM glucose + Ex-4 samples). For MIN6 pseudo-islets, sonicated islets were diluted 1:50 and the collected supernatants were either analyzed undiluted (2.8 mM glucose samples), in a dilution of 1:2 (16.7 mM glucose), 1:4 (2.8 mM glucose, positive control Ex-4) or 1:5 (16.7 mM glucose, positive control).

2.2.4.3 Production and Purification of Recombinant Proteins

Two days before transfection, 2.5x 10^5 CHO-S cells were seeded per well in a 6 well plate. Cells of each well were transfected with 4 µg of the SP-6xHis-Fc-LCN13-pEFIRES-PURO plasmid using lipofectamine 3000 reagent (Life Technlogies) according to the manufacturer's instructions. Cells were incubated with the DNA-lipid complex in 1.5 mL Opti-MEM medium for 6 h at 37°C. Afterwards, medium was changed to DMEM/F12 medium supplemented with 10% FBS for another 48 h. Successfully transfected cells were subsequently selected by culturing the cells in DMEM/F12 medium supplemented with 25 ug/ml puromycin. Medium changes were performed daily until no apparent cell death was observed anymore, after which medium was changed every other day. After reaching confluence, cells of one well were transferred to a 25 cm^2 flask, then to a 75 cm^2 flask from which they were split to three 150 cm^2 flasks. For further cell expansion, cells of each 150 cm^2 flask were transferred to 100 mL

serum-free OptiCHO medium supplemented with 0.5 mg/mL alanyl-glutamin and 25 ug/ml puromycin in a 0.5 L rectangular bottle. After 5 to 7 days at 37°C in a shaking incubator (120 rpm), the cell suspension of each bottle was transferred to a 1 L rectangular bottle to which 200 mL fresh culture medium with puromycin was added. The cells were grown for further 5 days during which the temperature was reduced to 31°C. Afterwards, cell suspensions were spun down at 9500 g and 4°C for 15 min. The supernatants were pooled in a 2 L bottle and 1M NaCl, 5 mM imidazole as well as 1x Halt™ Protease Phosphatase Inhibitor-Cocktail (Life Technologies) were added. The solution was stirred on ice, filtered using a bottle top vacuum filter with a pore size of 0.45 µm and degassed (during continuous stirring under vacuum). Afterwards, the pH was adjusted to 7.2. In the meanwhile, HisTrap™ HP 5ml chromatography columns (GE Healthcare) were connected to a ÄKTA pure 25 (GE Healthcare), washed with 50 mL ultrapure H_2O and equilibrated using 50 mL of washing buffer 1 (WB1) supplemented with 0.2 M NaCl, 0.02 M $NaHPO_4$ and 5 mM imidazole at a pH of 7.2. Then, the degassed culture medium was loaded on the column at a flow rate of 1 mL/min. In order to clean columns from unwanted material, 50 mL of both WB1 and WB2 (0.2 M NaCl, 0.02 M $NaHPO_4$, 20 mM imidazole, pH 7.2) were passed through the column at a flow rate of 2 mL/min. The 6xHis-Fc-LCN13 protein was collected in 7 fractions, each of 5 mL elution buffer containing 0.2 M NaCl, 0.02 M $NaHPO_4$, 400 mM imidazole at a pH of 7.2. For elution a flow rate of 1 mL/min was chosen. The fraction containing the elution peak (fraction 3) was dialyzed against 4 L of DPBS using a dialysis membrane under stirring at 4°C. DPBS was changed every 2 hours for 3 times. Afterwards, the purified protein was snap frozen and stored at -80°C.
For the Fc control, the same workflow was performed. Stably transfected CHO-S cells were kindly provided by Dr. Anastasia Georgiadi.

2.2.5 In-Solution Digest and Mass Spectrometry Analysis of Fc-LCN13

In solution digest and LC-MS/MS analysis of our in-house produced recombinant proteins were performed by the Research Unit Protein Science of the Helmholtz Zentrum München. 10 µg Fc-LCN13 and 12 µg of the Fc control were typsinized following a modified filter-aided sample preparation (FASP) protocol described before (Grosche et al., 2016). In the following, acidified peptides were analyzed by LC-MS/MS in the data-dependent acquisition (DDA) mode using a Q Exactive HF mass spectrometer (Thermo Fisher Scientific) coupled to an UItiMate 3000 RSLC nano-HPLC (Dionex) as described in (Lepper et al., 2018). The samples were automatically loaded onto the HPLC system, consisting of a C18 trap column and a C18 analytical column (Acquity UPLC M-Class HSS T3 column, 1.8 µm, 75 µm x 250 mm; Waters). After 5 minutes, the peptides were eluted from the trap column and separated by the analytical column using a non-linear acetonitrile gradient (flow rate: 250 nL/min for 90 minutes in total).

MS scans were performed at a resolution of 60 000 and the 10 most abundant peptide ions of each MS1 cycle were subjected to fragmentation and further analysis by a second mass spectrometer (MS2). Label-free quantification was performed using Progenesis QI software for proteomics (v3.0, Nonlinear Dynamics, Waters) as described before (Grosche et al., 2016). Peptide identification on the basis of the generated MS/MS spectra was performed with Mascot (version 2.5.1) using the SwissProt mouse database containing 16,868 sequences. The following Mascot search parameters were chosen: trypsin (with up to 1 missed cleavage allowed), peptide tolerance of 10 ppm, fragment tolerance of 0.02 Da, carbamidomethylation as fixed modification, methionine oxidation as well as asparagine and glutamine de-amidation as variable modifications. The false discovery rate (FDR) of the Mascot search against a decoy database was set to below 1%. Identified peptides were re-imported in the Progenesis QI software for proteomics. Normalized abundances of each protein were calculated by summing up the abundances of all unique peptides for the respective protein. In general, only proteins which were quantified by at least two unique peptides and identified by at least three spectral counts were included into the analysis.

2.2.6 Statistics

Data are shown as mean ± SEM. Statistical analysis was performed using Graph Pad Prism v. 8. Normal distribution was assumed for all data. In one-factorial designs with more than 2 groups, equality of variances was assessed by Brown-Forsythe test. In case of equal variances, regular one-way ANOVA with Tukey's multiple comparison test was performed. Data with unequal variances were assessed using Welch's ANOVA with Dunnett's T3 multiple comparison test. For multifactorial study designs and repeated measures, two-way ANOVA with Tukey's multiple comparison test was applied. When the repeated measures factor had more than two levels, Geisser-Greenhouse correction was used. As post hoc analysis, either Tukey's, Sidak's or Dunnett's multiple comparison test was chosen. Performed statistical tests are indicated in the figure legends.

3. Results

Parts of the results presented here were submitted as research article to the journal Life Science Alliance on the 30th of August 2020:

Lipocalin 13 enhances insulin secretion but is dispensable for systemic metabolic control

Lea Bühler [1,2,4], Adriano Maida [1,2,4], Anastasia Georgiadi [1,2,4], Elena Vogl [1,2,4], Andrea Takacs [1,2,4], Oliver Kluth [4,5], Annette Schürmann [4,5,6], Annette Feuchtinger [7], Christine von Törne[8], Foivos Tsokanos [1,2,4], Katarina Klepac [1,2,4], Gretchen Wolff [1,2,4], Mina Sakurai [1,2,4], Bilgen Ekim Üstünel [1,2,4], Peter Nawroth [2,4], and Stephan Herzig[1,2,3,4]

1. Institute for Diabetes and Cancer (IDC), Helmholtz Centre Munich, German Research Center for Environmental Health, Neuherberg, Germany

2. Joint Heidelberg-IDC Transnational Diabetes Program, Inner Medicine I, Heidelberg University Hospital, Heidelberg, Germany

3. Chair Molecular Metabolic Control, Medical Faculty, Technical University Munich, Germany

4. German Center for Diabetes Research (DZD), Neuherberg, Germany

5. Department of Experimental Diabetology, German Institute of Human Nutrition Potsdam-Rehbruecke (DIfE), Nuthetal, Germany

6. Institute of Nutritional Science, University of Potsdam, Potsdam, Germany

7. Research Unit Analytical Pathology, Helmholtz Centre Munich, German Research Center for Environmental Health, Neuherberg, Germany

8. Research Unit Protein Science, Helmholtz Centre Munich, German Research Center for Environmental Health, Munich, Germany

For clarification, author contributions are declared in the figure legends and summarized in Table 32.

3.1 Liver-Specific LCN13 Knockdown neither Affects Glucose nor Lipid Homeostasis

It is becoming increasingly clear that inter-tissue crosstalk plays a major role in metabolic health and disease. In this context, LCN13 has been identified as an endocrine factor regulating both glucose and lipid homeostasis (Cho et al., 2011; Ekim Ustunel et al., 2016; Sheng et al., 2011). The LCN13 coding sequence consists of 176 amino acids with a putative N-terminal signal peptide (amino acid 1 to 18) which facilitates its secretion into the blood stream (Suzuki et al., 2004). To ascertain the source of circulating LCN13, we screened a diverse set of tissues derived from C57BL/6N wild type mice by quantitative real-time polymerase chain reaction (qRT-PCR). *Lcn13* mRNA expression was highly tissue-specific, as it was almost exclusively detected in liver lysates (Figure 5).

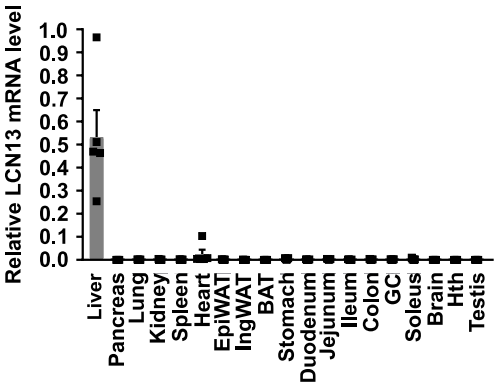

Figure 5 | LCN13 is Primarily Expressed in Liver

Lcn13 mRNA abundance was measured in tissue extracts by qRT-PCR in 13 week old C57BL/6N mice (n = 5 mice per group). Values are shown as mean ± SEM. Average ct value for liver samples was 28.7, for all other organs above 34. EpiWAT, epididymal white adipose tissue; IngWAT, inguinal white adipose tissue; BAT, brown adipose tissue; GC, gastrocnemius muscle; Hth, hypothalamus. Study was designed, conducted and analyzed by Lea Katharina Bühler.

To further investigate the physiological role of LCN13 in glucose metabolism, we knocked down LCN13 specifically in the liver of wild type mice by liponanoparticle (LNP)-mediated small interfering RNA (siRNA) delivery to hepatocytes. Besides the *Lcn13*-targeted siRNA, a siRNA targeting luciferase was used as control. In a preceding time course and dose response experiment, we identified a LNP dose of 0.5 mg/kg as sufficient to knockdown hepatic LCN13 (Figure 6a). Hepatic knockdown (KD) was already apparent two days after LNP injection and lasted up to two weeks. In a subsequent experiment, 0.5 mg/kg LNP achieved a knockdown of 69% and 93% compared to PBS and siRNA control injected mice after 2 weeks, respectively (Figure 6b).

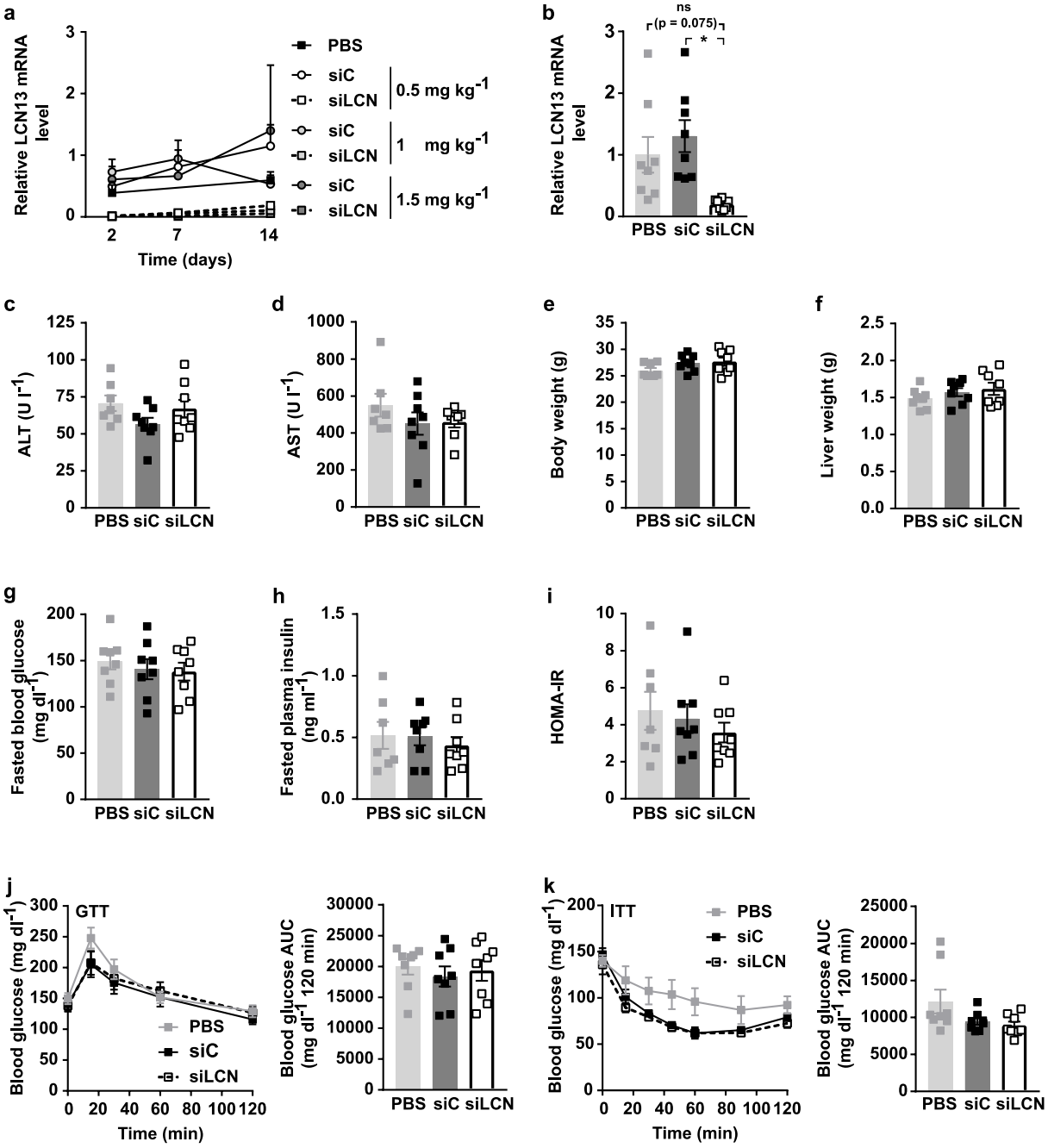

Figure 6 | LNP-Mediated Knockdown of LCN13 Does not Deteriorate Insulin Sensitivity or Glucose Tolerance in Lean Wild Type Mice

C57BL/6N males (8 weeks) were i.v. injected with PBS, liponanoparticles (LNP) carrying either a siRNA directed against *Lcn13* mRNA (siLCN) or a control siRNA targeting luciferase (siC) (0.5, 1 or 1.5 mg/kg, n = 3-4 mice per group). (**a**) *Lcn13* mRNA abundance was measured in liver extracts by qRT-PCR 2, 7 and 14 days after LNP injection. C57BL/6N males (8 weeks) were injected with PBS, LNP carrying siLCN or siC (0.5 mg/kg, n = 8 mice per group). (**b**) *Lcn13* mRNA abundance was measured in liver extracts by qRT-PCR 2 weeks after LNP injection. (**c**) Alanine transaminase (ALT) and (**d**) aspartate transaminase (AST) levels were measured in serum 2 weeks after LNP injection. (**e**) Body weight and weight of (**f**) liver were measured 2 weeks after LNP injection. (**g**) Fasting (5h) blood glucose, (**h**) corresponding plasma insulin levels and (**i**) resulting HOMA-IR index 1 week after LNP injection. (**j**) i.p. GTT was performed 1 week after LNP injection (fasted for 5 hs, 2 g/kg D-glucose). (**k**) i.p. ITT was performed 2 weeks after LNP injection (fasted for 5 hs, 1 U/kg insulin). Values are shown as mean ± SEM. Studies were designed by Lea Katharina Bühler, conducted by Elena Vogl and analyzed by Lea

Katharina Bühler. Statistical analysis: In (**b**), data was analyzed by Welch's ANOVA with Dunnett's T3 multiple comparison test. In (**j, k**), GTT and ITT data were analyzed by two-way ANOVA with Geisser-Greenhouse correction and Tukey's multiple comparisons test. All other data were analyzed by ordinary one-way ANOVA with Tukey's multiple comparison test. * $p \leq 0.05$.

Treatment with LNP did not lead to apparent liver damage as both alanine transaminase (ALT) and aspartate transaminase (AST) enzyme levels in serum remained unchanged (Figure 6c, d). LCN13 KD mice did not differ in body nor in liver weight from control mice (Figure 6e, f). Furthermore, all mice regardless of the treatment exhibited similar fasting plasma glucose and insulin levels (Figure 6g, h). Therefore, the comparable homeostasis model assessment evaluation of insulin resistance (HOMA-IR) resulted in similar values for all mice (Figure 6i). In line with this, glucose and insulin tolerance remained unchanged upon LCN13 KD (Figure 6j, k). We subsequently investigated whether LCN13 reduction had an impact on lipid homeostasis. Serum cholesterol, triglycerides, high-density lipoprotein (HDL)-cholesterol and low-density lipoprotein (LDL)-cholesterol levels did not differ between LCN13 KD and control mice (Figure 7a-d). Likewise, triglycerides, cholesterol, phospholipids and NEFA amounts in liver lysates did not change upon LCN13 knockdown (Figure 7e-h). Collectively, these results indicated that liver-specific LCN13 KD did not have any effect on systemic or hepatic parameters of glucose and lipid homeostasis in lean animals.

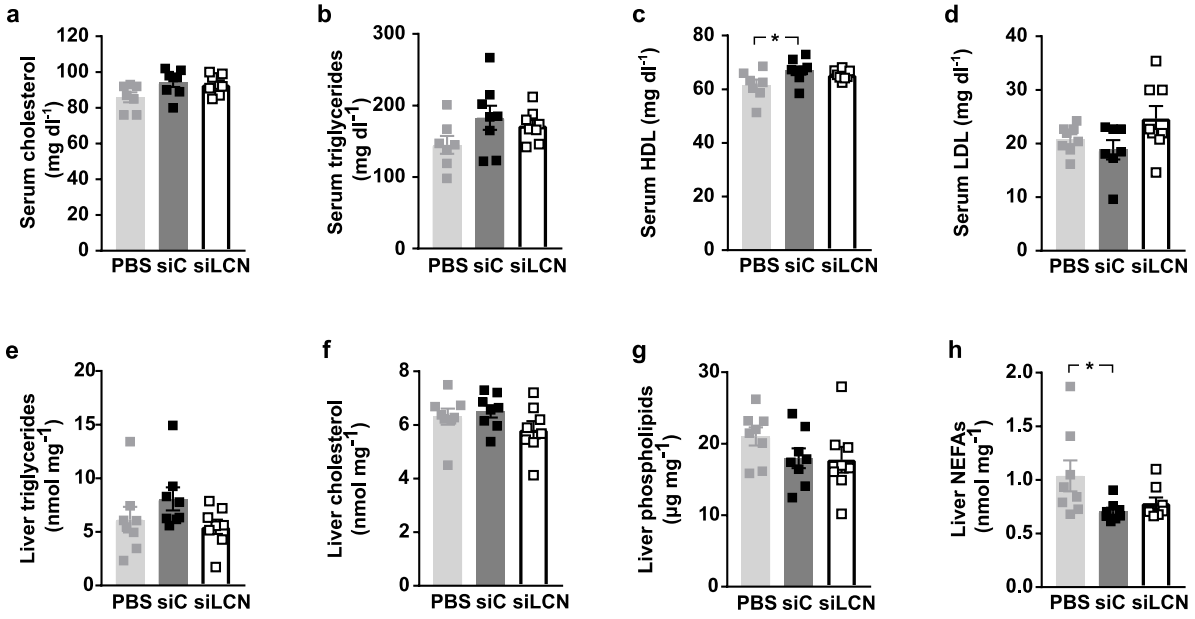

Figure 7 | LNP-Mediated Knockdown of LCN13 Does not Change Lipid Parameters in Serum or Liver in Lean Wild Type Mice

C57BL/6N males (8 weeks) were injected with PBS, LNP carrying either a siRNA directed against *Lcn13* mRNA (siLCN) or a control siRNA targeting luciferase (siC) (0.5 mg/kg, n = 8 mice per group). (**a**)

Cholesterol, (**b**) triglyceride, (**c**) high-density lipoprotein (HDL) and (**d**) low-density lipoprotein (LDL) levels were measured in serum 2 weeks after LNP injection. (**e**) Triglyceride, (**f**) cholesterol, (**g**) phospholipids and (**h**) non-esterified fatty acid (NEFA) levels were determined in liver extracts 2 weeks after LNP injection. Values are shown as mean ± SEM. Study was designed by Lea Katharina Bühler, conducted by Elena Vogl and analyzed by Lea Katharina Bühler. Statistical analysis: All data were analyzed by ordinary one-way ANOVA with Tukey's multiple comparison test. * $p \leq 0.05$.

3.2 Increased LCN13 Availability in the Circulation Does not Influence Glucose Homeostasis

To better understand the role of LCN13 in health, we next examined metabolic consequences of increased circulating LCN13 levels in lean wild type mice. The amount of LCN13 in the blood was experimentally elevated using two different approaches, firstly by multiple intraperitoneal (i.p.) injections of recombinant Fc-LCN13 protein and, secondly, by adeno-associated virus (AAV)-mediated hepatic overexpression.

We produced a LCN13 protein fused to the fragment crystallizable region (Fc) of the human immunoglobulin G (IgG) heavy-chain at its N-terminus in order to extend its half-life. We manufactured the recombinant protein in Chinese hamster ovary (CHO) cells, allowing for mammalian post-translational modifications, and perhaps preserved bioactivity. As a negative control, we purified unfused Fc tag. An additional polyhistidine tag cloned N-terminal to the Fc region facilitated protein purification via immobilized metal ion affinity chromatography (IMAC). The elution profile showed a clear peak in elution fraction number three (Figure 8a), which we subsequently analyzed by sodium dodecyl sulfate polyacrylamide gel electrophoresis (SDS-PAGE). Successful protein purification was verified by coomassie staining as well as immunoblotting with αhuman IgG and αLCN13 (Figure 8b, c). As result of the Fc tag, the recombinant Fc-LCN13 had a predicted molecular weigth of 46 kDa. However, more than one distinct band was detected by the antibodies, a finding which was also reported by others (Cho et al., 2011; Sheng et al., 2011). Of note, the molecular weights of these forms were higher than the predicted 46 kDa, potentially due to post-translational modifications. Additionally, we confirmed the identity and enrichment of the produced recombinant Fc-LCN13 protein by in-solution digest followed by mass spectrometry (MS) analysis (Table 31).

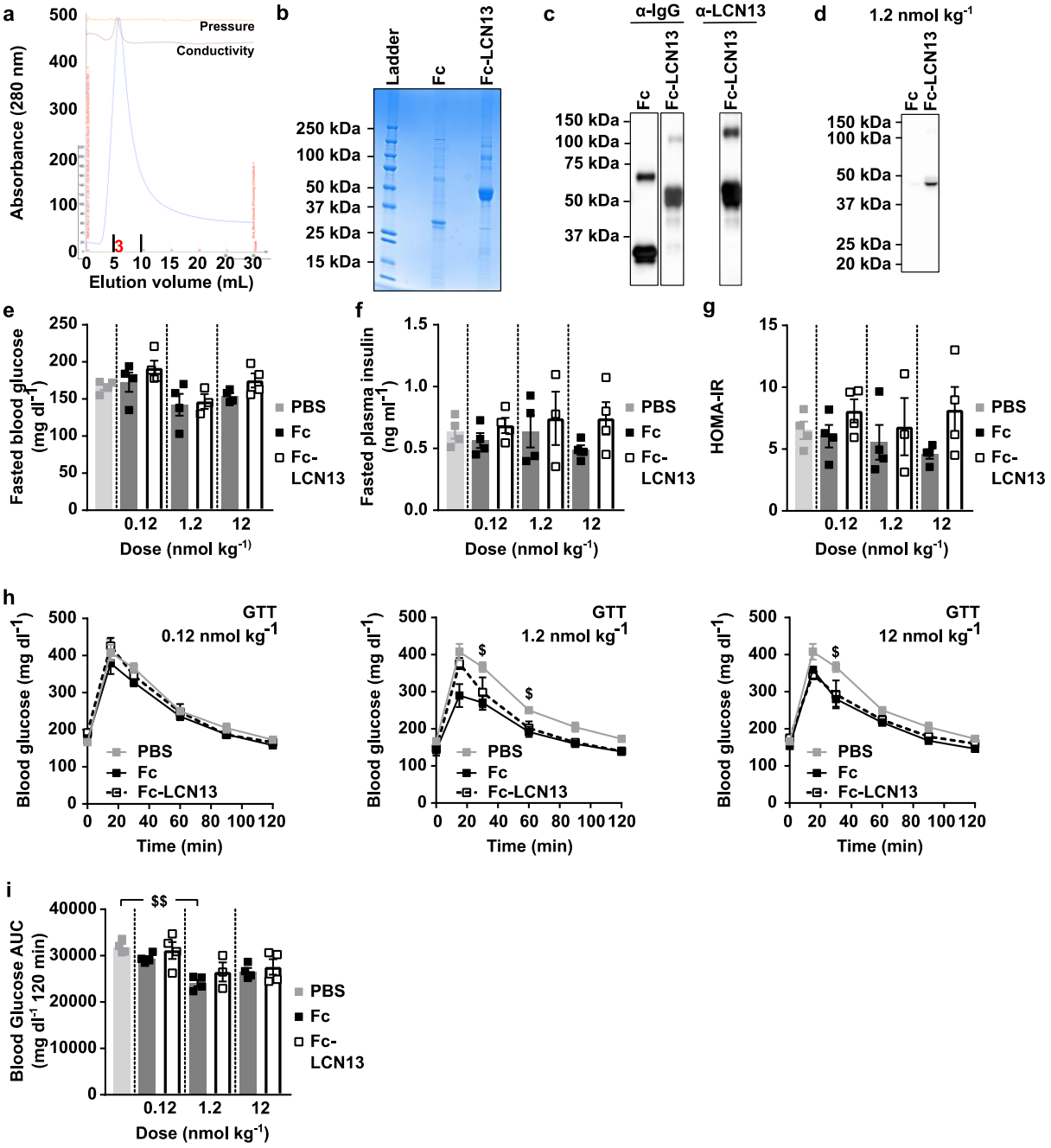

Figure 8 | Treatment with Recombinant Mammalian LCN13 Does not Improve Glucose Homeostasis in Lean Wild Type Mice

(a) Elution profile of Fc-LCN13 during purification via immobilized metal ion affinity chromatography (IMAC). SDS-PAGE of elution fraction three followed by (**b**) coomassie staining as well as (**c**) immunoblotting with αhuman IgG and αLCN13. C57BL/6N males (11 weeks) were i.p. injected with 0.12, 1.2 or 12 nmol/kg recombinant mammalian Fc-LCN13 every other day for 12 days (n = 4 mice per group). As control the same molar concentration of the Fc tag or PBS was injected. Used molar concentrations equal 0.012, 0.12 and 1.2 mg/kg Fc-LCN13 as well as 0.008, 0.08 and 0.8 mg/kg Fc. To secure potential acute effects, mice were additionally injected with the recombinant proteins 2 h before starting the GTT. (**d**) Plasma collected 24 h after recombinant protein administration was immunoblotted with αhuman IgG and αLCN13. (**e**) Fasting (5h) blood glucose, (**f**) plasma insulin levels and (**g**) resulting HOMA-IR after 12 days. (**h**) GTT after 12 days (fasted for 5 h, 2 g/kg D-glucose) and (**i**) corresponding areas under the curve (AUC). Values are shown as mean ± SEM. Fc-LCN13 was produced by Lea Katharina Bühler and purified by Dr. Anastasia Georgiadi. Animal studies were designed, conducted

and analyzed by Lea Katharina Bühler. Statistical analysis: In (**h**), GTT data were analyzed by two-way ANOVA with Geisser-Greenhouse correction and Tukey's multiple comparisons test. All other data were analyzed by ordinary one-way ANOVA with Tukey's multiple comparison test. $ indicates significance between PBS and Fc. $ p≤0.05; $$ p≤0.01.

After successful validation of protein purification, we i.p. injected mice with 0.12, 1.2 or 12 nmol/kg of either Fc-LCN13 or Fc control every other day over the course of twelve days. The injected recombinant protein was detected in the circulation (Figure 8d). Mice with elevated LCN13 levels did not differ with regard to fasting levels of circulating glucose or insulin levels, nor HOMA-IR values across the different treatment groups (Figure 8e-g). Likewise, administration of recombinant Fc-LCN13 did not improve glucose tolerance compared to the Fc-control (Figure 8h, i).

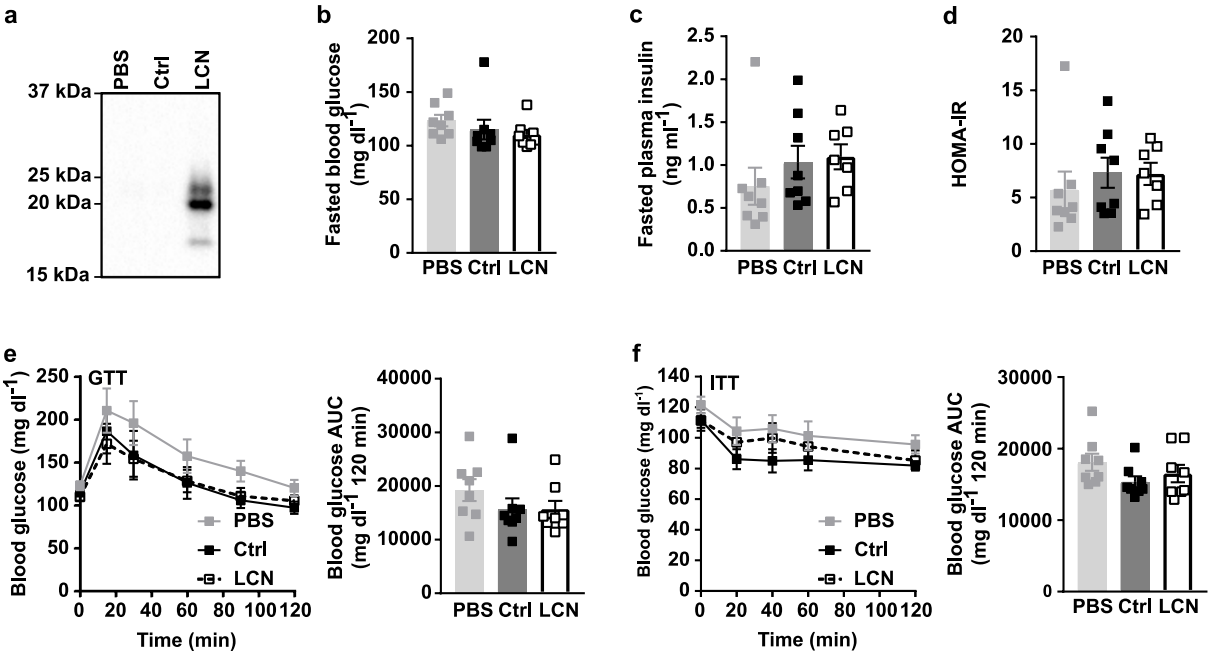

Figure 9 | Increased Endogenous LCN13 Levels Do not Influence Glucose or Insulin Tolerance

C57BL/6N males (7 weeks) were injected with PBS, a control AAV encoding for a mutated, untranslated GFP (Ctrl) or a LCN13 overexpressing AAV (LCN) (5x 10^{11} vg/mouse, n = 8 mice per group). (**a**) Plasma, collected 4 weeks after AAV injection, was immunoblotted with αLCN13. (**b**) Fasting (5h) blood glucose, (**c**) corresponding plasma insulin levels and (**d**) resulting HOMA-IR index 4 weeks after AAV injection. (**e**) i.p. GTT was performed 4 weeks after AAV injection (fasted for 5 hs, 2 g/kg D-glucose). (**f**) i.p. ITT was performed 5 weeks after AAV injection (fasted for 5 h, 0.75 U/kg insulin). Values are shown as mean ± SEM. Study was designed, conducted and analyzed by Lea Katharina Bühler. Statistical analysis: In (**e, f**), GTT and ITT data were analyzed by two-way ANOVA with Geisser-Greenhouse correction and Tukey's multiple comparisons test. All other data were analyzed by ordinary one-way ANOVA with Tukey's multiple comparison test.

In a complementary approach, we raised endogenous LCN13 levels by AAV-mediated, hepatocyte-specific overexpression. Control mice were either injected with PBS or a control AAV encoding for a mutated, untranslated GFP. Liver-specific LCN13 overexpression (OE) resulted in a pronounced increase in LCN13 blood levels (Figure 9a). Reminiscent of the recombinantly produced Fc-LCN13, liver-derived LCN13, although predicted to have a molecular weight of 18 kDa, migrated at multiple molecular weights. Of note, we were unable to detect endogenous LCN13 levels in control mice by the applied technique. The rise of available LCN13 in the circulation did not affect HOMA-IR values, derived from fasting blood glucose and insulin levels (Figure 9 b-d). Concordantly, both glucose and insulin tolerance tests did not reveal any benefit of higher LCN13 expression (Figure 9e, f). Overall, enhancing circulating LCN13 levels in lean wild type mice did not affect glucose homeostasis.

3.3 LCN13 Has neither Curative nor Preventive Effects on Diet-Induced Metabolic Dysfunction

As LCN13 might solely become indispensable under pathological conditions, we investigated its role in diet-induced metabolic dysfunction. Mice were fed a high fat diet (HFD, 60% of calories from fat) for 14 weeks, after which they were i.v. injected with either the LCN13 OE or the control AAV. Successful LCN13 overexpression was demonstrated by increased LCN13 plasma levels three weeks after AAV administration (Figure 10a). *Lcn13* mRNA amounts in liver extracts of LCN13 OE mice were strongly elevated compared to control mice even 16 weeks after AAV injection (Figure 10b). Of note, HFD itself did not significantly alter *Lcn13* mRNA expression in liver compared to mice on a 10% control low fat diet (LFD). AAV administration did not harm liver integrity, as ALT and AST levels were comparable to the PBS-injected group (Figure 10c, d). Long-term LCN13 overexpression over the course of 16 weeks did not affect body or liver weights of respective animals (Figure 10e, f). In line with this, also the weight of white adipose tissues, muscle as well as pancreas did not differ across the different treatment groups (Figure 10g-j). Three weeks after AAV administration, LCN13 OE mice showed slightly reduced fasting blood glucose and insulin levels which resulted in a significant lower HOMA-IR value compared to PBS-injected mice (Figure 10k-m). Eleven weeks later, however, all mice showed comparable plasma glucose and insulin levels as well as HOMA-IR upon fasting (Figure 10k-m). Mice with LCN13-overexpression did not display altered responses to glucose nor to insulin challenge conducted at both one and three months after AAV injection (Figure 10n-q). In accordance, random-fed blood glucose levels as well as the parameter for long-term glycemic control HbA1c did not reveal any positive effect of LCN13 overexpression (Figure 10r, s).

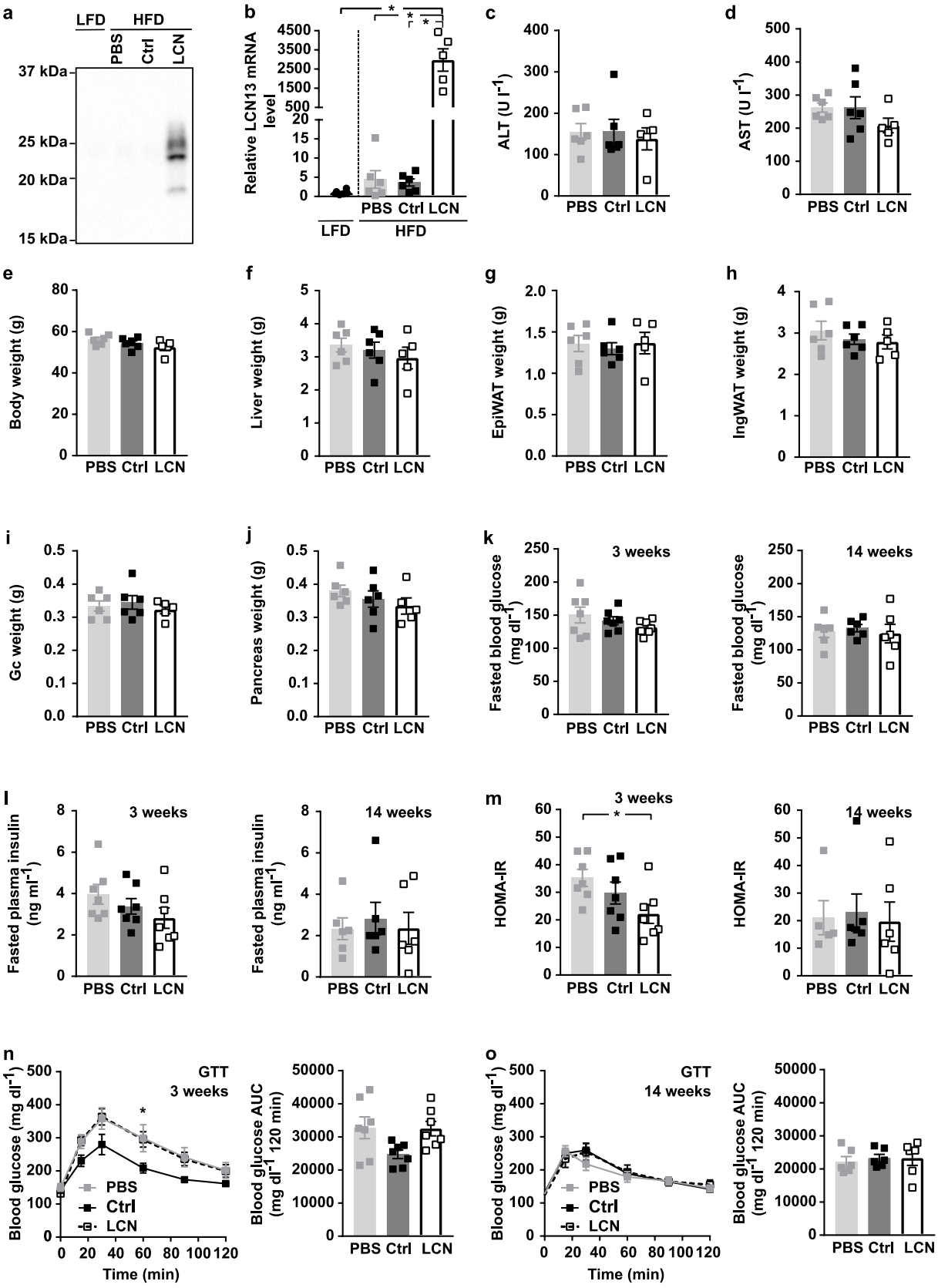
a
LFD
HFD
PBS
Ctrl
LCN
37 kDa
25 kDa
20 kDa
15 kDa
b
Relative LCN13 mRNA level
PBS Ctrl LCN
LFD
HFD
c
ALT (U l-1)
d
AST (U l-1)
e
Body weight (g)
f
Liver weight (g)
g
EpiWAT weight (g)
h
IngWAT weight (g)
i
Gc weight (g)
j
Pancreas weight (g)
k
Fasted blood glucose (mg dl-1)
3 weeks
14 weeks
l
Fasted plasma insulin (ng ml-1)
3 weeks
14 weeks
m
HOMA-IR
3 weeks
14 weeks
n
GTT
3 weeks
Blood glucose (mg dl-1)
Time (min)
PBS
Ctrl
LCN
Blood glucose AUC (mg dl-1 120 min)
o
GTT
14 weeks
Blood glucose (mg dl-1)
Time (min)
Blood glucose AUC (mg dl-1 120 min)

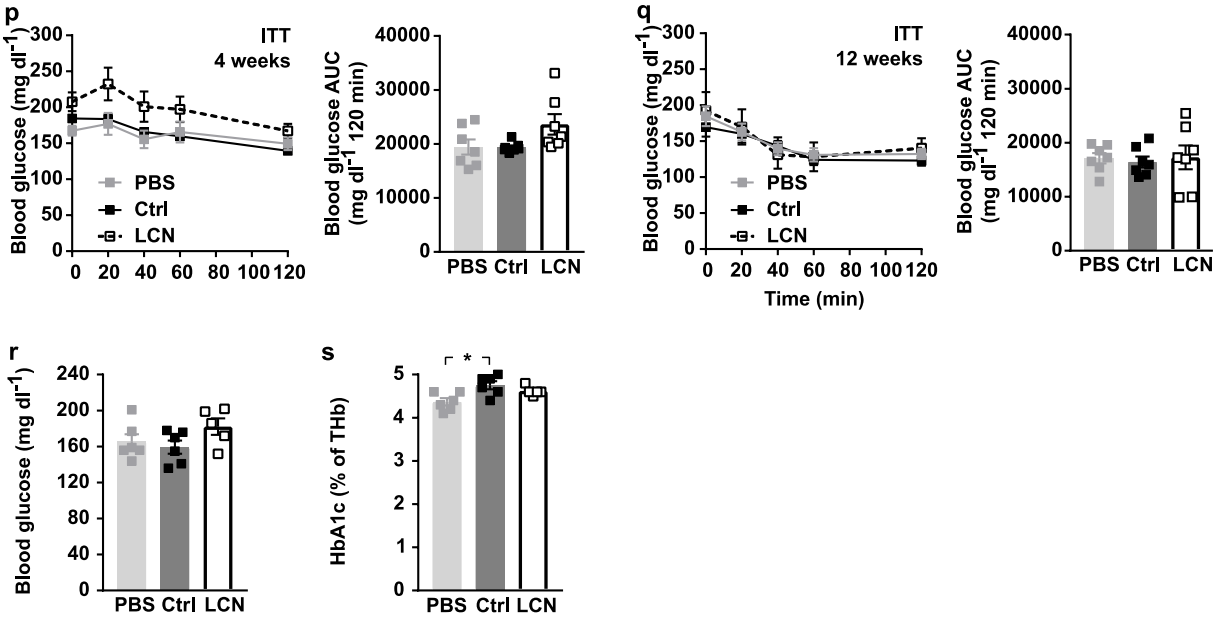

Figure 10 | AAV-Mediated Overexpression of LCN13 Has no Curative Effect on Diet-Induced Metabolic Dysfunction

C57BL/6N males (7 weeks) were fed either a 60% high fat diet (HFD) or a control low fat diet (LFD; 10% calories from fat) for 14 weeks. Subsequently, they were injected with PBS, a control AAV encoding for a mutated, untranslated GFP (Ctrl) or a LCN13 overexpressing AAV (LCN) (5x 10^{11} vg/mouse, n = 5-7 mice per group). (**a**) Plasma, collected 3 weeks after AAV injection, was immunoblotted with αLCN13. (**b**) *Lcn13* mRNA abundance was measured in liver extracts by qRT-PCR 16 weeks after AAV injection. (**c**) Alanine transaminase (ALT) and (**d**) aspartate transaminase (AST) were measured in serum 16 weeks after AAV injection. (**e**) Body weight, and the weights of (**f**) liver, (**g**) epididymal white adipose tissue (EpiWAT), (**h**) inguinal white adipose tissue (IngWAT), (**i**) gastrocnemius (GC) muscle as well as (**j**) pancreas were measured 16 weeks after AAV injection. (**k**) Fasting (16h) blood glucose, (**l**) corresponding plasma insulin levels and (**m**) resulting HOMA-IR index 3 and 14 weeks after AAV injection. (**n**) i.p. GTT was performed 3 weeks after AAV injection (fasted for 16 h, 1 g/kg D-glucose). * indicates significance between LCN and Ctrl. (**o**) i.p. GTT was performed 14 weeks after AAV injection (fasted for 16 h, 1 g/kg D-glucose). (**p**) i.p. ITT was performed 4 weeks after AAV injection (fasted for 5 hs, 1 U/kg insulin). (q) i.p. ITT was performed 12 weeks after AAV injection (fasted for 5 hs, 1.5 U/kg insulin). (**r**) Random fed blood glucose and (**s**) HbA1c levels in same mice 16 weeks after AAV injection. Values are shown as mean ± SEM. Study was designed, conducted and analyzed by Lea Katharina Bühler. Statistical analysis: In (**b**), data was analyzed by Welch's ANOVA with Dunnett's T3 multiple comparison test. In (**n-q**), GTT and ITT data were analyzed by two-way ANOVA with Geisser-Greenhouse correction and Tukey's multiple comparisons test. All other data were analyzed by ordinary one-way ANOVA with Tukey's multiple comparison test. * $p \leq 0.05$.

Next, we analyzed lipid parameters in serum covering cholesterol, triglycerides, HDL-cholesterol and LDL-cholesterol which did not change upon LCN13 overexpression (Figure 11a-d). We also measured liver expression of Stearoyl coenzyme A desaturase 1 (*Scd1*) and peroxisome proliferator-activated receptor gamma (*Pparg*) which play crucial roles in lipogenesis and lipid accumulation (Ferre, 2004; Paton and Ntambi, 2009). The increase of available LCN13 did not influence the expression of the analyzed genes in HFD-fed mice (Figure 11e, f).

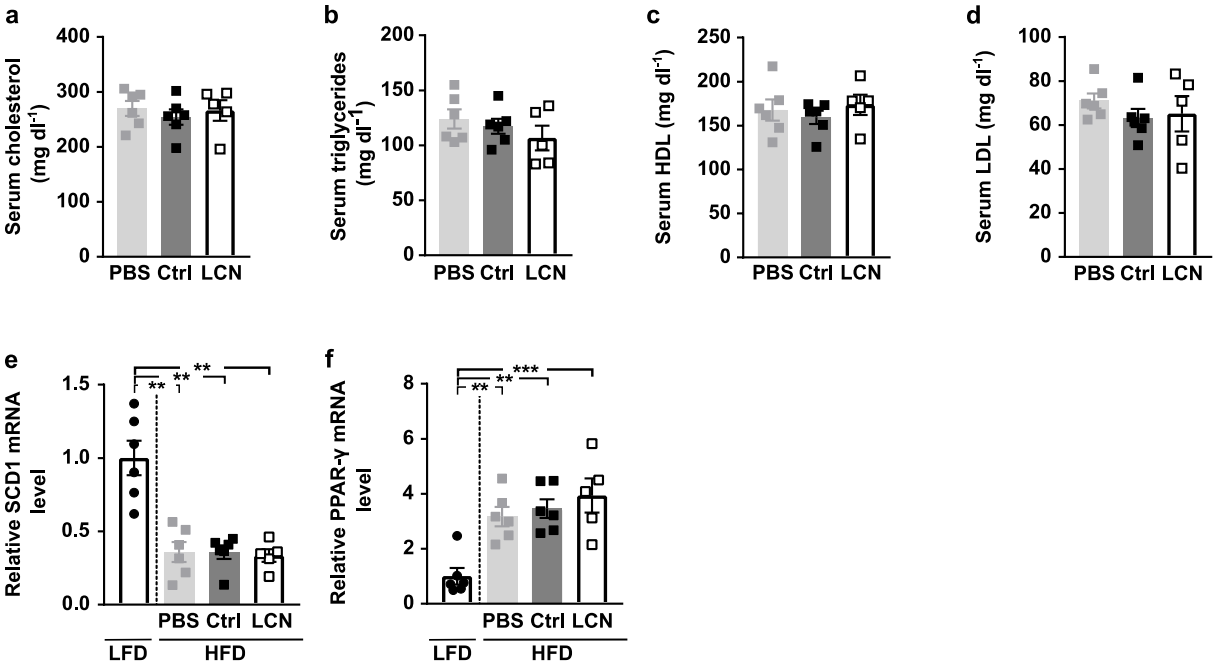

Figure 11 | AAV-Mediated Overexpression of LCN13 Does not Influence Lipid Metabolism in Mice on HFD

C57BL/6N males (7 weeks) were fed either a 60% high fat diet (HFD) or a control low fat diet (LFD; 10%) for 14 weeks. Subsequently, they were injected with PBS, an empty control AAV (Ctrl) or a LCN13 overexpressing AAV (LCN) (5x 10^{11} vg/mouse, n = 5-7 mice per group). (**a**) Cholesterol, (**b**) triglyceride, (**c**) HDL and (**d**) LDL levels were measured in serum 16 weeks after AAV injection. (**e**) Stearoyl coenzyme A desaturase 1 (*Scd1*) and (**f**) peroxisome proliferator-activated receptor gamma (*Pparg*) mRNA abundances were measured in liver extracts by qRT-PCR 16 weeks after AAV injection. Values are shown as mean ± SEM. Study was designed, conducted and analyzed by Lea Katharina Bühler. Statistical analysis: In (**e**), data was analyzed by Welch's ANOVA with Dunnett's T3 multiple comparison test. All other data were analyzed by ordinary one-way ANOVA with Tukey's multiple comparison test. ** p≤0.01; *** p≤0.001

To ensure elevated LCN13 levels within its therapeutic time window, we next designed a HFD study in which animals were subjected to AAV-mediated hepatic LCN13 overexpression, before the HFD was given (Figure 12a). LCN13 overexpression was confirmed both at the protein and the mRNA level in plasma and liver extracts respectively (Figure 9a, Figure 12b). Reminiscent of the previous HFD study, in which hepatic *Lcn13* levels were increased in already obese mice, *Lcn13* mRNA levels did not differ between chow and HFD control groups.

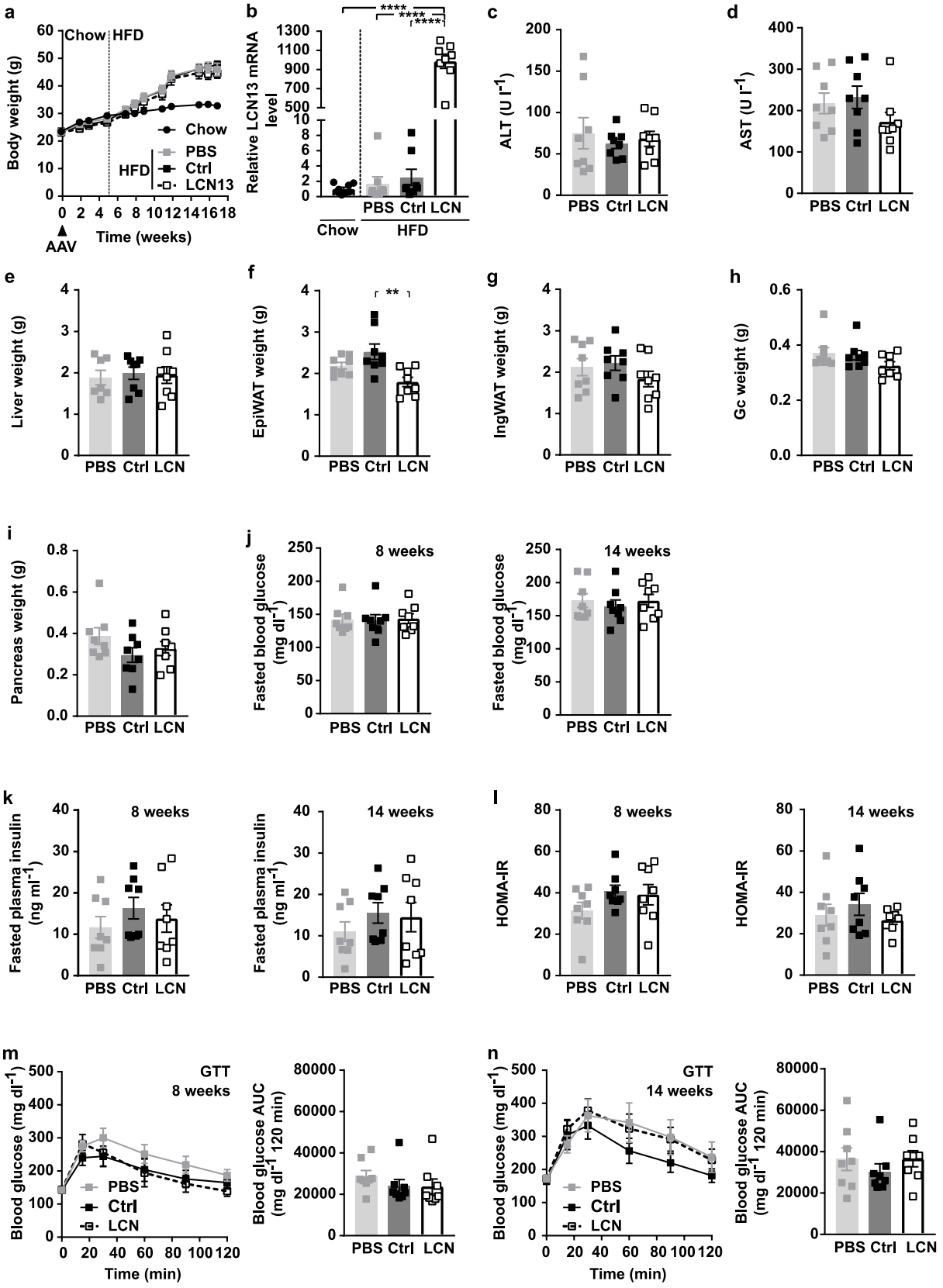
a
Body weight (g)
Chow
HFD
Chow
PBS
Ctrl
LCN13
Time (weeks)
AAV
b
Relative LCN13 mRNA level
****
****
****
PBS Ctrl LCN
Chow
HFD
c
ALT (U l-1)
PBS Ctrl LCN
d
AST (U l-1)
PBS Ctrl LCN
e
Liver weight (g)
PBS Ctrl LCN
f
EpiWAT weight (g)
**
PBS Ctrl LCN
g
IngWAT weight (g)
PBS Ctrl LCN
h
Gc weight (g)
PBS Ctrl LCN
i
Pancreas weight (g)
PBS Ctrl LCN
j
Fasted blood glucose (mg dl-1)
8 weeks
PBS Ctrl LCN
Fasted blood glucose (mg dl-1)
14 weeks
PBS Ctrl LCN
k
Fasted plasma insulin (ng ml-1)
8 weeks
PBS Ctrl LCN
Fasted plasma insulin (ng ml-1)
14 weeks
PBS Ctrl LCN
l
HOMA-IR
8 weeks
PBS Ctrl LCN
HOMA-IR
14 weeks
PBS Ctrl LCN
m
Blood glucose (mg dl-1)
GTT
8 weeks
PBS
Ctrl
LCN
Time (min)
Blood glucose AUC (mg dl-1 120 min)
PBS Ctrl LCN
n
Blood glucose (mg dl-1)
GTT
14 weeks
PBS
Ctrl
LCN
Time (min)
Blood glucose AUC (mg dl-1 120 min)
PBS Ctrl LCN

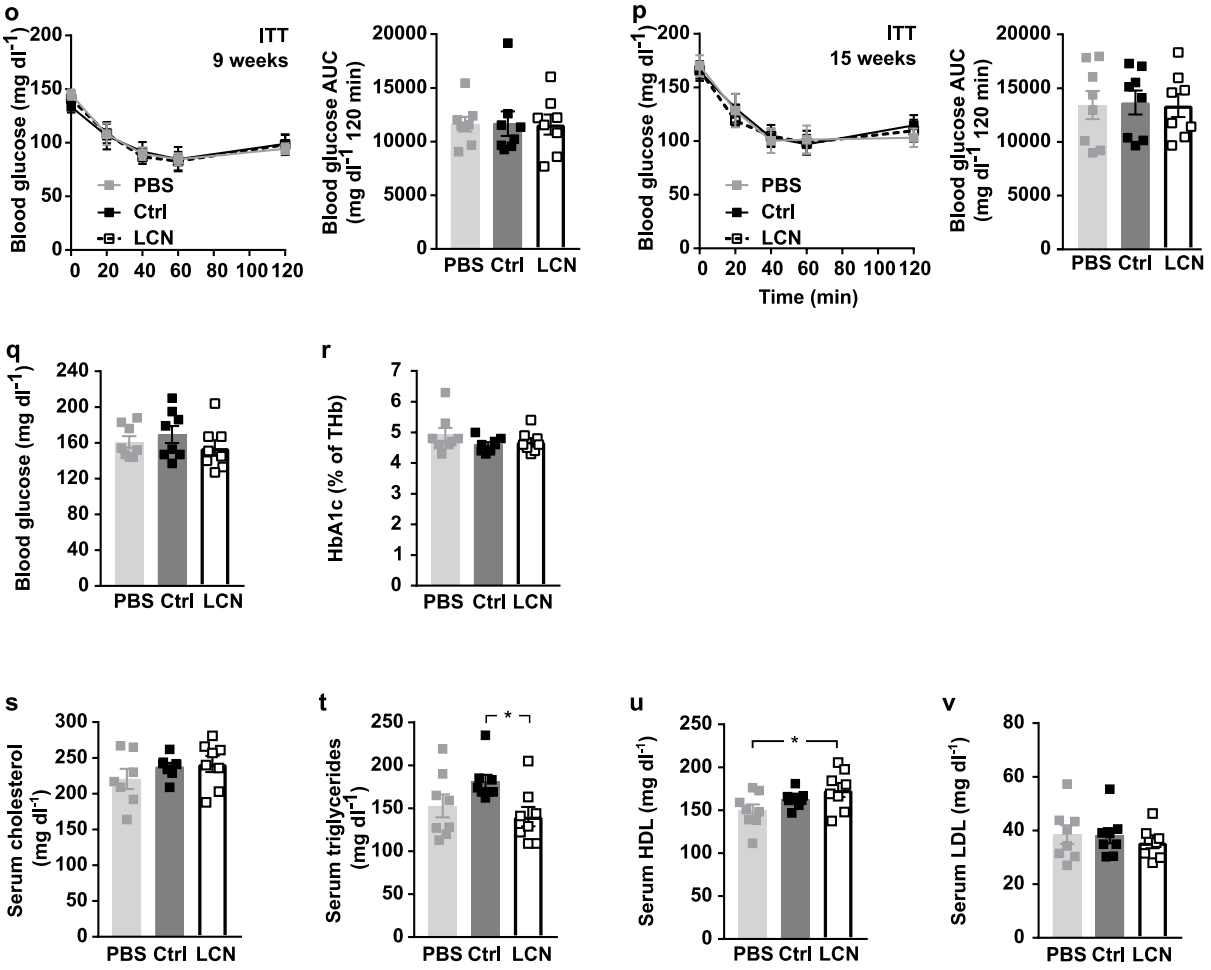

Figure 12 | AAV-Mediated Overexpression of LCN13 Has no Preventive Effect on Diet-Induced Metabolic Dysfunction

C57BL/6N males (7 weeks) were injected with PBS, a control AAV encoding for a mutated, untranslated GFP (Ctrl) or a LCN13 overexpressing AAV (LCN) (5x 10^{11} vg/mouse, n = 8 mice per group). After 5 weeks, the cow diet was switched to a 60 % high fat diet (HFD). Control mice were continuously fed with chow diet. Metabolic phenotyping conducted before HFD start is summarized in Figure 9. (**a**) Body weight over the course of 17 weeks. Dashed line indicates start of HFD feeding. (**b**) *Lcn13* mRNA abundance was measured in liver extracts by qRT-PCR 17 weeks after AAV injection. (**c**) Alanine transaminase (ALT) and (**d**) aspartate transaminase (AST) were measured in serum 17 weeks after AAV injection. Weights of (**e**) liver, (**f**) epididymal white adipose tissue (EpiWAT), (**g**) inguinal white adipose tissue (IngWAT), (**h**) gastrocnemius (GC) muscle as well as (**i**) pancreas were measured 17 weeks after AAV injection. (**j**) Fasting (5h) blood glucose, (**k**) corresponding plasma insulin levels and (**l**) resulting HOMA-IR index 8 and 14 weeks after AAV injection. i.p. GTT was performed (**m**) 8 and (**n**) 14 weeks after AAV injection (fasted for 5 h, 2 g/kg D-glucose). i.p. ITT was performed (**o**) 9 and (**p**) 15 weeks after AAV injection (fasted for 5 h, 1.2 and 1.5 U/kg insulin, respectively). (**q**) Random fed blood glucose and (**r**) HbA1c levels in same mice 17 weeks after AAV injection. (**s**) Cholesterol, (**t**) triglyceride, (**u**) high density lipoprotein (HDL) and (**v**) low density lipoprotein (LDL) levels were measured in serum 17 weeks after AAV injection. Values are shown as mean ± SEM. Study was designed, conducted and analyzed by Lea Katharina Bühler. Statistical analysis: In (**b**), data was analyzed by Welch's ANOVA with Dunnett's T3 multiple comparison test. In (**m-p**), GTT and ITT data were analyzed by two-way ANOVA with Geisser-Greenhouse correction and Tukey's multiple comparisons test. All other data were analyzed by ordinary one-way ANOVA with Tukey's multiple comparison test. * $p \leq 0.05$; ** $p \leq 0.01$; **** $p \leq 0.0001$.

Seventeen weeks after AAV administration, all mice on HFD had comparable body and organ weights, except for the epididymal fat whose weight was significantly reduced in LCN13 OE mice compared to mice receiving the control virus (Figure 12e-i). Both eight and fourteen weeks after AAV administration, glucose and insulin levels upon fasting as well as HOMA-IR levels were uniform in all mice on HFD, regardless of the treatment (Figure 12j-l). The rise of LCN13 liver and blood levels had no impact on glucose homeostasis or insulin sensitivity (Figure 12m-p). Random fed blood glucose and long-term blood glucose levels were comparable between all mice (Figure 12q, r). Similarly, all analyzed serum lipids did not differ significantly between LCN13 OE mice and the two control groups (Figure 12s-v). Taken together, these data showed that, regardless of the time point of administration, hepatocyte-specific AAV-mediated LCN13 overexpression did not improve diet-induced insulin resistance and glucose intolerance in mice.

3.4 Replenishing Circulating LCN13 Levels Has no Curative Effect in Mice with Monogenic Type 2 Diabetes

The db/db mouse is a genetic mouse model of diabetes, homozygous for a specific spontaneous single point mutation in the leptin receptor gene (*Lepr*^{db}; Chen et al., 1996). Seeing that LCN13 levels tended to be decreased in db/db mice compared to control mice of the same genetic background (not consistently significant; Figure 13a), made us wonder whether elevating its hepatic expression level could ameliorate the diabetic phenotype of these mice. Efficacious hepatic LCN13 overexpression and secretion into the circulation was validated (Figure 13a, b). LCN13 overexpression did not compromise liver health shown by unaltered ALT and AST serum levels (Figure 13c, d). 15 weeks of LCN13 overexpression did not influence body weight nor the weights of liver, adipose, muscle and pancreatic tissues (Figure 13e-j). Fasting blood glucose and insulin levels did not reveal any differences (Figure 13k, l). In line with this, the calculated HOMA-IR values were comparable across the different treatment groups (Figure 13m). Blood glucose control assessed in the random-fed state or via HbA1c was not influenced by higher LCN13 levels (Figure 13n, o). The rise of available LCN13 in the circulation did also not affect the response to glucose or insulin challenge (Figure 13p, q). Subsequently, we analyzed lipid metabolism via serum parameters and liver expression of the lipogenic genes *Scd1* and *Pparg*. All analyzed parameters were akin (Figure 14). In summary, reminiscent of the mouse model of diet-induced metabolic dysfunction, elevated LCN13 levels did neither improve systemic insulin sensitivity nor glucose and lipid homeostasis in db/db mice.

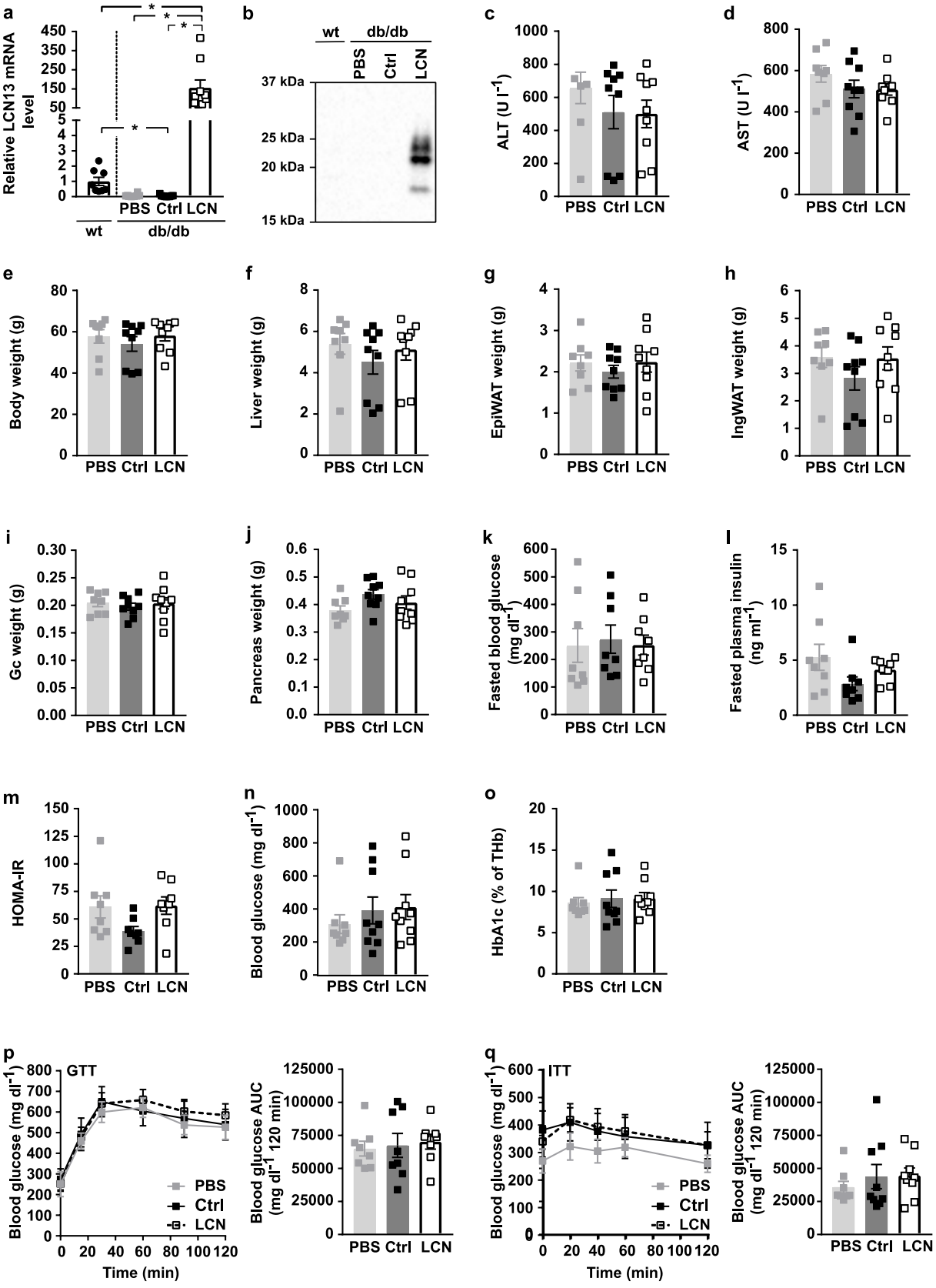

Figure 13 | AAV-Mediated Overexpression of LCN13 in db/db Mice Does not Improve the Diabetic Phenotype

db/db males (B6.BKS(D)-*Lepr*^{db}/J, 7 weeks) were injected with PBS, a control AAV encoding for a mutated, untranslated GFP (Ctrl) or a LCN13 overexpressing AAV (LCN13) (5x 10^{11} vg/mouse, n = 8-9

mice per group). Mice with the same genetic background (C57BL/6J, 7 weeks) were used as wildtype controls (wt). (**a**) *Lcn13* mRNA abundance was measured in liver extracts by qRT-PCR 15 weeks after AAV injection. (**b**) Plasma, collected 4 weeks after AAV injection, was immunoblotted with an LCN13 antibody. (**c**) Alanine transaminase (ALT) and (**d**) aspartate transaminase (AST) were measured in serum 15 weeks after AAV injection. (**e**) Body weight and the weight of (**f**) liver, (**g**) epididymal white adipose tissue (EpiWAT), (**h**) inguinal white adipose tissue (IngWAT), (**i**) gastrocnemius (GC) muscle as well as (**j**) pancreas were measured 15 weeks after AAV injection. (**k**) Fasting (16h) blood glucose, (**l**) corresponding plasma insulin levels and (**m**) resulting HOMA-IR index 10 weeks after AAV injection. (**n**) Random fed blood glucose and (**o**) HbA1c levels in same mice 15 weeks after AAV injection. (**p**) i.p. GTT was performed 10 weeks after AAV injection (fasted for 16 h, 1 g/kg D-glucose). (**q**) i.p. ITT was performed 14 weeks after AAV injection (fasted for 5 h, 2 U/kg insulin). Values are shown as mean ± SEM. Study was designed, conducted and analyzed by Lea Katharina Bühler. Statistical analysis: In (**a**), data was analyzed by Welch's ANOVA with Dunnett's T3 multiple comparison test. In (**p, q**), GTT and ITT data were analyzed by two-way ANOVA with Geisser-Greenhouse correction and Tukey's multiple comparisons test. All other data were analyzed by ordinary one-way ANOVA with Tukey's multiple comparison test.* $p \leq 0.05$.

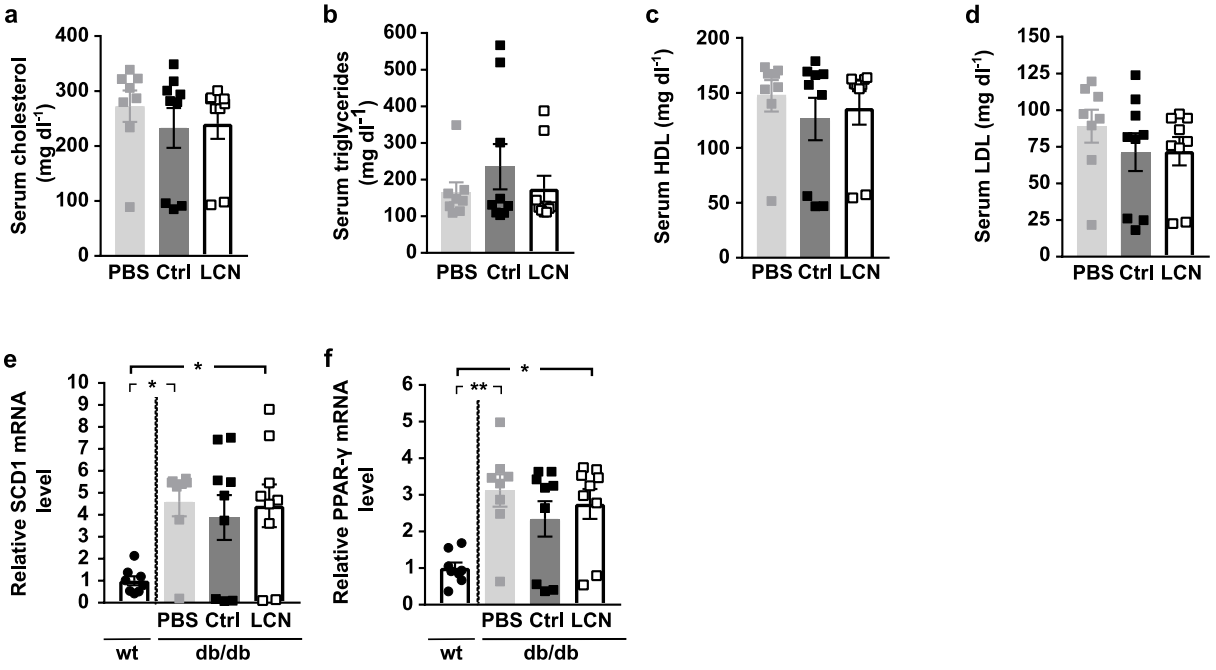

Figure 14 | AAV-Mediated Overexpression of LCN13 Does not Influence Lipid Metabolism in db/db Mice

db/db males (B6.BKS(D)-*Lepr*^{db}/J, 7 weeks) were injected with PBS, a control AAV encoding for a mutated, untranslated GFP (Ctrl) or a LCN13 overexpressing AAV (LCN) (5x 10^{11} vg/mouse, n = 8-9 mice per group). Mice with the same genetic background (C57BL/6J, 7 weeks) were used as wildtype controls (wt). (**a**) Cholesterol, (**b**) triglyceride, (**c**) high density lipoprotein (HDL) and (**d**) low density lipoprotein (LDL) levels were measured in serum 15 weeks after AAV injection. (**e**) Stearoyl coenzyme A desaturase 1 (*Scd1*) and (**f**) peroxisome proliferator-activated receptor gamma (*Pparg*) mRNA abundances were measured in liver extracts by qRT-PCR 15 weeks after AAV injection. Values are shown as mean ± SEM. Study was designed, conducted and analyzed by Lea Katharina Bühler. Statistical analysis: All data were analyzed by ordinary one-way ANOVA with Tukey's multiple comparison test. * $p \leq 0.05$; ** $p \leq 0.01$.

Supra-physiological LCN13 levels, achieved in all preceding experiments, could lead to desensitization and/or hepatic ER stress and accumulation of misfolded proteins. To address whether these factors could have confounded beneficial effects of LCN13 treatment, we additionally tested two lower doses of the LCN13 overexpressing AAV in db/db mice. The administered viral doses of $5x10^9$, $5x10^{10}$ and $5x10^{11}$ resulted in 5, 70 and 511 times higher hepatic *Lcn13* mRNA levels compared to wild type controls, respectively (Figure 15a). The varying *Lcn13* expression levels in liver were mirrored by LCN13 plasma levels (Figure 15b). As before, there was no apparent liver damage upon AAV injection (Figure 15c, d) and no variations in body or organ weights (Figure 15e-j). There was no significant difference in fasting blood glucose and insulin levels or in HOMA-IR values between the different treatment groups (Figure 15k-m). All db/db mice showed similar glucose and insulin tolerance and did also not differ in serum lipids regardless of the administered AAV amount (Figure 15n-s). Overall, the investigated viral doses covered a wide range of LCN13 levels in the circulation but did not have any effect on glucose or insulin metabolism. Thus, the high viral dose applied in all other experiments did not appear to be the reason why LCN13 overexpression had not improved diabetes.

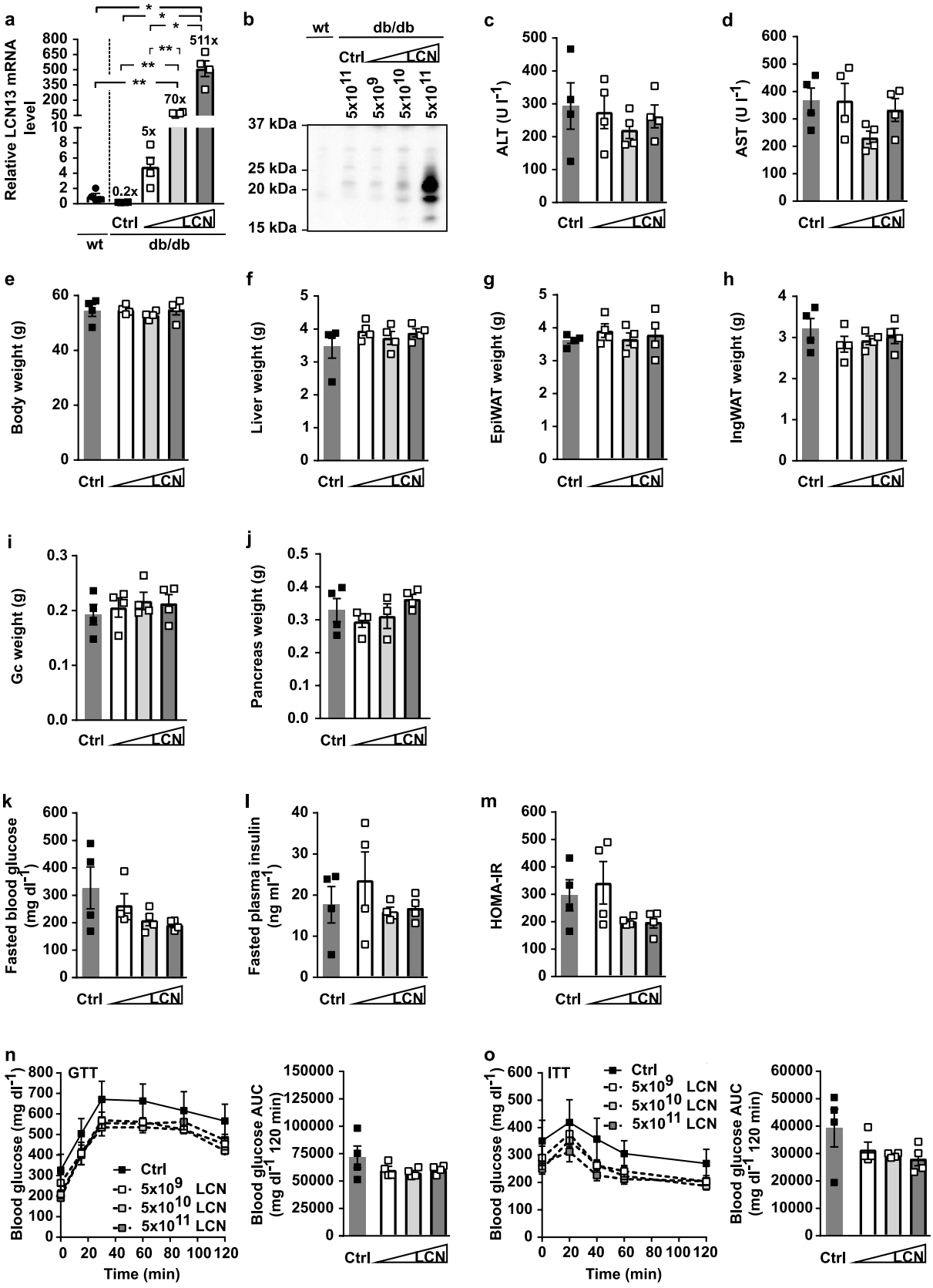
a
Relative LCN13 mRNA level
0.2x
5x
70x
511x
Ctrl
LCN
wt
db/db
b
wt
db/db
Ctrl
LCN
5x10^11
5x10^9
5x10^10
5x10^11
37 kDa
25 kDa
20 kDa
15 kDa
c
ALT (U l^-1)
d
AST (U l^-1)
e
Body weight (g)
f
Liver weight (g)
g
EpiWAT weight (g)
h
IngWAT weight (g)
i
Gc weight (g)
j
Pancreas weight (g)
k
Fasted blood glucose (mg dl^-1)
l
Fasted plasma insulin (ng ml^-1)
m
HOMA-IR
n
GTT
Blood glucose (mg dl^-1)
Time (min)
Ctrl
5x10^9 LCN
5x10^10 LCN
5x10^11 LCN
Blood glucose AUC (mg dl^-1 120 min)
o
ITT
Blood glucose (mg dl^-1)
Time (min)
Ctrl
5x10^9 LCN
5x10^10 LCN
5x10^11 LCN
Blood glucose AUC (mg dl^-1 120 min)

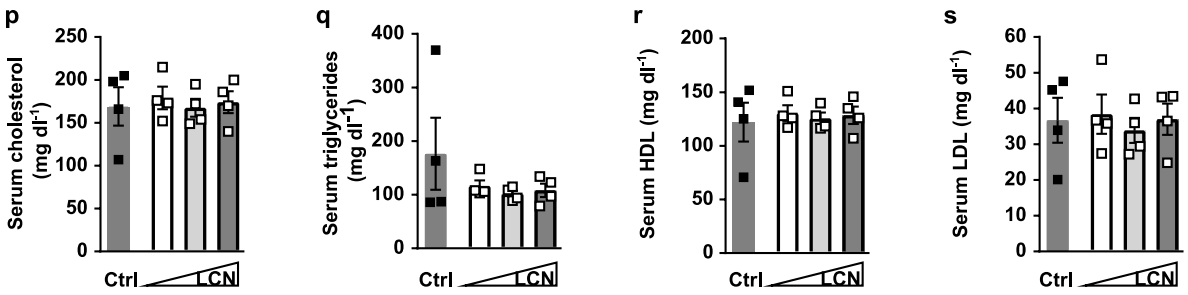

Figure 15 | Titrated Levels of Overexpressed LCN13 in db/db Mice Does not Influence Experimental Outcome

db/db males (B6.BKS(D)-*Lepr*^{db}/J, 7 weeks) were injected with PBS, a control AAV encoding for a mutated, untranslated GFP (Ctrl) (5x 10^{11} vg/mouse) or different doses of the LCN13 overexpressing AAV (LCN) (5x $10^{9,\ 10\ or\ 11}$ vg/mouse, n = 4 mice per group). Mice with the same genetic background (C57BL/6J, 7 weeks) were used as wildtype controls (wt). (**a**) Plasma, collected 3 weeks after AAV injection, was immunoblotted with an LCN13 antibody. (**b**) *Lcn13* mRNA abundance was measured in liver extracts by qRT-PCR 6 weeks after AAV injection. (**c**) Alanine transaminase (ALT) and (**d**) aspartate transaminase (AST) levels were measured in serum 6 weeks after AAV injection. (**e**) Body weight and the weight of (**f**) liver, (**g**) epididymal white adipose tissue (EpiWAT), (**h**) inguinal white adipose tissue (IngWAT), (**i**) gastrocnemius (GC) muscle as well as (**j**) pancreas were measured 6 weeks after AAV injection. (**k**) Fasting (5h) blood glucose, (**l**) corresponding plasma insulin levels and (**m**) resulting HOMA-IR index 4 weeks after AAV injection. (**n**) i.p. GTT was performed 4 weeks after AAV injection (fasted for 5 hs, 1 g/kg D-glucose). (**o**) i.p. ITT was performed 5 weeks after AAV injection (fasted for 5 hs, 3 U/kg insulin). (**p**) Cholesterol, (**q**) triglyceride, (**r**) high density lipoprotein (HDL) and (**s**) low density lipoprotein (LDL) were measured in serum 6 weeks after AAV injection. Values are shown as mean ± SEM. Study was designed, conducted and analyzed by Lea Katharina Bühler. Statistical analysis: In (**a, k-n**), data were analyzed by Welch's ANOVA with Dunnett's T3 multiple comparison test. In (**n-o**), GTT and ITT data were analyzed by two-way ANOVA with Geisser-Greenhouse correction and Tukey's multiple comparisons test. All other data were analyzed by ordinary one-way ANOVA with Tukey's multiple comparison test. * p≤0.05; ** p≤0.01.

3.5 Other Lipocalin Family Members Do not Compensate for Varying Levels of LCN13

To better understand why LCN13 did not regulate glucose and lipid metabolism in our studies, we screened for the expression of other lipocalin family members in metabolically relevant organs in response to decreased or increased hepatic *Lcn13* levels. We hypothesized that other lipocalins could compensate for changes in *Lcn13* expression. This was likely because other lipocalins have also been implicated in metabolic control (see Table 1). Interestingly, different lipocalins, such as bovine odorant binding protein (OBP) and the mouse major urinary protein, can bind to the same receptor (Boudjelal et al., 1996; Flower, 2000). From this we concluded that also LCN13/OBP2A could compete with other lipocalins for the same receptor expressed on peripheral tissues. Therefore, a compensatory up or downregulation of such lipocalin family members could explain why we did not observe any effect upon changes in LCN13 expression. We included lipocalin family members which share a high amino acid sequence similarity with LCN13 such as LCN14 (65%), LCN3 (56%), LCN4 (48%) and prostaglandin D2 synthase (PTGDS; 39%). In addition, we also analyzed lipocalins which were already reported to play a role in glucose metabolism and insulin sensitivity. These included LCN2, LCN5, LCN14, apolipoprotein D (ApoD), apolipoprotein M (ApoM), MUP1, PTGDS and RBP4 (see Table 1). Firstly, we measured the expression of the stated lipocalin family members in liver, white adipose tissues as well as in muscle of wild type mice in response to LNP-mediated hepatic knockdown of LCN13. None of the analyzed lipocalin family members were differently expressed upon LCN13 knockdown (Figure 16). To further examine the connection between LCN13 and other lipocalin family members, we measured their expression in db/db mice whose downregulated LCN13 levels were replenished by administration of the LCN13 OE AAV. *Lcn2* mRNA levels were increased in liver, inguinal white adipose tissue and in muscle of db/db mice compared to wild type controls, which is congruent with the literature (Yan et al., 2007; Figure 17a, c, d). Similarly to the knockdown study, LCN13 overexpression did not affect the expression of other lipocalin family members. Of note, even though the LCN13 OE AAV encodes for LCN13 under the control of the hepatocyte-specific promoter LP1, *Lcn13* mRNA evels were also slightly increased in iWAT compared to control groups albeit to a much lower extend than in the liver. Collectively, the expression of the investigated lipocalin family members were not coupled to experimentally manipulated hepatic *Lcn13* levels.

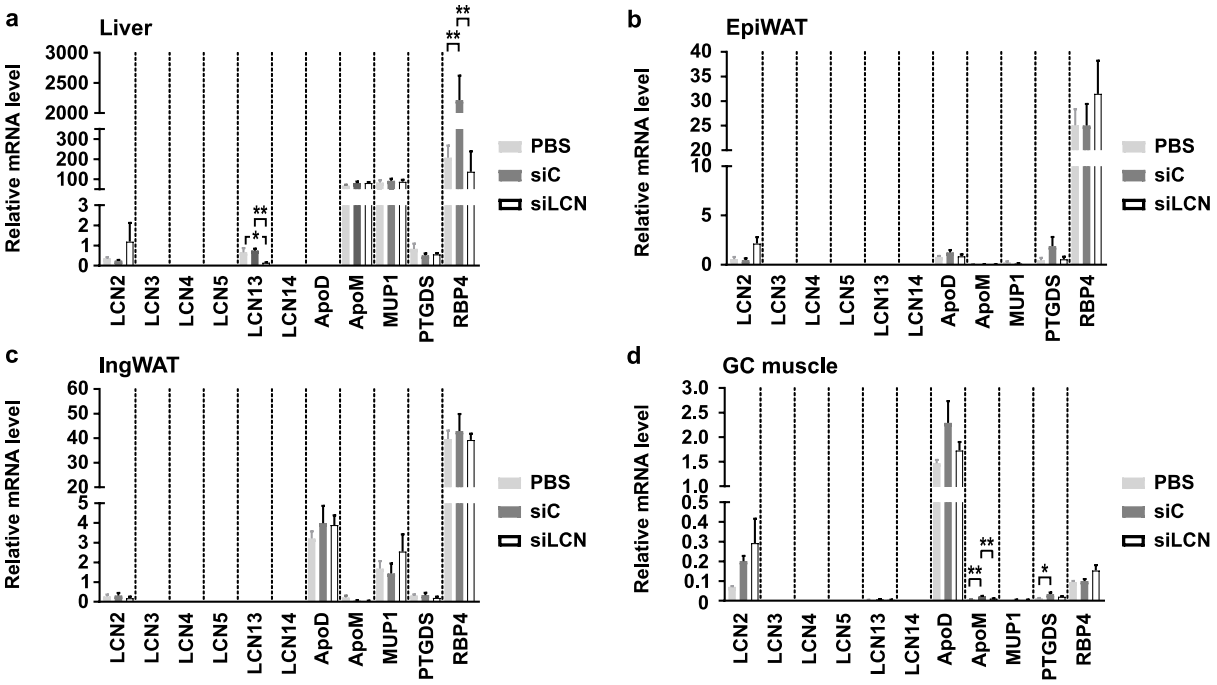

Figure 16 | LNP-Mediated Knockdown of LCN13 Is not Accompanied by Expression Changes of Other Lipocalin Family Members in Liver, Adipose Tissues or Muscle

C57BL/6N males (8 weeks) were injected with PBS, liponanoparticles (LNP) carrying either a siRNA directed against Lcn13 mRNA (siLCN) or a control siRNA targeting luciferase (siC) (0.5 mg/kg, n = 8 mice per group). mRNA abundances of lipocalin family members including *Lcn2*, *Lcn3*, *Lcn4*, *Lcn5*, *Lcn13*, *Lcn14*, Apolipoprotein D (*Apod*), Apolipoprotein M (*Apom*), Major urinary protein 1 (*Mup1*), Prostaglandin D2 synthase (*Ptgds*) and Retinol binding protein 4 (*Rbp4*) were measured in (**a**) liver, (**b**) epididymal white adipose tissue (EpiWAT), (**c**) inguinal white adipose tissue (IngWAT) and (**d**) gastrocnemius (GC) muscle extracts by qRT-PCR 2 weeks after LNP injection. Values are shown as mean ± SEM. Study was designed by Lea Katharina Bühler, conducted by Elena Vogl and analyzed by Lea Katharina Bühler. Statistical analysis: Outliers were identified by the ROUT method (Q = 1%). Data with unequal variances were assessed using Welch's ANOVA with Dunnett's T3 multiple comparison test. All other data were analyzed by ordinary one-way ANOVA with Tukey's multiple comparison test. * $p \leq 0.05$; ** $p \leq 0.01$.

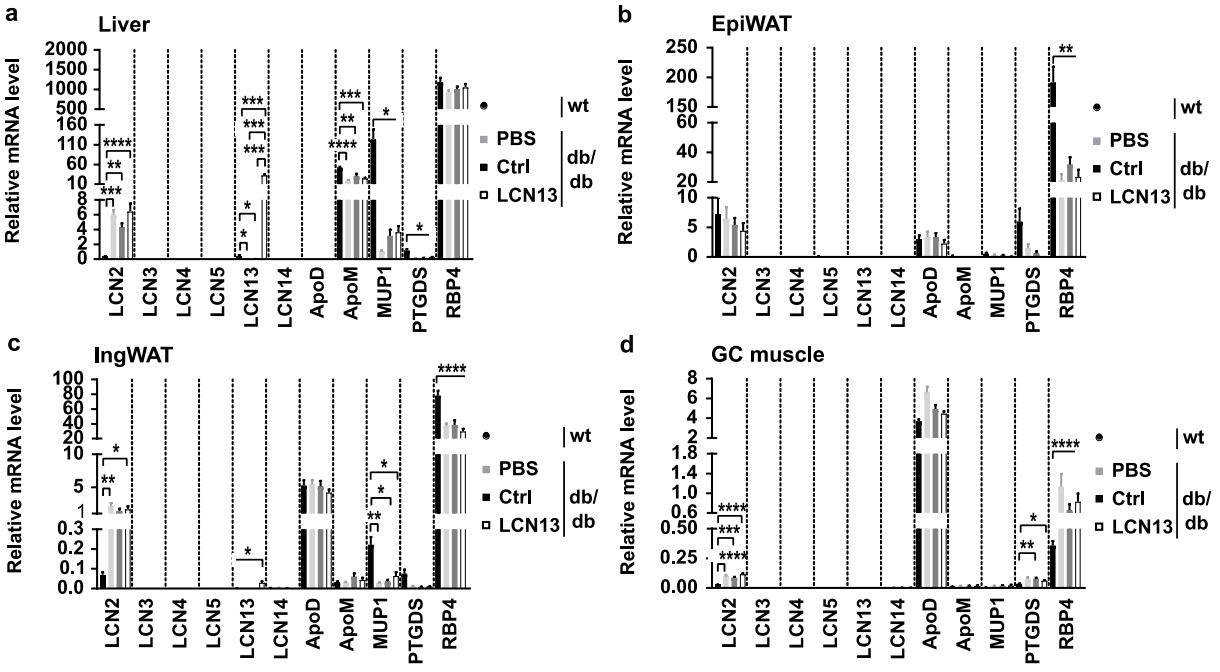

Figure 17 | AAV-Mediated Overexpression of LCN13 in db/db Mice Does not Influence the Expression of Other Lipocalin Family Members in Liver, Adipose Tissues or Muscle

db/db males (B6.BKS(D)-Leprdb/J, 7 weeks) were injected with PBS, a control AAV encoding for a mutated, untranslated GFP (Ctrl) or an LCN13 overexpressing AAV (LCN) (5x 10^{11}vg/mouse, n = 8-9 mice per group). Mice with the same genetic background (C57BL/6J, 7 weeks) were used as wildtype controls (wt). mRNA abundances of *Lcn2*, *Lcn3*, *Lcn4*, *Lcn5*, *Lcn13*, *Lcn14*, Apolipoprotein D (*Apod*), Apolipoprotein M (*Apom*), Major urinary protein 1 (*Mup1*), Prostaglandin D2 synthase (*Ptgds*) and Retinol binding protein 4 (*Rbp4*) were measured in (**a**) liver, (**b**) epididymal white adipose tissue (eWAT), (**c**) inguinal white adipose tissue (iWAT) and (**d**) gastrocnemius (Gc) muscle extracts by qRT-PCR 15 weeks after AAV injection. Values are shown as mean ± SEM. Study was designed, conducted and analyzed by Lea Katharina Bühler. Statistical analysis: Outliers were identified by the ROUT method (Q = 1%). Data with unequal variances were assessed using Welch's ANOVA with Dunnett's T3 multiple comparison test. All other data were analyzed by ordinary one-way ANOVA with Tukey's multiple comparison test. * $p \leq 0.05$; ** $p \leq 0.01$; *** $p \leq 0.001$; **** $p \leq 0.0001$.

3.6 LCN13 Potentiates Insulin Secretion *in Vitro*

In the previous section, we addressed the question whether the expression of other lipocalin family members is coupled to LCN13 expression and, thereby, could explain why LCN13 KD and OE did not affect systemic metabolism in mice. As LCN13 is also a potential carrier of an unknown cargo which could mediate its effects (Flower, 1996), a difference in cargo diversity and accessibility between this and previous studies of the Rui laboratory could be another confounding variable. Moreover, if LCN13 had opposing effects on different tissues and cell types, this could explain why we did not see any differences in the overall metabolic phenotype *in vivo*. Therefore, in order to circumvent these obstacles, we decided to investigate the effects of LCN13 in an isolated *in vitro* system. We chose the murine pancreatic β-cell line MIN6 as a potential target, because β-cells play a pivotal role in glucose handling and exhibit a comprised function in both T1D and T2D (Chen et al., 2017a). Of note, other lipocalin family members, such as APOM, were shown to promote both insulin secretion and β-cell survival (Kurano et al., 2014; Moon et al., 2013). Our decision to study LCN13 effects on MIN6 cells was further based on the finding that they express a potential receptor for OBPs and/or their cargo (Blache et al., 1998).

To ensure sufficient cell-to-cell contact which is indispensible for β-cell functionality (Hauge-Evans et al., 1999), we grew MIN6 cells as pseudo-islets by shaking them in low attachment plates. After three days, pseudo-islets reached a size comparable to primary islets isolated from 8 to12 week old wild type mice (Figure 18a, b). High glucose (16.7 mM) enhanced GSIS by MIN6 cells (Figure 18c). Exendin-4 (Ex-4) is an incretin mimetic which is known to enhance glucose-dependent insulin secretion (Goke et al., 1993). In line with this, Ex-4 increased insulin secretion by MIN6 pseudo-islets upon high glucose incubation. However, it also increased insulin release in low glucose-treated islets. In contrast, recombinant LCN13 produced in E.coli, increased insulin secretion exclusively upon stimulation by high glucose. MIN6 pseudo-islets are comprised of solely β-cells, whereas in primary mouse islets β-cells are surrounded by a more complex microenvironment consisting of other cell types, such as α-, δ-, ε- and γ-cells. Therefore, we investigated whether LCN13 affected insulin secretion also *ex vivo* in isolated primary mouse islets. Indeed, LCN13 raised glucose-dependent insulin secretion to a level comparable to Ex-4 stimulation (Figure 18d). Importantly, this effect was solely observed upon chronic (12-24 h pre-treatment), but not acute (1 h) LCN13 stimulation. Moreover, insulin content remained unchanged both in MIN6 pseudo-islets and primary islets regardless of the treatment (Figure 18c-d). In conclusion, data from pseudo- and primary mouse islets consistently showed that LCN13 increased glucose-stimulated insulin secretion.

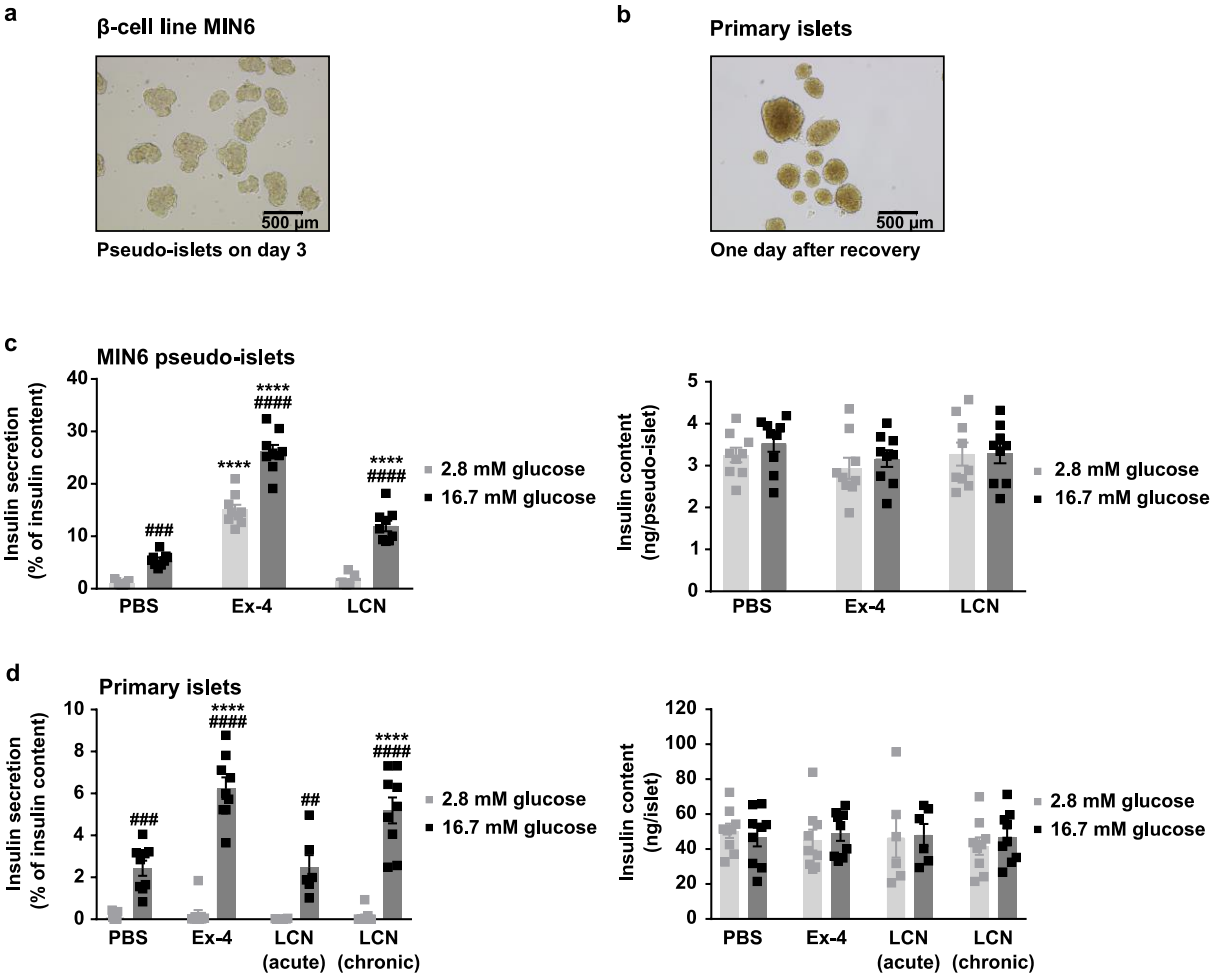

Figure 18 | LCN13 Increases GSIS by Both MIN6 Pseudo-islets and Primary Islets

Comparison of (**a**) MIN6 pseudo-islets, 3 days after pseudo-islet growth initiation, and (**b**) primary islets, one day after isolation from C57BL/6N males (8-12 weeks). Glucose-stimulated insulin secretion (GSIS) assay with (**c**) MIN6 pseudo-islets (n = 3 independent experiments, each with 3 technical replicates per condition) and (**d**) primary islets (n = 2-3 independent experiments, each with 3 technical replicates per condition): Pseudo-islets and primary islets were pre-incubated in low glucose (2.8 mM) for 1 h, before they were transferred into low (2.8 mM) or high (16.7 mM) glucose for 2 or 1 h, respectively. Islets were either acutely (during GSIS assay only) or chronically (12-14 h pre-incubation as well as during the GSIS assay) treated with 10 nM recombinant bacterial LCN13 (LCN). PBS served as negative control, while 10 nM Exendin-4 (Ex-4) was used as positive control. Afterwards, both insulin secretion in the supernatant and insulin content of the islets were measured by Insulin ELISA. Insulin secretion is shown as percentage of total insulin content (insulin content and secreted insulin). Likewise, insulin content per islet was calculated as sum of insulin content and secreted insulin. Values are shown as mean ± SEM. Experiments were designed, conducted and analyzed by Lea Katharina Bühler. Statistical analysis: Data were analyzed by two-way ANOVA. Effects attributed to glucose (#) were analyzed by comparing low glucose with high glucose stimulation within the same treatment (Sidak's multiple comparison test). Ex-4 and LCN effects (*) were analyzed by comparing respective values with the PBS control group upon either low or high glucose stimulation (Dunnett's multiple comparison test). $^{\#\#}$ $p \leq 0.01$; $^{\#\#\#}$ $p \leq 0.001$, $^{\#\#\#\#}p \leq 0.0001$. **** $p \leq 0.0001$.

4. Discussion

The liver is a central regulator of systemic energy homeostasis. As a source of circulating endocrine factors, called hepatokines, it shapes the metabolic response of various organs, including adipose tissue, muscle and the pancreas (El Ouaamari et al., 2016; El Ouaamari et al., 2013; Iroz et al., 2015). The liver secretome is responsive to pathological changes, such as liver steatosis, which is a common feature of T2D. This altered hepatokine profile was shown to drive metabolic dysfunction (Meex et al., 2015; Meex and Watt, 2017). In this context, we have characterised LCN13 as a hepatokine with insulin sensitizing properties which is downregulated in T2D patients (Ekim Ustunel et al., 2016). These data were in accordance with earlier findings published by another group which showed reduced LCN13 levels both in liver and the circulation in different mouse models of obesity and diabetes (Cho et al., 2011; Sheng et al., 2011). In this study, we aimed to further investigate the role of LCN13 in physiology as well as in the pathological context of T2D, in order to assess its applicability as biomarker and therapeutic target for T2D.

LCN13, also known as OBP2A, belongs to the lipocalin family sub-group of odorant binding proteins. The human LCN13 orthologue was detected in the mucus covering the olfactory cleft where it is thought to carry, deactivate and/or select odorant molecules, thereby contributing to olfactory perception (Briand et al., 2002). Its gene variant hOBP$_{IIa\alpha}$ (170 amino acids; UniProtKB accession: Q9NY56) was shown to have high binding affinity for aldehydes, such as undecanal, lilial and vanillin, as well as for long chain fatty acids (Briand et al., 2002). The ability to bind such a diverse set of hydrophobic compounds can be explained by its large hydrophobic ligand binding pocket which exhibits a high structural flexibility (Schiefner et al., 2015). Applying site-directed mutagenesis, a single lysine residue (K112) was identified to convey specificity for medium-size aldehydes and small carboxylic acids (C9-C12; Tcatchoff et al., 2006). Aligning the mature protein sequence of the mouse LCN13 (UniProtKB accession: Q8K1H9) and the aforementioned human LCN13 variant, revealed that this specific lysine residue is conserved across the two different species (data not shown). Thus, mouse LCN13 could, in theory, exhibit similar ligand specificity. Nonetheless, with an identity and similarity of 39% and 60%, respectively, we can not exclude the possibility that amino acid differences in the ligand-binding pocket or in the four loops governing its entrance lead to inter-species differences in cargo binding properties. It is currently unknown whether LCN13 exerts its regulatory role in metabolism as apoprotein or as holoprotein, in complex with a yet to be identified cargo. Native ligands of LCN13 could be identified *in vivo* by hepatocyte-specific AAV-mediated expression of a tagged LCN13 protein or by a transgenic mouse line which overexpresses a tag-fused LCN13. Tag affinity purification and lipid extraction followed by liquid chromatography coupled to mass spectrometry (LC-MS)-based lipidomics could help to

identify its cargo/s (Cajka and Fiehn, 2014).

Similarly, the exact molecular mechanisms, underlying the metabolic functions of LCN13, remain elusive. LCN13 could potentially convey its signal via olfactory receptors which are G protein-coupled receptors (GPCR). Interestingly, olfactory receptor expression is not restricted to olfactory sensory neurons, but is rather distributed throughout the body (Massberg and Hatt, 2018). A putative olfactory receptor was, for example, reported to be expressed in the β-cell line MIN6 (Blache et al., 1998). This prompted us to investigate whether LCN13 had a positive effect on β-cell insulin secretion *in vitro*. Indeed, we could consistently show that LCN13 stimulated glucose-dependent insulin secretion by both MIN6 and primary islets (Figure 18). The observation that pre-treatment of LCN13 was needed to see this positive effect enables us to speculate about the possible underlying mechanism. The requirement for chronic LCN13 availability is indicative of transcriptional regulation. Previous studies have shown that LCN13 inhibits gluconeogenic and lipogenic genes while promoting genes involved in β-oxidation in hepatocytes both *in vitro* and *in vivo* (Cho et al., 2011; Sheng et al., 2011). Possible target genes in β-cells could include enzymes involved in glucose metabolism, such as GK, or proteins promoting glucose uptake, like glucose transporter 2 (GLUT2). GK and GLUT2 upregulation was speculated to be able to enhance GSIS due to increased fuel utilisation (García-Ocaña et al., 2001). However, GLUT2 or GK overexpression alone did not promote GSIS in β-cells *in vitro* and *ex vivo*, respectively (Ishihara et al., 1995; Lu et al., 2018). Therefore, additional or other LCN13-induced changes are likely required. Importantly, LCN13 seems not to control the expression of insulin, as insulin content remained unchanged even after chronic treatment with LCN13. Bulk RNA sequencing (RNA-seq) data from MIN6 cells or single cell RNA-seq (scRNA-seq) data of primary islets could lead to the identification of LCN13 responsive genes which are responsible for the observed increase in insulin secretion.

There are several possibilities of how LCN13 could affect gene expression. If LCN13 acted on an olfactory receptor, downstream signalling would be dependent on the type of G protein coupled to this receptor (Massberg and Hatt, 2018). Other receptors could facilitate the uptake of LCN13's putative cargo which, in turn, could function as transcriptional regulator. Such a process is, for example, exploited by the lipocalin RBP4, its ligand retinol and its transmembrane receptor STRA6. Upon receptor binding of RBP4, retinol is taken up by the target cell via its direct diffusion into the lipid bilayer (Chen et al., 2016). Once inside the cell retinol is either stored in the form of retinylesters or metabolized to retinonic acids which drive gene expression by binding to retinoic acid receptor (RAR) and retinoid X receptor (RXR), which are both nuclear receptor transcription factors. Besides cargo uptake, such a transmembrane receptor could additionally regulate target cell transcription via receptor downstream signalling elicited by either apo- or holo-LCN13. Holo-RBP4, for instance, was suggested to exert transcriptional effects via STRA6-mediated JAK-STAT signalling (Berry et

al., 2011). Lastly, apo- or holo-LCN13 itself could function as an intracellular signalling molecule. In line with this, stress-induced cellular uptake of the lipocalin APOD followed by its nuclear translocation was demonstrated by a previous study (Do Carmo et al., 2007). The receptor or receptors of LCN13 expressed by LCN13-responsive cells, including hepatocytes, adipocytes, muscle cells and β-cells, could be identified by the TRICEPS/HATRIC-based ligand receptor capture (LRC) approach coupled to flow cytometry-based validation (Frei et al., 2013; Lopez-Garcia et al., 2018; Sobotzki et al., 2018). To address whether LCN13 is taken up by target cells and resides in specific subcellular localisations, LCN13-responsive cells could be treated with a LCN13-GFP fusion protein followed by confocal microscopy-based analysis. Alternatively, mammalian recombinant LCN13 could be detected by immunostainings using a primary and subsequently a fluorophore-labeled secondary antibody. If LCN13 was detected intracellularly, its internalisation could be blocked by dynamin inhibitors, which prevent receptor-mediated endocytosis. Thereby, one would be able to address the question whether cellular uptake of LCN13 is necessary for its metabolic actions.

By analysing a broad spectrum of tissues by qRT-PCR, we found *Lcn13* mRNA expression highly restricted to the liver of healthy C57BL/6N mice (Figure 5). Looking at publically available expression data at the EMBL-EBI Expression Atlas, *Lcn13* indeed seems to be most consistently expressed in liver of mice, albeit it was also found in thymus and the olfactory system (Barbosa-Morais et al., 2012; Huntley et al., 2016; Merkin et al., 2012; Nakahara et al., 2016; Petryszak et al., 2015; Soumillon et al., 2013). The latter is not surprising as LCN13 is an odorant binding protein which was detected in the mucus of the olfactory cleft in humans (Briand et al., 2002). In contrast to our finding, data generated by the Rui laboratory displayed LCN13 expression in liver, muscle as well as pancreas both at the mRNA (RT-PCR) and the protein level in C57BL/6 mice of the same sex and comparable age to our study (Cho et al., 2011). Not much is known about the transcriptional regulation of LCN13 which renders it difficult to explain these discrepancies. We previously identified TSC22D4 as a direct transcriptional repressor of *Lcn13* in the liver (Ekim Ustunel et al., 2016). Interestingly, TSC22D4 is downregulated in mice fed a HFD (Jones et al., 2013). Because neither we nor the Rui laboratory observed increased *Lcn13* levels in HFD-fed mice, *Lcn13* expression seems to be governed by additional, yet to be identified transcription factors in this context.

Whether nutritional cues affect *Lcn13* expression is not entirely clear. Cho *et al.* reported reduced plasma levels in 16 hour-fasted mice compared to their randomly fed counterparts (Cho et al., 2011). We, in contrast, did not observe any decline of *Lcn13* at the mRNA level upon 3, 6 or 9 h of fasting during the dark phase (6 p.m. – 9 p.m./12 or 3 a.m.; n = 4 mice per group; data not shown). Similarly, fasting for 8 h during the light phase (10 a.m. – 6 p.m.) with subsequent refeeding during the dark phase (6 p.m. – 9 p.m./12 or 3 a.m.) did not change hepatic *Lcn13* mRNA levels (n = 4 mice per group; data not shown). Intermittent fasting,

however, strongly reduced *Lcn13* expression in our hands (n = 8-10 mice; data not shown). Furthermore, Cho *et al.* showed significant downregulation of hepatic *Lcn13* mRNA and circulating LCN13 protein levels in HFD-fed mice (45% HFD) compared to chow-fed control mice (Cho et al., 2011). This finding could neither be confirmed in this nor in our previous study where mice fed with a 60% HFD were compared to mice receiving either a 10% LFD or a chow diet (Ekim Ustunel et al., 2016). We cannot exclude that differences in the used diets are accountable for the stated discrepancies.

In our previous publication, we demonstrated reduced hepatic *Lcn13* levels in mice fed a methionine/choline-deficient (MCD) diet as early as after 1 week of MCD diet start (Ekim Ustunel et al., 2016). MCD diet is known to lead to liver inflammation which promotes NASH development. Therefore, *Lcn13* expression could be responsive to inflammation. To gain further insight whether *Lcn13* mRNA expression is changed upon alterations in inflammatory liver diseases, we looked at relevant data sets at the NCBI gene expression and hybridization array data repository (Gene Expression Omnibus (GEO) database; Barrett et al., 2013; Edgar et al., 2002). One study used MCD together with a HFD to induce NASH which significantly downregulated hepatic *Lcn13* (accession: GSE35961 ; Kita et al., 2012). Administration of metformin, which reduced steatosis and inflammation in the same publication, did however not reverse *Lcn13* levels. *Lcn13* is also downregulated in the fatty liver Shionogi (FLS) mouse which spontaneously develops NASH compared to dd Shionogi (DS) mice which are a model of simple steatosis (accession: GSE45624; Semba et al., 2013). In a third study, high-cholesterol and HFD did not lead to a decline in liver *Lcn13* mRNA (GSE51432; Kobori et al., 2014). Taken together, inflammation might regulate *Lcn13* expression, albeit the specific experimental design seems to be of importance.

Changes in the gut microbial community can not only lead to changes in the hepatic transcriptome, but also to low grade inflammation in mice and humans (Cani et al., 2007; Cani et al., 2012; Leone et al., 2015; Montagner et al., 2016; Oh et al., 2019; Pussinen et al., 2011). Therefore, we looked at data generated by RNA sequencing of livers derived from mice with an altered gut microbiome. Germ-free, conventionalized or conventionally raised specific-pathogen-free mice fed a regular chow diet did not exhibit changes in hepatic *Lcn13* expression (accession: GSE53590; Leone et al., 2015). Low dose penicillin treatment given from birth onwards changed the microbial community composition, increased body fat percentage, but neither lobular inflammation nor hepatic *Lcn13* expression measured in mice at the age of 30 weeks, regardless whether they were continuously fed a chow or from week 17 onwards a 45% HFD (acccession: GSE58086; Cox et al., 2014). Thus, alterations in the gut microbiota seem not to profoundly affect *Lcn13* mRNA expression.

To investigate its pharmacological potential in healthy wild type mice, we manipulated hepatic and/or circulating LCN13 levels by AAV-driven hepatic overexpression or by i.p. injection of

recombinant mammalian Fc-LCN13 protein. Our in-house produced recombinant LCN13 protein was generated in a mammalian system allowing for relevant posttranslational modifications. Additionally, it excludes the possibility of bacterial contaminations which could induce an inflammatory response. In accordance, by establishing LP1 promoter-driven, AAV-mediated hepatic LCN13 overexpression, we lowered the probability of inducing inflammation which is a common feature of adenoviral-delivered, CMV-driven transgene expression (see below). Neither of the described complementary treatment approaches affected glucose clearance or insulin responsiveness in healthy mice (Figure 8 and 9). We can of course not rule out the possibility that endogenous LCN13 levels already pass the threshold needed for its maximum positive metabolic effect which would render pharmacological LCN13 amounts ineffective. However, supporting a negligible role of endogenous LCN13 in glucose homeostasis, LNP-mediated hepatocyte-specific knockdown of LCN13 did neither affect glucose nor lipid metabolism in healthy mice (Figure 6 and 7). Contradicting these findings, Sheng *et al.* reported detrimental metabolic effects upon neutralization of circulating LCN13 in healthy wild type mice. Injection of anti-LCN13 serum resulted in a worsened glucose tolerance and a change in the hepatic expression profile favouring lipogenesis over β-oxidation (Sheng et al., 2011). It could be that residual LCN13 levels following LNP administration were higher and sufficient for sustaining its metabolic effects, compared to the ones Sheng *et al.* achieved with their neutralisation approach. Importantly, Sheng *et al.* neutralized circulating, while we manipulated hepatic LCN13 expression and do not know the effects on its circulating levels. As we did, however, not observe any tendency towards decreased glucose tolerance, despite clear downregulation of hepatic *Lcn13* mRNA with a knockdown of 69% and 93% compared to PBS and siRNA control injected mice respectively, this scenario seems rather unlikely. Differences in sub-strain, diet, inflammation status and intestinal flora might be more plausible reasons for these contradictive results and will be commented further below.

After we found no indication for a metabolic regulatory role of LCN13 in healthy wild type mice, we addressed its importance under pathophysiology, including nutritional- as well as genetically induced obesity and diabetes. We speculated that LCN13 might only become indispensable under certain pathological stimuli, as other proteins with redundant roles could curtail the importance of LCN13 in healthy animals and might be suppressed exclusively upon metabolic dysfunction. Alternatively, factors needed for its metabolic regulatory role might be enriched under specific pathological conditions. Unexpectedly, we did neither observe any curative nor preventive effect of AAV-mediated LCN13 overexpression on HFD-induced metabolic dysfunction (Figure 10-12). Mimicking these results, also db/db mice treated with LCN13 overexpressing AAV did not display any differences in the applied metabolic readouts (Figure 13 and 14). These results are at odds to those published by the Rui laboratory. Using *Lcn13* transgenic mice, they observed an improvement in glucose clearance, insulin

responsiveness as well as in hepatic steatosis after HFD feeding (Cho et al., 2011; Sheng et al., 2011). In the created transgenic mouse line, *Lcn13* transgene expression was driven by the ubiquitous CAG (CMV enhancer, chicken beta-Actin promoter and rabbit beta-Globin splice acceptor site) promoter. The CAG promoter is constitutively active in virtually all cell types, except for erythrocytes and hair which does not reflect its physiological expression status (Niwa et al., 1991; Okabe et al., 1997). The fact that this promoter is already active in the unfertilized egg, makes it impossible to differentiate developmental from purely metabolic effects (Okabe et al., 1997). However, the same group also studied the therapeutic efficacy of LCN13 by adenovirus-mediated LCN13 overexpression in mice which had been fed a HFD for 10 weeks beforehand as well as in db/db mice (Cho et al., 2011). Improved glucose and insulin tolerance in all mentioned mouse models supported their conclusion that LCN13 is a key regulator of systemic energy homeostasis. Possible explanations for the observed discrepancies with respect to our study will be highlighted in the following sections.

Unresponsiveness of LCN13 Expression to Metabolic Dysfunction. Opposing the results generated by the Rui laboratory, we did not see any difference in hepatic *Lcn13* mRNA levels comparing mice on chow or LFD with obese, diabetic mice fed a HFD (Figure 10b and 12b). Even though db/db mice showed a clear trend towards reduced liver *Lcn13* mRNA expression, these changes were not consistently significant (Figure 13a and 15a). These background levels of LCN13 could be sufficient for its positive metabolic effects which would render higher LCN13 levels elicited by AAV-mediated overexpression ineffective. If this was true, LCN13 would however not play a major role in sustaining metabolic health under the conditions tested in this study. To address this issue, a comparison of the relative levels of circulating LCN13 between our studies and the ones of the Rui laboratory would be essential. However, quantification of LCN13 in serum remains difficult, because high-affinity antibodies and functional ELISA kits are not available. One possibility to address the importance of disease-mediated LCN13 downregulation could be to feed mice with a MCD diet. As in our previous study, MCD diet induced a significant downregulation of *Lcn13*, it might be worth to overexpress LCN13 in this scenario to see whether it could ameliorate liver steatosis.

Supra-physiological LCN13 Levels. Looking at LCN13 expression levels achieved by our exploited AAV approach revealed a striking increase compared to levels found in controls (Figure 10b, 12b and 13a). Similarly western blot data, published by the Rui laboratory, showed marked differences between wild type mice and mice overexpressing LCN13 (Cho et al., 2011; Sheng et al., 2011). Nevertheless, we saw the possibility that the high LCN13 levels achieved by AAV-mediated overexpression in our previous experiments could desensitize tissues towards LCN13 and/or might elicit hepatic ER stress and accumulation of misfolded proteins. To exclude that these factors indeed confounded beneficial effects of LCN13 treatment, we

tested different doses of the LCN13 overexpressing AAV. None of the used AAV concentrations showed any influence on metabolic traits in db/db mice (Figure 15). We achieved a range of LCN13 levels spanning 2 orders of magnitude, with the lowest concentration leading to a fivefold overexpression compared to wild type mice. Hence, we are convinced that the degree of LCN13 overexpression unlikely was the reason for the lack of beneficial metabolic effects.

Genetic Differences. Variances, arising due to the usage of distinct mouse strains, could lead to different expression levels of cargo, receptor or other indispensible molecules involved in the signalling pathway exploited by LCN13. Additionally the presence of an environmental or genetic factor with inhibitory or redundant effects in relation to LCN13 could explain why LCN13 did not affect metabolic dysfunction in this study. Divergence at the level of animal vendors might additionally lead to subtle differences of commensal microbiota which, in turn, could hinder data reproducibility (discussed below). Concerning healthy wild type mice on chow, LFD or HFD, although the Rui laboratory used the same genetic background (C57BL/6) of mice, the authors did not specify the sub-strain or the supplier (Cho et al., 2011; Sheng et al., 2011). The db/db mice used in the current work originated from the same strain and vendor [B6.BKS(D)-Leprdb/J (000697) mice from the Jackson laboratory] as those used by Cho and Sheng *et al*. However, db/db mice used in our previous work were on a different genetic background [BKS.Cg-Dock7m +/+ $Lepr^{db}$/J (000642) mice] (Ekim Ustunel et al., 2016). It needs to be pointed out that the establishment of LCN13 as a positive metabolic regulator was based on results of various mouse models of obesity and diabetes encompassing wild type mice on HFD, *Lcn13* transgenic mice on HFD, db/db, ob/ob as well as *Lcn13* transgenic mice crossed with $ob^{+/-}$ mice (Cho et al., 2011; Ekim Ustunel et al., 2016; Sheng et al., 2011). Therefore, the genetic background is unlikely the main driver of the unexpected findings presented here.

Differences in Transgene Delivery. Aside from distinct mouse lineages, also subtle differences in applied techniques can be possible confounders and the reason for a lack of reproducibility (Crestani et al., 2000). We exploited a pseudo-typed AAV2/8 virus which incorporates the AAV2 viral backbone packaged into the AAV8 capsid (Gao et al., 2002). AAV2/8 is highly efficient in transducing hepatocytes as well as skeletal and cardiac muscle cells (Akache et al., 2006; Gao et al., 2002; Nakai et al., 2005; Wang et al., 2005). While the commonly used CMV promoter is ubiquitously active, the herein used LP1 promoter is characterized by its hepatocyte-specificity (Cheng et al., 1993; Nathwani et al., 2006). Interestingly, we still observed a small, but significant *Lcn13* upregulation in inguinal white adipose tissue, but not in epididymal fat or skeletal muscle of db/db mice transduced with the AAV2-LP1-LCN13 plasmid (Figure 17). AAV are non-pathogenic, elicit only minor immune responses and are therefore able to establish long-term transgene expression (Chirmule et al.,

1999; Hernandez et al., 1999; Zaiss and Muruve, 2008). In line with this, McCaffrey *et al.* reported that AAV given at a comparable dose (3x 10^{11} vg/mouse) and via the same route (i.v. tail vein injection) as in our study failed to elicit a robust type I interferon (IFN) response (McCaffrey et al., 2008). Another publication showed that AAV elicits a mild, but detectable host defence, which is characterized by a highly transient (< 6h) cytokine and chemokine expression as well as leukocyte recruitment without marked toxicity or inflammation in the mouse liver, when given via the femoral vein at a comparable dose than used in this study (2.5x 10^{11} vg/mouse; Zaiss et al., 2002). Because we did not observe any apparent liver damage in AAV-injected mice, evaluated by ALT and AST levels measured between 6 and 17 weeks after AAV administration, we can at least exclude an ongoing, vigorous immune response towards viral gene and transgene products. Additional support for the lack of a confounding involvement of the innate and adaptive immune response is the robust AVV-mediated *Lcn13* overexpression seen throughout our experiments, even 17 weeks after virus injection (Figure 10b, 12b, 13a and 15a).

First generation adenoviruses (E1 and E3 genes deleted), which were used in previous studies of the Rui laboratory and Üstünel *et al.*, in contrast, induce both a strong early transcription-independent innate immune response as well as an adaptive immune response directed against viral gene products (Liu and Muruve, 2003; McCaffrey et al., 2008; Zaiss et al., 2002). The control transgene lacZ used by Cho and Sheng *et al.* is also known to be immunogenic, resulting in a β-galactosidase-targeted CTL response (Jooss et al., 1998; Song et al., 1997; Yang et al., 1996). Additionally, the ubiquitous CMV promoter used by the Rui laboratory, compared to the more hepatocyte-specific LP1 promoter, is also prone to foster an immune response (Zaiss and Muruve, 2008). Experiments with contradicting results to our study were performed between 1 and 2 weeks after adenovirus administration (Cho et al., 2011; Ekim Ustunel et al., 2016). Based on previous data which showed that i.v. femoral vein injection of Ad5 (ΔE1 and ΔE3, 1x10^{11} vg/mouse) induced an innate immune response peaking at 6 h after virus injection and an adaptive immune response apparent after 5 days, it could well be that in previous studies of Cho *et al.*, Sheng *et al.* and Üstünel *et al*. proinflammatory mediators and effector cells were present at the time point of experiments (Liu et al., 2003). A difference in background liver inflammation between this and previous studies could explain why we were unsuccessful in reproducing earlier findings. The odds are that certain inflammatory signals could be essential for the expression of LCN13's cargo, its receptor and/or indispensable downstream signalling molecules. Another plausible scenario explaining an inflammation-based discrepancy of data could be that LCN13 and a confounding factor X have redundant roles as insulin stimulants and sensitizers. If factor X was sufficient to maintain these beneficial effects, neither knockdown nor overexpression of LCN13 would lead to any observable difference in metabolic phenotype. Solely in the presence of a certain trigger, like inflammation,

factor X could be downregulated or inhibited which would render LCN13 indispensable. It is important to keep in mind, that obesity and diabetes themselves are associated with chronic low-grade inflammation. Therefore, low-grade inflammation was most certainly present in all mouse models of obesity and diabetes used by us and the Rui laboratory. It is unclear, whether an additional inflammatory stimulus, such as adenoviral infection or an altered gut microbiome (reviewed below) would be needed to trigger the abovementioned events and potentially explain the discrepancies between this and earlier studies (Cho et al., 2011; Ekim Ustunel et al., 2016; Sheng et al., 2011). Whether there were different levels of background liver inflammation in this and previous studies could be only answered by comparing liver histology, liver damage markers, such as ALT and AST in serum, as well as expression data covering inflammatory markers, like TNF-α or IFN-γ. To address the question whether adenovirus-induced host changes are required for beneficial LCN13-mediated metabolic effects, one could co-infect mice with an empty adenovirus and the herein used LCN13-overexpressing AAV. Importantly, the administration of anti-LCN13 serum to healthy wild type mice had detrimental metabolic effects in one of the previous studies (Sheng et al., 2011). More specifically, mice treated with anti-LCN13 serum exhibited higher fasting blood glucose levels and worsened glucose tolerance than control mice receiving pre-immune serum. Moreover, neutralisation of circulating LCN13 led to increased *Scd1* and decreased *Cpt1α* mRNA expression which is indicative of the induction of lipogenesis and suppression of β-oxidation, respectively. Thus, the technical aspect discussed here cannot be the only explanation for the observed discrepancies.

Distinct Disease Stages. To ensure significant overexpression, we generally conducted phenotyping at the earliest 3 weeks post-AAV injection. Therefore, our animals were overall older and possibly exhibited more advanced disease in comparison with previous studies which used adenoviruses as means to overexpress or knockdown LCN13. Indeed, calculating an approximate HOMA-IR value of 25 based on the data available for the db/db mice in the publication of Cho *et al.* (fasted for 16 hours: blood glucose ~ 120 mg/dL, plasma insulin ~ 3.4 ng/mL) shows that our control db/db mice, with an average HOMA-IR value of 50 (fasted for 16 hours: blood glucose ~ 244 mg/dL, plasma insulin ~ 4.1 ng/mL) were markedly more insulin resistant (Figure 13k-m; Cho et al., 2011). Similarly, control mice which were fed a 45% HFD for 11 weeks by Cho *et al.* showed a HOMA-IR value of 15 (fasted for 16 hours: (calculated) blood glucose ~ 129 mg/dL, plasma insulin ~ 1.9 ng/mL; Cho et al., 2011). In our experiment, control mice exhibited an average HOMA-IR value of 32 (fasted for 16 hours: blood glucose ~ 146 mg/dL, plasma insulin ~ 3.7 ng/mL) and 21 (fasted for 16 hours: blood glucose ~ 131 mg/dL, plasma insulin ~ 2.6 ng/mL) after 3 and 14 weeks on 60% HFD, respectively (Figure 10k-m). This could consequently imply that due to a further progressed disease stage, mice used in this study were not as responsive to LCN13 as in previous studies. Likewise, a disease-

related downregulation of its cargo or other factors involved in its signalling cascade might prevent positive metabolic effects of LCN13. And lastly, factors with inhibitory or redundant effects in relation to LCN13 could be upregulated upon advanced disease progression. Of note, a difference in disease stage cannot however explain the lack of effect upon LNP-mediated LCN13 KD.

Diet-Related Variables. Differences related to the ingested food could lead to changed cargo availability. The cargo of LCN13 could either be a lipophilic dietary component or a metabolite deriving from the gut microbiota (see below). Putative LCN13 ligands stemming from these two sources might reach the liver via chylomicrons where they could be further metabolized and/or loaded onto LCN13. Another possibility is the presence of an inhibitory cargo in our study arising from a specific dietary component which might have been absent in previous studies. For instance, a substance which binds to LCN13 and, thereby, blocks the binding and transportation of its normal cargo could prevent the beneficial metabolic action of LCN13. Chow diets used in this and in studies of the Rui laboratory differed mostly in fat (5.1 vs 9%, respectively) and fiber content (4.5 vs 2.4%, respectively). The chow diet used in our former publication had similar fat and fiber content (4.3% and 4.7%, respectively) to the diet used here (nutrients expressed as percent of mass; Ekim Ustunel et al., 2016). As all chow diets were obtained from varying vendors, the source of ingredients could also add up to the difference. While both HFDs were obtained from the same supplier, we used a 60% HFD in contrast to Cho and Sheng *et al.* who fed a 45% HFD. Lard and soybean oil are the lipid sources in both diets. The composition is, however, slightly different. While in the 60% HFD, lard constitutes 91% of the fat content, it only comprises 88% in the 45% diet. As LCN13's cargo might indeed be lipid-derived, these food variables could lead to incomparable results.

Other Environmental Factors. It is becoming increasingly clear that various environmental factors besides the ones discussed so far affect data reproducibility. Importantly, gene-by-environment interactions do not only play an important role in the analysis of behavioural but also of physiological phenotypes (Valdar et al., 2006). Month, sex, season and litter were, for example, shown to have effects on biochemical measures. Interestingly, glucose tolerance tests are highly affected by season, sex as well as by the experimenter. Furthermore, utilized housing systems and corresponding husbandry practices significantly affect reproducibility and data comparability (Hasenau, 2020). Physical environmental factors like temperature, humidity, light and sound can change experimental outcomes as well as the type of enrichment and sociological factors (Obrink and Rehbinder, 2000). Differences in the frequency of cage changes, cage size and group size can induce distinct levels of stress (Hasenau, 2020; Van Loo et al., 2001). Stress, in turn, increases glucocorticoid release known to have adverse effects on glucose metabolism (Kuo et al., 2015; Rosmond, 2005; Wiberg and Grice, 1963).

Here it is important to mention that in mice supplied by Charles River, we observed increased aggressive behaviour and abscesses at the lower belly/genital area which forced us to significantly reduce the cohort size in one of our experiments (n = 5 – 7 instead of 8 mice per group, Figure 10 and 11). Therefore, we decided to use mice with the same genetic background from another supplier (Janvier) for all other experiments shown in this work. Lastly, variances at the level of hygienic standards and barrier facilities between different laboratories could lead to differences in commensal and pathogenic microbes.

Different Microbial Communities. The above stated differences between this and previous studies, namely mouse strain, vendor source, age, diet, husbandry and pathogen status can all have an impact on the diversity and richness of the intestinal flora. The composition of the microbial community in turn might have an impact on the presence of background inflammation and microbial endocrine factors (De Filippo et al., 2010; Ericsson et al., 2015; Franklin and Ericsson, 2017; Hufeldt et al., 2010; Robosky et al., 2005; Rohde et al., 2007). Metabolic dysfunction and gastrointestinal barrier function are highly interconnected. Both humans and mice on HFD as well as leptin-deficient (ob/ob) and hyperleptinemic (db/db) mice exhibit increased gut permeability and endotoxemia (Brun et al., 2007; Cani et al., 2007; Pendyala et al., 2012). Alteration of the gut microbiome can lead to increased intestinal permeability, due to, for example, induction of Chemokine (C-C motif) ligand 5 (CCL5) secretion by epithelial cells and downregulation of tight junction proteins (Cani et al., 2012; Elinav et al., 2011; Feng et al., 2019; Henao-Mejia et al., 2012). This breach in the intestinal barrier leads to the systemic dissemination of microbial components which arrive first at the liver via the portal vein. HFD-induced dysbiosis and endotoxemia were reported to foster obesity and hepatic insulin resistance via TLR4-induced proinflammatory cytokine expression of IL-6, TNF-α, IL-1, and plasminogen activator inhibitor-1 (PAI-1; Cani et al., 2007). In line with this, lipopolysaccharides (LPS) as well as bacterial DNA drive NAFLD/NASH progression via TLR4/9-mediated upregulation of TNF-α (Henao-Mejia et al., 2012). It is worth to mention, that also enhanced chylomicron-mediated LPS uptake upon HFD feeding was suggested to play a causative role in HFD-linked endotoxemia (Ghoshal et al., 2009). In light of the aforementioned literature, differences at the level of gut microbiota composition, e.g. the ratio of Gram-negative (containing LPS) and Gram-positive microbes, could lead to levels of low-grade inflammation distinct in the different studies. Furthermore, also the disease stage could aggravate microbe-mediated inflammation, as not only changes in microbiota composition, but also hyperglycemia and elevated leptin levels were shown to comprise intestinal barrier integrity (Ahmad et al., 2017; Thaiss et al., 2018). As described above, inflammatory processes, in turn, could affect the expression of factors which influence LCN13 signalling.

Differences at the level of the microbiota composition could not only establish varying degrees of inflammation, but also distinct pools of signalling molecules. By converting dietary

components into signalling molecules, the microbiome actively takes part in inter-organ communication (Schroeder and Backhed, 2016). Indeed, many blood metabolites, especially amino acid-derived ones, originate from the gut microbiome (Sridharan et al., 2014; Wikoff et al., 2009). Imidazole propionate, a microbial metabolite deriving from histidine was, for example, shown to directly impair insulin signalling and, thereby, promoting T2D (Koh et al., 2018). In contrast, tryptophan-derived bacterial metabolites indole and tryptophol as well as microbially produced palmitoleic acid were identified as anti-inflammatory signals in the liver (Beaumont et al., 2018; Schirmer et al., 2016). Besides amino acids, non-digestible carbohydrates are also processed by the gut microbiota resulting in end-products including short chain fatty acids (SCFA), mainly acetate, propionate and butyrate. Binding to their cognate G protein-coupled receptors GPR41 (Ffar3) and GPR43 (Ffar2), SCFA can beneficially modulate systemic metabolism by inducing the secretion of GLP-1 and PYY by enteroendocrine L-cells (Samuel et al., 2008; Tolhurst et al., 2012). Furthermore, GPR43 activation by acetate reduces the inflammatory potential of neutrophils (Maslowski et al., 2009). Contradicting these beneficial effects of SCFA, one study reported that HFD-linked dysbiosis promotes hyperphagia, obesity and insulin resistance via an acetate-dependent microbiome-brain-β-cell axis (Perry et al., 2016). Besides diet-derived signal molecules, the microbiota additionally processes hepatic bile acids secreted into the intestinal lumen. Thereby, commensal microbiota enlarge the bile acid pool by generating secondary bile acids with endocrine functions as they can signal through the GPCR TGR5 leading to improved glucose metabolism via induction of intestinal GLP-1 secretion and increased energy expenditure in brown adipose tissue (Thomas et al., 2009; Watanabe et al., 2006). Furthermore, gut microbiota-derived bile acids were reported to promote diet-induced obesity by signalling through the nuclear receptor farnesoid X receptor (FXR; Parséus et al., 2017). Moreover, increased microbial metabolism of choline was implied in the establishment of NAFLD and insulin resistance by preventing phosphatidylcholine-dependent VLDL assembly and secretion (Dumas et al., 2006). All these examples highlight the extensive communication that exists between the microbiota and the host's organs, especially via the bidirectional gut-liver axis. The illustrated broad range of microbial endocrine metabolites derive from a diverse set of biological molecules, including, for example, dietary carbohydrates, amino acids and lipids as well as bile acids and choline. Such metabolites could function as LCN13's ligand or they could influence the expression of factors determining the tissue responsiveness towards LCN13. The microbiota-derived metabolite profile is highly dependent on the composition of the microbial community, for example the ratio of Bacteroidetes and Firmicules phyla. Thus, differences between this and previous studies at the level of the micobiome could be the basis for the observed discrepancies. A possible approach to address the importance of microbiota for the physiological relevance of LCN13 would be to manipulate its expression in germ-free mice or

upon modification of the microbial community by antibiotics treatment (Kennedy et al., 2018). The latter allows for studying the role of bacteria without affecting mouse development and could address whether specific bacteria, such as Gram-negative ones, are important in the experimental context of our study (Kennedy et al., 2018; Pappo et al., 1991). Whether inflammation in general is needed for the metabolic importance of LCN13 could be studied by injecting the microbe-derived inflammatory molecule LPS in wild type mice which have been pre-treated with LCN13-overexpression AAV. Both acute as well as chronic administration of LPS to mice leads to a state of insulin resistance (Cani et al., 2007; Sugita et al., 2002; Virkamäki and Yki-Järvinen, 1994). Furthermore, like the abovementioned adenoviral transgene delivery, both acute and chronic administration of LPS increases the levels of a broad range of proinflammatory cytokines, such as TNF-α, IL-1, IL-6 and INF-γ (Cani et al., 2007; Feingold et al., 1992; Varma et al., 2002). Therefore, such a LPS-based experiment could answer the question whether inflammation, evoked by adenovirus infection or commensal microbiota is a requirement for LCN13 to become an important metabolic regulator.

Redundancy of Lipocalin Family Members. Lipocalin family members are characterized by redundant functions and some for their potential to bind to the same receptor (Table 1; Flower, 2000). Therefore, we hypothesized that other lipocalin family members could have obscured the metabolic regulatory effect of LCN13 in our study. LCN14 (OBP2B) was one of the top candidates, because, firstly, it exhibits a high sequence similarity with LCN13 (65%) and, secondly, its metabolic influences are similar to the ones reported for LCN13 (Lee et al., 2016). MUP1 was also reported to have metabolic functions reminiscent of LCN13 and a mouse MUP was shown to compete with the bovine odorant binding protein for the same receptor (Boudjelal et al., 1996; Hui et al., 2009; Zhou et al., 2009). First, we investigated whether manipulation of LCN13 levels influences the expression of other lipocalin family members in metabolic relevant organs, including liver, white adipose tissues and muscle. This hypothesis was based on findings of previous publications suggesting that LCN13 is involved in transcriptional regulation. For instance, Cho and Sheng *et al.* reported that LCN13 inhibits gluconeogenic and lipogenic genes while promoting genes involved in β-oxidation in hepatocytes both *in vitro* and *in vivo* (Cho et al., 2011; Sheng et al., 2011). We investigated mRNA levels of lipocalins with either high sequence similarity (LCN3, LCN4, LCN14, PTGDS and RBP4) and/or known metabolic functions (APOD, APOM, LCN2, LCN5, LCN14, MUP1, PTGDS and RBP4) in our previous LCN13 knockdown and db/db study. We speculated that another lipocalin protein with a redundant, but indispensable role in energy homeostasis could be reciprocally regulated compared to LCN13. In this scenario, LCN13 knockdown would lead to an upregulation of the redundant lipocalin which took on LCN13's task. Upon LCN13 overexpression this redundant lipocalin would be downregulated and would, due to its indispensability, obscure beneficial

effects of LCN13. Both upon LCN13 knockdown and overexpression, none of the investigated lipocalin family members were differentially expressed (Figure 16 and 17). Therefore, a direct transcriptional effect of LCN13 on other proteins of the lipocalin family cannot explain our findings. Nevertheless, it could still be that discrepancies between this and other studies stem from LCN family members, their cargo or other factors affecting their activity. Such a situation could arise if the protein landscape needed for another lipocalin family member to exert the same effects as LCN13, which would make LCN13 dispensable, were exclusively present in this study. To validate this possibility, one could knockdown other lipocalins together with and without LCN13 to see whether the presence of another family member obscured LCN13's action in our study. In summary, disparities between the current and previous studies might be related to differences in diet, disease stage, inflammation as well as the microbiome. All of these variables might have led to unfavourable cargo availability, LCN13 unresponsiveness and the presence and/or importance of redundant proteins, including other lipocalin family members, in this study.

Supporting the idea that LCN13 is a part of a rather delicate and complex system, controversial roles in systemic metabolism were attributed to other lipocalin family members, such as LCN2 (Table 1). Most intriguingly, three laboratories studied the metabolic phenotype of LCN2 knockout mice, which led to three different conclusions. Law et al. reported that LCN2 deficiency protects mice from obesity-induced insulin resistance, while Guo et al. showed LCN2-dependent promotion of metabolic dysfunction (Guo et al., 2010; Law et al., 2010). In a third study, LCN2 did not affect diet-induced insulin resistance (Jun et al., 2011).

5. Conclusion

Harnessing the liver secretome to combat diabetes and other components of the metabolic syndrome is gaining increasing interest (Iroz et al., 2015; Meex and Watt, 2017). The hepatokine LCN13, which is downregulated in diabetic mice and humans, seemed to be such a promising therapeutic target (Cho et al., 2011; Ekim Ustunel et al., 2016; Sheng et al., 2011). Besides its already established role as insulin sensitizer, we could show that recombinant bacterial LCN13 has also direct effects on insulin secreting β-cells both *in* and *ex vivo*. In stark contrast to these data as well as to previously published ones, we did not observe any metabolic role for LCN13 *in vivo*.

Our study exhibits several strengths, including the minimization of obstructive inflammatory responses in each of the applied techniques. Firstly, we produced recombinant LCN13 protein in a mammalian system, which excludes the possibility of bacterial contamination. Secondly, we applied hepatocyte-specific knockdown of LCN13 with the help of a LNP-based approach with chemically altered siRNA (2'-O-methyl- and phosphorothioate-modifications). These modifications confer increased siRNA stability while simultaneously eliminating its immunostimulatory potential (Judge et al., 2006; Selvam et al., 2017). Thirdly, we exploited AAV-driven, instead of adenovirus-mediated overexpression and, lastly, we used a rather tissue-specific LP1 promoter, instead of the ubiquitously active CMV promoter. The absence of detrimental side effects of LNP or AAV administration was proven in all studies by unchanged ALT and AST levels. Moreover, quality assurance involved the confirmation of manipulated hepatic mRNA and/or plasma protein levels of LCN13. The identity of the mammalian Fc-LCN13 protein was additionally confirmed by MS analysis. Another strength of this work is the broad time window, spanning 3 to 15 weeks post-AAV infection, in which metabolic phenotyping was conducted. We further excluded the possibility that the amount of viral particles administered and the interconnected high LCN13 overexpression levels were the reason for the lack of effect on the diabetic phenotype.

Lipocalin family members are characterized by redundant roles and the potential for binding to the same receptor (Table 1; Flower, 2000). Additionally, odorant binding proteins are known to be able to bind to a diverse set of cargos with comparable chemical properties (Briand et al., 2002; Pelosi, 1994; Tcatchoff et al., 2006). Therefore, only minimal changes in the system due to, for example, variances at the level of diet, presence of background inflammation or the composition of the microbial gut community could determine whether LCN13's regulatory capacity plays a role in a specific experimental setting. This idea is supported by the fact that the importance of other lipocalin family members in systemic energy homeostasis remains a matter of debate. By targeted induction of inflammation, manipulation of the gut microbiome or

simultaneous knockdown of additional LCN family members one might get a clearer picture of which factors could influence LCN13’s regulatory role in metabolism.

6. Appendix

6.1 Mass Spectrometry Analysis

Table 31 | Mass Spectrometry Analysis of Recombinant Mammalian Proteins

Mass spectrometry analysis of the recombinant mammalian Fc-LCN13 and the Fc control after in-solution digest was designed, conducted and analyzed by Dr. Christine von Törne. The ratio of Fc-LCN13 and Fc control was calculated by the normalized abundances of these two proteins.

						Normalized abundance		Raw abundance		Spectral count	
Gene symbol	**UniProt**	**Pep. count**	**Unique pep.**	**Conf. score**	**ratio FC-LCN13 / Fc Ctrl**	**Fc Ctrl**	**Fc-LCN13**	**Fc Ctrl**	**Fc-LCN13**	**Fc Ctrl**	**Fc-LCN 13**
Obp2a	**Q8K1H9**	**34**	**34**	**3417**	**570.9**	**72278378**	**41264273897**	**63882558**	**35823599124**	**0**	**254**
Gdf11	Q9Z1W4	2	2	204	474.6	3270	1552002	2890	1347371	0	4
Cep170	Q6A065	5	5	260	338.7	2491	843744	2202	732497	0	3
Sema3c	Q62181	38	38	2641	113.8	3805760	433088443	3363685	375985939	3	74
Prnp	P04925	4	4	173	77.7	100929	7842802	89206	6808733	1	3
Lpl	P11152; Q9WVG5	12	12	857	77.3	990648	76556003	875575	66462131	2	20
Hgf	Q08048	15	15	876	75.1	787543	59152245	696062	51353050	4	21
Psap	Q61207	5	5	387	72.5	760817	55151894	672441	47880143	2	8
Sart1	Q9Z315	10	10	720	61.8	80833	4996892	71444	4338054	0	11
Hexb	P20060	3	3	176	61.1	444783	27192162	393117	23606888	1	6
Fip1l1	Q9D824	4	4	292	56.0	713463	39980856	630588	34709399	0	7
Vegfc	P97953	8	8	546	53.8	392202	21088875	346644	18308317	0	12
Igfbp4	P47879	10	10	764	51.0	1235425	63007012	1091919	54699568	2	20
Sepp1	P70274	2	2	87	43.3	338434	14637962	299122	12707954	1	3
Sulf2	Q8CFG0; Q8K007	15	15	907	41.4	3735867	154495548	3301911	134125384	0	25
Bmp1	P98063; Q9WVM6; Q62381	5	5	227	38.9	57201	2222449	50557	1929420	0	5
Olfml3	Q8BK62	6	6	387	34.2	261225	8921303	230881	7745033	0	8
Crlf1	Q9JM58	9	8	545	27.1	273495	7414630	241726	6437015	0	9
C1qtnf4	Q8R066	26	25	2500	23.9	18137207	433353988	16030398	376216472	1	67
Mcm2	P97310	9	9	443	23.8	137394	3268172	121435	2837265	0	7
Nudt21	Q9CQF3	5	5	291	19.1	224152	4290018	198115	3724381	0	3
Cpsf7	Q8BTV2	5	5	419	18.6	109312	2027764	96614	1760405	0	6
Sbsn	Q8CIT9	2	2	172	18.5	1006568	18664377	889645	16203487	1	7
Loxl3	Q9Z175	16	16	984	18.4	2655525	48818247	2347060	42381584	5	18
Larp1	Q6ZQ58	6	6	361	17.0	76177	1297378	67328	1126319	0	3
Ssb	P32067; Q8CFW7	18	17	1364	16.7	3371115	56228783	2979528	48815045	2	22
U2surp	Q6NV83	4	4	263	16.0	160360	2564755	141732	2226593	0	5

Rps19	Q9CZX8	7	7	361	15.3	416484	6372761	368105	5532515	0	6
Cpsf6	Q6NVF9	9	9	666	14.3	853897	12238545	754709	10624899	0	11
Rps5	P97461	5	5	439	13.9	267852	3731020	236738	3239087	0	4
Nono	Q99K48	14	11	988	13.7	1769015	24170120	1563528	20983301	3	18
Prpf4b	Q61136	7	7	560	11.5	3002105	34613941	2653382	30050110	4	8
Cdk11b	P24788; Q03173	4	4	136	10.8	190566	2066893	168430	1794374	0	3
Htra1	Q9R118	7	7	317	10.8	189145	2033822	167174	1765663	2	7
Slc39a10	Q6P5F6	4	4	259	10.5	1578324	16598984	1394987	14410416	2	7
Top1	Q04750; Q8R4U6	14	14	617	10.0	2313618	23102083	2044869	20056085	4	20
Zc3h4	Q6ZPZ3	4	4	178	9.8	198431	1939979	175381	1684194	1	3
Mamdc2	Q8CG85	5	5	316	9.5	139004	1327071	122858	1152097	2	5
Sema3b	Q62177	13	13	730	9.4	2824860	26609680	2496726	23101207	6	17
Nucb1	Q02819	24	23	1878	9.2	10367485	95237280	9163203	82680290	13	38
Lamb1	P02469; Q9D659	23	23	1560	9.0	3938718	35515775	3481198	30833037	10	27
Rbbp6	P97868	4	4	289	8.2	446513	3640486	394646	3160490	1	6
Sfpq	Q8VIJ6	27	23	1638	7.7	11003357	85252736	9725213	74012204	6	24
Ccdc80	Q8R2G6	10	10	504	7.7	3490805	26871564	3085315	23328561	3	9
Itih5	Q8BJD1	5	5	218	7.7	207075	1589384	183021	1379825	1	5
Thbs1	P35441	25	25	1475	7.7	5880847	45072375	5197730	39129604	13	26
Dhx15	O35286; A2A4P0	13	13	530	7.3	794629	5814530	702325	5047887	1	11
Supt16h	Q920B9	4	4	201	7.2	239951	1717973	212079	1491459	0	3
Pxdn	Q3UQ28	41	41	3046	7.1	22600702	160308421	19975416	139171832	26	61
Vegfa	Q00731	8	8	421	7.1	11055131	78111524	9770973	67812557	4	11
Hnrnpl	Q8R081	20	20	1179	6.5	2931168	19173489	2590685	16645474	4	16
Nrp1	P97333	28	28	1843	6.2	31050443	192768026	27443639	167351654	22	45
Prpf40a	Q9R1C7; Q80W14	4	4	318	5.9	594063	3534062	525057	3068098	2	4
Neu1	O35657	3	3	132	5.8	101068	586523	89328	509190	0	3
Bgn	P28653	6	6	312	5.7	817574	4674873	722605	4058493	2	7
Rps23	P62267	5	5	282	5.4	258451	1405749	228429	1220402	0	3
Ctsz	Q9WUU7	3	3	282	5.0	1273366	6415829	1125452	5569905	3	4
Ltbp1	Q8CG19	43	42	3682	5.0	71576759	355199279	63262439	308366424	33	84
Rbm25	B2RY56	6	5	309	4.8	871838	4224467	770565	3667473	4	5
Rps2	P25444	5	5	254	4.4	155966	681870	137849	591966	3	5
Ltbp3	Q61810	3	2	177	4.3	111509	484984	98557	421039	1	3
Loxl4	Q924C6	4	4	264	3.6	297267	1057913	262736	918428	2	3
Dnajc10	Q9DC23	16	16	827	3.5	7817359	27626685	6909299	23984120	13	5
Luc7l2	Q7TNC4	7	3	417	3.5	320467	1108662	283242	962485	2	4
Ctsb	P10605	6	6	714	3.4	23608133	80456074	20865824	69847979	13	16
Rps4x	P62702	13	13	793	3.0	1475804	4439669	1304375	3854300	0	7
Krt10	P02535	13	5	814	3.0	8489027	25153107	7502946	21836682	5	6
Rack1	P68040	5	5	246	2.7	875185	2378550	773524	2064939	5	4
Tgfb1	P04202	9	9	523	2.7	6109869	16347190	5400150	14191821	7	4

Krt2	Q3TTY5	9	6	448	2.7	3194858	8466843	2823745	7350494	2	3
Pafah1b3	Q61205	10	9	480	2.6	1851900	4888942	1636784	4244338	3	8
Ext2	P70428	3	3	139	2.6	304147	781248	268817	678241	0	3
Aebp1	Q640N1	6	6	346	2.4	1857989	4489606	1642166	3897653	3	6
Nbl1	Q61477	2	2	146	2.4	1482770	3553847	1310533	3085274	4	5
Nid1	P10493	33	32	2608	2.3	182062203	415194042	160913951	360450906	56	66
Ctcf	Q61164; A2APF3	3	3	122	2.0	442316	867931	390937	753494	0	3
Prpf8	Q99PV0	6	6	342	1.9	276980	514864	244806	446980	5	3
Cbl	P22682; Q3TTA7	8	8	551	1.6	4558343	7385827	4028848	6412010	5	4
Npm1	Q61937	4	4	386	1.5	1600103	2453217	1414236	2129761	5	6
Krt1	P04104; Q6IFZ6	9	3	705	1.5	9786223	14578733	8649461	12656534	4	4
Calu	O35887	22	22	1644	1.4	4235706	5906921	3743688	5128096	3	3
Clu	Q06890	6	5	328	1.4	4650827	6402914	4110589	5558693	6	5
Eef1a1	P10126; P62631	10	9	662	1.4	5896314	8087793	5211401	7021421	12	8
Kpna3	O35344	4	4	174	1.3	256069	335319	226324	291107	1	3
Mycbp	Q9EQS3	2	2	180	1.3	1350733	1702099	1193832	1477678	4	3
Smad4	P97471; P15919	5	5	344	1.2	772806	962372	683037	835484	5	6
Glud1	P26443	8	8	482	1.2	1750557	2073948	1547214	1800499	6	5
Lgmn	O89017	9	9	879	1.2	59402044	68320102	52501933	59312129	17	15
Nucb2	P81117	8	8	670	1.1	16812330	18918082	14859418	16423742	10	7
Lamc1	P02468; E9Q5R7	8	8	450	1.1	1264688	1364990	1117782	1185017	6	4
Gapdh	P16858; Q64467	11	11	668	1.0	13337530	13342448	11788249	11583253	9	10
Xxylt1	Q3U4G3	9	9	587	0.9	5638427	5232506	4983470	4542602	8	7
Spp1	P10923	3	3	189	0.9	3966050	3666358	3505356	3182950	2	3
Serpine1	P22777	6	6	435	0.9	7421629	6738365	6559537	5849915	7	7
Clstn1	Q9EPL2; Q9ER65	17	16	1026	0.9	13020181	11655414	11507763	10118653	16	12
Gtf2a1	Q99PM3	4	4	308	0.8	18902769	15630410	16707033	13569548	7	4
Glg1	Q61543	24	24	1660	0.8	7944640	6325014	7021795	5491064	22	19
Crip2	Q9DCT8	5	5	304	0.8	5920904	4709953	5233135	4088948	3	3
Aga	Q64191	4	4	258	0.8	22383343	17225305	19783306	14954157	4	6
Sf3b4	Q8QZY9	6	6	598	0.8	8628830	6621134	7626509	5748140	5	8
Eftud2	O08810	13	13	667	0.7	2102595	1419889	1858359	1232677	11	7
Actb	P60710; Q8BFZ3	17	8	1308	0.6	23623807	14682146	20879677	12746312	13	10
Serbp1	Q9CY58	16	16	1199	0.6	6420099	3927967	5674344	3410066	7	3
Lama5	Q61001	18	18	1098	0.6	7111200	4273722	6285166	3710234	17	12
Dkk3	Q9QUN9	5	4	371	0.5	5999223	3186122	5302356	2766034	2	4
Prdx4	O08807	6	3	335	0.5	1924763	980903	1701183	851571	4	3
Zranb2	Q9R020	2	2	208	0.5	186500	91987	164836	79859	0	3
Gtf2a2	Q80ZM7	3	3	273	0.5	1962538	907301	1734571	787674	4	3

Hspg2	Q05793	99	98	7923	0.5	1042984179	479282632	921831672	416089446	237	154
Tubb5	P99024; P68372; Q7TMM9; Q9D6F9; Q9ERD7; Q922F4; A2AQ07	10	10	467	0.4	2875877	1229250	2541817	1067174	9	4
Ilf3	Q9Z1X4; Q91WM1	12	12	648	0.4	2331463	864542	2060641	750553	7	4
Vim	P20152; P15331; P31001	14	13	810	0.4	3963022	1468654	3502679	1275013	7	4
Sf3b3	Q921M3	20	20	1143	0.3	7343092	2197072	6490122	1907389	19	6
Eef1g	Q9D8N0	9	8	521	0.3	5428760	1577597	4798158	1369591	7	5
Lgals1	P16045	4	4	367	0.3	15413960	4457957	13623483	3870177	5	3
Cspg4	Q8VHY0	33	33	2193	0.3	69212740	19171496	61173024	16643743	30	21
Hnrnpf	Q9Z2X1	8	7	640	0.3	5972559	1649739	5278789	1432222	8	5
Fn1	P11276	64	63	4630	0.3	278266542	69902337	245943243	60685747	110	39
Eif5a	P63242; Q8BGY2	12	12	1209	0.2	26277511	6536861	23225129	5674979	28	9
Lmna	P48678; P21619	46	45	3160	0.2	237729521	56832529	210114982	49339187	42	9
Hsp90ab1	P11499; Q9CQN1; Q9D5S7	35	20	2197	0.2	40160969	9189087	35495892	7977510	32	15
Hspa8	P63017; P17156; P17879	19	15	1247	0.2	11535394	2636966	10195448	2289283	17	6
Eef2	P58252	25	25	1361	0.2	22614069	5102541	19987231	4429773	26	13
Hspa5	P20029	28	22	2050	0.2	23641074	5332986	20894939	4629834	28	6
Pkm	P52480; P53657	26	25	1739	0.2	92839275	20776134	82055112	18036811	38	14
Tinagl1	Q99JR5	11	11	908	0.2	56082279	11275587	49567790	9788906	23	11
Prdx1	P35700	10	7	388	0.2	10844159	2155176	9584507	1871017	8	3
Loxl1	P97873	11	11	1053	0.2	40284833	7944480	35605368	6897004	22	7
Agrn	A2ASQ1	10	10	547	0.2	16804699	3246436	14852674	2818395	10	3
Tgm2	P21981	14	14	927	0.2	35680902	6712790	31536227	5827712	18	7
Wdr1	O88342; Q7M707	17	17	1128	0.2	11030819	2040665	9749484	1771605	19	4
Cct8	P42932	17	16	938	0.2	11015937	1847598	9736331	1603993	15	3
Calr	P14211	7	7	438	0.2	5460088	886033	4825847	769210	8	4
Hist1h4a	P62806	8	8	548	0.2	97799777	15585177	86439405	13530279	24	9
Pdia3	P27773	15	15	849	0.2	34786852	5523904	30746029	4795580	22	4
Hsp90aa1	P07901	29	15	1844	0.2	22519263	3498554	19903437	3037271	21	9
Pgk1	P09411	18	15	1376	0.2	26598474	4060804	23508809	3525389	21	3
Nap1l1	P28656	5	4	275	0.1	1789959	242813	1582038	210799	2	3
Cnbp	P53996	9	9	863	0.1	32961809	3930238	29132982	3412038	16	8
Tcp1	P11983	12	12	864	0.1	8679302	1002759	7671119	870546	14	5

Cct3	P80318	13	12	683	0.1	8025918	896561	7093631	778350	12	3
Hsp90b1	P08113	34	32	2511	0.1	93478961	9688969	82620492	8411483	54	14
Cfl1	P18760	5	4	471	0.1	20357940	1927469	17993172	1673333	8	3
P4hb	P09103; Q8BUV8; Q8CII2	17	16	1048	0.1	34351268	2827313	30361042	2454533	25	9
Tkt	P40142	18	17	1317	0.1	50518373	4090637	44650185	3551289	29	6
Eno1	P17182; P21550; P17183	17	17	1466	0.1	72293335	5642762	63895778	4898767	32	8
Txndc5	Q91W90	14	14	921	0.1	257711295	19995030	227775683	17358694	33	5
Pgd	Q9DCD0	12	12	917	0.1	33754933	2181933	29833977	1894246	18	4
Ganab	Q8BHN3	12	12	608	0.1	4098998	239385	3622861	207823	12	3
Serpinh1	P19324	16	16	1202	0.1	37938969	2061016	33531998	1789272	20	7
Rplp0	P14869	7	6	458	0.0	7406893	270384	6546512	234734	8	3

Pep., peptide; conf., confidence

6.2 Author Contributions

Table 32 | Author contributions to this work

Figure/Table	Study	Contribution
Figure 5	LCN13 tissue expression screen	Designed, conducted and analyzed by Lea Katharina Bühler
Figure 6, 7 and 16	LCN13 knockdown study	Designed and analyzed by Lea Katharina Bühler Conducted by Elena Vogl
Figure 8	Wild type mice injected with recombinant Fc-LCN13	Designed, conducted and analyzed by Lea Katharina Bühler Protein production by Lea Katharina Bühler Protein purification by Dr. Anastasia Georgiadi
Figure 9 and 12	HFD study to test preventive potential of LCN13	Designed, conducted and analyzed by Lea Katharina Bühler
Figure 10 and 11	HFD study to test therapeutic potential of LCN13	Designed, conducted and analyzed by Lea Katharina Bühler
Figure 13, 14 and 17	db/db mice study to test therapeutic potential of LCN13	Designed, conducted and analyzed by Lea Katharina Bühler
Figure 15	AAV titration study	Designed, conducted and analyzed by Lea Katharina Bühler
Figure 18	GSIS of MIN6 pseudo-islets and primary islets	Designed, conducted and analyzed by Lea Katharina Bühler
Table 31	Mass spectrometry analysis of recombinant mammalian Fc-LCN13 and Fc control	Designed, conducted and analyzed by Christine von Törne

6.3 List of Abbreviations

Table 33 | Abbreviations

Abbreviation	Meaning
°C	Degree Celsius
AAV	Adeno-associated virus
ACC	Acetyl-CoA carboxylase
Ac-CoA	Acetyl-coenzyme A
ACS	Acetyl-CoA synthetase
ADA	American Diabetes Association
ADP	Adenosine diphosphate
ALT	Alanine transaminase
AMPK	5' adenosine monophosphate-activated protein kinase
APO	Apolipoprotein
AST	Aspartate transaminase
ATGL	Adipose triglyceride lipase
ATP	Adenosine triphosphate
AUC	Area under the curve
BAT	Brown adipose tissue
BSA	Bovine serum albumin
BW	Body weight
$CaCl_2$	Calcium chloride
CAG	CMV enhancer, chicken beta-Actin promoter and rabbit beta-Globin splice acceptor site
cAMP	Cyclic adenosine monophosphate
cAMP-GEFII	cAMP-regulated guanine nucleotide exchange factor II
CCL5	Chemokine (C-C motif) ligand 5
cDNA	Complementary DNA
CERS6	Ceramide synthase enzyme 6
CHO	Chinese hamster ovary
CMV	Cytomegalovirus
CO_2	Carbon dioxide
CoA	Coenzyme A
Conf.	Confidence
CPT-I	Carnitinepalmitoyltransferase I
CREB	cAMP response element-binding protein
CRTC2	CREB regulated transcription coactivator 2
Ctrl	Control
CVD	Cardiovascular disease
DAG	Diacylglycerol

DDA	Data-dependent acquisition
DHAP	Dihydroxyacetone phosphate
DIO	Diet-induced obese
DNA	Deoxyribonucleic acid
DPP4	Dipeptidyl peptidase 4
DPP4i	DPP4 inhibitor
DS	dd Shionogi
DTT	Dithiothreitol
EASD	European Association for the Study of Diabetes
EGFR	Epidermal growth factor receptor
EGP	Endogenous glucose production
EGR1	Early growth response protein 1
Epac 2	Exchange protein directly activated by cAMP 2
EpiWAT	Epididymal white adipose tissue
ER	Endoplasmatic reticulum
e^-TC	Electron transport chain
EtOH	Ethanol
Ex-4	Exendin-4
FA-CoA	Acyl-coenzyme A
$FADH_2$	Flavin adenine dinulceotide
FAS	Fatty acid synthase
FASP	Filter-aided sample preparation
Fc	Fragment crystallizable region
FDR	False discovery rate
FFA	Free fatty acid
FGF21	Fibroblast growth factor 21
FLS	Fatty liver Shionogi
FOXO	Forkhead box O transcription factor
FXR	Farnesoid X receptor
G-6-P	Glucose-6-phosphate
GC	Gastrocnemius muscle
GDH	Glutamate dehydrogenase
GEO	Gene Expression Omnibus
GFP	Green fluorescent protein
GIP	Glucose-dependent insulinotropic peptide
GK	Glucokinase
GL	Glycerolipid
Gln	Glutamine
GLP-1	Glucagon-like peptide-1
GLP-1RA	GLP-1 receptor agonist

Glu	Glutamate
GLUT2	Glucose transporter 2
GLUT4	Glucose transporter 4
GPCR	G protein-coupled receptor
GPR40	G-protein-coupled receptor 40
Gro3P	Glycerol-3-phosphate
GSIS	Glucose-stimulated insulin secretion
GSK3β	Glycogen synthase kinase 3 beta
GTT	Glucose tolerance test
h	Hour
HbA1c	Glycated hemoglobin
HBSS	Hank's Balanced Salt Solution
HCl	Hydrochloric acid
HDL	High-density lipoprotein
HEPES	4-(2-hydroxyethyl)-1-piperazineethanesulfonic acid
HFD	High fat diet
HOMA-IR	Homeostatic model assessment evaluation of insulin resistance
HPLC	High performance liquid chromatography
Hth	Hypothalamus
Hz	Hertz
i.p.	Intraperitoneal
i.v.	Intravenous
IAPP	Islet amyloid polypeptide
IFN	Interferon
IgG	Immunoglobulin G
IGNG	Intestinal gluconeogenesis
IGT	Impaired glucose tolerance
IKK	Inhibitor of nuclear factor kappa-B kinase
IL	Interleukin
IMAC	Immobilized metal ion affinity chromatography
IngWAT	Inguinal white adipose tissue
IP_3	Inositol 1,4,5-triphosphate
IR	Insulin receptor
IRE-1α	Inositol-requiring enzyme 1 alpha
IRS	Insulin receptor substrate
ITT	Insulin tolerance test
JNK	JUN N-terminal kinase
K_{ATP}	ATP-sensitive potassium channel
KCl	Potassium chloride
kDa	Kilodalton

kg	Kilogram
KH_2PO_4	Monopotassium chloride
KO	Knockout
KRB	Krebs-Ringer buffer
Kv	Voltage-dependent potassium channel
L	Litre
LC	Liquid chromatography
LCN	Lipocalin
LDL	Low-density lipoprotein
Leu	Leucine
LFD	Low fat diet
LNP	Liponanoparticle
LPS	Lipopolysaccharide
LRC	Ligand receptor capture
m	Mass
MAG	Monoacylglycerol
Mal-CoA	Malonyl-coenzyme A
MAPK	P38 mitogen-activated protein kinase
MCD	Methionine/choline-deficient
MCF	Metabolic coupling factor
MEF	Mouse embryonic fibroblast
MeOH	Methanol
mg	Milligram
$MgSO_4$	Magnesium sulphate
min	Minute
mL	Millilitre
mRNA	Messenger ribonucleic acid
MS	Mass spectrometry
mTORC1	Mammalian target of rapamycin complex 1
Munc13-1	Mammalian homologue of UNC-13-1
MUP1	Major urinary protein 1
Na	Natrium
NaCl	Natrium chloride
NAD	Nicotinamide adenine dinucleotide
NADP	Nicotinamide adenine dinucleotide phosphate
NAFLD	Non-alcoholic fatty liver disease
$NaHCO_3$	Sodium biocarbonate
$NaHPO_4$	Sodium hydrogenphosphate
NASH	Non-alcoholic steatohepatitis
NEFA	Non-esterified fatty acids

NF-κB	Nuclear factor kappa-B
NW	Normal weight
OB	Obese
OBP	Odorant-binding protein
Ob-Rb	Long form of the leptin receptor
OE	Overexpression
OXM	Oxyntomodulin
OXPHOS	Oxidative phosphorylation
PAGE	Polyacrylamide gel electrophoresis
PAI-1	Plasminogen activator inhibitor-1
PBS	Phosphate-buffered saline
PC	Pyruvate carboxylase
PCR	Polymerase chain reaction
PDE3B	Phosphodiesterase 3B
PDK	3-phosphoinositide-dependent protein kinase-1
PDK4	Pyruvate dehydrogenase kinase 4
PDX1	Pancreatic and duodenal homeobox 1
Pep.	Peptide
PEPCK	Phosphoenolpyruvate carboxykinase
pH	Power/Potential of hydrogen
PI3K	Phosphatidylinositol 3-kinase
PIP_2	Phosphatidylinositol 4,5-bisphosphate
PIP_3	Phosphatidylinositol (3,4,5)-trisphosphate
PKA	Protein kinase A
PKB	Protein kinase B
PKC	Protein kinase C
PKD1	Protein kinase D1
PKR	Protein kinase RNA-activated
PLC	Phospholipase C
PPAR	Peroxisome proliferator-activated receptor
PTGDS	Prostaglandin D2 synthase
PYY	Peptide YY
qRT-PCR	Quantitative real-time polymerase chain reaction
RAR	Retinoic acid receptor
RBP4	Retinol-binding protein 4
RNA	Ribonucleic acid
RNA-seq	RNA sequencing
ROS	Reactive oxygen species
Rpm	Rounds per min
RT	Room Temperature

RT-PCR	Real-time polymerase chain reaction
RXR	Retinoid X receptor
RYGB	Roux-en-Y gastric bypass
s	Second
S1P	Sphingosine 1-phosphate
S6K	Ribosomal protein S6 kinase beta-1
SCFA	Short chain fatty acid
scRNA-seq	Single cell RNA sequencing
SDS	Sodium dodecyl sulfate
SEM	Standard error of the mean
Ser	Serine
SGLT	Sodium-dependent glucose cotransporter
SGLT2i	SGLT2 inhibitor
siC	Control siRNA
siLCN	siRNA directed against *Lcn13* mRNA
siRNA	Small interfering RNA
SNP	Single nucleotide polymorphism
SOCS	Suppressor of cytokine signalling
SREBP1	Sterol regulatory element-binding protein-1
STRA6	Stimulated by retinoic acid 6
SU	Sulfonylurea
SUR	Sulfonylurea receptor
T1D	Type 1 diabetes
T2D	Type 2 diabetes
TAE	Tris-acetate-EDTA
TBC1D4	TBC1 domain family member 4
TBP	TATA-box binding protein
TBS	Tris buffered saline
TBS-T	Tris buffered saline with Tween 20
TCF7L2	Transcription factor 7-like 2
TE	Tris-EDTA
Thr	Threonine
TLR	Toll-like receptor
TNF-α	Tumor necrosis factor alpha
TSC2	Tuberous sclerosis complex 2
TSC22D4	Transforming growth factor beta-like stimulated clone 22 D4
TZD	Thiazolidinediones
U	Unit
UCP-2	Uncoupling protein-2
UPR	Unfolded protein response

V	Volume
VDCC	Voltage-dependent calcium channels
vg	Viral genome
VLDL	Very-low-density lipoprotein
VSG	Vertical sleeve gastrectomy
w	Weight
WAT	White adipose tissue
WB	Washing buffer
ZDF	Zucker diabetic fatty
ZF	Zucker fatty
α	Alpha
α-KG	Alpha-ketoglutarate
β	Beta
γ	Gamma
δ	Delta
ε	Epsilon
θ	Theta
κ	Kappa

6.4 List of Figures and Tables

6.4.1 Figures

6.4.2 Tables

7. References

Abella, V., Scotece, M., Conde, J., Gomez, R., Lois, A., Pino, J., Gomez-Reino, J.J., Lago, F., Mobasheri, A., and Gualillo, O. (2015). The potential of lipocalin-2/NGAL as biomarker for inflammatory and metabolic diseases. Biomarkers : biochemical indicators of exposure, response, and susceptibility to chemicals *20*, 565-571.

Action to Control Cardiovascular Risk in Diabetes Study Group, H.C.G., Michael E Miller, Robert P Byington, David C Goff Jr, J Thomas Bigger, John B Buse, William C Cushman, Saul Genuth, Faramarz Ismail-Beigi, Richard H Grimm Jr, Jeffrey L Probstfield, Denise G Simons-Morton, William T Friedewald (2008). Effects of Intensive Glucose Lowering in Type 2 Diabetes. New England Journal of Medicine *358*, 2545-2559.

Adeghate, E., Mohsin, S., Adi, F., Ahmed, F., Yahya, A., Kalasz, H., Tekes, K., and Adeghate, E.A. (2019). An update of SGLT1 and SGLT2 inhibitors in early phase diabetes-type 2 clinical trials. Expert opinion on investigational drugs *28*, 811-820.

Adina-Zada, A., Zeczycki, T.N., and Attwood, P.V. (2012). Regulation of the structure and activity of pyruvate carboxylase by acetyl CoA. Arch Biochem Biophys *519*, 118-130.

ADVANCE Collaborative Group, A.P., Stephen MacMahon, John Chalmers, Bruce Neal, Laurent Billot, Mark Woodward, Michel Marre, Mark Cooper, Paul Glasziou, Diederick Grobbee, Pavel Hamet, Stephen Harrap, Simon Heller, Lisheng Liu, Giuseppe Mancia, Carl Erik Mogensen, Changyu Pan, Neil Poulter, Anthony Rodgers, Bryan Williams, Severine Bompoint, Bastiaan E de Galan, Rohina Joshi, Florence Travert (2008). Intensive Blood Glucose Control and Vascular Outcomes in Patients with Type 2 Diabetes. New England Journal of Medicine *358*, 2560-2572.

Ahlqvist, E., Storm, P., Käräjämäki, A., Martinell, M., Dorkhan, M., Carlsson, A., Vikman, P., Prasad, R.B., Aly, D.M., Almgren, P.*, et al.* (2018). Novel subgroups of adult-onset diabetes and their association with outcomes: a data-driven cluster analysis of six variables. The Lancet Diabetes & Endocrinology *6*, 361-369.

Ahmad, R., Rah, B., Bastola, D., Dhawan, P., and Singh, A.B. (2017). Obesity-induces Organ and Tissue Specific Tight Junction Restructuring and Barrier Deregulation by Claudin Switching. Scientific reports *7*, 5125-5125.

Akache, B., Grimm, D., Pandey, K., Yant, S.R., Xu, H., and Kay, M.A. (2006). The 37/67-kilodalton laminin receptor is a receptor for adeno-associated virus serotypes 8, 2, 3, and 9. Journal of virology *80*, 9831-9836.

Akelma, A.Z., Abaci, A., Ozdemir, O., Celik, A., Avci, Z., Razi, C.H., Hizli, S., and Akin, O. (2012). The association of serum lipocalin-2 levels with metabolic and clinical parameters in obese children: a pilot study. Journal of pediatric endocrinology & metabolism : JPEM *25*, 525-528.

Ali, O. (2013). Genetics of type 2 diabetes. World J Diabetes *4*, 114-123.

Alkhouri, N., Lopez, R., Berk, M., and Feldstein, A.E. (2009). Serum retinol-binding protein 4 levels in patients with nonalcoholic fatty liver disease. J Clin Gastroenterol *43*, 985-989.

Arita, Y., Kihara, S., Ouchi, N., Takahashi, M., Maeda, K., Miyagawa, J., Hotta, K., Shimomura, I., Nakamura, T., Miyaoka, K.*, et al.* (1999). Paradoxical decrease of an adipose-specific protein, adiponectin, in obesity. Biochemical and biophysical research communications *257*, 79-83.

Arkan, M.C., Hevener, A.L., Greten, F.R., Maeda, S., Li, Z.W., Long, J.M., Wynshaw-Boris, A., Poli, G., Olefsky, J., and Karin, M. (2005). IKK-beta links inflammation to obesity-induced insulin resistance. Nature medicine *11*, 191-198.

Aroda, V.R., Henry, R.R., Han, J., Huang, W., DeYoung, M.B., Darsow, T., and Hoogwerf, B.J. (2012). Efficacy of GLP-1 receptor agonists and DPP-4 inhibitors: meta-analysis and systematic review. Clinical therapeutics *34*, 1247-1258.e1222.

Aronoff, S.L., Berkowitz, K., Shreiner, B., and Want, L. (2004). Glucose Metabolism and Regulation: Beyond Insulin and Glucagon. Diabetes Spectrum *17*, 183-190.

Back, S.H., and Kaufman, R.J. (2012). Endoplasmic reticulum stress and type 2 diabetes. Annu Rev Biochem *81*, 767-793.

Baker, W.A., Hitman, G.A., Hawrami, K., McCarthy, M.I., Riikonen, A., Tuomilehto-Wolf, E., Nissinen, A., Tuomilehto, J., Mohan, V., Viswanathan, M.*, et al.* (1994). Apolipoprotein D gene polymorphism: a new genetic marker for type 2 diabetic subjects in Nauru and south India. Diabetic medicine : a journal of the British Diabetic Association *11*, 947-952.

Balas, B., Baig, M.R., Watson, C., Dunning, B.E., Ligueros-Saylan, M., Wang, Y., He, Y.L., Darland, C., Holst, J.J., Deacon, C.F.*, et al.* (2007). The dipeptidyl peptidase IV inhibitor vildagliptin suppresses endogenous glucose production and enhances islet function after single-dose administration in type 2 diabetic patients. The Journal of clinical endocrinology and metabolism *92*, 1249-1255.

Barbosa-Morais, N.L., Irimia, M., Pan, Q., Xiong, H.Y., Gueroussov, S., Lee, L.J., Slobodeniuc, V., Kutter, C., Watt, S., Çolak, R.*, et al.* (2012). The Evolutionary Landscape of Alternative Splicing in Vertebrate Species. Science (New York, NY) *338*, 1587-1593.

Barclay, J.W., Morgan, A., and Burgoyne, R.D. (2005). Calcium-dependent regulation of exocytosis. Cell Calcium *38*, 343-353.

Baron, A.D., Schaeffer, L., Shragg, P., and Kolterman, O.G. (1987). Role of hyperglucagonemia in maintenance of increased rates of hepatic glucose output in type II diabetics. Diabetes *36*, 274-283.

Barrett, T., Wilhite, S.E., Ledoux, P., Evangelista, C., Kim, I.F., Tomashevsky, M., Marshall, K.A., Phillippy, K.H., Sherman, P.M., Holko, M.*, et al.* (2013). NCBI GEO: archive for functional genomics data sets--update. Nucleic acids research *41*, D991-995.

Beaumont, M., Neyrinck, A.M., Olivares, M., Rodriguez, J., de Rocca Serra, A., Roumain, M., Bindels, L.B., Cani, P.D., Evenepoel, P., Muccioli, G.G.*, et al.* (2018). The gut microbiota metabolite indole alleviates liver inflammation in mice. FASEB journal : official publication of the Federation of American Societies for Experimental Biology *32*, fj201800544-fj201800544.

Berg, A.H., Combs, T.P., Du, X., Brownlee, M., and Scherer, P.E. (2001). The adipocyte-secreted protein Acrp30 enhances hepatic insulin action. Nature medicine *7*, 947-953.

Berry, D.C., Jin, H., Majumdar, A., and Noy, N. (2011). Signaling by vitamin A and retinol-binding protein regulates gene expression to inhibit insulin responses. Proceedings of the National Academy of Sciences of the United States of America *108*, 4340-4345.

Blache, P., Gros, L., Salazar, G., and Bataille, D. (1998). Cloning and tissue distribution of a new rat olfactory receptor-like (OL2). Biochemical and biophysical research communications *242*, 669-672.

Bluher, M. (2019). Obesity: global epidemiology and pathogenesis. Nature reviews Endocrinology *15*, 288-298.

Boden, G., Duan, X., Homko, C., Molina, E.J., Song, W., Perez, O., Cheung, P., and Merali, S. (2008). Increase in endoplasmic reticulum stress-related proteins and genes in adipose tissue of obese, insulin-resistant individuals. Diabetes *57*, 2438-2444.

Boudjelal, M., Sivaprasadarao, A., and Findlay, J.B. (1996). Membrane receptor for odour-binding proteins. The Biochemical journal *317 (Pt 1)*, 23-27.

Brahimaj, A., Ligthart, S., Ikram, M.A., Hofman, A., Franco, O.H., Sijbrands, E.J., Kavousi, M., and Dehghan, A. (2017). Serum Levels of Apolipoproteins and Incident Type 2 Diabetes: A Prospective Cohort Study. Diabetes care *40*, 346-351.

Brandt, S.J., Götz, A., Tschöp, M.H., and Müller, T.D. (2018). Gut hormone polyagonists for the treatment of type 2 diabetes. Peptides *100*, 190-201.

Brereton, M.F., Iberl, M., Shimomura, K., Zhang, Q., Adriaenssens, A.E., Proks, P., Spiliotis, II, Dace, W., Mattis, K.K., Ramracheya, R.*, et al.* (2014). Reversible changes in pancreatic islet structure and function produced by elevated blood glucose. Nature communications *5*, 4639.

Briand, L., Eloit, C., Nespoulous, C., Bezirard, V., Huet, J.C., Henry, C., Blon, F., Trotier, D., and Pernollet, J.C. (2002). Evidence of an odorant-binding protein in the human olfactory mucus: location, structural characterization, and odorant-binding properties. Biochemistry *41*, 7241-7252.

Brose, N., Petrenko, A.G., Sudhof, T.C., and Jahn, R. (1992). Synaptotagmin: a calcium sensor on the synaptic vesicle surface. Science (New York, NY) *256*, 1021-1025.

Brun, P., Castagliuolo, I., Di Leo, V., Buda, A., Pinzani, M., Palu, G., and Martines, D. (2007). Increased intestinal permeability in obese mice: new evidence in the pathogenesis of nonalcoholic steatohepatitis. American journal of physiology Gastrointestinal and liver physiology *292*, G518-525.

Buteau, J., Foisy, S., Joly, E., and Prentki, M. (2003). Glucagon-like peptide 1 induces pancreatic beta-cell proliferation via transactivation of the epidermal growth factor receptor. Diabetes *52*, 124-132.

Buteau, J., Spatz, M.L., and Accili, D. (2006). Transcription factor FoxO1 mediates glucagon-like peptide-1 effects on pancreatic beta-cell mass. Diabetes *55*, 1190-1196.

Butler, A.E., Janson, J., Bonner-Weir, S., Ritzel, R., Rizza, R.A., and Butler, P.C. (2003). Beta-cell deficit and increased beta-cell apoptosis in humans with type 2 diabetes. Diabetes *52*, 102-110.

Cajka, T., and Fiehn, O. (2014). Comprehensive analysis of lipids in biological systems by liquid chromatography-mass spectrometry. Trends Analyt Chem *61*, 192-206.

Campfield, L.A., Smith, F.J., Guisez, Y., Devos, R., and Burn, P. (1995). Recombinant mouse OB protein: evidence for a peripheral signal linking adiposity and central neural networks. Science (New York, NY) *269*, 546-549.

Cani, P.D., Amar, J., Iglesias, M.A., Poggi, M., Knauf, C., Bastelica, D., Neyrinck, A.M., Fava, F., Tuohy, K.M., Chabo, C.*, et al.* (2007). Metabolic endotoxemia initiates obesity and insulin resistance. Diabetes *56*, 1761-1772.

Cani, P.D., Osto, M., Geurts, L., and Everard, A. (2012). Involvement of gut microbiota in the development of low-grade inflammation and type 2 diabetes associated with obesity. Gut Microbes *3*, 279-288.

Capulli, M., Ponzetti, M., Maurizi, A., Gemini-Piperni, S., Berger, T., Mak, T.W., Teti, A., and Rucci, N. (2018). A Complex Role for Lipocalin 2 in Bone Metabolism: Global Ablation in Mice Induces Osteopenia Caused by an Altered Energy Metabolism. Journal of bone and mineral research : the official journal of the American Society for Bone and Mineral Research *33*, 1141-1153.

Carey, D.G., Cowin, G.J., Galloway, G.J., Jones, N.P., Richards, J.C., Biswas, N., and Doddrell, D.M. (2002). Effect of rosiglitazone on insulin sensitivity and body composition in type 2 diabetic patients [corrected]. Obesity research *10*, 1008-1015.

Carey, D.G., Jenkins, A.B., Campbell, L.V., Freund, J., and Chisholm, D.J. (1996). Abdominal fat and insulin resistance in normal and overweight women: Direct measurements reveal a strong relationship in subjects at both low and high risk of NIDDM. Diabetes *45*, 633-638.

Castillo-Armengol, J., Fajas, L., and Lopez-Mejia, I.C. (2019). Inter-organ communication: a gatekeeper for metabolic health. EMBO reports *20*, e47903.

Cengiz, C., Ardicoglu, Y., Bulut, S., and Boyacioglu, S. (2010). Serum retinol-binding protein 4 in patients with nonalcoholic fatty liver disease: does it have a significant impact on pathogenesis? European journal of gastroenterology & hepatology *22*, 813-819.

Cervera, A., Wajcberg, E., Sriwijitkamol, A., Fernandez, M., Zuo, P., Triplitt, C., Musi, N., DeFronzo, R.A., and Cersosimo, E. (2008). Mechanism of action of exenatide to reduce postprandial hyperglycemia in type 2 diabetes. Am J Physiol Endocrinol Metab *294*, E846-852.

Chakrabarti, P., Kim, J.Y., Singh, M., Shin, Y.K., Kim, J., Kumbrink, J., Wu, Y., Lee, M.J., Kirsch, K.H., Fried, S.K.*, et al.* (2013). Insulin inhibits lipolysis in adipocytes via the evolutionarily conserved mTORC1-Egr1-ATGL-mediated pathway. Mol Cell Biol *33*, 3659-3666.

Chan, Y.K., Sung, H.K., Jahng, J.W., Kim, G.H., Han, M., and Sweeney, G. (2016). Lipocalin-2 inhibits autophagy and induces insulin resistance in H9c2 cells. Molecular and cellular endocrinology *430*, 68-76.

Chang, A.M., and Halter, J.B. (2003). Aging and insulin secretion. Am J Physiol Endocrinol Metab *284*, E7-12.

Charkoftaki, G., Wang, Y., McAndrews, M., Bruford, E.A., Thompson, D.C., Vasiliou, V., and Nebert, D.W. (2019). Update on the human and mouse lipocalin (LCN) gene family, including evidence the mouse Mup cluster is result of an "evolutionary bloom". Hum Genomics *13*, 11-11.

Charles, E.D., Neuschwander-Tetri, B.A., Pablo Frias, J., Kundu, S., Luo, Y., Tirucherai, G.S., and Christian, R. (2019). Pegbelfermin (BMS-986036), PEGylated FGF21, in Patients with Obesity and Type 2 Diabetes: Results from a Randomized Phase 2 Study. Obesity (Silver Spring, Md) *27*, 41-49.

Chavez, A.O., Molina-Carrion, M., Abdul-Ghani, M.A., Folli, F., Defronzo, R.A., and Tripathy, D. (2009). Circulating fibroblast growth factor-21 is elevated in impaired glucose tolerance and type 2 diabetes and correlates with muscle and hepatic insulin resistance. Diabetes care *32*, 1542-1546.

Chavez, J.A., and Summers, S.A. (2003). Characterizing the effects of saturated fatty acids on insulin signaling and ceramide and diacylglycerol accumulation in 3T3-L1 adipocytes and C2C12 myotubes. Arch Biochem Biophys *419*, 101-109.

Chen, C., Cohrs, C.M., Stertmann, J., Bozsak, R., and Speier, S. (2017a). Human beta cell mass and function in diabetes: Recent advances in knowledge and technologies to understand disease pathogenesis. Molecular metabolism *6*, 943-957.

Chen, C., Hosokawa, H., Bumbalo, L.M., and Leahy, J.L. (1994a). Mechanism of compensatory hyperinsulinemia in normoglycemic insulin-resistant spontaneously hypertensive rats. Augmented enzymatic activity of glucokinase in beta-cells. The Journal of clinical investigation *94*, 399-404.

Chen, H., Charlat, O., Tartaglia, L.A., Woolf, E.A., Weng, X., Ellis, S.J., Lakey, N.D., Culpepper, J., Moore, K.J., Breitbart, R.E.*, et al.* (1996). Evidence that the diabetes gene encodes the leptin receptor: identification of a mutation in the leptin receptor gene in db/db mice. Cell *84*, 491-495.

Chen, S., Ogawa, A., Ohneda, M., Unger, R.H., Foster, D.W., and McGarry, J.D. (1994b). More direct evidence for a malonyl-CoA-carnitine palmitoyltransferase I interaction as a key event in pancreatic beta-cell signaling. Diabetes *43*, 878-883.

Chen, X., Shen, T., Li, Q., Chen, X., Li, Y., Li, D., Chen, G., Ling, W., and Chen, Y.M. (2017b). Retinol Binding Protein-4 Levels and Non-alcoholic Fatty Liver Disease: A community-based cross-sectional study. Scientific reports *7*, 45100.

Chen, Y., Clarke, O.B., Kim, J., Stowe, S., Kim, Y.-K., Assur, Z., Cavalier, M., Godoy-Ruiz, R., von Alpen, D.C., Manzini, C.*, et al.* (2016). Structure of the STRA6 receptor for retinol uptake. Science (New York, NY) *353*, aad8266.

Cheng, L., Ziegelhoffer, P.R., and Yang, N.S. (1993). In vivo promoter activity and transgene expression in mammalian somatic tissues evaluated by using particle bombardment. Proceedings of the National Academy of Sciences of the United States of America *90*, 4455-4459.

Cheung, C.L., Cheung, T.T., Lam, K.S., and Cheung, B.M. (2013). Reduced serum beta-trace protein is associated with metabolic syndrome. Atherosclerosis *227*, 404-407.

Chia, C.W., Carlson, O.D., Kim, W., Shin, Y.K., Charles, C.P., Kim, H.S., Melvin, D.L., and Egan, J.M. (2009). Exogenous glucose-dependent insulinotropic polypeptide worsens post prandial hyperglycemia in type 2 diabetes. Diabetes *58*, 1342-1349.

Chirmule, N., Propert, K., Magosin, S., Qian, Y., Qian, R., and Wilson, J. (1999). Immune responses to adenovirus and adeno-associated virus in humans. Gene therapy *6*, 1574-1583.

Cho, K.W., Zhou, Y., Sheng, L., and Rui, L. (2011). Lipocalin-13 regulates glucose metabolism by both insulin-dependent and insulin-independent mechanisms. Mol Cell Biol *31*, 450-457.

Christoffersen, C., Federspiel, C.K., Borup, A., Christensen, P.M., Madsen, A.N., Heine, M., Nielsen, C.H., Kjaer, A., Holst, B., Heeren, J.*, et al.* (2018). The Apolipoprotein M/S1P Axis Controls Triglyceride Metabolism and Brown Fat Activity. Cell reports *22*, 175-188.

Christoffersen, C., Obinata, H., Kumaraswamy, S.B., Galvani, S., Ahnstrom, J., Sevvana, M., Egerer-Sieber, C., Muller, Y.A., Hla, T., Nielsen, L.B.*, et al.* (2011). Endothelium-protective sphingosine-1-phosphate provided by HDL-associated apolipoprotein M. Proceedings of the National Academy of Sciences of the United States of America *108*, 9613-9618.

Chung, H.S., and Choi, K.M. (2020). Organokines in disease. Advances in clinical chemistry *94*, 261-321.

Cipollone, F., Fazia, M., Iezzi, A., Ciabattoni, G., Pini, B., Cuccurullo, C., Ucchino, S., Spigonardo, F., De Luca, M., Prontera, C.*, et al.* (2004). Balance between PGD synthase and PGE synthase is a major determinant of atherosclerotic plaque instability in humans. Arteriosclerosis, thrombosis, and vascular biology *24*, 1259-1265.

Clemmensen, C., Chabenne, J., Finan, B., Sullivan, L., Fischer, K., Küchler, D., Sehrer, L., Ograjsek, T., Hofmann, S.M., Schriever, S.C.*, et al.* (2014). GLP-1/glucagon coagonism restores leptin responsiveness in obese mice chronically maintained on an obesogenic diet. Diabetes *63*, 1422-1427.

Codoner-Franch, P., Carrasco-Luna, J., Allepuz, P., Codoner-Alejos, A., and Guillem, V. (2016). Association of RBP4 genetic variants with childhood obesity and cardiovascular risk factors. Pediatric diabetes *17*, 576-583.

Colberg, S.R., Sigal, R.J., Fernhall, B., Regensteiner, J.G., Blissmer, B.J., Rubin, R.R., Chasan-Taber, L., Albright, A.L., Braun, B., American College of Sports, M.*, et al.* (2010).

Exercise and type 2 diabetes: the American College of Sports Medicine and the American Diabetes Association: joint position statement. Diabetes care *33*, e147-e167.

Combs, T.P., Berg, A.H., Obici, S., Scherer, P.E., and Rossetti, L. (2001). Endogenous glucose production is inhibited by the adipose-derived protein Acrp30. The Journal of clinical investigation *108*, 1875-1881.

Combs, T.P., Pajvani, U.B., Berg, A.H., Lin, Y., Jelicks, L.A., Laplante, M., Nawrocki, A.R., Rajala, M.W., Parlow, A.F., Cheeseboro, L.*, et al.* (2004). A transgenic mouse with a deletion in the collagenous domain of adiponectin displays elevated circulating adiponectin and improved insulin sensitivity. Endocrinology *145*, 367-383.

Considine, R.V., Sinha, M.K., Heiman, M.L., Kriauciunas, A., Stephens, T.W., Nyce, M.R., Ohannesian, J.P., Marco, C.C., McKee, L.J., Bauer, T.L.*, et al.* (1996). Serum immunoreactive-leptin concentrations in normal-weight and obese humans. The New England journal of medicine *334*, 292-295.

Consoli, A., Nurjhan, N., Capani, F., and Gerich, J. (1989). Predominant role of gluconeogenesis in increased hepatic glucose production in NIDDM. Diabetes *38*, 550-557.

Cooper, G.J., Willis, A.C., Clark, A., Turner, R.C., Sim, R.B., and Reid, K.B. (1987). Purification and characterization of a peptide from amyloid-rich pancreases of type 2 diabetic patients. Proceedings of the National Academy of Sciences of the United States of America *84*, 8628-8632.

Copps, K.D., and White, M.F. (2012). Regulation of insulin sensitivity by serine/threonine phosphorylation of insulin receptor substrate proteins IRS1 and IRS2. Diabetologia *55*, 2565-2582.

Cox, L.M., Yamanishi, S., Sohn, J., Alekseyenko, A.V., Leung, J.M., Cho, I., Kim, S.G., Li, H., Gao, Z., Mahana, D.*, et al.* (2014). Altering the intestinal microbiota during a critical developmental window has lasting metabolic consequences. Cell *158*, 705-721.

Crestani, F., Martin, J.R., Mohler, H., and Rudolph, U. (2000). Resolving differences in GABAA receptor mutant mouse studies. Nature neuroscience *3*, 1059.

Croset, M., Rajas, F., Zitoun, C., Hurot, J.M., Montano, S., and Mithieux, G. (2001). Rat small intestine is an insulin-sensitive gluconeogenic organ. Diabetes *50*, 740-746.

Cross, D.A., Alessi, D.R., Cohen, P., Andjelkovich, M., and Hemmings, B.A. (1995). Inhibition of glycogen synthase kinase-3 by insulin mediated by protein kinase B. Nature *378*, 785-789.

Cusi, K., Consoli, A., and DeFronzo, R.A. (1996). Metabolic effects of metformin on glucose and lactate metabolism in noninsulin-dependent diabetes mellitus. The Journal of clinical endocrinology and metabolism *81*, 4059-4067.

Daimon, M., Oizumi, T., Saitoh, T., Kameda, W., Hirata, A., Yamaguchi, H., Ohnuma, H., Igarashi, M., Tominaga, M., and Kato, T. (2003). Decreased serum levels of adiponectin are a risk factor for the progression to type 2 diabetes in the Japanese Population: the Funagata study. Diabetes care *26*, 2015-2020.

Davies, M.J., D'Alessio, D.A., Fradkin, J., Kernan, W.N., Mathieu, C., Mingrone, G., Rossing, P., Tsapas, A., Wexler, D.J., and Buse, J.B. (2018). Management of Hyperglycemia in Type 2 Diabetes, 2018. A Consensus Report by the American Diabetes Association (ADA) and the European Association for the Study of Diabetes (EASD). Diabetes care *41*, 2669-2701.

Day, J.W., Ottaway, N., Patterson, J.T., Gelfanov, V., Smiley, D., Gidda, J., Findeisen, H., Bruemmer, D., Drucker, D.J., Chaudhary, N.*, et al.* (2009). A new glucagon and GLP-1 co-agonist eliminates obesity in rodents. Nature chemical biology *5*, 749-757.

de Alvaro, C., Teruel, T., Hernandez, R., and Lorenzo, M. (2004). Tumor necrosis factor alpha produces insulin resistance in skeletal muscle by activation of inhibitor kappaB kinase in a p38 MAPK-dependent manner. The Journal of biological chemistry *279*, 17070-17078.

De Filippo, C., Cavalieri, D., Di Paola, M., Ramazzotti, M., Poullet, J.B., Massart, S., Collini, S., Pieraccini, G., and Lionetti, P. (2010). Impact of diet in shaping gut microbiota revealed by a comparative study in children from Europe and rural Africa. Proceedings of the National Academy of Sciences of the United States of America *107*, 14691-14696.

De Giorgio, M.R., Yoshioka, M., and St-Amand, J. (2009). Feeding induced changes in the hypothalamic transcriptome. Clinica chimica acta; international journal of clinical chemistry *406*, 103-107.

De la Chesnaye, E., Manuel-Apolinar, L., Zarate, A., Damasio, L., Espino, N., Revilla-Monsalve, M.C., and Islas-Andrade, S. (2015). Lipocalin-2 plasmatic levels are reduced in patients with long-term type 2 diabetes mellitus. International journal of clinical and experimental medicine *8*, 2853-2859.

Deacon, C.F., Nauck, M.A., Toft-Nielsen, M., Pridal, L., Willms, B., and Holst, J.J. (1995). Both subcutaneously and intravenously administered glucagon-like peptide I are rapidly degraded from the NH2-terminus in type II diabetic patients and in healthy subjects. Diabetes *44*, 1126-1131.

Defronzo, R.A. (2009). Banting Lecture. From the triumvirate to the ominous octet: a new paradigm for the treatment of type 2 diabetes mellitus. Diabetes *58*, 773-795.

DeFronzo, R.A., Ferrannini, E., Groop, L., Henry, R.R., Herman, W.H., Holst, J.J., Hu, F.B., Kahn, C.R., Raz, I., Shulman, G.I.*, et al.* (2015). Type 2 diabetes mellitus. Nature reviews Disease primers *1*, 15019.

DeFronzo, R.A., Hompesch, M., Kasichayanula, S., Liu, X., Hong, Y., Pfister, M., Morrow, L.A., Leslie, B.R., Boulton, D.W., Ching, A.*, et al.* (2013). Characterization of renal glucose reabsorption in response to dapagliflozin in healthy subjects and subjects with type 2 diabetes. Diabetes care *36*, 3169-3176.

DeFronzo, R.A., Okerson, T., Viswanathan, P., Guan, X., Holcombe, J.H., and MacConell, L. (2008). Effects of exenatide versus sitagliptin on postprandial glucose, insulin and glucagon secretion, gastric emptying, and caloric intake: a randomized, cross-over study. Current medical research and opinion *24*, 2943-2952.

Deglasse, J.P., Roma, L.P., Pastor-Flores, D., Gilon, P., Dick, T.P., and Jonas, J.C. (2019). Glucose Acutely Reduces Cytosolic and Mitochondrial H2O2 in Rat Pancreatic Beta Cells. Antioxidants & redox signaling *30*, 297-313.

Deng, S., Vatamaniuk, M., Huang, X., Doliba, N., Lian, M.M., Frank, A., Velidedeoglu, E., Desai, N.M., Koeberlein, B., Wolf, B.*, et al.* (2004). Structural and functional abnormalities in the islets isolated from type 2 diabetic subjects. Diabetes *53*, 624-632.

Desai, P.P., Bunker, C.H., Ukoli, F.A., and Kamboh, M.I. (2002). Genetic variation in the apolipoprotein D gene among African blacks and its significance in lipid metabolism. Atherosclerosis *163*, 329-338.

Do Carmo, S., Fournier, D., Mounier, C., and Rassart, E. (2009). Human apolipoprotein D overexpression in transgenic mice induces insulin resistance and alters lipid metabolism. Am J Physiol Endocrinol Metab *296*, E802-811.

Do Carmo, S., Levros, L.C., Jr., and Rassart, E. (2007). Modulation of apolipoprotein D expression and translocation under specific stress conditions. Biochimica et biophysica acta *1773*, 954-969.

Drucker, D.J. (2006). The biology of incretin hormones. Cell Metab *3*, 153-165.

Duckworth, W., Abraira, C., Moritz, T., Reda, D., Emanuele, N., Reaven, P.D., Zieve, F.J., Marks, J., Davis, S.N., Hayward, R.*, et al.* (2009). Glucose control and vascular complications in veterans with type 2 diabetes. The New England journal of medicine *360*, 129-139.

Dullaart, R.P., Plomgaard, P., de Vries, R., Dahlback, B., and Nielsen, L.B. (2009). Plasma apolipoprotein M is reduced in metabolic syndrome but does not predict intima media thickness. Clinica chimica acta; international journal of clinical chemistry *406*, 129-133.

Dumas, M.-E., Barton, R.H., Toye, A., Cloarec, O., Blancher, C., Rothwell, A., Fearnside, J., Tatoud, R., Blanc, V., Lindon, J.C.*, et al.* (2006). Metabolic profiling reveals a contribution of gut microbiota to fatty liver phenotype in insulin-resistant mice. Proceedings of the National Academy of Sciences of the United States of America *103*, 12511-12516.

Dushay, J., Chui, P.C., Gopalakrishnan, G.S., Varela-Rey, M., Crawley, M., Fisher, F.M., Badman, M.K., Martinez-Chantar, M.L., and Maratos-Flier, E. (2010). Increased fibroblast growth factor 21 in obesity and nonalcoholic fatty liver disease. Gastroenterology *139*, 456-463.

Edgar, R., Domrachev, M., and Lash, A.E. (2002). Gene Expression Omnibus: NCBI gene expression and hybridization array data repository. Nucleic acids research *30*, 207-210.

Edholm, T., Degerblad, M., Gryback, P., Hilsted, L., Holst, J.J., Jacobsson, H., Efendic, S., Schmidt, P.T., and Hellstrom, P.M. (2010). Differential incretin effects of GIP and GLP-1 on gastric emptying, appetite, and insulin-glucose homeostasis. Neurogastroenterology and motility : the official journal of the European Gastrointestinal Motility Society *22*, 1191-1200, e1315.

Ekim Ustunel, B., Friedrich, K., Maida, A., Wang, X., Krones-Herzig, A., Seibert, O., Sommerfeld, A., Jones, A., Sijmonsma, T.P., Sticht, C.*, et al.* (2016). Control of diabetic hyperglycaemia and insulin resistance through TSC22D4. Nature communications *7*, 13267.

El-Assaad, W., Buteau, J., Peyot, M.L., Nolan, C., Roduit, R., Hardy, S., Joly, E., Dbaibo, G., Rosenberg, L., and Prentki, M. (2003). Saturated fatty acids synergize with elevated glucose to cause pancreatic beta-cell death. Endocrinology *144*, 4154-4163.

El-Assaad, W., Joly, E., Barbeau, A., Sladek, R., Buteau, J., Maestre, I., Pepin, E., Zhao, S., Iglesias, J., Roche, E.*, et al.* (2010). Glucolipotoxicity alters lipid partitioning and causes mitochondrial dysfunction, cholesterol, and ceramide deposition and reactive oxygen species production in INS832/13 ss-cells. Endocrinology *151*, 3061-3073.

El Ouaamari, A., Dirice, E., Gedeon, N., Hu, J., Zhou, J.Y., Shirakawa, J., Hou, L., Goodman, J., Karampelias, C., Qiang, G.*, et al.* (2016). SerpinB1 Promotes Pancreatic beta Cell Proliferation. Cell Metab *23*, 194-205.

El Ouaamari, A., Kawamori, D., Dirice, E., Liew, C.W., Shadrach, J.L., Hu, J., Katsuta, H., Hollister-Lock, J., Qian, W.J., Wagers, A.J.*, et al.* (2013). Liver-derived systemic factors drive beta cell hyperplasia in insulin-resistant states. Cell reports *3*, 401-410.

Elinav, E., Strowig, T., Kau, A.L., Henao-Mejia, J., Thaiss, C.A., Booth, C.J., Peaper, D.R., Bertin, J., Eisenbarth, S.C., Gordon, J.I.*, et al.* (2011). NLRP6 inflammasome regulates colonic microbial ecology and risk for colitis. Cell *145*, 745-757.

Ellingsgaard, H., Hauselmann, I., Schuler, B., Habib, A.M., Baggio, L.L., Meier, D.T., Eppler, E., Bouzakri, K., Wueest, S., Muller, Y.D.*, et al.* (2011). Interleukin-6 enhances insulin secretion by increasing glucagon-like peptide-1 secretion from L cells and alpha cells. Nature medicine *17*, 1481-1489.

Elrick, H., Stimmler, L., Hlad, C.J., Jr., and Arai, Y. (1964). PLASMA INSULIN RESPONSE TO ORAL AND INTRAVENOUS GLUCOSE ADMINISTRATION. The Journal of clinical endocrinology and metabolism *24*, 1076-1082.

Emanuelli, B., Peraldi, P., Filloux, C., Chavey, C., Freidinger, K., Hilton, D.J., Hotamisligil, G.S., and Van Obberghen, E. (2001). SOCS-3 inhibits insulin signaling and is up-regulated in response to tumor necrosis factor-alpha in the adipose tissue of obese mice. The Journal of biological chemistry *276*, 47944-47949.

Ericsson, A.C., Davis, J.W., Spollen, W., Bivens, N., Givan, S., Hagan, C.E., McIntosh, M., and Franklin, C.L. (2015). Effects of vendor and genetic background on the composition of the fecal microbiota of inbred mice. PLoS One *10*, e0116704-e0116704.

Erion, D.M., and Shulman, G.I. (2010). Diacylglycerol-mediated insulin resistance. Nature medicine *16*, 400-402.

Fain, J.N., Cheema, P.S., Bahouth, S.W., and Lloyd Hiler, M. (2003). Resistin release by human adipose tissue explants in primary culture. Biochemical and biophysical research communications *300*, 674-678.

Farooqi, I.S., Jebb, S.A., Langmack, G., Lawrence, E., Cheetham, C.H., Prentice, A.M., Hughes, I.A., McCamish, M.A., and O'Rahilly, S. (1999). Effects of recombinant leptin therapy in a child with congenital leptin deficiency. The New England journal of medicine *341*, 879-884.

Feingold, K.R., Staprans, I., Memon, R.A., Moser, A.H., Shigenaga, J.K., Doerrler, W., Dinarello, C.A., and Grunfeld, C. (1992). Endotoxin rapidly induces changes in lipid metabolism that produce hypertriglyceridemia: low doses stimulate hepatic triglyceride production while high doses inhibit clearance. J Lipid Res *33*, 1765-1776.

Feng, Y., Huang, Y., Wang, Y., Wang, P., Song, H., and Wang, F. (2019). Antibiotics induced intestinal tight junction barrier dysfunction is associated with microbiota dysbiosis, activated NLRP3 inflammasome and autophagy. PLoS One *14*, e0218384-e0218384.

Ferdaoussi, M., Bergeron, V., Zarrouki, B., Kolic, J., Cantley, J., Fielitz, J., Olson, E.N., Prentki, M., Biden, T., MacDonald, P.E.*, et al.* (2012). G protein-coupled receptor (GPR)40-dependent potentiation of insulin secretion in mouse islets is mediated by protein kinase D1. Diabetologia *55*, 2682-2692.

Ferrannini, E., Muscelli, E., Frascerra, S., Baldi, S., Mari, A., Heise, T., Broedl, U.C., and Woerle, H.-J. (2014). Metabolic response to sodium-glucose cotransporter 2 inhibition in type 2 diabetic patients. The Journal of clinical investigation *124*, 499-508.

Ferrannini, E., Muscelli, E., Natali, A., Gabriel, R., Mitrakou, A., Flyvbjerg, A., Golay, A., and Hojlund, K. (2007). Association of fasting glucagon and proinsulin concentrations with insulin resistance. Diabetologia *50*, 2342-2347.

Ferre, P. (2004). The biology of peroxisome proliferator-activated receptors: relationship with lipid metabolism and insulin sensitivity. Diabetes *53 Suppl 1*, S43-50.

Finan, B., Clemmensen, C., Zhu, Z., Stemmer, K., Gauthier, K., Müller, L., De Angelis, M., Moreth, K., Neff, F., Perez-Tilve, D.*, et al.* (2016). Chemical Hybridization of Glucagon and Thyroid Hormone Optimizes Therapeutic Impact for Metabolic Disease. Cell *167*, 843-857.e814.

Finan, B., Ma, T., Ottaway, N., Müller, T.D., Habegger, K.M., Heppner, K.M., Kirchner, H., Holland, J., Hembree, J., Raver, C.*, et al.* (2013). Unimolecular dual incretins maximize metabolic benefits in rodents, monkeys, and humans. Science translational medicine *5*, 209ra151.

Finan, B., Yang, B., Ottaway, N., Smiley, D.L., Ma, T., Clemmensen, C., Chabenne, J., Zhang, L., Habegger, K.M., Fischer, K.*, et al.* (2015). A rationally designed monomeric peptide triagonist corrects obesity and diabetes in rodents. Nature medicine *21*, 27-36.

Finan, B., Yang, B., Ottaway, N., Stemmer, K., Müller, T.D., Yi, C.-X., Habegger, K., Schriever, S.C., García-Cáceres, C., Kabra, D.G.*, et al.* (2012). Targeted estrogen delivery reverses the metabolic syndrome. Nature medicine *18*, 1847-1856.

Fisher, F.M., Kleiner, S., Douris, N., Fox, E.C., Mepani, R.J., Verdeguer, F., Wu, J., Kharitonenkov, A., Flier, J.S., Maratos-Flier, E.*, et al.* (2012). FGF21 regulates PGC-1alpha

and browning of white adipose tissues in adaptive thermogenesis. Genes & development *26*, 271-281.

Flower, D.R. (1996). The lipocalin protein family: structure and function. The Biochemical journal *318 (Pt 1)*, 1-14.

Flower, D.R. (2000). Beyond the superfamily: the lipocalin receptors. Biochimica et biophysica acta *1482*, 327-336.

Forbes, J.M., and Cooper, M.E. (2013). Mechanisms of diabetic complications. Physiological reviews *93*, 137-188.

Fosgerau, K., Jessen, L., Lind Tolborg, J., Østerlund, T., Schæffer Larsen, K., Rolsted, K., Brorson, M., Jelsing, J., and Skovlund Ryge Neerup, T. (2013). The novel GLP-1-gastrin dual agonist, ZP3022, increases β-cell mass and prevents diabetes in db/db mice. Diabetes, obesity & metabolism *15*, 62-71.

Franklin, C.L., and Ericsson, A.C. (2017). Microbiota and reproducibility of rodent models. Lab Anim (NY) *46*, 114-122.

Fraze, E., Donner, C.C., Swislocki, A.L., Chiou, Y.A., Chen, Y.D., and Reaven, G.M. (1985). Ambient plasma free fatty acid concentrations in noninsulin-dependent diabetes mellitus: evidence for insulin resistance. The Journal of clinical endocrinology and metabolism *61*, 807-811.

Frei, A.P., Moest, H., Novy, K., and Wollscheid, B. (2013). Ligand-based receptor identification on living cells and tissues using TRICEPS. Nat Protoc *8*, 1321-1336.

Fu, Z., Gilbert, E.R., and Liu, D. (2013). Regulation of insulin synthesis and secretion and pancreatic Beta-cell dysfunction in diabetes. Current diabetes reviews *9*, 25-53.

Fujimori, K., Aritake, K., and Urade, Y. (2007). A novel pathway to enhance adipocyte differentiation of 3T3-L1 cells by up-regulation of lipocalin-type prostaglandin D synthase mediated by liver X receptor-activated sterol regulatory element-binding protein-1c. The Journal of biological chemistry *282*, 18458-18466.

Gaich, G., Chien, J.Y., Fu, H., Glass, L.C., Deeg, M.A., Holland, W.L., Kharitonenkov, A., Bumol, T., Schilske, H.K., and Moller, D.E. (2013). The effects of LY2405319, an FGF21 analog, in obese human subjects with type 2 diabetes. Cell Metab *18*, 333-340.

Gao, G.P., Alvira, M.R., Wang, L., Calcedo, R., Johnston, J., and Wilson, J.M. (2002). Novel adeno-associated viruses from rhesus monkeys as vectors for human gene therapy. Proceedings of the National Academy of Sciences of the United States of America *99*, 11854-11859.

García-Ocaña, A., Vasavada, R.C., Cebrian, A., Reddy, V., Takane, K.K., López-Talavera, J.C., and Stewart, A.F. (2001). Transgenic overexpression of hepatocyte growth factor in the beta-cell markedly improves islet function and islet transplant outcomes in mice. Diabetes *50*, 2752-2762.

Gedulin, B.R., Rink, T.J., and Young, A.A. (1997). Dose-response for glucagonostatic effect of amylin in rats. Metabolism: clinical and experimental *46*, 67-70.

Geerling, J.J., Boon, M.R., van der Zon, G.C., van den Berg, S.A., van den Hoek, A.M., Lombes, M., Princen, H.M., Havekes, L.M., Rensen, P.C., and Guigas, B. (2014). Metformin lowers plasma triglycerides by promoting VLDL-triglyceride clearance by brown adipose tissue in mice. Diabetes *63*, 880-891.

Gerich, J.E. (2010). Role of the kidney in normal glucose homeostasis and in the hyperglycaemia of diabetes mellitus: therapeutic implications. Diabetic medicine : a journal of the British Diabetic Association *27*, 136-142.

Gerstein, H.C., Miller, M.E., Byington, R.P., Goff, D.C., Jr., Bigger, J.T., Buse, J.B., Cushman, W.C., Genuth, S., Ismail-Beigi, F., Grimm, R.H., Jr.*, et al.* (2008). Effects of intensive glucose lowering in type 2 diabetes. The New England journal of medicine *358*, 2545-2559.

Ghoshal, S., Witta, J., Zhong, J., de Villiers, W., and Eckhardt, E. (2009). Chylomicrons promote intestinal absorption of lipopolysaccharides. J Lipid Res *50*, 90-97.

Goke, R., Fehmann, H.C., Linn, T., Schmidt, H., Krause, M., Eng, J., and Goke, B. (1993). Exendin-4 is a high potency agonist and truncated exendin-(9-39)-amide an antagonist at the glucagon-like peptide 1-(7-36)-amide receptor of insulin-secreting beta-cells. The Journal of biological chemistry *268*, 19650-19655.

Gough, S.C., Bode, B., Woo, V., Rodbard, H.W., Linjawi, S., Poulsen, P., Damgaard, L.H., and Buse, J.B. (2014). Efficacy and safety of a fixed-ratio combination of insulin degludec and liraglutide (IDegLira) compared with its components given alone: results of a phase 3, open-label, randomised, 26-week, treat-to-target trial in insulin-naive patients with type 2 diabetes. The lancet Diabetes & endocrinology *2*, 885-893.

Graham, T.E., Yang, Q., Bluher, M., Hammarstedt, A., Ciaraldi, T.P., Henry, R.R., Wason, C.J., Oberbach, A., Jansson, P.A., Smith, U.*, et al.* (2006). Retinol-binding protein 4 and insulin resistance in lean, obese, and diabetic subjects. The New England journal of medicine *354*, 2552-2563.

Grant, S.F., Thorleifsson, G., Reynisdottir, I., Benediktsson, R., Manolescu, A., Sainz, J., Helgason, A., Stefansson, H., Emilsson, V., Helgadottir, A.*, et al.* (2006). Variant of transcription factor 7-like 2 (TCF7L2) gene confers risk of type 2 diabetes. Nature genetics *38*, 320-323.

Griffin, M.E., Marcucci, M.J., Cline, G.W., Bell, K., Barucci, N., Lee, D., Goodyear, L.J., Kraegen, E.W., White, M.F., and Shulman, G.I. (1999). Free fatty acid-induced insulin resistance is associated with activation of protein kinase C theta and alterations in the insulin signaling cascade. Diabetes *48*, 1270-1274.

Grimm, D., Kern, A., Rittner, K., and Kleinschmidt, J.A. (1998). Novel tools for production and purification of recombinant adenoassociated virus vectors. Human gene therapy *9*, 2745-2760.

Guardado-Mendoza, R., Davalli, A.M., Chavez, A.O., Hubbard, G.B., Dick, E.J., Majluf-Cruz, A., Tene-Perez, C.E., Goldschmidt, L., Hart, J., Perego, C.*, et al.* (2009). Pancreatic islet

amyloidosis, beta-cell apoptosis, and alpha-cell proliferation are determinants of islet remodeling in type-2 diabetic baboons. Proceedings of the National Academy of Sciences of the United States of America *106*, 13992-13997.

Guo, H., Jin, D., Zhang, Y., Wright, W., Bazuine, M., Brockman, D.A., Bernlohr, D.A., and Chen, X. (2010). Lipocalin-2 Deficiency Impairs Thermogenesis and Potentiates Diet-Induced Insulin Resistance in Mice. Diabetes *59*, 1376-1385.

Gustavsson, N., Wu, B., and Han, W. (2012). Calcium sensing in exocytosis. Adv Exp Med Biol *740*, 731-757.

Haeusler, R.A., Hartil, K., Vaitheesvaran, B., Arrieta-Cruz, I., Knight, C.M., Cook, J.R., Kammoun, H.L., Febbraio, M.A., Gutierrez-Juarez, R., Kurland, I.J.*, et al.* (2014). Integrated control of hepatic lipogenesis versus glucose production requires FoxO transcription factors. Nature communications *5*, 5190.

Haeusler, R.A., McGraw, T.E., and Accili, D. (2018). Biochemical and cellular properties of insulin receptor signalling. Nat Rev Mol Cell Biol *19*, 31-44.

Halaas, J.L., Gajiwala, K.S., Maffei, M., Cohen, S.L., Chait, B.T., Rabinowitz, D., Lallone, R.L., Burley, S.K., and Friedman, J.M. (1995). Weight-reducing effects of the plasma protein encoded by the obese gene. Science (New York, NY) *269*, 543-546.

Hamano, K., Totsuka, Y., Ajima, M., Gomi, T., Ikeda, T., Hirawa, N., Eguchi, Y., Yamakado, M., Takagi, M., Nakajima, H.*, et al.* (2002). Blood sugar control reverses the increase in urinary excretion of prostaglandin D synthase in diabetic patients. Nephron *92*, 77-85.

Han, M.S., Jung, D.Y., Morel, C., Lakhani, S.A., Kim, J.K., Flavell, R.A., and Davis, R.J. (2013). JNK expression by macrophages promotes obesity-induced insulin resistance and inflammation. Science (New York, NY) *339*, 218-222.

Hasenau, J.J. (2020). Reproducibility and Comparative aspects of Terrestrial Housing Systems and Husbandry Procedures in Animal Research Facilities on Study Data. ILAR Journal.

Hatting, M., Tavares, C.D.J., Sharabi, K., Rines, A.K., and Puigserver, P. (2018). Insulin regulation of gluconeogenesis. Ann N Y Acad Sci *1411*, 21-35.

Hauge-Evans, A.C., Squires, P.E., Persaud, S.J., and Jones, P.M. (1999). Pancreatic beta-cell-to-beta-cell interactions are required for integrated responses to nutrient stimuli: enhanced Ca2+ and insulin secretory responses of MIN6 pseudoislets. Diabetes *48*, 1402-1408.

Haukeland, J.W., Dahl, T.B., Yndestad, A., Gladhaug, I.P., Loberg, E.M., Haaland, T., Konopski, Z., Wium, C., Aasheim, E.T., Johansen, O.E.*, et al.* (2012). Fetuin A in nonalcoholic fatty liver disease: in vivo and in vitro studies. European journal of endocrinology *166*, 503-510.

Heinrichsdorff, J., and Olefsky, J.M. (2012). Fetuin-A: the missing link in lipid-induced inflammation. Nature medicine *18*, 1182-1183.

Henao-Mejia, J., Elinav, E., Jin, C., Hao, L., Mehal, W.Z., Strowig, T., Thaiss, C.A., Kau, A.L., Eisenbarth, S.C., Jurczak, M.J.*, et al.* (2012). Inflammasome-mediated dysbiosis regulates progression of NAFLD and obesity. Nature *482*, 179-185.

Hernandez, Y.J., Wang, J., Kearns, W.G., Loiler, S., Poirier, A., and Flotte, T.R. (1999). Latent adeno-associated virus infection elicits humoral but not cell-mediated immune responses in a nonhuman primate model. Journal of virology *73*, 8549-8558.

Hofmann, C., Lorenz, K., Braithwaite, S.S., Colca, J.R., Palazuk, B.J., Hotamisligil, G.S., and Spiegelman, B.M. (1994). Altered gene expression for tumor necrosis factor-alpha and its receptors during drug and dietary modulation of insulin resistance. Endocrinology *134*, 264-270.

Holman, R.R., Paul, S.K., Bethel, M.A., Matthews, D.R., and Neil, H.A. (2008). 10-year follow-up of intensive glucose control in type 2 diabetes. The New England journal of medicine *359*, 1577-1589.

Holman, R.R., Thorne, K.I., Farmer, A.J., Davies, M.J., Keenan, J.F., Paul, S., and Levy, J.C. (2007). Addition of biphasic, prandial, or basal insulin to oral therapy in type 2 diabetes. The New England journal of medicine *357*, 1716-1730.

Holzer, R.G., Park, E.J., Li, N., Tran, H., Chen, M., Choi, C., Solinas, G., and Karin, M. (2011). Saturated fatty acids induce c-Src clustering within membrane subdomains, leading to JNK activation. Cell *147*, 173-184.

Hu, E., Liang, P., and Spiegelman, B.M. (1996). AdipoQ is a novel adipose-specific gene dysregulated in obesity. The Journal of biological chemistry *271*, 10697-10703.

Huang, C.J., Lin, C.Y., Haataja, L., Gurlo, T., Butler, A.E., Rizza, R.A., and Butler, P.C. (2007). High expression rates of human islet amyloid polypeptide induce endoplasmic reticulum stress mediated beta-cell apoptosis, a characteristic of humans with type 2 but not type 1 diabetes. Diabetes *56*, 2016-2027.

Huang, S., Rutkowsky, J.M., Snodgrass, R.G., Ono-Moore, K.D., Schneider, D.A., Newman, J.W., Adams, S.H., and Hwang, D.H. (2012). Saturated fatty acids activate TLR-mediated proinflammatory signaling pathways. J Lipid Res *53*, 2002-2013.

Hufeldt, M.R., Nielsen, D.S., Vogensen, F.K., Midtvedt, T., and Hansen, A.K. (2010). Variation in the gut microbiota of laboratory mice is related to both genetic and environmental factors. Comparative medicine *60*, 336-347.

Hui, X., Zhu, W., Wang, Y., Lam, K.S., Zhang, J., Wu, D., Kraegen, E.W., Li, Y., and Xu, A. (2009). Major urinary protein-1 increases energy expenditure and improves glucose intolerance through enhancing mitochondrial function in skeletal muscle of diabetic mice. The Journal of biological chemistry *284*, 14050-14057.

Huntley, M.A., Lou, M., Goldstein, L.D., Lawrence, M., Dijkgraaf, G.J.P., Kaminker, J.S., and Gentleman, R. (2016). Complex regulation of ADAR-mediated RNA-editing across tissues. BMC Genomics *17*, 61-61.

Ibrahimi, A., Teboul, L., Gaillard, D., Amri, E.Z., Ailhaud, G., Young, P., Cawthorne, M.A., and Grimaldi, P.A. (1994). Evidence for a common mechanism of action for fatty acids and thiazolidinedione antidiabetic agents on gene expression in preadipose cells. Molecular pharmacology *46*, 1070-1076.

Inagaki, N., Gonoi, T., Clement, J.P.t., Namba, N., Inazawa, J., Gonzalez, G., Aguilar-Bryan, L., Seino, S., and Bryan, J. (1995). Reconstitution of IKATP: an inward rectifier subunit plus the sulfonylurea receptor. Science (New York, NY) *270*, 1166-1170.

International Diabetes Federation (2019). IDF Diabetes Atlas, 9th edn (Brussels, Belgium: International Diabetes Federation).

Iroz, A., Couty, J.P., and Postic, C. (2015). Hepatokines: unlocking the multi-organ network in metabolic diseases. Diabetologia *58*, 1699-1703.

Ishihara, H., Asano, T., Tsukuda, K., Katagiri, H., Inukai, K., Anai, M., Yazaki, Y., Miyazaki, J., Kikuchi, M., and Oka, Y. (1995). Human GLUT-2 overexpression does not affect glucose-stimulated insulin secretion in MIN6 cells. The American journal of physiology *269*, E897-902.

Ishii, A., Katsuura, G., Imamaki, H., Kimura, H., Mori, K.P., Kuwabara, T., Kasahara, M., Yokoi, H., Ohinata, K., Kawanishi, T.*, et al.* (2017). Obesity-promoting and anti-thermogenic effects of neutrophil gelatinase-associated lipocalin in mice. Scientific reports *7*, 15501.

Ishikura, S., Bilan, P.J., and Klip, A. (2007). Rabs 8A and 14 are targets of the insulin-regulated Rab-GAP AS160 regulating GLUT4 traffic in muscle cells. Biochemical and biophysical research communications *353*, 1074-1079.

Ivarsson, R., Quintens, R., Dejonghe, S., Tsukamoto, K., in 't Veld, P., Renstrom, E., and Schuit, F.C. (2005). Redox control of exocytosis: regulatory role of NADPH, thioredoxin, and glutaredoxin. Diabetes *54*, 2132-2142.

Ix, J.H., Shlipak, M.G., Brandenburg, V.M., Ali, S., Ketteler, M., and Whooley, M.A. (2006). Association between human fetuin-A and the metabolic syndrome: data from the Heart and Soul Study. Circulation *113*, 1760-1767.

Ix, J.H., Wassel, C.L., Kanaya, A.M., Vittinghoff, E., Johnson, K.C., Koster, A., Cauley, J.A., Harris, T.B., Cummings, S.R., Shlipak, M.G.*, et al.* (2008). Fetuin-A and incident diabetes mellitus in older persons. JAMA *300*, 182-188.

Jones, A., Friedrich, K., Rohm, M., Schafer, M., Algire, C., Kulozik, P., Seibert, O., Muller-Decker, K., Sijmonsma, T., Strzoda, D.*, et al.* (2013). TSC22D4 is a molecular output of hepatic wasting metabolism. EMBO molecular medicine *5*, 294-308.

Jooss, K., Ertl, H.C., and Wilson, J.M. (1998). Cytotoxic T-lymphocyte target proteins and their major histocompatibility complex class I restriction in response to adenovirus vectors delivered to mouse liver. Journal of virology *72*, 2945-2954.

Judge, A.D., Bola, G., Lee, A.C., and MacLachlan, I. (2006). Design of noninflammatory synthetic siRNA mediating potent gene silencing in vivo. Molecular therapy : the journal of the American Society of Gene Therapy *13*, 494-505.

Jun, L.S., Siddall, C.P., and Rosen, E.D. (2011). A minor role for lipocalin 2 in high-fat diet-induced glucose intolerance. Am J Physiol Endocrinol Metab *301*, E825-E835.

Kahn, S.E. (2001). Clinical review 135: The importance of beta-cell failure in the development and progression of type 2 diabetes. The Journal of clinical endocrinology and metabolism *86*, 4047-4058.

Kahn, S.E., D'Alessio, D.A., Schwartz, M.W., Fujimoto, W.Y., Ensinck, J.W., Taborsky, G.J., Jr., and Porte, D., Jr. (1990). Evidence of cosecretion of islet amyloid polypeptide and insulin by beta-cells. Diabetes *39*, 634-638.

Kahn, S.E., Haffner, S.M., Heise, M.A., Herman, W.H., Holman, R.R., Jones, N.P., Kravitz, B.G., Lachin, J.M., O'Neill, M.C., Zinman, B.*, et al.* (2006a). Glycemic durability of rosiglitazone, metformin, or glyburide monotherapy. The New England journal of medicine *355*, 2427-2443.

Kahn, S.E., Hull, R.L., and Utzschneider, K.M. (2006b). Mechanisms linking obesity to insulin resistance and type 2 diabetes. Nature *444*, 840-846.

Kahn, S.E., Prigeon, R.L., McCulloch, D.K., Boyko, E.J., Bergman, R.N., Schwartz, M.W., Neifing, J.L., Ward, W.K., Beard, J.C., Palmer, J.P.*, et al.* (1993). Quantification of the relationship between insulin sensitivity and beta-cell function in human subjects. Evidence for a hyperbolic function. Diabetes *42*, 1663-1672.

Kang, L., He, Z., Xu, P., Fan, J., Betz, A., Brose, N., and Xu, T. (2006). Munc13-1 is required for the sustained release of insulin from pancreatic beta cells. Cell Metab *3*, 463-468.

Kanno, T., Suga, S., Wu, J., Kimura, M., and Wakui, M. (1998). Intracellular cAMP potentiates voltage-dependent activation of L-type Ca2+ channels in rat islet beta-cells. Pflugers Archiv : European journal of physiology *435*, 578-580.

Kawamori, D., Kurpad, A.J., Hu, J., Liew, C.W., Shih, J.L., Ford, E.L., Herrera, P.L., Polonsky, K.S., McGuinness, O.P., and Kulkarni, R.N. (2009). Insulin signaling in alpha cells modulates glucagon secretion in vivo. Cell Metab *9*, 350-361.

Kelley, D.E., Mintun, M.A., Watkins, S.C., Simoneau, J.A., Jadali, F., Fredrickson, A., Beattie, J., and Thériault, R. (1996). The effect of non-insulin-dependent diabetes mellitus and obesity on glucose transport and phosphorylation in skeletal muscle. The Journal of clinical investigation *97*, 2705-2713.

Kennedy, E.A., King, K.Y., and Baldridge, M.T. (2018). Mouse Microbiota Models: Comparing Germ-Free Mice and Antibiotics Treatment as Tools for Modifying Gut Bacteria. Front Physiol *9*, 1534-1534.

Kharitonenkov, A., Shiyanova, T.L., Koester, A., Ford, A.M., Micanovic, R., Galbreath, E.J., Sandusky, G.E., Hammond, L.J., Moyers, J.S., Owens, R.A.*, et al.* (2005). FGF-21 as a novel metabolic regulator. The Journal of clinical investigation *115*, 1627-1635.

Kilimnik, G., Kim, A., Steiner, D.F., Friedman, T.C., and Hara, M. (2010). Intraislet production of GLP-1 by activation of prohormone convertase 1/3 in pancreatic α-cells in mouse models of ß-cell regeneration. Islets *2*, 149-155.

Kita, Y., Takamura, T., Misu, H., Ota, T., Kurita, S., Takeshita, Y., Uno, M., Matsuzawa-Nagata, N., Kato, K.-I., Ando, H.*, et al.* (2012). Metformin prevents and reverses inflammation in a non-diabetic mouse model of nonalcoholic steatohepatitis. PLoS One *7*, e43056.

Kitamura, T., Nakae, J., Kitamura, Y., Kido, Y., Biggs, W.H., 3rd, Wright, C.V.E., White, M.F., Arden, K.C., and Accili, D. (2002). The forkhead transcription factor Foxo1 links insulin signaling to Pdx1 regulation of pancreatic beta cell growth. The Journal of clinical investigation *110*, 1839-1847.

Kleinert, M., Parker, B.L., Jensen, T.E., Raun, S.H., Pham, P., Han, X., James, D.E., Richter, E.A., and Sylow, L. (2018). Quantitative proteomic characterization of cellular pathways associated with altered insulin sensitivity in skeletal muscle following high-fat diet feeding and exercise training. Scientific reports *8*, 10723.

Kobori, M., Ni, Y., Takahashi, Y., Watanabe, N., Sugiura, M., Ogawa, K., Nagashimada, M., Kaneko, S., Naito, S., and Ota, T. (2014). β-Cryptoxanthin alleviates diet-induced nonalcoholic steatohepatitis by suppressing inflammatory gene expression in mice. PLoS One *9*, e98294.

Koh, A., Molinaro, A., Stahlman, M., Khan, M.T., Schmidt, C., Manneras-Holm, L., Wu, H., Carreras, A., Jeong, H., Olofsson, L.E.*, et al.* (2018). Microbially Produced Imidazole Propionate Impairs Insulin Signaling through mTORC1. Cell *175*, 947-961.e917.

Kumar, S., Lau, R., Hall, C., Palaia, T., Brathwaite, C.E., and Ragolia, L. (2015). Bile acid elevation after Roux-en-Y gastric bypass is associated with cardio-protective effect in Zucker Diabetic Fatty rats. International journal of surgery (London, England) *24*, 70-74.

Kumar, S., Lau, R., Hall, C.E., Palaia, T., Rideout, D.A., Brathwaite, C.E., and Ragolia, L. (2016). Lipocalin-type prostaglandin D2 synthase (L-PGDS) modulates beneficial metabolic effects of vertical sleeve gastrectomy. Surgery for obesity and related diseases : official journal of the American Society for Bariatric Surgery *12*, 1523-1531.

Kumar, S., Palaia, T., Hall, C., Lee, J., Stevenson, M., and Ragolia, L. (2018). Lipocalin-Type Prostaglandin D2 Synthase (L-PGDS) Knockout Mice Exhibits Hepatosteatosis Mediated by Enhanced Cd36 Hepatic Expression as a Result of Hyperinsulinemia. Diabetes *67*, 39-LB.

Kumar, S., Srivastava, A., Palaia, T., Hall, C., Lee, J., Stevenson, M., Zhao, C.L., and Ragolia, L. (2020). Lipocalin-type prostaglandin D2 synthase deletion induces dyslipidemia and non-alcoholic fatty liver disease. Prostaglandins & other lipid mediators *149*, 106429.

Kunnari, A.M., Savolainen, E.R., Ukkola, O.H., Kesäniemi, Y.A., and Jokela, M.A. (2009). The expression of human resistin in different leucocyte lineages is modulated by LPS and TNFalpha. Regulatory peptides *157*, 57-63.

Kuo, T., McQueen, A., Chen, T.-C., and Wang, J.-C. (2015). Regulation of Glucose Homeostasis by Glucocorticoids. Adv Exp Med Biol *872*, 99-126.

Kurano, M., Hara, M., Tsuneyama, K., Sakoda, H., Shimizu, T., Tsukamoto, K., Ikeda, H., and Yatomi, Y. (2014). Induction of insulin secretion by apolipoprotein M, a carrier for sphingosine 1-phosphate. Biochimica et biophysica acta *1841*, 1217-1226.

Kurano, M., Tsukamoto, K., Shimizu, T., Kassai, H., Nakao, K., Aiba, A., Hara, M., and Yatomi, Y. (2020). Protection Against Insulin Resistance by Apolipoprotein M/Sphingosine 1-Phosphate. Diabetes.

Lara-Castro, C., and Garvey, W.T. (2008). Intracellular lipid accumulation in liver and muscle and the insulin resistance syndrome. Endocrinology and metabolism clinics of North America *37*, 841-856.

Law, I.K., Xu, A., Lam, K.S., Berger, T., Mak, T.W., Vanhoutte, P.M., Liu, J.T., Sweeney, G., Zhou, M., Yang, B.*, et al.* (2010). Lipocalin-2 deficiency attenuates insulin resistance associated with aging and obesity. Diabetes *59*, 872-882.

Lazar, M.A. (2007). Resistin- and Obesity-associated metabolic diseases. Hormone and metabolic research = Hormon- und Stoffwechselforschung = Hormones et metabolisme *39*, 710-716.

Lee, J.T., Huang, Z., Pan, K., Zhang, H.J., Woo, C.W., Xu, A., and Wong, C.M. (2016). Adipose-derived lipocalin 14 alleviates hyperglycaemia by suppressing both adipocyte glycerol efflux and hepatic gluconeogenesis in mice. Diabetologia *59*, 604-613.

Leone, V., Gibbons, S.M., Martinez, K., Hutchison, A.L., Huang, E.Y., Cham, C.M., Pierre, J.F., Heneghan, A.F., Nadimpalli, A., Hubert, N.*, et al.* (2015). Effects of diurnal variation of gut microbes and high-fat feeding on host circadian clock function and metabolism. Cell host & microbe *17*, 681-689.

Leto, D., and Saltiel, A.R. (2012). Regulation of glucose transport by insulin: traffic control of GLUT4. Nat Rev Mol Cell Biol *13*, 383-396.

Li, Y., Cao, X., Li, L.X., Brubaker, P.L., Edlund, H., and Drucker, D.J. (2005). beta-Cell Pdx1 expression is essential for the glucoregulatory, proliferative, and cytoprotective actions of glucagon-like peptide-1. Diabetes *54*, 482-491.

Light, P.E., Manning Fox, J.E., Riedel, M.J., and Wheeler, M.B. (2002). Glucagon-like peptide-1 inhibits pancreatic ATP-sensitive potassium channels via a protein kinase A- and ADP-dependent mechanism. Molecular endocrinology (Baltimore, Md) *16*, 2135-2144.

Lim, W.H., Wong, G., Lim, E.M., Byrnes, E., Zhu, K., Devine, A., Pavlos, N.J., Prince, R.L., and Lewis, J.R. (2015). Circulating Lipocalin 2 Levels Predict Fracture-Related Hospitalizations in Elderly Women: A Prospective Cohort Study. Journal of bone and mineral research : the official journal of the American Society for Bone and Mineral Research *30*, 2078-2085.

Lindsay, R.S., Funahashi, T., Hanson, R.L., Matsuzawa, Y., Tanaka, S., Tataranni, P.A., Knowler, W.C., and Krakoff, J. (2002). Adiponectin and development of type 2 diabetes in the Pima Indian population. Lancet (London, England) *360*, 57-58.

Linnemann, A.K., Neuman, J.C., Battiola, T.J., Wisinski, J.A., Kimple, M.E., and Davis, D.B. (2015). Glucagon-Like Peptide-1 Regulates Cholecystokinin Production in β-Cells to Protect From Apoptosis. Molecular endocrinology (Baltimore, Md) *29*, 978-987.

Liu, Q., and Muruve, D.A. (2003). Molecular basis of the inflammatory response to adenovirus vectors. Gene therapy *10*, 935-940.

Liu, Q., Zaiss, A.K., Colarusso, P., Patel, K., Haljan, G., Wickham, T.J., and Muruve, D.A. (2003). The role of capsid-endothelial interactions in the innate immune response to adenovirus vectors. Human gene therapy *14*, 627-643.

Liu, Y.Q., Jetton, T.L., and Leahy, J.L. (2002). beta-Cell adaptation to insulin resistance. Increased pyruvate carboxylase and malate-pyruvate shuttle activity in islets of nondiabetic Zucker fatty rats. The Journal of biological chemistry *277*, 39163-39168.

Liu, Z., Chang, G.Q., and Leibowitz, S.F. (2001). Apolipoprotein D interacts with the long-form leptin receptor: a hypothalamic function in the control of energy homeostasis. FASEB journal : official publication of the Federation of American Societies for Experimental Biology *15*, 1329-1331.

Lopez-Garcia, L.A., Demiray, L., Ruch-Marder, S., Hopp, A.-K., Hottiger, M.O., Helbling, P.M., and Pavlou, M.P. (2018). Validation of extracellular ligand–receptor interactions by Flow-TriCEPS. BMC Research Notes *11*, 863.

Lowell, B.B., and Shulman, G.I. (2005). Mitochondrial dysfunction and type 2 diabetes. Science (New York, NY) *307*, 384-387.

Lu, B., Kurmi, K., Munoz-Gomez, M., Jacobus Ambuludi, E.J., Tonne, J.M., Rakshit, K., Hitosugi, T., Kudva, Y.C., Matveyenko, A.V., and Ikeda, Y. (2018). Impaired β-cell glucokinase as an underlying mechanism in diet-induced diabetes. Disease models & mechanisms *11*.

Lukinius, A., Wilander, E., Westermark, G.T., Engstrom, U., and Westermark, P. (1989). Co-localization of islet amyloid polypeptide and insulin in the B cell secretory granules of the human pancreatic islets. Diabetologia *32*, 240-244.

Lyssenko, V., Lupi, R., Marchetti, P., Del Guerra, S., Orho-Melander, M., Almgren, P., Sjogren, M., Ling, C., Eriksson, K.F., Lethagen, A.L.*, et al.* (2007). Mechanisms by which common variants in the TCF7L2 gene increase risk of type 2 diabetes. The Journal of clinical investigation *117*, 2155-2163.

MacDonald, P.E., Salapatek, A.M., and Wheeler, M.B. (2003). Temperature and redox state dependence of native Kv2.1 currents in rat pancreatic beta-cells. The Journal of physiology *546*, 647-653.

Madiraju, A.K., Erion, D.M., Rahimi, Y., Zhang, X.M., Braddock, D.T., Albright, R.A., Prigaro, B.J., Wood, J.L., Bhanot, S., MacDonald, M.J.*, et al.* (2014). Metformin suppresses gluconeogenesis by inhibiting mitochondrial glycerophosphate dehydrogenase. Nature *510*, 542-546.

Maeda, N., Takahashi, M., Funahashi, T., Kihara, S., Nishizawa, H., Kishida, K., Nagaretani, H., Matsuda, M., Komuro, R., Ouchi, N.*, et al.* (2001). PPARgamma ligands increase expression and plasma concentrations of adiponectin, an adipose-derived protein. Diabetes *50*, 2094-2099.

Maedler, K., Carr, R.D., Bosco, D., Zuellig, R.A., Berney, T., and Donath, M.Y. (2005). Sulfonylurea induced beta-cell apoptosis in cultured human islets. The Journal of clinical endocrinology and metabolism *90*, 501-506.

Magnusson, I., Rothman, D.L., Katz, L.D., Shulman, R.G., and Shulman, G.I. (1992). Increased rate of gluconeogenesis in type II diabetes mellitus. A 13C nuclear magnetic resonance study. The Journal of clinical investigation *90*, 1323-1327.

Mancini, A.D., and Poitout, V. (2013). The fatty acid receptor FFA1/GPR40 a decade later: how much do we know? Trends in endocrinology and metabolism: TEM *24*, 398-407.

Marroquí, L., Gonzalez, A., Ñeco, P., Caballero-Garrido, E., Vieira, E., Ripoll, C., Nadal, A., and Quesada, I. (2012). Role of leptin in the pancreatic β-cell: effects and signaling pathways. Journal of molecular endocrinology *49*, R9-17.

Marso, S.P., Bain, S.C., Consoli, A., Eliaschewitz, F.G., Jodar, E., Leiter, L.A., Lingvay, I., Rosenstock, J., Seufert, J., Warren, M.L.*, et al.* (2016a). Semaglutide and Cardiovascular Outcomes in Patients with Type 2 Diabetes. The New England journal of medicine *375*, 1834-1844.

Marso, S.P., Daniels, G.H., Brown-Frandsen, K., Kristensen, P., Mann, J.F., Nauck, M.A., Nissen, S.E., Pocock, S., Poulter, N.R., Ravn, L.S.*, et al.* (2016b). Liraglutide and Cardiovascular Outcomes in Type 2 Diabetes. The New England journal of medicine *375*, 311-322.

Maslowski, K.M., Vieira, A.T., Ng, A., Kranich, J., Sierro, F., Yu, D., Schilter, H.C., Rolph, M.S., Mackay, F., Artis, D.*, et al.* (2009). Regulation of inflammatory responses by gut microbiota and chemoattractant receptor GPR43. Nature *461*, 1282-1286.

Massberg, D., and Hatt, H. (2018). Human Olfactory Receptors: Novel Cellular Functions Outside of the Nose. Physiological reviews *98*, 1739-1763.

Mathews, S.T., Chellam, N., Srinivas, P.R., Cintron, V.J., Leon, M.A., Goustin, A.S., and Grunberger, G. (2000). Alpha2-HSG, a specific inhibitor of insulin receptor autophosphorylation, interacts with the insulin receptor. Molecular and cellular endocrinology *164*, 87-98.

Mathews, S.T., Singh, G.P., Ranalletta, M., Cintron, V.J., Qiang, X., Goustin, A.S., Jen, K.L., Charron, M.J., Jahnen-Dechent, W., and Grunberger, G. (2002). Improved insulin sensitivity and resistance to weight gain in mice null for the Ahsg gene. Diabetes *51*, 2450-2458.

Mayerson, A.B., Hundal, R.S., Dufour, S., Lebon, V., Befroy, D., Cline, G.W., Enocksson, S., Inzucchi, S.E., Shulman, G.I., and Petersen, K.F. (2002). The effects of rosiglitazone on insulin sensitivity, lipolysis, and hepatic and skeletal muscle triglyceride content in patients with type 2 diabetes. Diabetes *51*, 797-802.

McCaffrey, A.P., Fawcett, P., Nakai, H., McCaffrey, R.L., Ehrhardt, A., Pham, T.T., Pandey, K., Xu, H., Feuss, S., Storm, T.A.*, et al.* (2008). The host response to adenovirus, helper-dependent adenovirus, and adeno-associated virus in mouse liver. Molecular therapy : the journal of the American Society of Gene Therapy *16*, 931-941.

Meex, R.C., Hoy, A.J., Morris, A., Brown, R.D., Lo, J.C., Burke, M., Goode, R.J., Kingwell, B.A., Kraakman, M.J., Febbraio, M.A.*, et al.* (2015). Fetuin B Is a Secreted Hepatocyte Factor Linking Steatosis to Impaired Glucose Metabolism. Cell Metab *22*, 1078-1089.

Meex, R.C.R., and Watt, M.J. (2017). Hepatokines: linking nonalcoholic fatty liver disease and insulin resistance. Nature reviews Endocrinology *13*, 509-520.

Meier, J.J., Gallwitz, B., Siepmann, N., Holst, J.J., Deacon, C.F., Schmidt, W.E., and Nauck, M.A. (2003). Gastric inhibitory polypeptide (GIP) dose-dependently stimulates glucagon secretion in healthy human subjects at euglycaemia. Diabetologia *46*, 798-801.

Mentlein, R., Gallwitz, B., and Schmidt, W.E. (1993). Dipeptidyl-peptidase IV hydrolyses gastric inhibitory polypeptide, glucagon-like peptide-1(7-36)amide, peptide histidine methionine and is responsible for their degradation in human serum. European journal of biochemistry *214*, 829-835.

Merkin, J., Russell, C., Chen, P., and Burge, C.B. (2012). Evolutionary dynamics of gene and isoform regulation in Mammalian tissues. Science (New York, NY) *338*, 1593-1599.

Merovci, A., Solis-Herrera, C., Daniele, G., Eldor, R., Fiorentino, T.V., Tripathy, D., Xiong, J., Perez, Z., Norton, L., Abdul-Ghani, M.A.*, et al.* (2014). Dapagliflozin improves muscle insulin sensitivity but enhances endogenous glucose production. The Journal of clinical investigation *124*, 509-514.

Meyer, C., Stumvoll, M., Nadkarni, V., Dostou, J., Mitrakou, A., and Gerich, J. (1998). Abnormal renal and hepatic glucose metabolism in type 2 diabetes mellitus. The Journal of clinical investigation *102*, 619-624.

Mezza, T., Muscogiuri, G., Sorice, G.P., Clemente, G., Hu, J., Pontecorvi, A., Holst, J.J., Giaccari, A., and Kulkarni, R.N. (2014). Insulin resistance alters islet morphology in nondiabetic humans. Diabetes *63*, 994-1007.

Milner, K.L., van der Poorten, D., Xu, A., Bugianesi, E., Kench, J.G., Lam, K.S., Chisholm, D.J., and George, J. (2009). Adipocyte fatty acid binding protein levels relate to inflammation and fibrosis in nonalcoholic fatty liver disease. Hepatology (Baltimore, Md) *49*, 1926-1934.

Minami, K., Yano, H., Miki, T., Nagashima, K., Wang, C.-Z., Tanaka, H., Miyazaki, J.-I., and Seino, S. (2000). Insulin secretion and differential gene expression in glucose-responsive and -unresponsive MIN6 sublines. American Journal of Physiology-Endocrinology and Metabolism *279*, E773-E781.

Mithieux, G., Bady, I., Gautier, A., Croset, M., Rajas, F., and Zitoun, C. (2004). Induction of control genes in intestinal gluconeogenesis is sequential during fasting and maximal in diabetes. Am J Physiol Endocrinol Metab *286*, E370-375.

Miwa, Y., Takiuchi, S., Kamide, K., Yoshii, M., Horio, T., Tanaka, C., Banno, M., Miyata, T., Sasaguri, T., and Kawano, Y. (2004). Identification of gene polymorphism in lipocalin-type prostaglandin D synthase and its association with carotid atherosclerosis in Japanese hypertensive patients. Biochemical and biophysical research communications *322*, 428-433.

Miyazaki, Y., Glass, L., Triplitt, C., Matsuda, M., Cusi, K., Mahankali, A., Mahankali, S., Mandarino, L.J., and DeFronzo, R.A. (2001). Effect of rosiglitazone on glucose and non-esterified fatty acid metabolism in Type II diabetic patients. Diabetologia *44*, 2210-2219.

Miyazaki, Y., Matsuda, M., and DeFronzo, R.A. (2002). Dose-response effect of pioglitazone on insulin sensitivity and insulin secretion in type 2 diabetes. Diabetes care *25*, 517-523.

Montagner, A., Korecka, A., Polizzi, A., Lippi, Y., Blum, Y., Canlet, C., Tremblay-Franco, M., Gautier-Stein, A., Burcelin, R., Yen, Y.C*., et al.* (2016). Hepatic circadian clock oscillators and nuclear receptors integrate microbiome-derived signals. Scientific reports *6*, 20127.

Moon, H., Chon, J., Joo, J., Kim, D., In, J., Lee, H., Park, J., and Choi, J. (2013). FTY720 preserved islet beta-cell mass by inhibiting apoptosis and increasing survival of beta-cells in db/db mice. Diabetes/metabolism research and reviews *29*, 19-24.

Mori, K., Emoto, M., Yokoyama, H., Araki, T., Teramura, M., Koyama, H., Shoji, T., Inaba, M., and Nishizawa, Y. (2006). Association of serum fetuin-A with insulin resistance in type 2 diabetic and nondiabetic subjects. Diabetes care *29*, 468.

Morley, J.E., and Flood, J.F. (1991). Amylin decreases food intake in mice. Peptides *12*, 865-869.

Mosialou, I., Shikhel, S., Liu, J.M., Maurizi, A., Luo, N., He, Z., Huang, Y., Zong, H., Friedman, R.A., Barasch, J*., et al.* (2017). MC4R-dependent suppression of appetite by bone-derived lipocalin 2. Nature *543*, 385-390.

Mraz, M., Bartlova, M., Lacinova, Z., Michalsky, D., Kasalicky, M., Haluzikova, D., Matoulek, M., Dostalova, I., Humenanska, V., and Haluzik, M. (2009). Serum concentrations and tissue expression of a novel endocrine regulator fibroblast growth factor-21 in patients with type 2 diabetes and obesity. Clinical endocrinology *71*, 369-375.

Mukhopadhyay, S., and Bhattacharya, S. (2016). Plasma fetuin-A triggers inflammatory changes in macrophages and adipocytes by acting as an adaptor protein between NEFA and TLR-4. Diabetologia *59*, 859-860.

Mutanen, A., Heikkila, P., Lohi, J., Raivio, T., Jalanko, H., and Pakarinen, M.P. (2014). Serum FGF21 increases with hepatic fat accumulation in pediatric onset intestinal failure. Journal of hepatology *60*, 183-190.

Nakahara, T.S., Cardozo, L.M., Ibarra-Soria, X., Bard, A.D., Carvalho, V.M.A., Trintinalia, G.Z., Logan, D.W., and Papes, F. (2016). Detection of pup odors by non-canonical adult vomeronasal neurons expressing an odorant receptor gene is influenced by sex and parenting status. BMC Biol *14*, 12-12.

Nakai, H., Fuess, S., Storm, T.A., Muramatsu, S.-i., Nara, Y., and Kay, M.A. (2005). Unrestricted hepatocyte transduction with adeno-associated virus serotype 8 vectors in mice. Journal of virology *79*, 214-224.

Nakamura, T., Furuhashi, M., Li, P., Cao, H., Tuncman, G., Sonenberg, N., Gorgun, C.Z., and Hotamisligil, G.S. (2010). Double-stranded RNA-dependent protein kinase links pathogen sensing with stress and metabolic homeostasis. Cell *140*, 338-348.

Nathwani, A.C., Gray, J.T., Ng, C.Y., Zhou, J., Spence, Y., Waddington, S.N., Tuddenham, E.G., Kemball-Cook, G., McIntosh, J., Boon-Spijker, M.*, et al.* (2006). Self-complementary adeno-associated virus vectors containing a novel liver-specific human factor IX expression cassette enable highly efficient transduction of murine and nonhuman primate liver. Blood *107*, 2653-2661.

Nauck, M.A., Baller, B., and Meier, J.J. (2004). Gastric inhibitory polypeptide and glucagon-like peptide-1 in the pathogenesis of type 2 diabetes. Diabetes *53 Suppl 3*, S190-196.

Nauck, M.A., Heimesaat, M.M., Behle, K., Holst, J.J., Nauck, M.S., Ritzel, R., Hufner, M., and Schmiegel, W.H. (2002). Effects of glucagon-like peptide 1 on counterregulatory hormone responses, cognitive functions, and insulin secretion during hyperinsulinemic, stepped hypoglycemic clamp experiments in healthy volunteers. The Journal of clinical endocrinology and metabolism *87*, 1239-1246.

Nauck, M.A., Heimesaat, M.M., Orskov, C., Holst, J.J., Ebert, R., and Creutzfeldt, W. (1993). Preserved incretin activity of glucagon-like peptide 1 [7-36 amide] but not of synthetic human gastric inhibitory polypeptide in patients with type-2 diabetes mellitus. The Journal of clinical investigation *91*, 301-307.

NICE-SUGAR Study Investigators, S.F., Dean R Chittock, Steve Yu-Shuo Su, Deborah Blair, Denise Foster, Vinay Dhingra, Rinaldo Bellomo, Deborah Cook, Peter Dodek, William R Henderson, Paul C Hébert, Stephane Heritier, Daren K Heyland, Colin McArthur, Ellen McDonald, Imogen Mitchell, John A Myburgh, Robyn Norton, Julie Potter, Bruce G Robinson, Juan J Ronco (2009). Intensive versus Conventional Glucose Control in Critically Ill Patients. New England Journal of Medicine *360*, 1283-1297.

Niwa, H., Yamamura, K., and Miyazaki, J. (1991). Efficient selection for high-expression transfectants with a novel eukaryotic vector. Gene *108*, 193-199.

Nolan, C.J., Leahy, J.L., Delghingaro-Augusto, V., Moibi, J., Soni, K., Peyot, M.L., Fortier, M., Guay, C., Lamontagne, J., Barbeau, A.*, et al.* (2006). Beta cell compensation for insulin resistance in Zucker fatty rats: increased lipolysis and fatty acid signalling. Diabetologia *49*, 2120-2130.

Nonogaki, K., Fuller, G.M., Fuentes, N.L., Moser, A.H., Staprans, I., Grunfeld, C., and Feingold, K.R. (1995). Interleukin-6 stimulates hepatic triglyceride secretion in rats. Endocrinology *136*, 2143-2149.

Obrink, K.J., and Rehbinder, C. (2000). Animal definition: a necessity for the validity of animal experiments? Laboratory animals *34*, 121-130.

Oh, H.Y.P., Ellero-Simatos, S., Manickam, R., Tan, N.S., Guillou, H., and Wahli, W. (2019). Depletion of Gram-Positive Bacteria Impacts Hepatic Biological Functions During the Light Phase. Int J Mol Sci *20*, 812.

Okabe, M., Ikawa, M., Kominami, K., Nakanishi, T., and Nishimune, Y. (1997). 'Green mice' as a source of ubiquitous green cells. FEBS letters *407*, 313-319.

Okamoto, H., Hribal, M.L., Lin, H.V., Bennett, W.R., Ward, A., and Accili, D. (2006). Role of the forkhead protein FoxO1 in beta cell compensation to insulin resistance. The Journal of clinical investigation *116*, 775-782.

Ozaki, N., Shibasaki, T., Kashima, Y., Miki, T., Takahashi, K., Ueno, H., Sunaga, Y., Yano, H., Matsuura, Y., Iwanaga, T.*, et al.* (2000). cAMP-GEFII is a direct target of cAMP in regulated exocytosis. Nature cell biology *2*, 805-811.

Ozcan, U., Cao, Q., Yilmaz, E., Lee, A.H., Iwakoshi, N.N., Ozdelen, E., Tuncman, G., Gorgun, C., Glimcher, L.H., and Hotamisligil, G.S. (2004). Endoplasmic reticulum stress links obesity, insulin action, and type 2 diabetes. Science (New York, NY) *306*, 457-461.

Pal, D., Dasgupta, S., Kundu, R., Maitra, S., Das, G., Mukhopadhyay, S., Ray, S., Majumdar, S.S., and Bhattacharya, S. (2012). Fetuin-A acts as an endogenous ligand of TLR4 to promote lipid-induced insulin resistance. Nature medicine *18*, 1279-1285.

Pappo, I., Becovier, H., Berry, E.M., and Freund, H.R. (1991). Polymyxin B reduces cecal flora, TNF production and hepatic steatosis during total parenteral nutrition in the rat. The Journal of surgical research *51*, 106-112.

Parséus, A., Sommer, N., Sommer, F., Caesar, R., Molinaro, A., Ståhlman, M., Greiner, T.U., Perkins, R., and Bäckhed, F. (2017). Microbiota-induced obesity requires farnesoid X receptor. Gut *66*, 429-437.

Paton, C.M., and Ntambi, J.M. (2009). Biochemical and physiological function of stearoyl-CoA desaturase. Am J Physiol Endocrinol Metab *297*, E28-E37.

Paton, C.M., Rogowski, M.P., Kozimor, A.L., Stevenson, J.L., Chang, H., and Cooper, J.A. (2013). Lipocalin-2 increases fat oxidation in vitro and is correlated with energy expenditure in normal weight but not obese women. Obesity (Silver Spring, Md) *21*, E640-648.

Pelleymounter, M.A., Cullen, M.J., Baker, M.B., Hecht, R., Winters, D., Boone, T., and Collins, F. (1995). Effects of the obese gene product on body weight regulation in ob/ob mice. Science (New York, NY) *269*, 540-543.

Pelosi, P. (1994). Odorant-binding proteins. Critical reviews in biochemistry and molecular biology *29*, 199-228.

Pendyala, S., Walker, J.M., and Holt, P.R. (2012). A high-fat diet is associated with endotoxemia that originates from the gut. Gastroenterology *142*, 1100-1101.e1102.

Perdomo, G., and Henry Dong, H. (2009). Apolipoprotein D in lipid metabolism and its functional implication in atherosclerosis and aging. Aging (Albany NY) *1*, 17-27.

Perdomo, G., Kim, D.H., Zhang, T., Qu, S., Thomas, E.A., Toledo, F.G.S., Slusher, S., Fan, Y., Kelley, D.E., and Dong, H.H. (2010). A role of apolipoprotein D in triglyceride metabolism. J Lipid Res *51*, 1298-1311.

Perry, R.J., Peng, L., Barry, N.A., Cline, G.W., Zhang, D., Cardone, R.L., Petersen, K.F., Kibbey, R.G., Goodman, A.L., and Shulman, G.I. (2016). Acetate mediates a microbiome-brain-beta-cell axis to promote metabolic syndrome. Nature *534*, 213-217.

Petryszak, R., Keays, M., Tang, Y.A., Fonseca, N.A., Barrera, E., Burdett, T., Füllgrabe, A., Fuentes, A.M.-P., Jupp, S., Koskinen, S.*, et al.* (2015). Expression Atlas update—an integrated database of gene and protein expression in humans, animals and plants. Nucleic acids research *44*, D746-D752.

Pi, J., Bai, Y., Zhang, Q., Wong, V., Floering, L.M., Daniel, K., Reece, J.M., Deeney, J.T., Andersen, M.E., Corkey, B.E.*, et al.* (2007). Reactive oxygen species as a signal in glucose-stimulated insulin secretion. Diabetes *56*, 1783-1791.

Pocai, A., Carrington, P.E., Adams, J.R., Wright, M., Eiermann, G., Zhu, L., Du, X., Petrov, A., Lassman, M.E., Jiang, G.*, et al.* (2009). Glucagon-like peptide 1/glucagon receptor dual agonism reverses obesity in mice. Diabetes *58*, 2258-2266.

Polonsky, K.S., Given, B.D., and Van Cauter, E. (1988). Twenty-four-hour profiles and pulsatile patterns of insulin secretion in normal and obese subjects. The Journal of clinical investigation *81*, 442-448.

Prentki, M., Matschinsky, F.M., and Madiraju, S.R. (2013). Metabolic signaling in fuel-induced insulin secretion. Cell Metab *18*, 162-185.

Pussinen, P.J., Havulinna, A.S., Lehto, M., Sundvall, J., and Salomaa, V. (2011). Endotoxemia is associated with an increased risk of incident diabetes. Diabetes care *34*, 392-397.

Quarta, C., Clemmensen, C., Zhu, Z., Yang, B., Joseph, S.S., Lutter, D., Yi, C.X., Graf, E., García-Cáceres, C., Legutko, B.*, et al.* (2017). Molecular Integration of Incretin and Glucocorticoid Action Reverses Immunometabolic Dysfunction and Obesity. Cell Metab *26*, 620-632.e626.

Ragolia, L., Hall, C.E., and Palaia, T. (2008). Lipocalin-type prostaglandin D(2) synthase stimulates glucose transport via enhanced GLUT4 translocation. Prostaglandins & other lipid mediators *87*, 34-41.

Ragolia, L., Palaia, T., Hall, C.E., Maesaka, J.K., Eguchi, N., and Urade, Y. (2005). Accelerated glucose intolerance, nephropathy, and atherosclerosis in prostaglandin D2 synthase knock-out mice. The Journal of biological chemistry *280*, 29946-29955.

Rains, J.L., and Jain, S.K. (2011). Oxidative stress, insulin signaling, and diabetes. Free radical biology & medicine *50*, 567-575.

Ramracheya, R., Chapman, C., Chibalina, M., Dou, H., Miranda, C., González, A., Moritoh, Y., Shigeto, M., Zhang, Q., Braun, M.*, et al.* (2018). GLP-1 suppresses glucagon secretion in

human pancreatic alpha-cells by inhibition of P/Q-type Ca(2+) channels. Physiol Rep *6*, e13852-e13852.

Reaven, P.D., Emanuele, N.V., Wiitala, W.L., Bahn, G.D., Reda, D.J., McCarren, M., Duckworth, W.C., and Hayward, R.A. (2019). Intensive Glucose Control in Patients with Type 2 Diabetes - 15-Year Follow-up. The New England journal of medicine *380*, 2215-2224.

Redl, B. (2000). Human tear lipocalin. Biochimica et biophysica acta *1482*, 241-248.

Reinbothe, T.M., Ivarsson, R., Li, D.-Q., Niazi, O., Jing, X., Zhang, E., Stenson, L., Bryborn, U., and Renström, E. (2009). Glutaredoxin-1 mediates NADPH-dependent stimulation of calcium-dependent insulin secretion. Molecular endocrinology (Baltimore, Md) *23*, 893-900.

Riccardi, G., Giacco, R., and Rivellese, A.A. (2004). Dietary fat, insulin sensitivity and the metabolic syndrome. Clinical nutrition (Edinburgh, Scotland) *23*, 447-456.

Rieusset, J., Bouzakri, K., Chevillotte, E., Ricard, N., Jacquet, D., Bastard, J.-P., Laville, M., and Vidal, H. (2004). Suppressor of Cytokine Signaling 3 Expression and Insulin Resistance in Skeletal Muscle of Obese and Type 2 Diabetic Patients. Diabetes *53*, 2232.

Ritzel, R.A., Meier, J.J., Lin, C.Y., Veldhuis, J.D., and Butler, P.C. (2007). Human islet amyloid polypeptide oligomers disrupt cell coupling, induce apoptosis, and impair insulin secretion in isolated human islets. Diabetes *56*, 65-71.

Robosky, L.C., Wells, D.F., Egnash, L.A., Manning, M.L., Reily, M.D., and Robertson, D.G. (2005). Metabonomic identification of two distinct phenotypes in Sprague-Dawley (Crl:CD(SD)) rats. Toxicological sciences : an official journal of the Society of Toxicology *87*, 277-284.

Rodríguez-Gutiérrez, R., and Montori, V.M. (2016). Glycemic Control for Patients With Type 2 Diabetes Mellitus: Our Evolving Faith in the Face of Evidence. Circulation Cardiovascular quality and outcomes *9*, 504-512.

Rohde, C.M., Wells, D.F., Robosky, L.C., Manning, M.L., Clifford, C.B., Reily, M.D., and Robertson, D.G. (2007). Metabonomic evaluation of Schaedler altered microflora rats. Chemical research in toxicology *20*, 1388-1392.

Rosenstock, J., Einhorn, D., Hershon, K., Glazer, N.B., and Yu, S. (2002). Efficacy and safety of pioglitazone in type 2 diabetes: a randomised, placebo-controlled study in patients receiving stable insulin therapy. International journal of clinical practice *56*, 251-257.

Rosmond, R. (2005). Role of stress in the pathogenesis of the metabolic syndrome. Psychoneuroendocrinology *30*, 1-10.

Roumie, C.L., Hung, A.M., Greevy, R.A., Grijalva, C.G., Liu, X., Murff, H.J., Elasy, T.A., and Griffin, M.R. (2012). Comparative effectiveness of sulfonylurea and metformin monotherapy on cardiovascular events in type 2 diabetes mellitus: a cohort study. Annals of internal medicine *157*, 601-610.

Ruvinsky, I., and Meyuhas, O. (2006). Ribosomal protein S6 phosphorylation: from protein synthesis to cell size. Trends in biochemical sciences *31*, 342-348.

Samuel, B.S., Shaito, A., Motoike, T., Rey, F.E., Backhed, F., Manchester, J.K., Hammer, R.E., Williams, S.C., Crowley, J., Yanagisawa, M.*, et al.* (2008). Effects of the gut microbiota on host adiposity are modulated by the short-chain fatty-acid binding G protein-coupled receptor, Gpr41. Proceedings of the National Academy of Sciences of the United States of America *105*, 16767-16772.

Samuel, V.T., Liu, Z.X., Qu, X., Elder, B.D., Bilz, S., Befroy, D., Romanelli, A.J., and Shulman, G.I. (2004). Mechanism of hepatic insulin resistance in non-alcoholic fatty liver disease. The Journal of biological chemistry *279*, 32345-32353.

Samuel, V.T., Liu, Z.X., Wang, A., Beddow, S.A., Geisler, J.G., Kahn, M., Zhang, X.M., Monia, B.P., Bhanot, S., and Shulman, G.I. (2007). Inhibition of protein kinase Cepsilon prevents hepatic insulin resistance in nonalcoholic fatty liver disease. The Journal of clinical investigation *117*, 739-745.

Samuel, V.T., and Shulman, G.I. (2016). The pathogenesis of insulin resistance: integrating signaling pathways and substrate flux. The Journal of clinical investigation *126*, 12-22.

Sano, H., Eguez, L., Teruel, M.N., Fukuda, M., Chuang, T.D., Chavez, J.A., Lienhard, G.E., and McGraw, T.E. (2007). Rab10, a target of the AS160 Rab GAP, is required for insulin-stimulated translocation of GLUT4 to the adipocyte plasma membrane. Cell Metab *5*, 293-303.

Satoh, H., Nguyen, M.T., Miles, P.D., Imamura, T., Usui, I., and Olefsky, J.M. (2004). Adenovirus-mediated chronic "hyper-resistinemia" leads to in vivo insulin resistance in normal rats. The Journal of clinical investigation *114*, 224-231.

Schiefner, A., Freier, R., Eichinger, A., and Skerra, A. (2015). Crystal structure of the human odorant binding protein, OBPIIa. Proteins *83*, 1180-1184.

Schiefner, A., and Skerra, A. (2015). The menagerie of human lipocalins: a natural protein scaffold for molecular recognition of physiological compounds. Accounts of chemical research *48*, 976-985.

Schirmer, M., Smeekens, S.P., Vlamakis, H., Jaeger, M., Oosting, M., Franzosa, E.A., Ter Horst, R., Jansen, T., Jacobs, L., Bonder, M.J.*, et al.* (2016). Linking the Human Gut Microbiome to Inflammatory Cytokine Production Capacity. Cell *167*, 1125-1136.e1128.

Schlehuber, S., and Skerra, A. (2005). Lipocalins in drug discovery: from natural ligand-binding proteins to "anticalins". Drug discovery today *10*, 23-33.

Schmid, A., Leszczak, S., Ober, I., Schaffler, A., and Karrasch, T. (2016). Short-Term Regulation of Lipocalin-2 but not RBP-4 During Oral Lipid Tolerance Test and Oral Glucose Tolerance Test. Hormone and metabolic research = Hormon- und Stoffwechselforschung = Hormones et metabolisme *48*, 99-105.

Schroeder, B.O., and Backhed, F. (2016). Signals from the gut microbiota to distant organs in physiology and disease. Nature medicine *22*, 1079-1089.

Schwartz, D.R., and Lazar, M.A. (2011). Human resistin: found in translation from mouse to man. Trends in endocrinology and metabolism: TEM *22*, 259-265.

Seldin, M.M., Koplev, S., Rajbhandari, P., Vergnes, L., Rosenberg, G.M., Meng, Y., Pan, C., Phuong, T.M.N., Gharakhanian, R., Che, N.*, et al.* (2018). A Strategy for Discovery of Endocrine Interactions with Application to Whole-Body Metabolism. Cell Metab *27*, 1138-1155.e1136.

Selvam, C., Mutisya, D., Prakash, S., Ranganna, K., and Thilagavathi, R. (2017). Therapeutic potential of chemically modified siRNA: Recent trends. Chem Biol Drug Des *90*, 665-678.

Semba, T., Nishimura, M., Nishimura, S., Ohara, O., Ishige, T., Ohno, S., Nonaka, K., Sogawa, K., Satoh, M., Sawai, S.*, et al.* (2013). The FLS (fatty liver Shionogi) mouse reveals local expressions of lipocalin-2, CXCL1 and CXCL9 in the liver with non-alcoholic steatohepatitis. BMC gastroenterology *13*, 120.

Sheng, L., Cho, K.W., Zhou, Y., Shen, H., and Rui, L. (2011). Lipocalin 13 protein protects against hepatic steatosis by both inhibiting lipogenesis and stimulating fatty acid beta-oxidation. The Journal of biological chemistry *286*, 38128-38135.

Shi, H., Kokoeva, M.V., Inouye, K., Tzameli, I., Yin, H., and Flier, J.S. (2006). TLR4 links innate immunity and fatty acid-induced insulin resistance. The Journal of clinical investigation *116*, 3015-3025.

Shibasaki, T., Sunaga, Y., Fujimoto, K., Kashima, Y., and Seino, S. (2004). Interaction of ATP sensor, cAMP sensor, Ca2+ sensor, and voltage-dependent Ca2+ channel in insulin granule exocytosis. The Journal of biological chemistry *279*, 7956-7961.

Shulman, G.I., Rothman, D.L., Jue, T., Stein, P., DeFronzo, R.A., and Shulman, R.G. (1990). Quantitation of muscle glycogen synthesis in normal subjects and subjects with non-insulin-dependent diabetes by 13C nuclear magnetic resonance spectroscopy. The New England journal of medicine *322*, 223-228.

Simpson, S.H., Majumdar, S.R., Tsuyuki, R.T., Eurich, D.T., and Johnson, J.A. (2006). Dose-response relation between sulfonylurea drugs and mortality in type 2 diabetes mellitus: a population-based cohort study. CMAJ *174*, 169-174.

Sobotzki, N., Schafroth, M.A., Rudnicka, A., Koetemann, A., Marty, F., Goetze, S., Yamauchi, Y., Carreira, E.M., and Wollscheid, B. (2018). HATRIC-based identification of receptors for orphan ligands. Nature communications *9*, 1519.

Song, W., Kong, H.L., Traktman, P., and Crystal, R.G. (1997). Cytotoxic T lymphocyte responses to proteins encoded by heterologous transgenes transferred in vivo by adenoviral vectors. Human gene therapy *8*, 1207-1217.

Soumillon, M., Necsulea, A., Weier, M., Brawand, D., Zhang, X., Gu, H., Barthes, P., Kokkinaki, M., Nef, S., Gnirke, A.*, et al.* (2013). Cellular source and mechanisms of high transcriptome complexity in the mammalian testis. Cell reports *3*, 2179-2190.

Sramkova, V., Berend, S., Siklova, M., Caspar-Bauguil, S., Carayol, J., Bonnel, S., Marques, M., Decaunes, P., Kolditz, C.I., Dahlman, I.*, et al.* (2019). Apolipoprotein M: a novel adipokine decreasing with obesity and upregulated by calorie restriction. The American journal of clinical nutrition *109*, 1499-1510.

Sreekumar, R., Halvatsiotis, P., Schimke, J.C., and Nair, K.S. (2002). Gene expression profile in skeletal muscle of type 2 diabetes and the effect of insulin treatment. Diabetes *51*, 1913-1920.

Sridharan, G.V., Choi, K., Klemashevich, C., Wu, C., Prabakaran, D., Pan, L.B., Steinmeyer, S., Mueller, C., Yousofshahi, M., Alaniz, R.C.*, et al.* (2014). Prediction and quantification of bioactive microbiota metabolites in the mouse gut. Nature communications *5*, 5492.

Srinivas, P.R., Wagner, A.S., Reddy, L.V., Deutsch, D.D., Leon, M.A., Goustin, A.S., and Grunberger, G. (1993). Serum alpha 2-HS-glycoprotein is an inhibitor of the human insulin receptor at the tyrosine kinase level. Molecular endocrinology (Baltimore, Md) *7*, 1445-1455.

Stanford, K.I., and Goodyear, L.J. (2014). Exercise and type 2 diabetes: molecular mechanisms regulating glucose uptake in skeletal muscle. Adv Physiol Educ *38*, 308-314.

Stefan, N., Fritsche, A., Weikert, C., Boeing, H., Joost, H.-G., Häring, H.-U., and Schulze, M.B. (2008). Plasma fetuin-A levels and the risk of type 2 diabetes. Diabetes *57*, 2762-2767.

Stefan, N., and Haring, H.U. (2013). Circulating fetuin-A and free fatty acids interact to predict insulin resistance in humans. Nature medicine *19*, 394-395.

Stefan, N., Hennige, A.M., Staiger, H., Machann, J., Schick, F., Krober, S.M., Machicao, F., Fritsche, A., and Haring, H.U. (2006). Alpha2-Heremans-Schmid glycoprotein/fetuin-A is associated with insulin resistance and fat accumulation in the liver in humans. Diabetes care *29*, 853-857.

Steppan, C.M., Bailey, S.T., Bhat, S., Brown, E.J., Banerjee, R.R., Wright, C.M., Patel, H.R., Ahima, R.S., and Lazar, M.A. (2001). The hormone resistin links obesity to diabetes. Nature *409*, 307-312.

Steppan, C.M., Wang, J., Whiteman, E.L., Birnbaum, M.J., and Lazar, M.A. (2005). Activation of SOCS-3 by resistin. Mol Cell Biol *25*, 1569-1575.

Stonehouse, A., Okerson, T., Kendall, D., and Maggs, D. (2008). Emerging incretin based therapies for type 2 diabetes: incretin mimetics and DPP-4 inhibitors. Current diabetes reviews *4*, 101-109.

Stratford, S., Hoehn, K.L., Liu, F., and Summers, S.A. (2004). Regulation of insulin action by ceramide: dual mechanisms linking ceramide accumulation to the inhibition of Akt/protein kinase B. The Journal of biological chemistry *279*, 36608-36615.

Stratton, I.M., Adler, A.I., Neil, H.A., Matthews, D.R., Manley, S.E., Cull, C.A., Hadden, D., Turner, R.C., and Holman, R.R. (2000). Association of glycaemia with macrovascular and microvascular complications of type 2 diabetes (UKPDS 35): prospective observational study. BMJ (Clinical research ed) *321*, 405-412.

Sugita, H., Kaneki, M., Tokunaga, E., Sugita, M., Koike, C., Yasuhara, S., Tompkins, R.G., and Martyn, J.A. (2002). Inducible nitric oxide synthase plays a role in LPS-induced hyperglycemia and insulin resistance. Am J Physiol Endocrinol Metab *282*, E386-394.

Sun, E.W.L., Martin, A.M., Young, R.L., and Keating, D.J. (2019). The Regulation of Peripheral Metabolism by Gut-Derived Hormones. Front Endocrinol (Lausanne) *9*, 754-754.

Suzuki, K., Lareyre, J.J., Sanchez, D., Gutierrez, G., Araki, Y., Matusik, R.J., and Orgebin-Crist, M.C. (2004). Molecular evolution of epididymal lipocalin genes localized on mouse chromosome 2. Gene *339*, 49-59.

Talchai, C., Xuan, S., Lin, H.V., Sussel, L., and Accili, D. (2012). Pancreatic beta cell dedifferentiation as a mechanism of diabetic beta cell failure. Cell *150*, 1223-1234.

Tanaka, R., Miwa, Y., Mou, K., Tomikawa, M., Eguchi, N., Urade, Y., Takahashi-Yanaga, F., Morimoto, S., Wake, N., and Sasaguri, T. (2009). Knockout of the l-pgds gene aggravates obesity and atherosclerosis in mice. Biochemical and biophysical research communications *378*, 851-856.

Tang, J., Maximov, A., Shin, O.H., Dai, H., Rizo, J., and Sudhof, T.C. (2006). A complexin/synaptotagmin 1 switch controls fast synaptic vesicle exocytosis. Cell *126*, 1175-1187.

Tcatchoff, L., Nespoulous, C., Pernollet, J.C., and Briand, L. (2006). A single lysyl residue defines the binding specificity of a human odorant-binding protein for aldehydes. FEBS letters *580*, 2102-2108.

Terauchi, Y., Takamoto, I., Kubota, N., Matsui, J., Suzuki, R., Komeda, K., Hara, A., Toyoda, Y., Miwa, I., Aizawa, S.*, et al.* (2007). Glucokinase and IRS-2 are required for compensatory beta cell hyperplasia in response to high-fat diet-induced insulin resistance. The Journal of clinical investigation *117*, 246-257.

Terra, X., Auguet, T., Broch, M., Sabench, F., Hernandez, M., Pastor, R.M., Quesada, I.M., Luna, A., Aguilar, C., del Castillo, D.*, et al.* (2013). Retinol binding protein-4 circulating levels were higher in nonalcoholic fatty liver disease vs. histologically normal liver from morbidly obese women. Obesity (Silver Spring, Md) *21*, 170-177.

Thaiss, C.A., Levy, M., Grosheva, I., Zheng, D., Soffer, E., Blacher, E., Braverman, S., Tengeler, A.C., Barak, O., Elazar, M.*, et al.* (2018). Hyperglycemia drives intestinal barrier dysfunction and risk for enteric infection. Science (New York, NY) *359*, 1376-1383.

Thomas, C., Gioiello, A., Noriega, L., Strehle, A., Oury, J., Rizzo, G., Macchiarulo, A., Yamamoto, H., Mataki, C., Pruzanski, M.*, et al.* (2009). TGR5-mediated bile acid sensing controls glucose homeostasis. Cell Metab *10*, 167-177.

Tolhurst, G., Heffron, H., Lam, Y.S., Parker, H.E., Habib, A.M., Diakogiannaki, E., Cameron, J., Grosse, J., Reimann, F., and Gribble, F.M. (2012). Short-chain fatty acids stimulate glucagon-like peptide-1 secretion via the G-protein-coupled receptor FFAR2. Diabetes *61*, 364-371.

Trexler, A.J., and Taraska, J.W. (2017). Regulation of insulin exocytosis by calcium-dependent protein kinase C in beta cells. Cell Calcium *67*, 1-10.

Turnbull, F.M., Abraira, C., Anderson, R.J., Byington, R.P., Chalmers, J.P., Duckworth, W.C., Evans, G.W., Gerstein, H.C., Holman, R.R., Moritz, T.E.*, et al.* (2009). Intensive glucose control and macrovascular outcomes in type 2 diabetes. Diabetologia *52*, 2288-2298.

Turner, R.C., Cull, C.A., Frighi, V., and Holman, R.R. (1999). Glycemic control with diet, sulfonylurea, metformin, or insulin in patients with type 2 diabetes mellitus: progressive requirement for multiple therapies (UKPDS 49). UK Prospective Diabetes Study (UKPDS) Group. JAMA *281*, 2005-2012.

Turpin, S.M., Nicholls, H.T., Willmes, D.M., Mourier, A., Brodesser, S., Wunderlich, C.M., Mauer, J., Xu, E., Hammerschmidt, P., Brönneke, H.S.*, et al.* (2014). Obesity-induced CerS6-dependent C16:0 ceramide production promotes weight gain and glucose intolerance. Cell Metab *20*, 678-686.

U.K. Prospective Diabetes Study Group (1995). U.K. prospective diabetes study 16. Overview of 6 years' therapy of type II diabetes: a progressive disease. U.K. Prospective Diabetes Study Group. Diabetes *44*, 1249-1258.

UK Prospective Diabetes Study (UKPDS) Group (1998). Intensive blood-glucose control with sulphonylureas or insulin compared with conventional treatment and risk of complications in patients with type 2 diabetes (UKPDS 33). UK Prospective Diabetes Study (UKPDS) Group. Lancet (London, England) *352*, 837-853.

Umino, H., Hasegawa, K., Minakuchi, H., Muraoka, H., Kawaguchi, T., Kanda, T., Tokuyama, H., Wakino, S., and Itoh, H. (2018). High Basolateral Glucose Increases Sodium-Glucose Cotransporter 2 and Reduces Sirtuin-1 in Renal Tubules through Glucose Transporter-2 Detection. Scientific reports *8*, 6791.

Urbanet, R., Nguyen Dinh Cat, A., Feraco, A., Venteclef, N., El Mogrhabi, S., Sierra-Ramos, C., Alvarez de la Rosa, D., Adler, G.K., Quilliot, D., Rossignol, P.*, et al.* (2015). Adipocyte Mineralocorticoid Receptor Activation Leads to Metabolic Syndrome and Induction of Prostaglandin D2 Synthase. Hypertension (Dallas, Tex : 1979) *66*, 149-157.

Valdar, W., Solberg, L.C., Gauguier, D., Cookson, W.O., Rawlins, J.N., Mott, R., and Flint, J. (2006). Genetic and environmental effects on complex traits in mice. Genetics *174*, 959-984.

Vallon, V., Platt, K.A., Cunard, R., Schroth, J., Whaley, J., Thomson, S.C., Koepsell, H., and Rieg, T. (2011). SGLT2 mediates glucose reabsorption in the early proximal tubule. Journal of the American Society of Nephrology : JASN *22*, 104-112.

Van Loo, P.L., Mol, J.A., Koolhaas, J.M., Van Zutphen, B.F., and Baumans, V. (2001). Modulation of aggression in male mice: influence of group size and cage size. Physiology & behavior *72*, 675-683.

van Schothorst, E.M., Keijer, J., Pennings, J.L., Opperhuizen, A., van den Brom, C.E., Kohl, T., Franssen-van Hal, N.L., and Hoebee, B. (2006). Adipose gene expression response of lean and obese mice to short-term dietary restriction. Obesity (Silver Spring, Md) *14*, 974-979.

Varma, T.K., Lin, C.Y., Toliver-Kinsky, T.E., and Sherwood, E.R. (2002). Endotoxin-induced gamma interferon production: contributing cell types and key regulatory factors. Clin Diagn Lab Immunol *9*, 530-543.

Vatner, D.F., Majumdar, S.K., Kumashiro, N., Petersen, M.C., Rahimi, Y., Gattu, A.K., Bears, M., Camporez, J.P., Cline, G.W., Jurczak, M.J.*, et al.* (2015). Insulin-independent regulation of hepatic triglyceride synthesis by fatty acids. Proceedings of the National Academy of Sciences of the United States of America *112*, 1143-1148.

Vijayaraghavan, S., Hitman, G.A., and Kopelman, P.G. (1994). Apolipoprotein-D polymorphism: a genetic marker for obesity and hyperinsulinemia. The Journal of clinical endocrinology and metabolism *79*, 568-570.

Vilsboll, T., Krarup, T., Madsbad, S., and Holst, J.J. (2002). Defective amplification of the late phase insulin response to glucose by GIP in obese Type II diabetic patients. Diabetologia *45*, 1111-1119.

Virkamäki, A., and Yki-Järvinen, H. (1994). Mechanisms of insulin resistance during acute endotoxemia. Endocrinology *134*, 2072-2078.

Virtue, S., Feldmann, H., Christian, M., Tan, C.Y., Masoodi, M., Dale, M., Lelliott, C., Burling, K., Campbell, M., Eguchi, N.*, et al.* (2012). A new role for lipocalin prostaglandin d synthase in the regulation of brown adipose tissue substrate utilization. Diabetes *61*, 3139-3147.

Wajngot, A., Chandramouli, V., Schumann, W.C., Ekberg, K., Jones, P.K., Efendic, S., and Landau, B.R. (2001). Quantitative contributions of gluconeogenesis to glucose production during fasting in type 2 diabetes mellitus. Metabolism: clinical and experimental *50*, 47-52.

Wang, C.H., Wang, C.C., Huang, H.C., and Wei, Y.H. (2013). Mitochondrial dysfunction leads to impairment of insulin sensitivity and adiponectin secretion in adipocytes. The FEBS journal *280*, 1039-1050.

Wang, Y., Lam, K.S., Kraegen, E.W., Sweeney, G., Zhang, J., Tso, A.W., Chow, W.S., Wat, N.M., Xu, J.Y., Hoo, R.L.*, et al.* (2007). Lipocalin-2 is an inflammatory marker closely associated with obesity, insulin resistance, and hyperglycemia in humans. Clinical chemistry *53*, 34-41.

Wang, Z., Zhu, T., Qiao, C., Zhou, L., Wang, B., Zhang, J., Chen, C., Li, J., and Xiao, X. (2005). Adeno-associated virus serotype 8 efficiently delivers genes to muscle and heart. Nature biotechnology *23*, 321-328.

Watanabe, M., Houten, S.M., Mataki, C., Christoffolete, M.A., Kim, B.W., Sato, H., Messaddeq, N., Harney, J.W., Ezaki, O., Kodama, T.*, et al.* (2006). Bile acids induce energy expenditure by promoting intracellular thyroid hormone activation. Nature *439*, 484-489.

Way, J.M., Harrington, W.W., Brown, K.K., Gottschalk, W.K., Sundseth, S.S., Mansfield, T.A., Ramachandran, R.K., Willson, T.M., and Kliewer, S.A. (2001). Comprehensive messenger ribonucleic acid profiling reveals that peroxisome proliferator-activated receptor gamma activation has coordinate effects on gene expression in multiple insulin-sensitive tissues. Endocrinology *142*, 1269-1277.

Weigle, D.S. (1987). Pulsatile Secretion of Fuel-Regulatory Hormones. Diabetes *36*, 764-775.

Weir, G.C., and Bonner-Weir, S. (2007). A dominant role for glucose in beta cell compensation of insulin resistance. The Journal of clinical investigation *117*, 81-83.

Weisberg, S.P., McCann, D., Desai, M., Rosenbaum, M., Leibel, R.L., and Ferrante, A.W., Jr. (2003). Obesity is associated with macrophage accumulation in adipose tissue. The Journal of clinical investigation *112*, 1796-1808.

Wente, W., Efanov, A.M., Brenner, M., Kharitonenkov, A., Koster, A., Sandusky, G.E., Sewing, S., Treinies, I., Zitzer, H., and Gromada, J. (2006). Fibroblast growth factor-21 improves pancreatic beta-cell function and survival by activation of extracellular signal-regulated kinase 1/2 and Akt signaling pathways. Diabetes *55*, 2470-2478.

Wiberg, G.S., and Grice, H.C. (1963). LONG-TERM ISOLATION STRESS IN RATS. Science (New York, NY) *142*, 507.

Wikoff, W.R., Anfora, A.T., Liu, J., Schultz, P.G., Lesley, S.A., Peters, E.C., and Siuzdak, G. (2009). Metabolomics analysis reveals large effects of gut microflora on mammalian blood metabolites. Proceedings of the National Academy of Sciences of the United States of America *106*, 3698-3703.

Wilding, J.P. (2014). The role of the kidneys in glucose homeostasis in type 2 diabetes: clinical implications and therapeutic significance through sodium glucose co-transporter 2 inhibitors. Metabolism: clinical and experimental *63*, 1228-1237.

Wilding, J.P., Woo, V., Soler, N.G., Pahor, A., Sugg, J., Rohwedder, K., and Parikh, S. (2012). Long-term efficacy of dapagliflozin in patients with type 2 diabetes mellitus receiving high doses of insulin: a randomized trial. Annals of internal medicine *156*, 405-415.

Wolfrum, C., Poy, M.N., and Stoffel, M. (2005). Apolipoprotein M is required for prebeta-HDL formation and cholesterol efflux to HDL and protects against atherosclerosis. Nature medicine *11*, 418-422.

Woods, S.C., Schwartz, M.W., Baskin, D.G., and Seeley, R.J. (2000). Food intake and the regulation of body weight. Annual review of psychology *51*, 255-277.

Wu, H., Jia, W., Bao, Y., Lu, J., Zhu, J., Wang, R., Chen, Y., and Xiang, K. (2008). Serum retinol binding protein 4 and nonalcoholic fatty liver disease in patients with type 2 diabetes mellitus. Diabetes research and clinical practice *79*, 185-190.

Xu, J., Lloyd, D.J., Hale, C., Stanislaus, S., Chen, M., Sivits, G., Vonderfecht, S., Hecht, R., Li, Y.S., Lindberg, R.A*., et al.* (2009). Fibroblast growth factor 21 reverses hepatic steatosis, increases energy expenditure, and improves insulin sensitivity in diet-induced obese mice. Diabetes *58*, 250-259.

Xu, S., and Venge, P. (2000). Lipocalins as biochemical markers of disease. Biochimica et biophysica acta *1482*, 298-307.

Yamamoto, Y., Hirose, H., Saito, I., Nishikai, K., and Saruta, T. (2004). Adiponectin, an adipocyte-derived protein, predicts future insulin resistance: two-year follow-up study in Japanese population. The Journal of clinical endocrinology and metabolism *89*, 87-90.

Yamauchi, T., Kamon, J., Ito, Y., Tsuchida, A., Yokomizo, T., Kita, S., Sugiyama, T., Miyagishi, M., Hara, K., Tsunoda, M.*, et al.* (2003). Cloning of adiponectin receptors that mediate antidiabetic metabolic effects. Nature *423*, 762-769.

Yamauchi, T., Kamon, J., Minokoshi, Y., Ito, Y., Waki, H., Uchida, S., Yamashita, S., Noda, M., Kita, S., Ueki, K.*, et al.* (2002). Adiponectin stimulates glucose utilization and fatty-acid oxidation by activating AMP-activated protein kinase. Nature medicine *8*, 1288-1295.

Yamauchi, T., Kamon, J., Waki, H., Terauchi, Y., Kubota, N., Hara, K., Mori, Y., Ide, T., Murakami, K., Tsuboyama-Kasaoka, N.*, et al.* (2001). The fat-derived hormone adiponectin reverses insulin resistance associated with both lipoatrophy and obesity. Nature medicine *7*, 941-946.

Yan, Q.W., Yang, Q., Mody, N., Graham, T.E., Hsu, C.H., Xu, Z., Houstis, N.E., Kahn, B.B., and Rosen, E.D. (2007). The adipokine lipocalin 2 is regulated by obesity and promotes insulin resistance. Diabetes *56*, 2533-2540.

Yang, G., Badeanlou, L., Bielawski, J., Roberts, A.J., Hannun, Y.A., and Samad, F. (2009). Central role of ceramide biosynthesis in body weight regulation, energy metabolism, and the metabolic syndrome. Am J Physiol Endocrinol Metab *297*, E211-E224.

Yang, Q., Graham, T.E., Mody, N., Preitner, F., Peroni, O.D., Zabolotny, J.M., Kotani, K., Quadro, L., and Kahn, B.B. (2005). Serum retinol binding protein 4 contributes to insulin resistance in obesity and type 2 diabetes. Nature *436*, 356-362.

Yang, Y., Jooss, K.U., Su, Q., Ertl, H.C., and Wilson, J.M. (1996). Immune responses to viral antigens versus transgene product in the elimination of recombinant adenovirus-infected hepatocytes in vivo. Gene therapy *3*, 137-144.

Yoneda, S., Uno, S., Iwahashi, H., Fujita, Y., Yoshikawa, A., Kozawa, J., Okita, K., Takiuchi, D., Eguchi, H., Nagano, H.*, et al.* (2013). Predominance of beta-cell neogenesis rather than replication in humans with an impaired glucose tolerance and newly diagnosed diabetes. The Journal of clinical endocrinology and metabolism *98*, 2053-2061.

Young, A.A., Gedulin, B.R., and Rink, T.J. (1996). Dose-responses for the slowing of gastric emptying in a rodent model by glucagon-like peptide (7-36) NH2, amylin, cholecystokinin, and other possible regulators of nutrient uptake. Metabolism: clinical and experimental *45*, 1-3.

Yu, C., Chen, Y., Cline, G.W., Zhang, D., Zong, H., Wang, Y., Bergeron, R., Kim, J.K., Cushman, S.W., Cooney, G.J.*, et al.* (2002). Mechanism by which fatty acids inhibit insulin activation of insulin receptor substrate-1 (IRS-1)-associated phosphatidylinositol 3-kinase activity in muscle. The Journal of biological chemistry *277*, 50230-50236.

Zaharia, O.P., Strassburger, K., Strom, A., Bönhof, G.J., Karusheva, Y., Antoniou, S., Bódis, K., Markgraf, D.F., Burkart, V., Müssig, K.*, et al.* (2019). Risk of diabetes-associated diseases

in subgroups of patients with recent-onset diabetes: a 5-year follow-up study. The Lancet Diabetes & Endocrinology *7*, 684-694.

Zaiss, A.K., Liu, Q., Bowen, G.P., Wong, N.C., Bartlett, J.S., and Muruve, D.A. (2002). Differential activation of innate immune responses by adenovirus and adeno-associated virus vectors. Journal of virology *76*, 4580-4590.

Zaiss, A.K., and Muruve, D.A. (2008). Immunity to adeno-associated virus vectors in animals and humans: a continued challenge. Gene therapy *15*, 808-816.

Zhang, H.H., Halbleib, M., Ahmad, F., Manganiello, V.C., and Greenberg, A.S. (2002). Tumor necrosis factor-alpha stimulates lipolysis in differentiated human adipocytes through activation of extracellular signal-related kinase and elevation of intracellular cAMP. Diabetes *51*, 2929-2935.

Zhang, J., Wu, Y., Zhang, Y., Leroith, D., Bernlohr, D.A., and Chen, X. (2008a). The role of lipocalin 2 in the regulation of inflammation in adipocytes and macrophages. Molecular endocrinology (Baltimore, Md) *22*, 1416-1426.

Zhang, X., Yeung, D.C., Karpisek, M., Stejskal, D., Zhou, Z.G., Liu, F., Wong, R.L., Chow, W.S., Tso, A.W., Lam, K.S.*, et al.* (2008b). Serum FGF21 levels are increased in obesity and are independently associated with the metabolic syndrome in humans. Diabetes *57*, 1246-1253.

Zhang, Y., Foncea, R., Deis, J.A., Guo, H., Bernlohr, D.A., and Chen, X. (2014). Lipocalin 2 expression and secretion is highly regulated by metabolic stress, cytokines, and nutrients in adipocytes. PLoS One *9*, e96997-e96997.

Zhang, Y., Proenca, R., Maffei, M., Barone, M., Leopold, L., and Friedman, J.M. (1994). Positional cloning of the mouse obese gene and its human homologue. Nature *372*, 425-432.

Zhang, Y., Zhou, F., Bai, M., Liu, Y., Zhang, L., Zhu, Q., Bi, Y., Ning, G., Zhou, L., and Wang, X. (2019). The pivotal role of protein acetylation in linking glucose and fatty acid metabolism to β-cell function. Cell Death Dis *10*, 66-66.

Zhao, A.Z., Bornfeldt, K.E., and Beavo, J.A. (1998). Leptin inhibits insulin secretion by activation of phosphodiesterase 3B. Journal of Clinical Investigation *102*, 869-873.

Zhao, S., Mugabo, Y., Iglesias, J., Xie, L., Delghingaro-Augusto, V., Lussier, R., Peyot, M.L., Joly, E., Taib, B., Davis, M.A.*, et al.* (2014). alpha/beta-Hydrolase domain-6-accessible monoacylglycerol controls glucose-stimulated insulin secretion. Cell Metab *19*, 993-1007.

Zhou, J.W., Tsui, S.K., Ng, M.C., Geng, H., Li, S.K., So, W.Y., Ma, R.C., Wang, Y., Tao, Q., Chen, Z.Y.*, et al.* (2011). Apolipoprotein M gene (APOM) polymorphism modifies metabolic and disease traits in type 2 diabetes. PLoS One *6*, e17324.

Zhou, Y., Jiang, L., and Rui, L. (2009). Identification of MUP1 as a regulator for glucose and lipid metabolism in mice. The Journal of biological chemistry *284*, 11152-11159.

Zierath, J.R., Livingston, J.N., Thorne, A., Bolinder, J., Reynisdottir, S., Lonnqvist, F., and Arner, P. (1998). Regional difference in insulin inhibition of non-esterified fatty acid release

from human adipocytes: relation to insulin receptor phosphorylation and intracellular signalling through the insulin receptor substrate-1 pathway. Diabetologia *41*, 1343-1354.